January 2015

Characterization And Catalytic Cracking Of Tar Obtained In Coal / Biomass / Municipal Solid Waste Gasification: The Use Of Basic Mineral Catalysts And Miscibility, Properties, And Corrosivity Of Petroleum-Biofuel Oils And Blends For Application In Oil-Fired Power Stations

Stacy Joan Bjorgaard

How does access to this work benefit you? Let us know!

Follow this and additional works at: https://commons.und.edu/theses

CHARACTERIZATION AND CATALYTIC CRACKING OF TAR OBTAINED IN
COAL / BIOMASS / MUNICIPAL SOLID WASTE GASIFICATION: THE USE OF
BASIC MINERAL CATALYSTS
AND
MISCIBILITY, PROPERTIES, AND CORROSIVITY OF PETROLEUM-BIOFUEL
OILS AND BLENDS FOR APPLICATION IN OIL-FIRED POWER STATIONS

by

Stacy Joan Bjorgaard
Bachelor of Science, University of North Dakota, 2010

A Dissertation
Submitted to the Graduate Faculty

of the

University of North Dakota

in partial fulfillment of the requirements

for the degree of

Doctor of Philosophy

Grand Forks, North Dakota
August
2015

ii
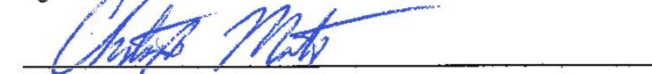
This dissertation, submitted by Stacy Bjorgaard in partial fulfillment of the requirements for the Degree of Doctor of Philosophy from the University of North Dakota, has been read by the Faculty Advisory Committee under whom the work has been done and is hereby approved.

_____
Michael Mann

_____
Bruce Folkedahl

_____
Christopher Martin

_____
Frank Bowman

_____
Steven Benson

This dissertation is being submitted by the appointed advisory committee as having met all of the requirements of the School of Graduate Studies at the University of North Dakota and is hereby approved.

_____
Wayne Swisher
Dean of the School of Graduate Studies

July 30, 2015

PERMISSION

Title   Characterization and Catalytic Cracking of Tar Obtained in Coal / Biomass / Municipal Solid Waste Gasification: The Use of Basic Mineral Catalysts
and
Miscibility, Properties, and Corrosivity of Petroleum-Biofuel Oils and Blends for Application in Oil-Fired Power Stations

Department   Chemical Engineering

Degree   Doctor of Philosophy

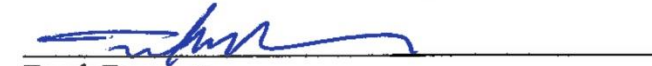In presenting this dissertation in partial fulfillment of the requirements for a graduate degree from the University of North Dakota, I agree that the library of this University shall make it freely available for inspection. I further agree that permission for extensive copying for scholarly purposes may be granted by the professor who supervised my dissertation work, or in his absence, by the Chairperson of the department or the dean of the School of Graduate Studies. It is understood that any copying or publication or other use of this dissertation or part thereof for financial gain shall not be allowed without my written permission. It is also understood that due recognition shall be given to me and to the University of North Dakota in any scholarly use which may be made of any material in my dissertation.

Stacy Joan Bjorgaard
30 July 2015

TABLE OF CONTENTS

LIST OF FIGURES

LIST OF TABLES

ACKNOWLEDGEMENTS

I wish to express my sincere appreciation to those around me for their guidance and support during my time in the doctoral program at the University of North Dakota.

I especially want to thank my advisor, Dr. Michael Mann, whose expertise, understanding, guidance, and mentorship provided me with the tools necessary to complete my undergraduate and graduate studies. His assistance made this project possible.

Dr. Bruce Folkedahl and Dr. Chris Martin have provided me with much encouragement and guidance in carrying out practical research. From locating equipment to assisting in the design and implementation of my experiments, they were invaluable in the focus and completion of this research.

Dr. Frank Bowman was very helpful in making sure I was completing the academic as well as research requirements for my doctorate. I am grateful for his guidance.

Dr. Steve Benson has provided much practical education, especially in the impurities arising in combustion and gasification and their final fates.

I recognize this research would not have been possible without the financial assistance of the Department of Defense's Strategic Environmental Research and Development program, the Department of Energy's Energy Efficiency and Renewable Energy Office, and the Electric Power Research Institute. I am grateful for their support in my graduate studies.

"If you can't repeat it, it's not science."
- Tory Belleci, *Mythbusters*, Episode 61: Deadly Straw, Primary Perception

"Serit arbores quae alteri saeclo prosint." ["One plants trees for the benefit of another age.]
- Marcus Tullius Cicero, *Cato Maior De Senectute* [*Essay to Cato the Elder On Old Age*]

ABSTRACT

To meet the metrics set forth by the Clean Power Plan, industry can use gasification or replacement of petroleum with biofuels. However, tars formed in gasification are difficult to remove, and biofuel-petroleum blends may have issues with fuel stability, corrosion, and miscibility.

Tar cracking was studied in both a laboratory-scale updraft gasifier, with a municipal solid waste feedstock, and tar cracking reactor system and in a bench-scale tar cracking reactor. The laboratory-scale system demonstrated that the optimal temperature was at least 800°C, that thermal cracking accounted for 85% of tar destruction, and that metal-based catalysts were the most promising. The bench-scale system, which used naphthalene as a model tar compound, demonstrated that a powder dolomite catalyst was most effective, that trona compared similarly to Plum Run dolomite, and that nahcolite was ineffective.

Hi-pour fuel oil, lo-pour fuel oil, crude jatropha oil, biocrude derived from animal renderings, biodiesel (refined biocrude), crude palm oil, and ultra-low sulfur diesel were blended at 75°F, 170°F, and 220°F. Flash points, pour points, and cloud points were determined for select oils and blends. 304 stainless steel, 316 stainless steel, brass, mild steel, and 410 stainless steel coupons were immersed in samples of each oil type and heated to 175°F to test for corrosive activity; these samples were examined every two weeks for fourteen weeks. Overall, blends containing biocrude and palm oil were

marginal to unacceptable due to the large proportion of waxes at ambient temperatures; all other fuel blends were acceptable for use in industry. Significant corrosion was observed on the brass in biocrude, brass in jatropha, brass in biodiesel, brass in palm, and brass in lo-pour fuel oil; the most significant corrosion was observed on the mild steel in biocrude. All samples had corrosion rates of < 1 mpy. Overall, the oils had the most effect on the brass samples.

CHAPTER I
INTRODUCTION

Recently greenhouse gas emissions have become a greater issue in the United

States, particularly as they relate to climate change. Figure 1-1 shows the breakdown of

greenhouse gas emissions in the United States as of 2014. The vast majority of the

emissions are carbon dioxide (CO_2); consequently, the Environmental Protection Agency

(EPA) has proposed the Clean Power Plan to reduce carbon emissions from existing

power plants. Additional regulations have been proposed for both modified and

reconstructed power plants as well as new power plants in separate documents (EPA,

2014d; EPA, 2013). The Clean Power Plan alone will allow the United States to cut

carbon pollution from the power sector by 30% by 2030. In addition, it will cut 54,000-

56,000 tons of $PM_{2.5}$, 424,000-471,000 tons of SO_2, and 407,000-428,000 tons of NO_2

(EPA, 2014a).

U.S. GREENHOUSE GAS POLLUTION INCLUDES:

CARBON DIOXIDE (CO2) 82%
Enters the atmosphere through burning fossil fuels (coal, natural gas, and oil), solid waste, trees and wood products, and also as a result of certain chemical reactions (e.g., manufacture of cement).

FLUORINATED GASES 3%
Hydrofluorocarbons, perfluorocarbons, and sulfur hexafluoride are synthetic, powerful greenhouse gases that are emitted from a variety of industrial processes.

NITROUS OXIDE (N2O) 6%
Emitted during agricultural and industrial activities, as well as during combustion of fossil fuels and solid waste.

METHANE (CH4) 9%
Emitted during the production and transport of coal, natural gas, and oil as well as from landfills.

10% COMMERCIAL & RESIDENTIAL
32% ELECTRICITY
10% AGRICULTURE
20% INDUSTRY
28% TRANSPORTATION

TOTAL U.S. GREENHOUSE GAS EMISSIONS BY ECONOMIC SECTOR IN 2012

SOURCE: EPA

Figure 1-1. United States greenhouse gas emissions, current as of 2014 (Web, accessed 2015).

The Clean Power Plan will be finalized by mid-summer 2015. At that point, the EPA will begin the regulatory process for proposing a federal plan. This plan was proposed to address the issues arising from climate change, including rising frequency and intensity of weather disasters, which cost the American economy more than $100 billion in 2012. Other pollutants, such as arsenic and mercury, are heavily regulated at power plants; however, there is not currently a limit on carbon. The Clean Power Plan will cut carbon pollution at power plants by 30% from 2005 levels (EPA, 2014c). Programs most strongly supported under the Clean Power Plan will include those targeting renewable energy or energy efficiency (EPA, 2014b). Thus, some plants may choose to meet the new carbon regulations by using gasification technologies or biofuels. These switches become more feasible in light of the 10- to 15-year window EPA will

provide after the finalization of the Clean Power Plan to plan and achieve reductions in

carbon pollution (EPA, 2014b). Two potential technologies for helping reduce CO_2

emissions and meeting the anticipated requirements of the Clean Power Plan are

gasification and the replacement of petroleum with biofuels.

1.1 Gasification

Gasification is a thermo-chemical process which breaks down a carbon-based

feedstock (e.g., coal, biomass, petroleum coke [petcoke], municipal solid wastes [MSW])

into its basic chemical constituents. The most common feedstock is coal, which is

exposed to steam and air or oxygen at high temperature and pressure. Gasification differs

from combustion primarily in that combustion takes place in the presence of excess

oxygen (O_2), while gasification takes place in an O_2-starved (i.e., reducing) environment

(EERC, 2007c).

Table 1-1 provides a list of reactions important in the gasification process. The

first four reactions are the primary reactions of gasification. The fifth reaction is the

Boudouard reaction. The sixth reaction is the formation of water from hydrogen and

oxygen. The seventh reaction is the formation of carbon dioxide and hydrogen from

elemental carbon and water. The eighth reaction is the water-gas shift reaction, which

converts carbon monoxide (CO) into carbon dioxide (CO_2) by splitting water and leaving

hydrogen (H_2). The final three reactions represent possible reactions for the production of

methane.

Table 1-1. Key Reactions in Gasification (after EERC, 2007d)

	Reaction	Heat of Formation (kJ/mol, 25°C)
1	$C + O_2 \rightarrow CO_2$	-390
2	$C + \frac{1}{2}O_2 \rightarrow CO$	-110
3	$CO + \frac{1}{2}O_2 \rightarrow CO_2$	-280
4	$C + H_2O \rightarrow CO + H_2$	130
5	$C + CO_2 \rightarrow 2CO$	170
6	$H_2 + \frac{1}{2}O_2 \rightarrow H_2O$	-240
7	$C + 2H_2O \rightarrow CO_2 + 2H_2$	90
8	$CO + H_2O \rightarrow CO_2 + H_2$	-41
9	$CO + 2H_2 \rightarrow CH4 + O\cdot$	36
10	$CO + 3H_2 \rightarrow CH_4 + H_2O$	-210
11	$2CO + 2H_2 \rightarrow CH_4 + CO_2$	-250

The generated gas largely consists of CO, H_2, CO_2, and H_2O and is known as syngas. Syngas has many potential applications: fuel to generate electricity using steam turbines, production of chemicals, production of liquid or gaseous fuels, and production of hydrogen. For example, a particularly H_2- and CO-rich syngas stream may be used to generate liquid fuels through the Fischer-Tropsch reaction (Folkedahl *et al*., 2011). Syngas, on average, has a composition of 0-6 wt% tar and oil, 28-40 vol% H_2, 16-63 vol% CO, 3-33 vol% CO_2, 0-10 vol% CH_4, 0.2-1 vol% H_2S, 0-0.1 vol% COS, 0-0.35 vol% NH_3, and 0-0.35 vol% HCN (EERC, 2007c). The composition of the syngas depends on both the feedstock and the gasification technology used.

The recent and projected growth of gasification will have many benefits for the United States. First, it is more economical to capture and sequester CO_2 generated through gasification than CO_2 generated through combustion (i.e., in a conventional coal-fired power plant). This increased efficiency is due to the economic advantage of separating CO_2 before combustion as opposed to after combustion. In addition, gasification will help decrease dependency on the foreign oil supply, as many products made from petroleum can be made from coal through gasification. Furthermore,

gasification boasts unusually wide feedstock flexibility: any carbonaceous material can be gasified. Moreover, gasification systems can approach near-zero emission levels, meeting the strictest EPA regulations pertaining to sulfur, particulate emissions, mercury, and NO_X removal. Finally, gasification processes can approach a considerably higher efficiency (60% overall) compared with conventional power plants (40% overall), excluding CO_2 capture and sequestration (EERC, 2007c).

Understanding the formation of tar in gasification depends on an understanding of gasifier technology and fuel types. There are four basic classes of gasifiers: fixed bed, fluidized bed, entrained flow, and transport. Typically the feedstock must be a solid (pulverized to 0.5-5 mm), though some entrained flow gasifiers can handle slurry feeds. Gas outlet temperatures range from 400°C (fixed bed) to 1400°C (entrained flow). For most gasifiers, the oxidant is either air or O_2; a notable exception is the entrained-flow gasifier, which is almost always O_2-blown. Residence time in a gasifier is usually on the order of seconds, with the exception of the fixed-bed gasifier; here, residence times are on the order of 15-30 minutes. Ash handling may be either slagging (molten) or non-slagging. There are many different commercial gasifiers; for example, the Lurgi and British-Gas Lurgi gasifiers are fixed bed, while the Shell and Prenflo gasifiers are entrained flow (EERC, 2007a). These various types were developed to gasify a variety of fuels, including coal, biomass, and municipal solid waste. The type of gasifier and fuel will impact the amount and types of impurities formed, including the formation of tar.

Since no feedstock is purely carbon and hydrogen, compounds in addition to those formed via the reactions in Table 1-1 form. Some of the most common compounds that are formed and which must be removed from syngas are ungasifiable slag, particulate

5

matter, tar, H₂S, COS, sodium, mercury, and ammonia. These compounds are present in varying amounts depending on the feedstock and gasification technology used (EERC, 2007b). Particulate matter is removed from syngas using cyclones, scrubbers, baghouses, or electrostatic precipitators (Encyclopaedia Britannica, 2009). Sulfur can be removed from the syngas by chemical absorption using amines, physical absorption using Selexol, and physical absorption using Rectisol (EERC, 2007b). The most common method of mercury removal was developed by the Eastman Chemical Company and involves passing the syngas through a bed of activated carbon impregnated with 10-15 wt% sulfur (USDoE NETL, 2002).

Tars are more difficult to remove. Current technologies, most commonly wet electrostatic precipitators, wet scrubbers, and wet cyclones, are only capable of removing 40-70% of tars in the case of wet electrostatic precipitators and wet cyclones and require large equipment sizes and consequently large capital investments. Using water to condense and remove tars, such as in wet scrubbers, leads to saponification, only 10-25% removal of tars, additional waste water treatment steps, and energy losses in cooling and reheating syngas. Tars may be thermally cracked, but this typically involves heating the syngas above the outlet temperature of the gasifier and thus imposes an energy penalty. Catalysts, most commonly basic minerals and/or nickel or other transition metals, may be used, but metal catalysts are expensive and susceptible to poisoning, while basic minerals are less active in cracking tars and may be friable, eluting out of fluidized and, to a lesser extent, fixed beds. Remaining tars may cause several problems, including causing the deterioration of turbine parts in electricity production, increasing maintenance costs because of the need for additional maintenance cycles for cleaning, and reducing the

6

effectiveness of heat exchange equipment. Therefore, additional work on tar destruction is needed, particularly in the dry cracking of tars (i.e., no additional water added) to reduce the energy penalty incurred in tar removal.

Given these difficulties in dealing with tars, much recent research has been done in tar cracking. Some technical issues that current tar cracking research attempts to address include whether thermal catalytic cracking can be used to treat the quantity and composition of tars arising from the countercurrent gasification of municipal solid waste and whether enough fuel value can be recovered from cracked tars to achieve a target conversion efficiency. Other issues include whether a recuperative heat exchanger within the cracking reactor can recycle enough thermal energy to help achieve the target conversion efficiency, whether fouling of heat transfer and catalyst surfaces can be reduced to levels that minimize maintenance requirements, and whether treated syngas is sufficiently clean so that maintenance requirements and operating lifetimes of downstream equipment are not adversely effected (Martin, 2011). Other research has been done in alternate catalysts, both metal- and mineral-based, to examine whether more effective catalysts with fewer fouling tendencies and lower costs can be discovered.

1.2 Biofuel Production

Another option to reduce CO_2 or meet renewable fuel mandates is to use biofuels for power generation. Since biofuels are considered carbon-neutral fuels, this allows for the displacement of CO_2 emissions associated with fossil fuel-based electricity generation.

The term *biofuels* refers both to the plant or animal biomass and refined products made from the biomass. These products may be combusted for energy, usually heat.

Biofuels exist in solid, liquid, and gaseous forms, analogous to fossil fuels. Biofuels provide an effective potential source for meeting future energy demands since they are extensively available, technology and infrastructure for use are already extant, and liquid fuel production is possible (Guo, 2014).

Combustion of biofuels, such as wood pellets, waste wood, and woody biomass, follows the following general equation:

$$C_6H_{10}O_5 + 6O_2 \rightarrow 6CO_2 + 5H_2O + heat + light$$
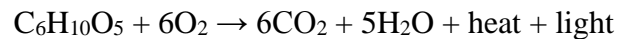
However, in conventional furnaces, combustion is incomplete; resulting products include smoke, creosote, carbon monoxide, methane, NO_X, and SO_X. Nevertheless, wood chips emit fewer NO_X and SO_X compounds than coal in combustion (Guo, 2014).

Bioethanol and other liquid biofuels may be produced from vegetative biomass through fermentation, in which the following series of reactions occur:

$$(C_6H_{10}O_5)_n \text{ (starch, cellulose, sugar)} + nH_2O \rightarrow nC_6H_{12}O_6$$

$$(C_5H_8O_4)_n \text{ (hemicellulose)} + nH_2O \rightarrow nC_5H_{10}O_5$$

$$C_6H_{12}O_6 \rightarrow 2CH_3CH_2OH + 2CO_2$$

$$C_5H_{10}O_5 \rightarrow 5CH_3CH_2OH + 5CO_2$$
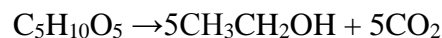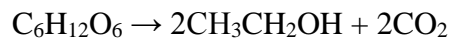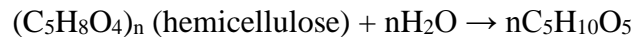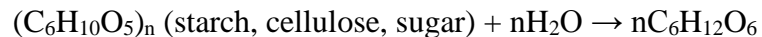
Bioethanol is currently used in gasoline blends or as a gasoline substitute in many countries (Guo, 2014).

Biodiesel may be derived from several different sources, including "vegetable oil, animal fats, algal lipids, or waste grease through 'transesterification' in the presence of alcohol and alkaline catalyst" (Guo, 2014). The generic equation is as follows:

$$Triglyceride + Methanol \rightarrow Biodiesel$$

This reaction occurs in the presence of a KOH or NaOH catalyst. Much as in the case of bioethanol, biodiesel is currently used in diesel blends in many countries (Guo, 2014).

Finally, biomass may be pyrolyzed (heated in the absence of air) to produce bio-ois, which may be directly burned or upgraded into various fuel oil grades (Guo, 2014).

Biogas can also be generated by the anaerobic digestion of organic wastes; that is, microorganisms are used to convert organic material into methane by the following reaction:

$$C_6H_{12}O_6 \rightarrow 3CO_2 + 3CH_4$$
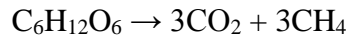
In addition, syngas can be generated from gasification or pyrolysis of biomass. This syngas may then be converted to chemicals or combusted for energy generation (Guo, 2014).

Of particular interest to this study are power plants operating using fuel oil. Oil is fairly simple to burn and produces less ash than coal. Fuel oils, derived from petroleum, are usually atomized before combustion. The combustible fraction of fuel oil is primarily made up of carbon and hydrogen with smaller amounts of sulfur, nitrogen, oxygen, water, and sediment. Table 1-2 shows some characteristics of typical liquid fuels, including gasoline, kerosene, gas oil, and fuel oil (Singer, 1981).

Table 1-2. Characteristics of Liquid Fuels (after Singer, 1981).

	$^\circ$ API	% C	% H_2	% S	% N_2	% O_2	HHV (Btu/lb)	A at zero excess air (lb/10^6 Btu)	CO_2 at zero excess air (%)
Gasoline	60	85.0	14.8	-	0.1	0.1	20200	746	14.87
Kerosene	45	85.0	14.0	-	0.5	0.5	19900	742	15.12
Gas oil	30	85.0	12.8	0.8	0.74	0.7	19300	745	15.48
Fuel oil	15	85.5	11.5	1.6	0.7	0.7	18500	758	15.90

9

Fuel oil falls into two general categories: distillate and residual. Fuel oils No. 1 and No. 2 are distillate oils, which are derived from vaporization in petroleum refineries. These are lighter oils; No. 1 is the kerosene cut that boils off right after the cut used for gasoline and fuels vaporizing pot-type boilers, while No. 2 is a distillate home heating oil. No. 3-5 fuel oils are residual oils and heavier distillate oils; No. 3 is an archaic designation for fuels that are now typically designated No. 2, No. 4 is a commercial heating oil for burners without preheaters, and No. 5 is a residual heating oil which requires preheating (Perry, 1950). No. 6 fuel oil is a heavy residual oil typically usually used for steam generation. No. 6 oil contains vanadium, sodium, and sulfur impurities, which can lead to operating problems, but is cheap. Residual fuel oils are not vaporized by heating, and these oils are typically black, high viscosity fluids. They require heating for handling and combustion (Kitto, 2005).

Biofuels are sometimes mixed with petroleum-based oils to increase the renewable content of the fuel, with a goal of meeting renewable portfolio standards, and may be a strategy for meeting the proposed Clean Power Plan. They are most commonly mixed with No. 2 or No. 6 oils; however, issues with fuel stability, corrosion, and miscibility can occur for some fuel blends. Therefore, miscibility of biofuel and petroleum blends and corrosivity of biofuels as compared to fuel oils need to be studied.

1.3 Hypotheses

With regards to required work in tar cracking to advance the efficacy of gasification in lowering CO_2 emissions, it was hypothesized that a robust, efficient, and compact syngas-cleaning system which complemented distributed-scale updraft gasifier technology could be used to generate a conversion efficiency in excess of 50%. A key

aspect of this system would be that it was dry, requiring no additional water in the form of steam. This system was tested in the form of a laboratory-scale updraft gasifier and tar cracker. In addition, the word "compact" was here defined as fitting within an 8' x 8' x 20' envelope for the full-scale system.

In addition, it was hypothesized that nahcolite and trona would be effective catalysts for cracking tars formed in updraft gasification. Here, "effective" was defined as 75% conversion of tars to syngas and small hydrocarbons. Nahcolite and trona were tested using a bench-scale, dry tar cracking reactor and naphthalene as a model tar compound to determine whether they would prove effective catalysts for cracking tars formed in updraft gasification (primary tars, typically simple 1-2 benzene ring structures), at least as guard bed materials which could protect the transition metal catalysts used for additional cracking of tars to syngas. This testing was done in support of the aforementioned updraft gasifier and tar cracking work to further examine the efficacy of mineral catalysts.

With regards to required work in biofuels to advance their efficacy in lowering CO_2 emissions, it was hypothesized that no 50:50 blend of biofuel and petroleum-based fuels would present a problem at 75°F, 170°F, or 220°F, all at atmospheric pressure. For this work, "problem" was defined as any event which would be detrimental if observed in industry, including but not limited to the formation of gel or sludge, excessive settling of waxes out of solution, incomplete miscibility, smoking at higher temperatures, and semi-polymerization of oil.

It was also hypothesized that no biofuel or petroleum-based fuel would prove significantly corrosive to a specific set of metal samples, comprised of samples of 316

stainless steel, 304 stainless steel, 410 stainless steel, brass, and mild steel. For this work, "significantly corrosive" was defined as having a corrosion rate in excess of 0.5 mils per year (mpy).

In addition, it was hypothesized that it would be possible to determine the pour point and cloud point of biofuels using simple methods. In this case, "simple methods" was defined as those testing methods which are accurate, precise, repeatable, simple to execute, and, preferably, may be performed in the field to confirm fuel properties before accepting them at the plant.

CHAPTER II
LITERATURE REVIEW – TAR CRACKING

2.1 World Energy and Liquid Fuel Overview

It is commonly accepted that global energy demands will continue to rise over the coming decades. With the continuing overall economic growth in underdeveloped and undeveloped countries, these countries will demand more and more energy. Specifically, electricity generation is projected to rise to more than triple the generation level in 1990 by the year 2035, and overall total energy consumption is expected to more than double in the same time period (as shown in Figure 2-1).

Figure 67. Growth in world electric power generation and total energy consumption, 1990-2035
(index, 1990 = 1)
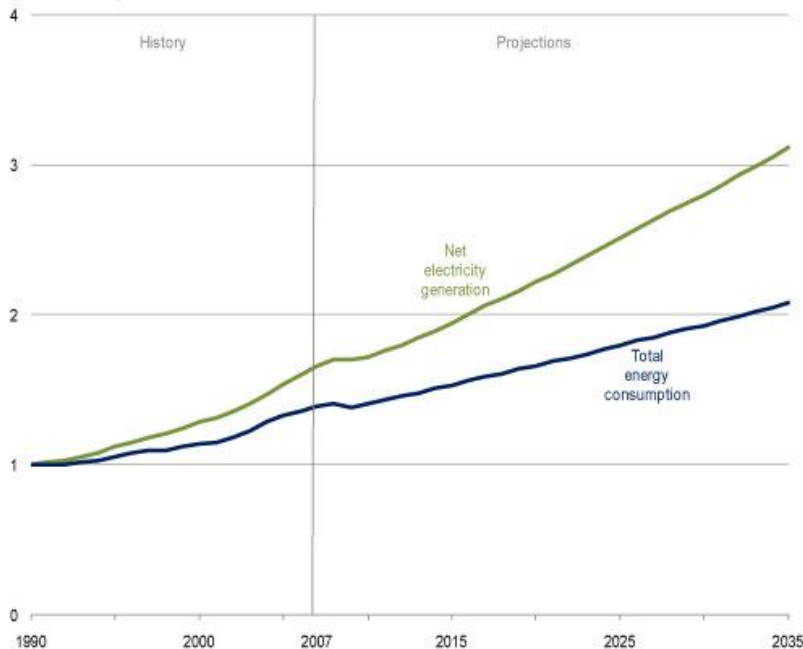
Figure 2-1. Expected growth in world electric power generation and total energy consumption, 1990-2035 (US EIA, 2010a).

Increasing electricity demand will be met mainly by electricity from coal.
According to Figure 2-2, coal currently supplies about 42% of the electricity generated,
and this share is projected to rise slightly to 43% by 2035. This outlook, of course, bars
any major global greenhouse gas policies and assumes that the price of oil and natural gas
will remain sufficiently high to make coal the cheapest energy source available. This is
especially true in developing coal-rich countries such as China and India.

Figure 70. World net electricity generation by fuel, 2007-2035
(trillion kilowatthours)

■ Liquids   ■ Nuclear   ■ Renewables   ■ Natural gas   ■ Coal
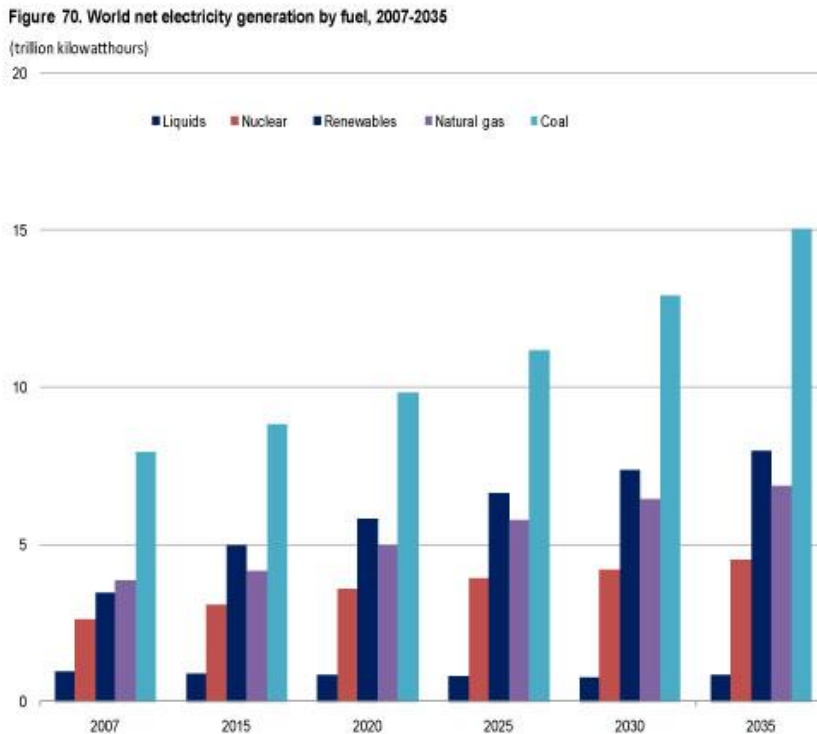
Figure 2-2. World net electricity generation by fuel, 2007-2035 (US EIA, 2010a).

Over the next several decades, the proportion of renewable energy used in energy
generation is expected to rise. Renewable energy sources include hydropower,
geothermal, solar, and wind. Municipal solid waste and biomass are also included as
renewable resources. Although biomass gives off CO_2 when it is burned, it is commonly
accepted that this carbon is returned to plant life in growing the next crops for biomass.

14

Figure 2-3 shows the expected overall usage of fuel sources in energy generation. Figure 2-4 shows the breakdown of different sources in electricity generation; note that renewable sources are expected to make an ever-increasing contribution to electricity generation.

Figure 16. World marketed energy use by fuel type, 1990-2035
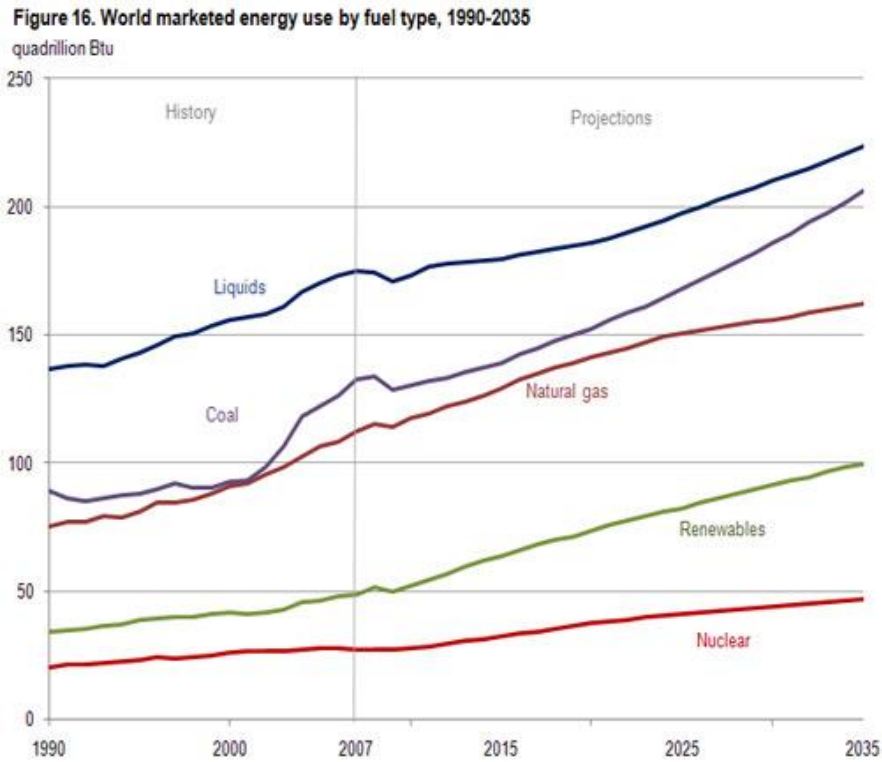
Figure 2-3. World marketed energy use by fuel type, 1990-2035 (US EIA, 2010c).

Figure 18. World electricity generation by fuel, 2007-2035
trillion kilowatthours
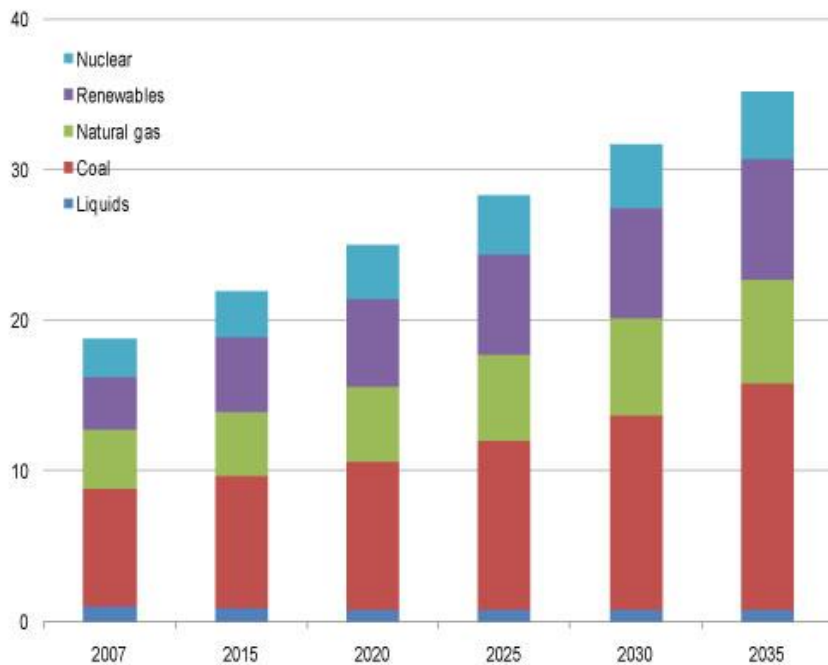
Figure 2-4. World electricity generation by fuel, 2007-2035 (US EIA, 2010c).

Combustion of coal for electricity generation is not the only use for coal. Coal

may also be indirectly liquefied to produce synthesis gas (a mixture of H_2, CO, CO_2,

H_2O, and possibly CH_4) or directly liquefied to produce a liquid hydrocarbon mixture.

Overall liquid fuel consumption is also projected to rise, largely as a consequence of the

aforementioned economic development and increasing prosperity around the world. The

use of coal for liquid fuels in these areas may become more important, especially if the

price of oil remains high and production remains centralized in politically unstable

regions of the world.

Figure 2-5 shows the expected unconventional liquid fuel production in 2035 as a

function of projected oil prices. These unconventional liquids include currently

undeveloped/developing oil products, gas-to-liquids, coal-to-liquids, and biofuels.

16

Figure 30. World production of unconventional liquid fuels in three cases, 2007 and 2035

million barrels per day

Legend:
- Shale Oil/Other
- Gas-to-Liquids
- Coal-to-Liquids
- Extra-Heavy Oil
- Biofuels
- Oil Sands/Bitumen

2007

2035: Reference, Low Oil Price, High Oil Price
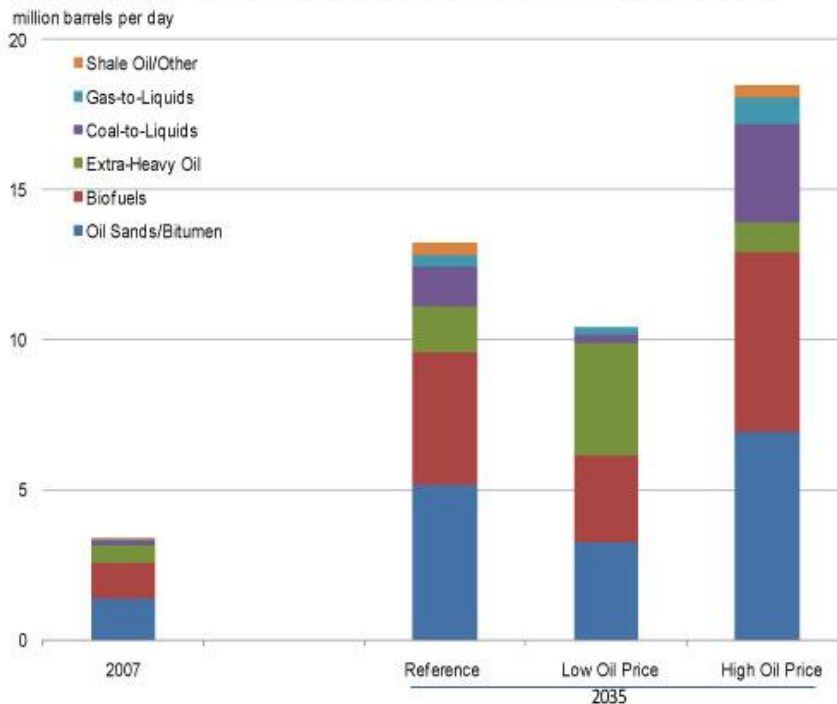
Figure 2-5. World production of unconventional liquid fuels in three cases, 2007 and 2035 (US EIA, 2010b).

The most well-known liquid fuel currently produced from biomass is ethanol. However, biomass, like coal, may be gasified to produce synthesis gas (henceforth, 'syngas'), from which many chemical products may be produced, including liquid fuels through the Fischer-Tropsch process, synthetic natural gas by synthesis over a nickel-based catalyst, hydrogen for electricity generation in turbines with combined cycle, or dimethyl ether. Municipal solid waste may be used in similar applications.

2.2 Gasification and Tar Production

The most common methods to obtain energy from coal, biomass, and municipal solid wastes are through combustion and gasification. Combustion involves feeding the fuel and excess air to a furnace at high temperatures to produce a flue gas primarily composed of water and CO_2. This flue gas is then used to generate energy by heating

17

water into steam, then using the steam to operate turbines. Gasification involves feeding the fuel and either air or pure oxygen along with steam to a gasifier at somewhat lower temperatures. The main difference between gasification and combustion is that in gasification air is fed at sub-stoichiometric ratios, so combustion reactions do not proceed to completion. That is, instead of producing a flue gas that is primarily composed of CO_2 and H_2O, gasification produces a syngas composed primarily of CO and H_2 along with smaller amounts of CO_2, H_2O, and CH_4.

There are some difficulties in gasifying coal, biomass, and municipal solid wastes. Due to the impurities present in coal, biomass, and municipal solid waste, the resulting gases may require additional processing to remove impurities. Gasifying these sources produces particulate matter, alkali metals (e.g., Na and K compounds), heavy metals and trace elements (e.g., mercury and lead), NH_3, H_2S, HCl, and tars. These compounds need to be removed before the syngas can be used. Particulate matter can be removed by filtering or scrubbing. Alkali metals can be removed by cooling, absorption, condensation, or filtering. Heavy metals and trace elements are typically removed by condensation, filtering, or using guard beds (especially in the case of Hg with activated carbon). NH_3 can be removed by scrubbing; if it is later converted to NO_X, it may be removed using selective catalytic reduction. H_2S and HCl can be removed by using limestone or dolomite, zinc-based guard beds before more sulfur-sensitive beds, scrubbing, or adsorption. Later shifting of syngas using the water-gas shift reaction may lead to the formation of CO_2, which can be captured using chemisorption or physisorption methods.

However, tars present a large challenge for cleaning. The precise definition of tars is a subject for much debate, but for this dissertation, tar will be defined as follows: "the organics produced under thermal or partial-oxidation regimes (gasification) of any organic material are called "tars" and are generally assumed to be largely aromatic" (Milne *et al*., 1998). Generally tars consist of five classes. Table 2-1 summarizes these tar classes, their properties, and representative compounds.

Table 2-1. List of tar compounds that are considered for different tar classes (after Li and Suzuki, 2009).

Tar class	Class name	Property	Representative compounds
1	GC-undetectable	Very heavy tars, cannot be detected by GC	Determined by subtracting the GC-detectable tar fraction from the total gravimetric tar
2	Heterocyclic aromatics	Tars containing hetero atoms; highly water soluble compounds	Pyridine, phenol, cresols, quinoline, isoquinoline, dibenzophenol
3	Light aromatic (1 ring)	Usually light hydrocarbons with single ring; do not pose a problem regarding condensability and solubility	Toluene, ethylbenzene, xylenes, styrene
4	Light PAH compounds (2-3 rings)	2 and 3 ring compounds; condense at low temperature even at very low concentration	Indene, naphthalene, methylnaphthalene, biphenyl, acenaphthalene, fluorine, phenanthrene, anthracene
5	Heavy PAH compounds (4-7 rings)	Larger than 3-ring, these compounds condense at high-temperatures at low concentrations	Fluoranthene, pyrene, chrysene, perylene, coronene

Tars must be removed or converted because they lead to filter plugging; internal condensation and deposition; and damage caused by impingement, especially in turbines when the tar molecules impact on the turbine blades. Typical methods for dealing with tar formation are wet and dry mechanical methods; thermal cracking; and catalytic cracking

(Han and Kim, 2008; Gerber, 2007; Li and Suzuki, 2009; Xu *et al*., 2010; Anis and Zainal, 2011; Siedlecki *et al.*, 2011).

Gasifier technology also plays a role in which tars are produced and in what amounts. Most tars are produced in fixed bed gasifiers, which are operated in two basic but distinct modes: downdraft and updraft. Downdraft gasifiers tend to produce a very clean syngas, with a possibility of a tar concentration less than 500 mg / Nm^3. However, it is difficult to scale up a downdraft gasifier. In an updraft gasifier, tar yields are much higher since the tar passes through a relatively cold drying region before exiting the gasifier, and concentrations may be up to 100 g / m^3. However, since the thermal efficiency of the updraft gasifier is far superior to the downdraft gasifier, it is beneficial to crack the tars (Siedlecki *et al*., 2011). In addition, different tars are formed in each gasifier. Downdraft gasifier tars tend to consist of tertiary tars at low levels, while primary tars tend to dominate the tar composition produced by updraft gasifiers (Milne *et al*., 1998).

The most common methods for tar cleaning using dry mechanical methods are cyclones, particle separators, fabric and ceramic filters, activated carbon adsorbers, and sand bed filters (Anis and Zainal, 2011). Occasionally the ceramic filtration methods for processing tar are combined with a catalytic element such as nickel, which has known tar-cracking properties. Loadings as low as 1 wt% nickel on a ceramic filter have demonstrated complete conversion of naphthalene to syngas at temperatures as low as 800°C (Zhao *et al*., 2000). In addition, Ni and Mg loaded onto alumina discs may almost completely remove naphthalene and benzene (model tars) at 900°C, although it would be better to run at 850°C; with that in mind, conversions of 99.0% were achieved at 850°C,

but conversions of only 77% were achieved at 800°C (Ma *et al.*, 2005). Nickel supported on a ceramic candle filter is capable of operating at temperatures up to 850°C and removing 98.5% of naphthalene (model tar compound) from an initial concentration of 7.8 g / Nm^3 (Simeone *et al.*, 2010).

The most common methods for tar cleaning using wet mechanical methods are wet electrostatic precipitators, wet scrubbers, and wet cyclones. These are the most common methods of removing tars from syngas and are widely applied in industry. Wet electrostatic precipitators are capable of removing 40-70% of tars, but achieving this removal requires a large equipment size and consequently a large capital investment. Wet scrubbers use water to condense and remove tars, but have several key disadvantages, including saponification, poor solubility of hydrocarbons (10-25% removal), waste water treatment, and energy losses in cooling and reheating syngas. Wet cyclones are capable of removing 30-70% of tars, but suffer from many of the same disadvantages as wet electrostatic precipitators and wet scrubbers (Anis and Zainal, 2011).

For updraft gasifiers, since the potential energy of tars is significant, it is more advantageous to crack tars than to remove them using mechanical methods (Virginie *et al.*, 2010b). Cracking tars increases the overall energy of the syngas. There are two primary methods of tar cracking, as mentioned earlier: thermal and catalytic. Thermal cracking of tars has been studied for a very long time; the earliest conclusive reference to thermal cracking was published in 1935 and refers to even earlier thermal cracking work (Frolich and Wieszevich, 1935). Thermal cracking of tars usually takes place at temperatures above 1000°C; however, some studies have taken place at temperatures as low as 700°C (Han and Kim, 2008; Anis and Zainal, 2011). Results of up to 99%

conversion have been observed in the presence of excess air, though recent results indicate tar reduction of 78% at 600°C (Phuphuakrat *et al*., 2010). However, this involves heating the gas above gasification temperatures, decreasing the overall thermal efficiency. Since the process is less efficient, it has been studied less in recent years. Much of the recent research has focused on kinetics of thermal cracking and modeling work, especially of model compounds with occasional studies of real gasification tars (Nunn *et al*., 1985). For example, thermal decomposition of toluene at atmospheric pressure and temperatures ranging from 700-950°C has been modeled (Taralas *et al*., 2003; McCoy, 1996). Additional research has been published discussing the use of NiO as an oxygen carrier in chemical looping combustion to remove tars (Mendiara *et al*., 2011). Moreover, tar conversion tends to form products such as methane, ethylene, propylene, cyclopentene, cyclopentadiene, benzene, and toluene as opposed to more synthesis gas, especially at lower temperatures (Anis and Zainal, 2011).

In order to form more synthesis gas at lower temperatures (typically 750-900°C), it is necessary to use catalytic cracking methods. The most common catalysts used are basic minerals, iron, nickel, and rhodium (Gerber, 2007; Xu *et al*., 2010; Anis and Zainal, 2011).

2.3 Metal-based Catalysts

Nickel catalysts are among the most commonly studied catalysts for tar cracking. In addition to the aforementioned work combining the nickel catalysts with filters in mechanical separation, nickel has been supported on alumina, dolomite, olivine, and biomass char. The decomposition of synthetic tar and ammonia over Ni monolith catalyst has been studied; it was found that complete conversion was only possible above 850°C

(Pfeifer and Hofbauer, 2008). The cracking of tars from waste polyethylene over a

NiO/Al_2O_3 catalyst was studied, and it was found that the highest conversions occurred at

900°C (He et $al.$, 2009). The effects of different supports (including MgO, Al_2O_3, SiO_2,

and NaY [zeolites]) on the activity of Ni in coal pyrolysis was studied, and it was

determined that MgO was the best support (Liu, 2009). Char and char-supported nickel

catalysts have also been studied; although it was determined that char has some catalytic

activity in tar cracking, this may be due to the presence of trace elements such as Mg and

Fe in the char, which are known to be catalytically active (Wang et $al.$, 2011). The effects

of nickel catalysts supported on brown coal char and Al_2O_3 were compared; coal char

may produce a more stable catalyst long-term than the more conventional alumina

support (Xiao et $al.$, 2011). The cracking of tars produced in gasifying pig compost over

Ni/Al_2O_3 catalysts was studied; it was determined that the catalyst led to complete

cracking of tars into H_2, CO, CO_2, and a small amount of residual carbon (Zhang et $al.$,

2011).

Unsupported nickel catalysts have also been studied recently, including recent

studies of Raney nickel in the gasification of activated sludge (Afif et $al.$, 2011). These

catalysts are promising because of their increased surface area.

Nickel catalysts have also been promoted with a variety of metals. The

gasification of waste wood for hydrogen production over a $Ni-CaO/Al_2O_3$ catalyst was

studied; this catalyst was able to produce a nearly tar-free syngas and H_2 concentration

around 57% (Kawamoto et $al.$, 2009). A trimetallic catalyst consisting of Ni, La, and Fe

supported on Al_2O_3 achieved 99% tar conversion at 800°C and did not exhibit any signs

of coking (Li et $al.$, 2009b). A Ni-Cu-Zn-Al catalyst was prepared by co-precipitation

(Kan *et al*., 2010). The decomposition of 1-methylnaphthalene over a NiMo catalyst was studied; developed models could very nearly predict experimental results (Dou *et al*., 2008). The pyrolysis of plant-based biomass with Ni-Mo catalyst was studied; it was determined that the overall temperature could be lowered while maintaining an acceptable tar production level (Hao *et al*., 2010). It was also found that a commercially-available zirconia-promoted Ni catalyst was more active than dolomite for tar cracking (Yoon *et al*., 2010). The reforming of toluene and naphthalene over Ni/MgO-Al$_2$O$_3$ catalysts was studied; it was determined that not only were the tar compounds fully cracked to small molecules, the catalyst showed relatively high sulfur tolerance (Yue *et al*., 2010). Similar studies were done using 1-methylnaphthalene as a model tar compound (Yang *et al*., 2010). Other research has determined that the most effective catalysts for gasifying coke were Fe/Ni/other metals in a 35/55/10 atomic ratio (Zhao *et al*., 2010). The gasification of waste tires over a nickel-ceria catalyst has been studied; it was determined that when 5% CeO$_2$ was added to the catalyst, a modest increase in gas and H$_2$ yield was obtained (Elbaba *et al*., 2011). The addition of ceria and zirconia to Ni catalysts was studied; it was determined that, at 800°C, 80% of 1-methylnaphthalene and 99% of toluene were converted to small molecules while avoiding coking issues (Łamacz *et al*., 2009; Łamacz *et al*., 2010).

Although nickel catalysts are effective at cracking tars and show some reforming activity which increases the H$_2$ and CO content of the syngas, they are not without their drawbacks. Ni catalysts are easily poisoned by sulfur and suffer from coking issues. In addition, Ni is a toxic metal (Virginie, 2010a).

A common way to protect Ni from sulfur poisoning is to place a guard bed of dolomite in front of a bed of Ni catalyst. This configuration has been used to obtain maximum H_2 concentrations of 52% and H_2 / CO ratios between 1.87 and 4.45 (Lv *et al.*, 2007). This configuration has also been used in the co-gasification of coal and wastes to obtained H_2 concentrations greater than 50% (Pinto *et al.*, 2009).

Rhodium catalysts are not commonly studied, partly because of the expense of rhodium. Ideally catalysts would be relatively cheap. However, rhodium-perovskite (a La compound) catalysts supported on Al_2O_3 have been studied. It was determined that these catalysts are resistant to coking and able to convert tars into syngas with only small amounts of CH_4 and CO_2 (Ammendola *et al.*, 2009). In addition, it was found that the activity of Rh-perovskite catalysts was superior to dolomite, olivine, and Ni (Ammendola *et al.*, 2010).

Iron-mixed oxides catalysts are less commonly studied as well, partly because most studies focus on attempting to harness the catalytic properties of several catalysts (such as by supporting Ni on dolomite). Nevertheless, the decomposition of tars produced in gasification of cedar sawdust over a Fe_3O_4 catalyst has been studied. It was found that the production of H_2 and CO_2 increased while the production of CO decreased because Fe also catalyzes the water-gas shift reaction (Uddin *et al.*, 2008).The reforming of naphthalene over Fe supported on Al_2O_3 and ZrO_2 was also studied. It was determined that by adding a small amount of CuO, the overall cracking properties were increased (Noichi *et al.*, 2010). (Coincidently, this is a similar composition to several well-documented Fischer-Tropsch catalysts.) Iron-based catalysts using biomass tars created in

a fluidized bed have been studied; evidence of tar-cracking properties was observed (Nemanova *et al*., 2010).

2.4 Mineral-based Catalysts

Basic mineral catalysts include dolomite, olivine, and calcite. Dolomite is a carbonate of calcium and magnesium and is usually represented as $CaMg(CO_3)_2$ or $CaCO_3 \cdot MgCO_3$. It is typically used in the concrete industry as an aggregate, in the production of magnesium, as a buffer in saltwater aquariums, and as a flux for smelting iron and steel. Olivine is a carbonate of iron and silica and is usually represented as $(Mg,Fe)_2SiO_4$. It is a solid solution of foresterite (Mg_2SiO_4) and fayalite (Fe_2SiO_4) (Świerczyński, 2006). It is used in the aluminum foundry industry and may be used to sequester CO_2. Calcite is a carbonate of calcium and is represented by the chemical formula $CaCO_3$. Its typical uses are in optical applications.

Much of the current work using dolomite involves comparing other catalysts (Ni, olivine, etc.) to the performance of dolomite (Kim *et al*., 2011; Yoon *et al*., 2010; Ruoppolo *et al*., 2010). However, dolomite is still studied for its own catalytic merits occasionally. The cracking of tars produced in olive oil waste gasification over dolomite was studied; catalyzing with dolomite led to a large increase in hydrogen concentration and activation energies and pre-exponential factors were determined for overall tar cracking (Encinar *et al*., 2008). The effect of dolomite in cracking tars formed in pine sawdust gasification was studied, and the maximum tar conversion achieved was 66% at 750°C (Gusta, 2008). The kinetics of tar cracking over dolomite were studied, and it was found that a first-order combustion model fit the data obtained well (Li *et al*., 2009a). The effect of Chinese dolomites in gasifying birch was studied. It was determined that not all

dolomites demonstrate equal catalytic properties; while four performed acceptably (< 60% conversion), Anhui dolomite did not exhibit any catalytic activity (10-20% conversion) (Yu *et al*., 2009). The pyrolysis of MSW over dolomite was studied, and it was determined that H_2 concentration more than doubled in the presence of the catalyst (He *et al*., 2010). However, dolomite is very friable and tends to elute from fluidized beds.

Olivine catalysts have been studied in methane, toluene, and naphthalene reforming. It was found that, while the catalysts were able to reform naphthalene, they were unable to reform methane at the tested conditions (Kuhn *et al*., 2008b). The gasification of plastic wastes with olivine as a catalyst has been studied; it was determined that the tar concentration dropped to undetectable levels and the H_2 concentration tripled over uncatalyzed gasification (Mastellone and Arena, 2008). The gasification of plastic wastes with olivine as tar-cracking catalyst was studied, and it was found that tars were cracked to compounds $<C_2H_M$ (Arena *et al*., 2009). Biomass gasification over iron-enhanced olivine was examined; it was determined that adding iron increased hydrogen and gas yield and decreased tar as compared to olivine alone (Rapagnà *et al*., 2010). Toluene reforming over iron-enhanced olivine led to 91% conversion at 825°C, which was three times higher than olivine alone (Virginie *et al*., 2010a; Virginie *et al*., 2010b). Gasification of mixed plastic wastes over olivine has been studied, but it was determined that the process is only economically viable for low-grade plastic wastes at this point in time (Arena *et al*., 2011). The cracking of biomass-derived tars over olivine at 720-900°C and 1-5 bars was studied; it was determined that higher temperatures had a greater influence on cracking than pressure (Kitzler *et al*., 2011). The

cracking of 1-methylnaphthalene in a synthetic syngas mixture over olivine at 850°C was studied. The bed setup was similar to a chemical looping combustion bed; however, it was found that olivine was carrying very little oxygen, and most of the activity (75% conversion) was likely due to the catalytic properties of olivine (Koppatz *et al*., 2011). Olivine has lower activity than dolomite partly due to its smaller surface area, but it has better mechanical properties.

One of the most common methods of studying the catalytic activity of olivine is to compare its activity with the well-documented activity of dolomite. The catalytic activity of olivine and dolomite was compared for MSW gasification. It was found that the activity of olivine was almost completely inhibited when feedstocks were changed, making dolomite the superior catalyst in this application (Arena *et al*., 2010).

Coal gasification with CaO as bed material has been studied, but it was determined that CaO is ineffective as a steam-reforming catalyst for tar cracking at the relatively low temperatures (600-670°C) required for CO_2 removal (Corella *et al*., 2008b). Corella *et al*. observed this result for reacted and coked catalyst and found that coking occurred very quickly, within one hour of startup; fresh catalyst reduced this issue, and they found that high CaO/coal ratios are required for technical feasibility (Corella *et al*., 2008b). The catalytic activity of CaO, which is the calcined form of $CaCO_3$, was studied, and it was discovered that not only does CaO exhibit catalytic cracking properties, but it can also be used in CO_2 capture (Widyawati *et al*., 2011).

Tar-cracking and Cl-removing abilities of limestone (CaO) and dolomite were studied, and it was determined that limestone has a very low tolerance for chlorine (Corella *et al*., 2008a). The catalytic activity of dolomite, olivine, and Ni was compared,

and it was found that activity declined in the following order: Ni > dolomite > olivine (Miccio *et al*., 2009). The catalytic activity of dolomite, olivine, and calcite have been compared for the steam reforming of phenol; it was found that olivine was more active at lower temperatures (650°C) and dolomite was more effective at high temperatures (800°C), while the activity of calcite was nearly constant (Constantinou *et al*., 2010).

2.5 Combinations of Metal- and Mineral-based Catalysts

Impregnating basic minerals, especially dolomite and olivine, with Ni has become increasingly prominent over the last several years. The catalytic activity of Ni-CeO_2/olivine in decomposing benzene and toluene was studied, and it was found that adding ceria increased activity and coking resistance (Zhang *et al*., 2007). The decomposition of naphthalene over Ni/olivine was studied, and it was determined that the catalyst was resistant to coking in the presence of excess steam (Kuhn *et al*., 2008a). The steam reforming of toluene over Ni/olivine and olivine was studied; the research group found that significantly lower temperatures could be used with Ni/olivine, discovered the presence of a NiO-MgO solid solution after calcining, and were able to determine kinetic data including the activation energy (Świerczynski *et al*., 2007; Świerczynski *et al*., 2008). Coconut shell gasification over a Ni/dolomite catalyst was studied, and it was determined that tar was reduced from 19.55% without catalyst to 1.4% with catalyst (Chaiprasert and Vitidsant, 2009). Simultaneous tar cracking and CO_2 capture using a Ni/dolomite catalyst was studied, and it was found that, once the catalyst was saturated with CO_2 from sorption, the catalytic activity for tar cracking significantly decreased (Di Felice, 2009). Ni/dolomite and Ni-WO_3/dolomite catalysts were studied for the gasification of bamboo; it was found that both catalysts had acceptable activity, but the

29

Ni-WO$_3$/dolomite catalyst was superior (Ketcong, 2009). The catalytic steam gasification of biomass over olivine catalysts, some of which were Ni-impregnated, was studied. The research group found that adding Ni to olivine led to a modest increase in gas content as compared to olivine alone. In addition, they determined that iron oxide migrates to the catalyst surface and, when Ni is present, forms a Fe-Ni alloy which increases the catalytic activity (Michel, 2010).

2.6 Other Catalysts

Several other catalysts have been studied to a lesser degree with varied results. These include biomass char, activated carbon, ilmenite, limonite, platinum group metals, mixed rare earth oxides, and tungsten (Sun *et al.*, 2011; Chaiwat *et al.*, 2010; Abu El-Rub *et al.*, 2008; Kuzentsov, 2009; Mun *et al.*, 2011; Min *et al.*, 2011; Li *et al.*, 2007; Magrini *et al.*, 2011; Adusumilli, 2009; Pansare *et al.*, 2008).

However, there are additional basic minerals which may have catalytic properties for cracking gasification tars. Based on previous studies, additional materials that may have cracking properties include nahcolite and trona (Young and Timpe, 1995). Nahcolite is the technical name for sodium bicarbonate and has the chemical formula NaHCO$_3$. It may be purified to form baking soda. Trona is a dicarbonate of sodium and is usually represented as Na$_3$H(CO$_3$)$_2$·2H$_2$O. It is the primary source of sodium carbonate (baking soda) in the United States.

References to trona and nahcolite as cracking catalysts are not plentiful in the literature. Trona was used as a biomass gasification catalyst once. Although it produced better results than using no catalyst at all, the performance was inferior to the reference catalysts sodium bicarbonate and potassium carbonate (Mudge *et al.*, 1981). In a recent

review, the use of nahcolite in HCl sorption from flue gases was mentioned (Ohtsuka *et al*., 2009).

There are also very few references to Na-based oxide catalysts. Sodium oxides would be the calcined form of nahcolite and trona. Nevertheless, the gasification of coal over limestone, sodium carbonate, and dolomite was studied, and it was determined that sodium carbonate was a better catalyst than either limestone or dolomite and sodium carbonate was capable of increasing carbon conversion to 81% (without catalyst, carbon conversion was 69%) (Zhou *et al*., 2007). The effect of solid additives, including Na_2CO_3, K_2CO_3, $CaCO_3$, $MgCO_3$, Fe_2O_3, and $CaSO_4$, on the pyrolysis of bituminous coal was studied, and it was determined that Na_2CO_3 reduced tars to their lowest observed levels. However, the research group had mechanically combined pure Na_2CO_3 with the coal prior to combustion, and it is unclear whether the mineral form of nahcolite or trona would have better tar-cracking properties (Ahmad *et al*., 2009). Still, these results are promising.

2.7 Summary

Based on the literature review and the relative paucity of work done in sodium-based catalysts, nahcolite and trona were selected as potential tar-cracking catalysts. For activity comparison, the well-known catalysts dolomite and olivine were selected. In addition, a Ni-based catalyst – NREL 60 – was selected for testing to examine a catalyst with high potential for tar cracking.

CHAPTER III
EXPERIMENTAL METHODS AND MATERIALS – TAR CRACKING

Two different systems were used to carry out the gasification and tar cracking experiments. The first system was a laboratory-scale updraft gasifier and tar cracking reactor; the results observed on the first system drove the development of a second system, which was a bench-scale tar cracking reactor. These two systems are treated separately where practicable.

3.1 Laboratory-Scale Updraft Gasifier and Tar Cracking Reactor

The scope of work of the laboratory-scale system was selected to address the following:

1.) Demonstrate that the catalytic gas cleanup system can enable conversion efficiencies in excess of 50%; and

2.) Show that such a system can comply with maximum size limitations, in this case, an 8' x 8' x 20' envelope, for the full-scale system.

3.) Identify a range of conditions for bench-scale tar cracking system tests.

An overall schematic of such a system is shown in Figure 3-1. For this work, the gasifier and tar cracking reactor were built at laboratory scale as opposed to the pilot scale of the full system.
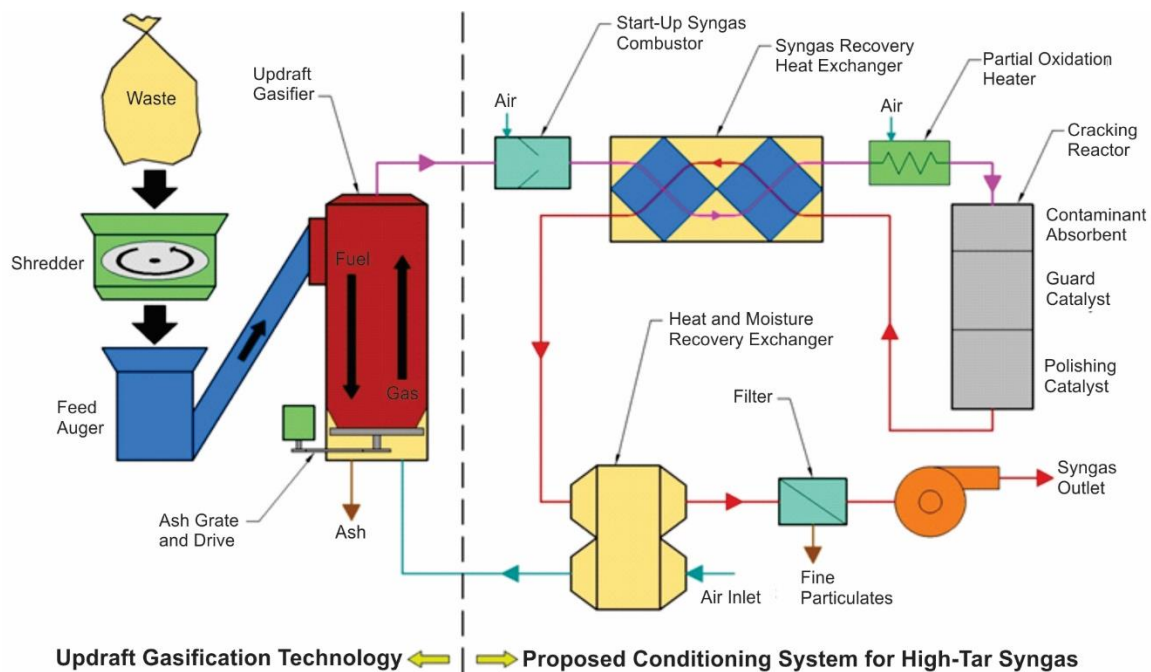
Figure 3-1. Schematic of updraft gasifier and thermo-catalytic tar cracking reactor.

The laboratory-scale gasifier and its associated hopper had a 4 inch O.D., and the system (gasifier and hopper together) was approximately 72 inches tall. The unit was built with 304 stainless steel and lined with a ceramic sleeve (3 inch I.D.). The air-blown gasifier was capable of handling gravity-fed fuel feed rates of 0.25-1 kg/h and countercurrent air flow rates of 4-10 slpm. Operating pressures were 0.25-0.75 psig. The gasifier was electrically heated maintain the desired test temperature (oxidation [up to 1500°C] at the bottom of the fuel bed to ~260°C at the outlet), counteracting the heat loss due to the system's small size (Martin and Dunham, 2013).

Generated syngas was sent to the catalyst oven through heated lines, maintained at 550°F, which were constructed of insulated 0.25 inch O.D. 304 stainless steel tubing. The catalyst oven was heated to 600-900°C, depending on test requirements, using an electric furnace. Tar-laden syngas was fed into the oven and split into four streams; three

of the pathways contained catalyst beds, and the fourth was empty. This allowed three catalysts to be simultaneously tested and compared to the effects of thermal cracking alone, which was evaluated by the empty bed line. The catalyst bed reactors were built from 304 stainless steel tubing and were 0.5 to 1 inch in diameter. Bed heights varied from 0.5 to 8 inches depending on the particle size of the catalyst evaluated. The reactor diameter and bed height were manipulated to achieve target space velocities of 4000-5000 hr^{-1}. Syngas flowed downward through the catalyst beds, which were supported on stainless steel mesh discs (Martin and Dunham, 2013).

After the catalytic oven, tars (here defined as organics that condensed at room temperature [~20°C]) were sampled in 0.25 inch O.D., 150 mm long 304 stainless steel tubes packed with glass wool and a disc of quartz filter media. The tubes were weighed before each test, exposed to a known volume of gas, dried to remove moisture, and reweighed. A typical eight-hour test would include the exposure of two sets of tar-sampling tubes, each of which were exposed for 20-30 minutes. Tar loading was calculated from the weight gain and measured gas volume (Martin and Dunham, 2013).

The gas then entered a series of ice condensers (0°C) to remove moisture and condensable hydrocarbons. The gas was then passed through a coalescing filter and backup thimble filter to remove any aerosols. Cleaned gas was passed through a mass flow meter and a rotameter to measure and control gas flow through each pathway. Each gas stream could be routed to a laser gas analyzer (LGA) for further analysis; the LGA was capable of identifying and measuring the concentration of CO, H_2O, H_2, O_2, N_2, CO_2, CH_4, and C_xH_y (interpreted as equivalent volume of propane).

A block diagram of this system is shown in Figure 3-2.
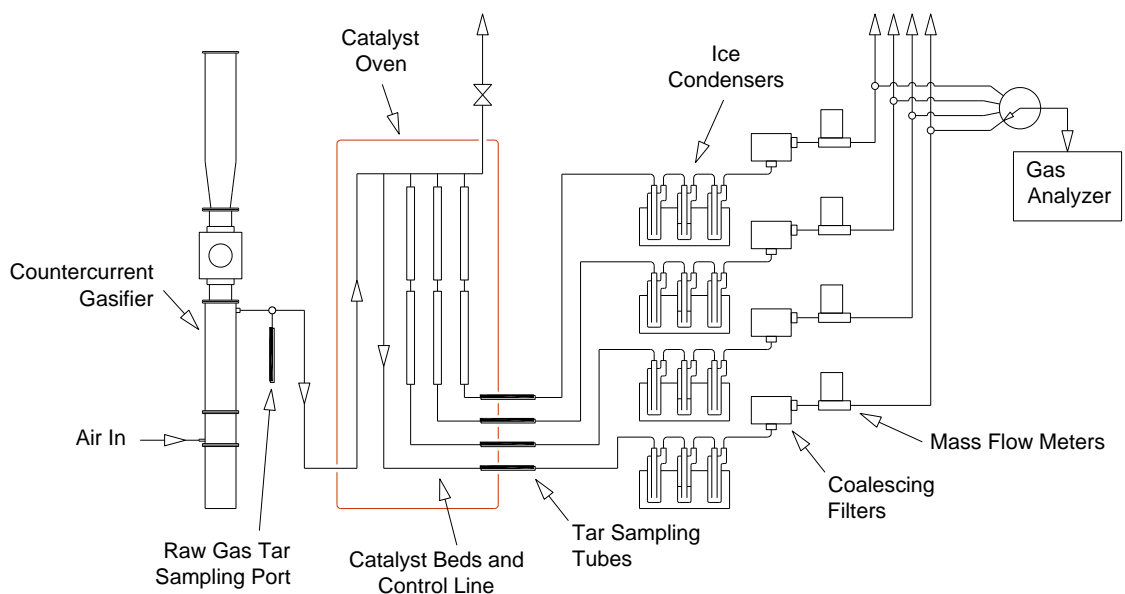
Figure 3-2. Block flow diagram of countercurrent gasifier and thermo-catalytic tar cracking reactor.

A fuel mixture was developed to simulate a municipal solid waste stream. Clean raw materials were used to reduce variability associated with uncontrolled components in the fuel, which would be present in actual waste products. While there is no single representative waste composition, for this set of experiments, the formulation was based on findings at the Force Provider Training Module in Fort Polk, Louisiana (Ruppert, 2004). For all tests, a fuel comprised of 40% cardboard, 40% saturated soybeans, 9.5% polyethylene, 9.5% polystyrene, and 1% polyvinylchloride was fed to the gasifier. Cardboard was selected to represent paper-based wastes, and soybeans were selected to represent food-based wastes (providing moisture, sulfur, and nitrogen). Among the plastics, polyethylene was selected because of its prevalence in packaging wastes, polystyrene was selected because of its inclusion of the aromatic ring structure which is a fundamental monomer in many tars, and polyvinylchloride was selected because of its

high chlorine concentration. Figure 3-3 shows a photographic representation of this raw

feed mixture (soybeans are dry in this image), and Table 3-1 gives the proximate/ultimate

analysis of the feed on an as-fired basis.

Figure 3- ... ier.

Table 3-1. Proximate/Ultimate Analysis of Gasifier Feed, as-fired

Proximate Analysis	
Moisture, %	28.2
Volatiles and Fixed Carbon, %	69.8
Ash, %	2.0
Ultimate Analysis	
C, %	43.2
H, %	8.6
N, %	1.1
S, %	0.1
Cl, %	0.3
O, % (by difference)	44.6
Heating Value, kJ/kg	19,100

Figure 3-4 shows the laboratory-scale gasifier and tar cracking system, and Figure

3-5 shows examples of the tar collected on the filter media.

Figure 3-4. Laboratory-scale updraft gasifier and tar cracker.

Figure 3-5. Tars collected on filter media.

The laboratory-scale system was used to perform a screening study of various catalysts, which were selected based on literature review, vendor recommendations, and EERC and NREL expertise. Table 3-2 shows the catalysts used in the screening study. Temperatures of the catalyst oven, in which tars were cracked, ranged from 600°C to 900°C. Condensed tars in the ice bath and on the final filter were weighed, and samples were collected before and after the tar cracker to determine the destruction efficiency (Martin, 2013).

Table 3-2. Catalyst Candidates.

Category	Catalyst
Natural Materials (guard candidates)	Dolomite
	Calcium carbonate
	Olivine
	Activated Carbon
Generic Metals-Based (commercially available)	Pt-Alumina
	Automotive Oxidation
	Woodstove Oxidation
Proprietary Metals-Based (commercially available)	Tar Cracking, Vendors A-C
	Reforming, Vendor A
Laboratory-Developed	NREL 60
	EERC

3.2 Bench-Scale Tar Cracking Reactor

The bench-scale tar cracking reactor system was a tubular reactor, approximately 12 inches in length with an O.D. of 0.5 inches, with a six-inch single-point thermocouple running axially from the top of the reactor to approximately the center. This reactor was surrounded by ceramic heaters and a layer of insulation. The reactor and heaters were contained in a heated cabinet to prevent the naphthalene and cracked product vapors from condensing.

Synthetic syngas was made by blending a mixture of purified hydrogen, nitrogen, carbon monoxide, and carbon dioxide. The total flow rate used was 0.5 slpm, and the flow rate of each individual gas was as follows: 0.09 slpm H_2 (18%), 0.10 slpm CO (20%), and 0.31 slpm N_2 (62%). These concentrations were selected to most accurately replicate conditions seen in air-blown gasification, with the exception of the omission of CO_2; this was done to avoid condensation issues in the impinger. Gases were fed from pressurized cylinders and stepped down to 75 psig through a regulator. They were then fed through individual stainless steel lines to Porter 200 series mass flow controllers. These controllers were metered using LabView software to set the desired flow rates.

After the mass flow controllers, the gases then were combined in a stainless steel manifold.

The combined syngas was fed into a permeation source containing naphthalene. This source was controlled using a four-way valve; in the "on" position, gas flow passed through the permeation source, sweeping naphthalene on its way past, while in the "off" position, the gas flow bypassed the permeation source. The amount of naphthalene collected in the syngas was controlled by controlling the temperature of the permeation source. The source, valve, and associated tubing were all contained in a heating mantle which was heated to the required temperature for the desired naphthalene concentration. The internal temperature of the permeation source was measured using a K-type thermocouple and recorded by the LabView software.

All tests were performed in a BTRS-Jr autoclave heated to 750°, 800°, 850°, or 900°C, depending on the experimental run. Tests were conducted at atmospheric pressure, and the effluent stream from the reactor was condensed in an impinger using liquid nitrogen (LN$_2$). Figure 3-6 shows a schematic of the bench-scale tar cracking reactor setup.
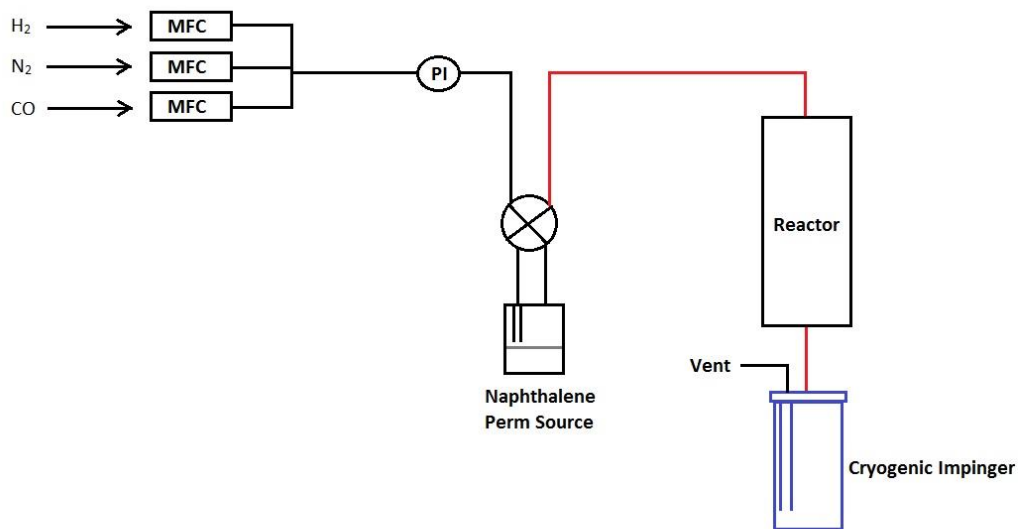
Figure 3-6. Bench-scale tar cracking reactor schematic.

Figures 3-7 through 3-13 show various sections of the bench-scale reactor system.

Figure 3-7 shows the gas cylinders and impinger. Figure 3-8 shows the pressure

indicator, the mass flow controllers, and the stainless steel manifold. Figure 3-9 shows

the heated mantle containing the naphthalene permeation source, the four-way valve for

controlling the permeation source, and the entering and exiting lines to the reactor, taped

and insulated together. Figure 3-10 shows the controls for heating the naphthalene

permeation source heating mantle and insulated, heat-taped lines leading to and away

from the reactor. Figure 3-11 shows the autoclave with the heating controls for the

cabinet and reactor itself. Figure 3-12 shows the insulated reactor and reactor cabinet in

the autoclave.
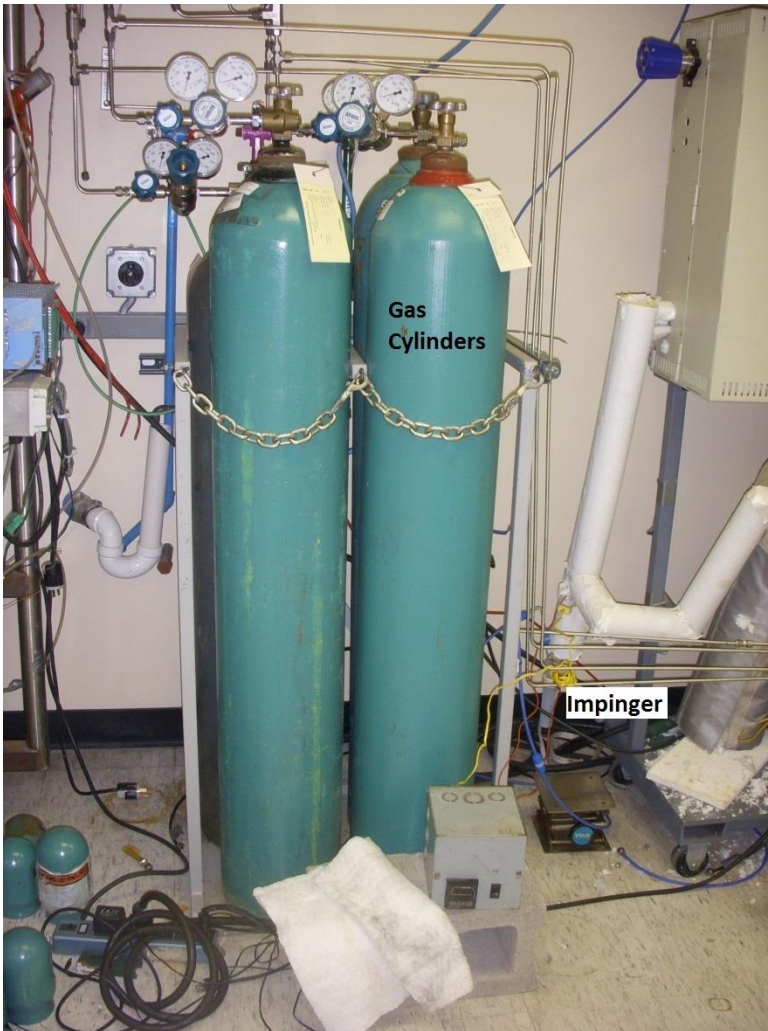
Figure 3-7. Gas cylinders and impinger.

Figure 3-8. Mass flow controllers, pressure indicator, and stainless steel manifold for mixing syngas.
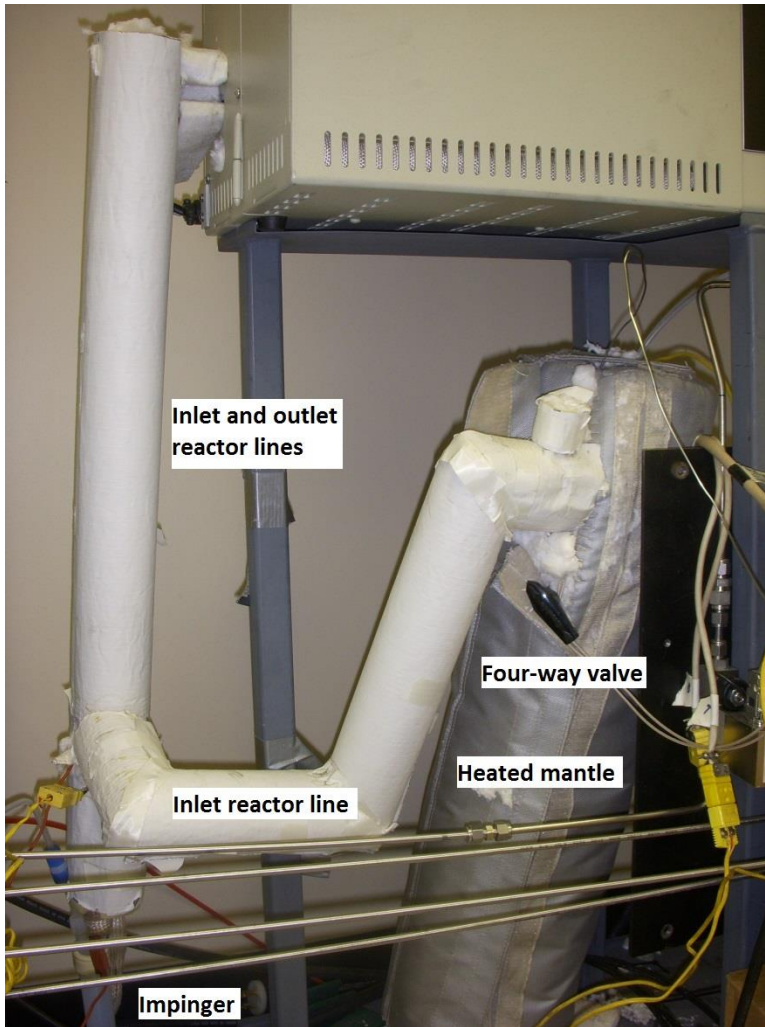
Figure 3-9. Heated mantle around the naphthalene permeation source, four-way valve, and insulated, heat-taped inlet and outlet lines to the reactor.
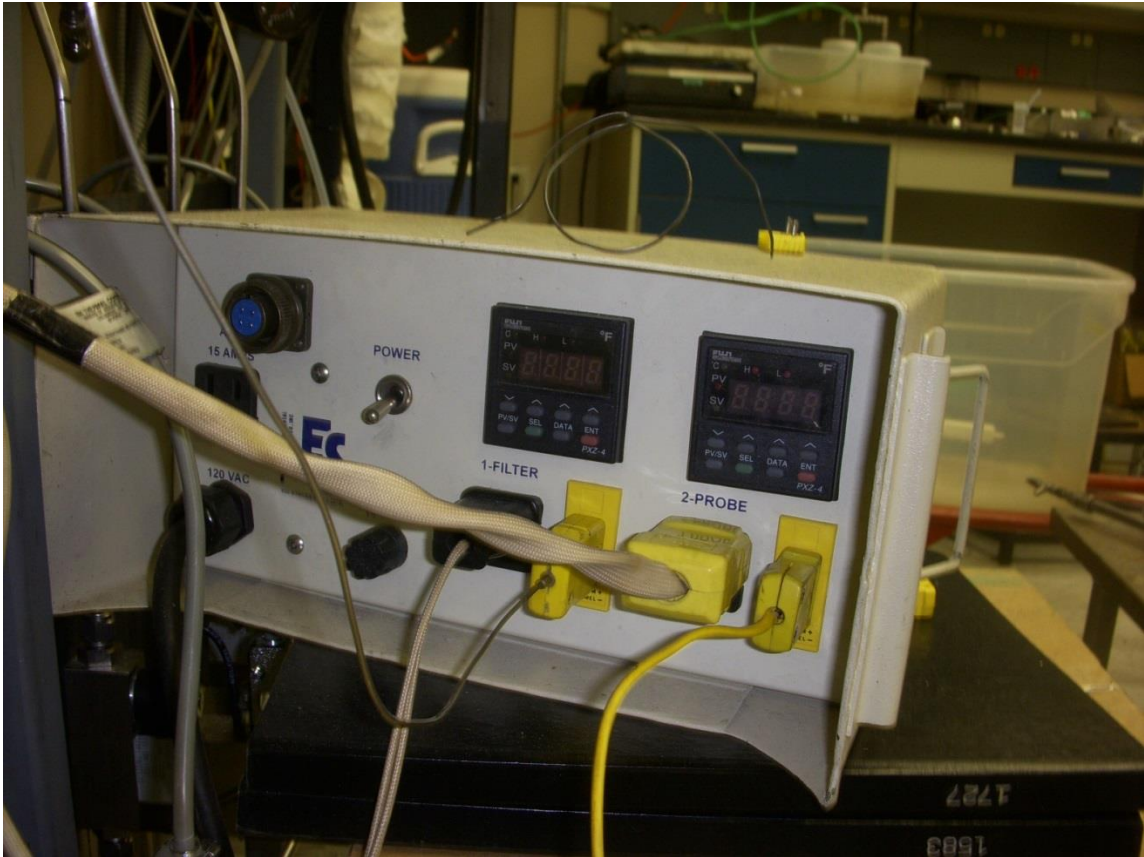
Figure 3-10. Heating controls for the naphthalene permeation source heating mantle and heat-taped inlet and outlet lines for the reactor.
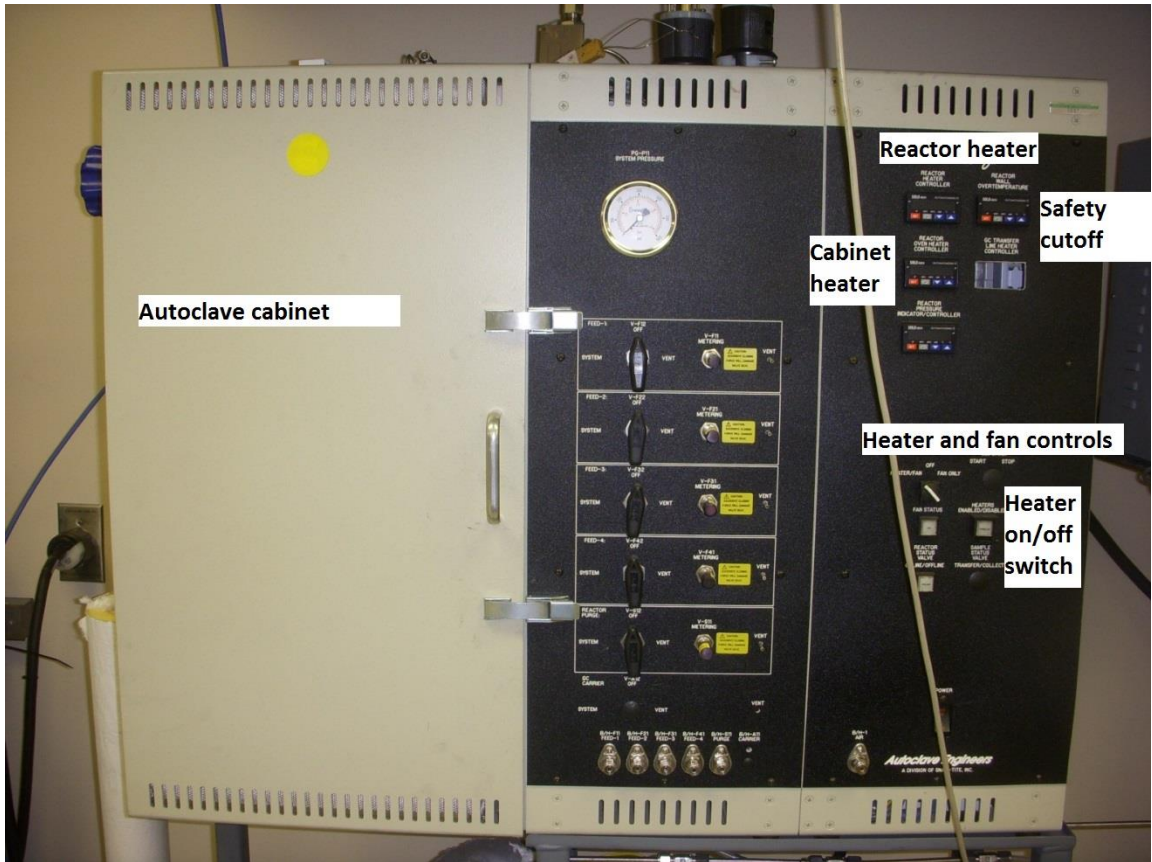
Figure 3-11. Autoclave cabinet and heating controls.
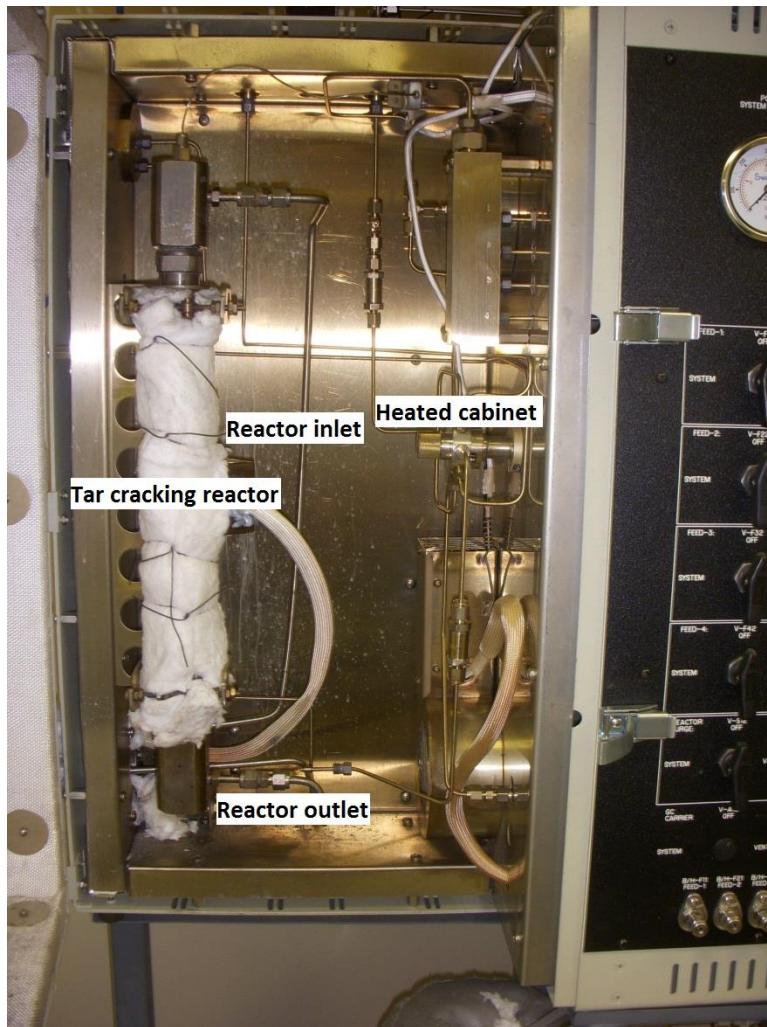
Figure 3-12. Tar cracking reactor (insulated) and cabinet.

Six catalysts were tested: two dolomites (one fine powder [> 55% CaO], one from

Plum Run [66.6% CaO]), olivine, nahcolite, trona, and NREL's nickel-based catalyst.

Figure 3-13 shows samples of the tested mineral catalysts. Table 3-3 shows the average

particle sizes and the bulk density of the tested catalysts.

(a) – trona
(b) – nahcolite
(c) – olivine
(d) – powder dolomite
(e) – Plum Run dolomite
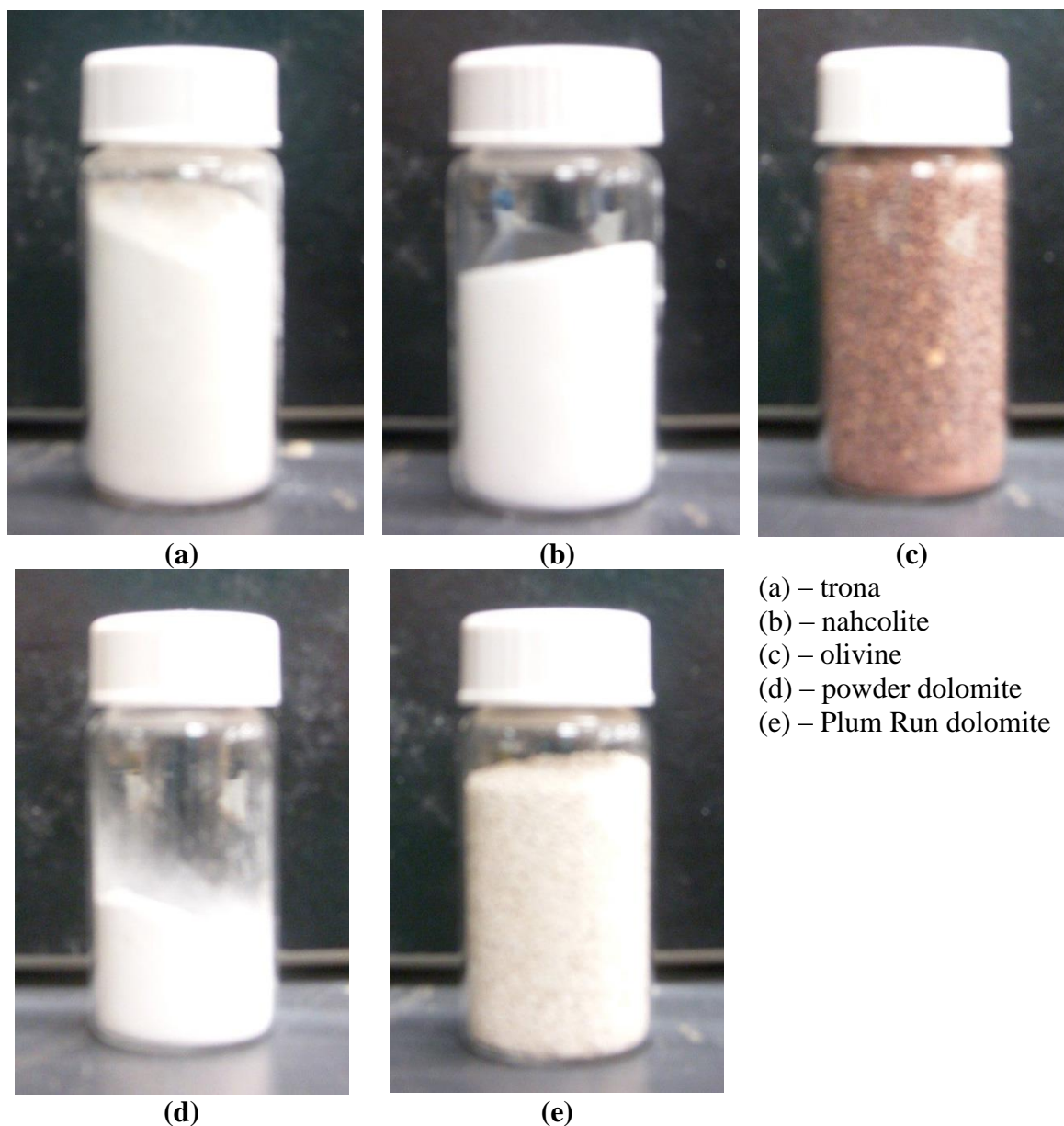
Figure 3-13. Calcined catalysts as tested in the bench-scale tar cracking reactor.

Table 3-3. Particle sizes and bulk densities of tested catalysts.

Catalyst	Average Particle Size (µm)	Bulk Density (g/mL)
Powder dolomite	90	0.59
Trona	70	0.98
Nahcolite	180	1.14
Olivine	2100	2.03
Plum Run Dolomite	1000	0.73
NREL Ni-based Catalyst	250	1.41

Table 3-4 shows the experimental design and run order used in the experiments. "Empty bed" runs refer to those with no material in the reactor at all, and "no catalyst" runs refer to those containing the packing material, including alumina pellets, mesh screens, and quartz wool, but no specific catalytic materials.

Table 3-4. Experimental design and run order.

Temperature (°C)	750	800	850	900
Empty bed – N_2	–	–	–	1
Empty bed	3	2	4	1
No catalyst	3	2	4	1
Trona	4	2	1	3
Nahcolite	2	1	4 (5)	3
Olivine	3	4 (5)	2	1
Powder Dolomite	3	2	4	1
Plum Run Dolomite	2	4	3	1
NREL Ni-based catalyst	3	2	1	4

Catalyst was loaded into the reactor bed according to Figure 3-14. From the bottom of the reactor, 5.625" of 1/8" alumina pellets were loaded in order to raise the bed to the heated zone of the reactor and to just below the height of the thermocouple, thereby ensuring the temperature of the catalyst was as close as possible to the temperature of the reactor without introducing error from heat transfer through bed materials in contact with the thermocouple, while using inert materials. A mesh screen was inserted next to hold the catalyst bed in place. A 0.25" quartz wool plug was inserted to hold the catalyst material above the metal screen. A 0.5" bed of catalytic material was inserted next. A similar 0.25" plug of quartz wool and mesh screen were inserted to secure the bed from above.
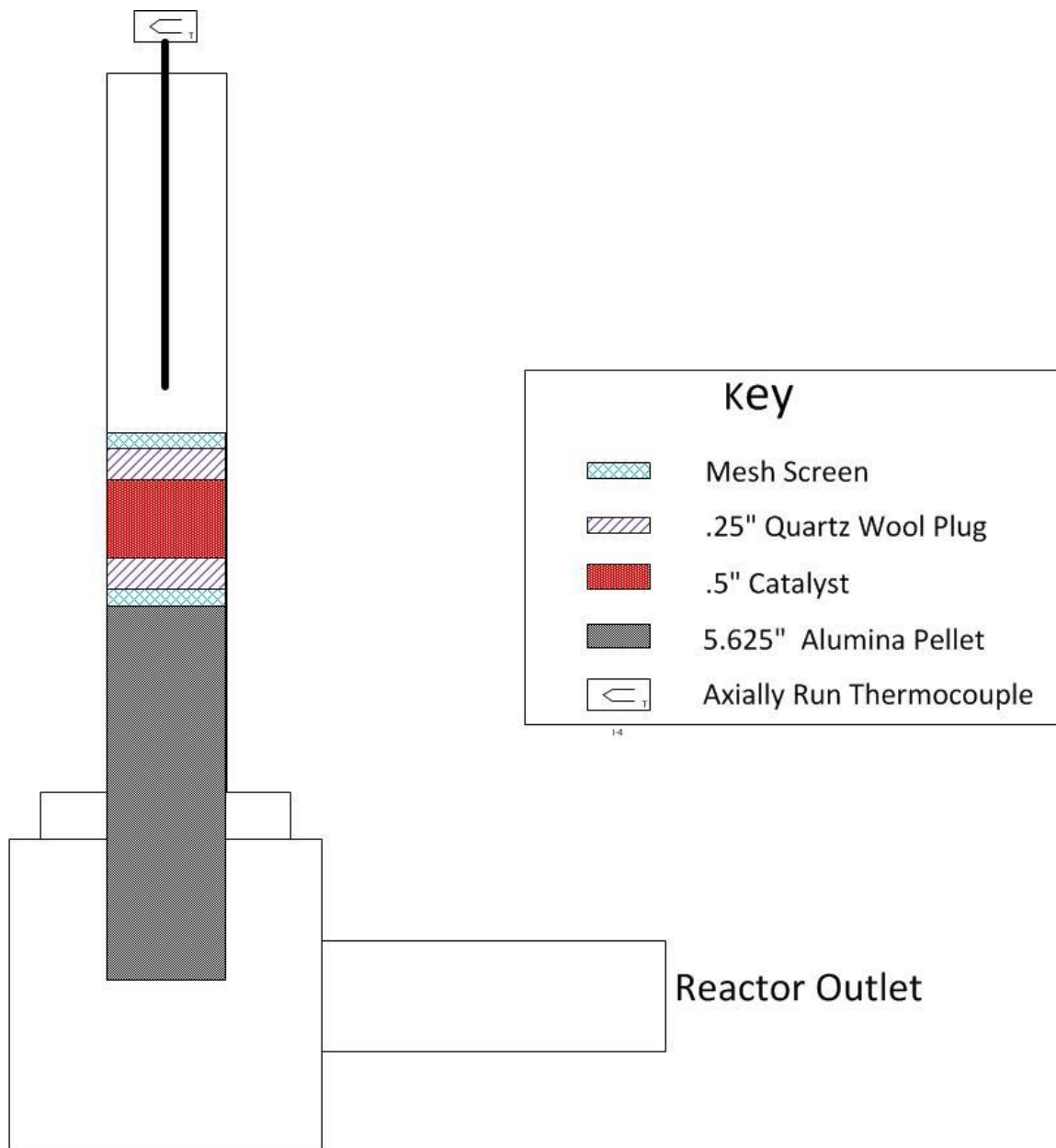
Figure 3-14. Reactor loading schematic.

Baseline data was obtained on the bench-scale system by running the reactor with no bed material in place at 300°F for 4-6 hours to confirm the level of mass balance closure for naphthalene. The naphthalene heater was set at 175°F, slightly below the melting point of naphthalene (176.5°F). The exit stream was condensed in an impinger

using liquid nitrogen. All pieces (the naphthalene permeation source, the impinger, connectors, etc.) were weighed on a five-place balance to determine the mass balance closure level. The impinger was plumbed in reverse to ensure better residence time for condensation and to prevent "plugs" of naphthalene from forming in the entrance tube, thus blocking the system. Typical impingers are plumbed so that the inlet gas enters through the tube extending almost the entire length of the impinger and the outlet gas leaves through the second opening at the top of the impinger. However, when the impinger was set up in this way, it was found that the naphthalene was condensing in the tube, leading to blockages and subsequent rises in system pressure. To prevent this from happening, the impinger was plumbed so that the gas would enter through the opening at the impinger top without a tube and exit through the axial tube of the impinger.

Table 3-5 shows selected results of the mass balance closure. Mass balance closures ranged from 83% to 110% for the tests using LN_2. Using LN_2 for condensation provided more consistent results than any ice-water bath test that was attempted, especially for the removal of water on the outside (and occasionally inside) of the impingers. For those tests using LN_2, the average feed concentration was 4.06 g/m^3, the average collected concentration was 3.70 g/m^3, and the average percent difference was 8.9%.

Runs were performed according to the following set of procedures:

Before the start of every run, the naphthalene permeation source was heated to the desired feed temperature overnight. The autoclave cabinet heater and ceramic heaters surrounding the reactor were turned on about 60-90 minutes before the start of the test to allow the reactor to heat to the desired testing temperature; H_2, CO, and N_2 flows were

started at this time as well. LabView was used to record data, and the recording was started. The cryogenic trap, a 300-mL Dewar flask, was filled with LN_2. The run started with the opening of the four-way valve to open the naphthalene permeation source and the starting of a timer.

During the run, the cryogenic trap was topped off every 90 minutes to ensure constant temperatures at the impinger. At the same time, the pressure indicator was checked to ensure that blockages were not forming in the system. Blockages required that the run be terminated since they caused the system pressure to increase, which altered the reaction kinetics and posed a safety hazard.

At the end of the run, the four-way valve was closed to the impinger source, H_2 and CO flows were turned off, and N_2 flow was turned up to 0.5 slpm for 30 minutes to flush the system of any naphthalene/tar deposits. The heaters were then shut off, the N_2 flow was shut off, and all source and collection pots were removed and weighed. Tar deposits were recovered by dissolving them in 10 mL of acetone.

Table 3-5. Mass balance closure results.

Heater Setpoint (°F)	Condensation Media	Total Fed (g)	Total Collected (g)	Mass Balance Closure (%)	Feed Concentration (g/Nm^3)	Collected Concentration (g/Nm^3)
90	Ice-water	0.101	0.130	129		
90	Ice-water	0.038	0.140	368		
110	Ice-water	0.253	0.222	88		
110	Ice-water	0.170	0.243	143		
110	Ice-water	0.078	0.220	629		
110	Ice-water	0.089	0.178	200		
130	Ice-water	0.443	0.032	7		
130	Ice-water	0.483	0.100	21		
130	Ice-water	0.290	0.425	147		
130	Ice-water	0.183	0.070	38		
150	Ice-water	0.285	0.237	83		
150	Ice-water	0.202	0.293	145		
170	Ice-water	0.456	0.289	63		
175	Liquid nitrogen	0.743	0.821	110	3.30	3.64
175	Liquid nitrogen	0.678	0.582	86	4.21	3.61
175	Liquid nitrogen	0.751	0.622	83	4.66	3.86

- Mass balance closure calculated as total collected divided by total fed.

CHAPTER IV
TAR CRACKING – RESULTS AND DISCUSSION

4.1 Laboratory-Scale Updraft Gasifier and Tar Cracking Reactor

The tar-laden syngas from the updraft gasifier exited the gasifier and was fed through tar sampling tubes and into the tar cracking reactor. The average raw gas tar loading, as measured using the tar sampling tubes discussed in Chapter 3, was 39.4 g/dscm, placing the gasifier solidly in the updraft tars regime (10-50 g/dcsm). A GC-MS analysis of the soluble tar condensates revealed a very complex mixture that could not be completely identified. This was expected, as tar is very complex; usually only about 50% of the constituent compounds can be positively identified, and the remainder can be identified only in terms of their basic structures (e.g., 1-ring aromatic compounds, 2-ring aromatic compounds, alkenes, etc.). The identified compounds were sorted into broad categories which give qualitative insight into the fate of the constituents. Aliphatic hydrocarbons are most likely derived from the polyethylene. The higher-order polycyclic aromatic hydrocarbons (PAHs) are likely derived from the styrene and represent secondary (e.g., naphthalene) and tertiary (e.g., phenanthrene, anthracene) gasification tars. Nitrogen, chlorine, and sulfur atoms were observed in the compounds containing heteroatoms; their sources were discussed in Chapter 3. Figure 4-1 shows a breakdown of the raw gas tar condensate (Martin and Dunham, 2013).
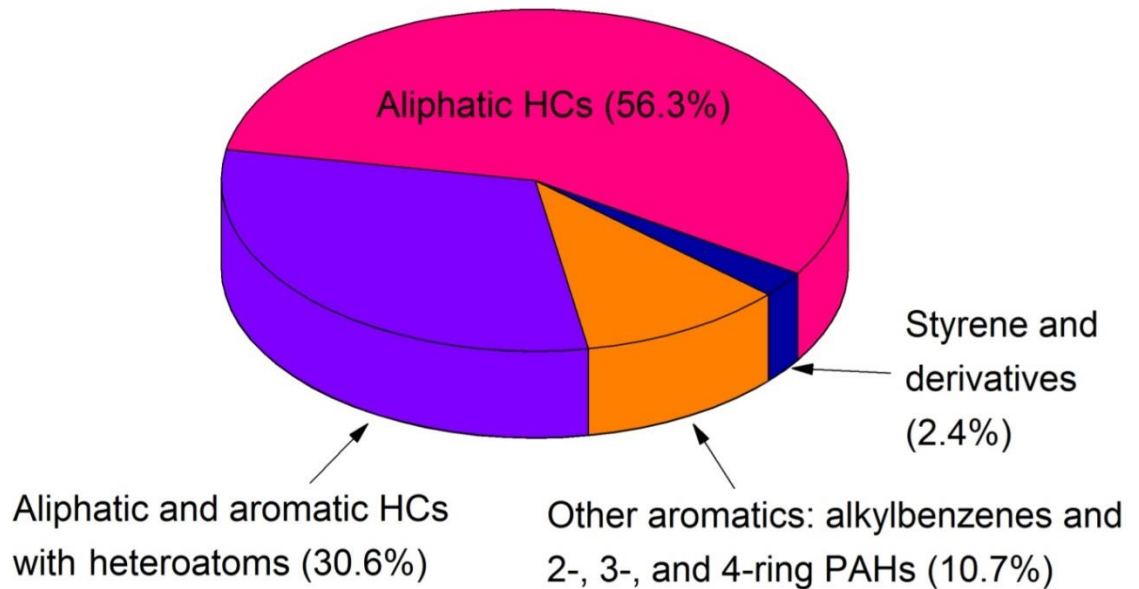
Figure 4-1. Categorical breakdown of identifiable compounds in raw gas tar condensate.

Figure 4-2 shows the gas composition on a dry basis after it is fed through tar-cracking beds containing various cracking catalysts at 900°C. As discussed in Chapter 3, three of the four parallel beds contained tar cracking catalysts, while the fourth bed was left empty to examine the effects of thermal cracking. The gas analyzer was switched from stream to stream to determine the gas composition of each exit stream. The decreasing C_xH_y and CH_4 content in the exit streams of the beds containing catalyst indicates decomposition of these compounds and, presumably, the more complex tars. Increasing CO and H_2 content arises from the conversion of hydrocarbons, including the tars. Thus, in this series of tests, the methane reforming catalyst provided the most complete cracking to CO and H_2; however, the woodstove oxidation catalyst and automotive oxidation catalyst provided some reforming over thermal cracking alone (Martin and Dunham, 2013).
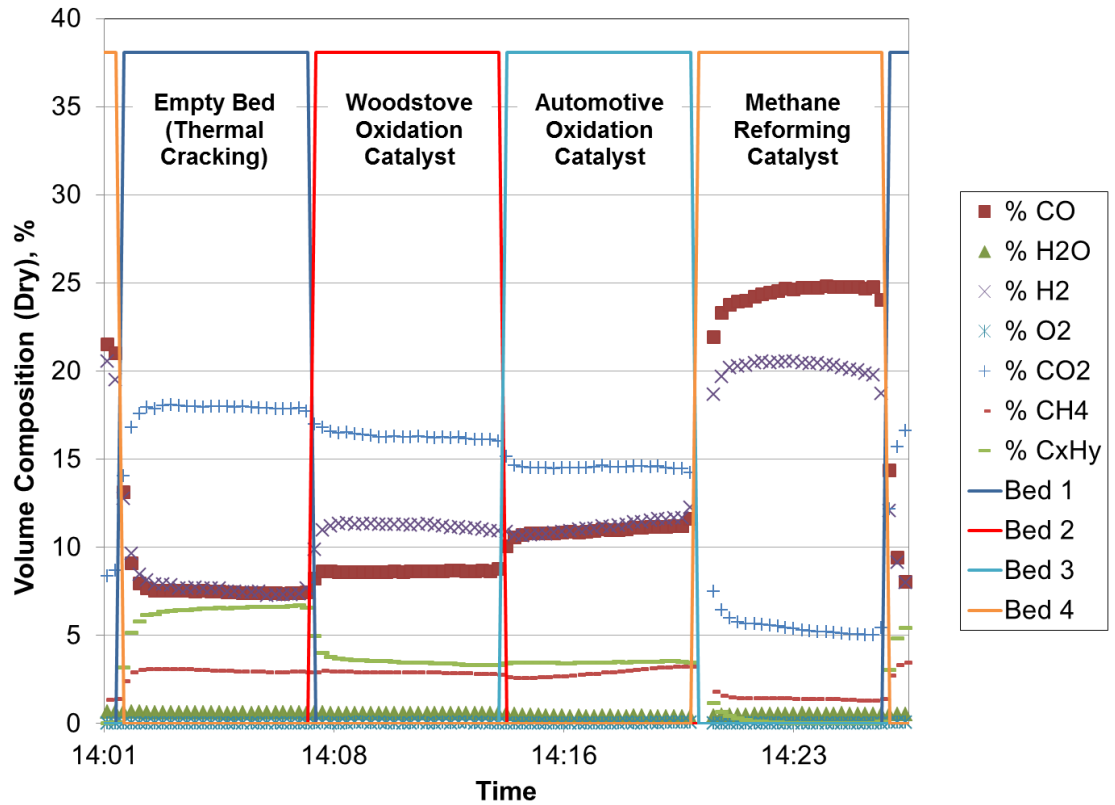
Figure 4-2. Fuel gas composition, post-cracking beds.

Figure 4-3 shows the results of temperature screening on the various tested

catalysts. It is apparent that a considerable amount of thermal cracking was occurring, as

tar loadings in the empty bed decreased from almost 40 g/dscm to about 7.2 g/dscm just

from heating the tar to 600°C-700°C and to 5.8 g/dscm at 900°C. The most effective

catalyst overall was the spray dried calcium carbonate, but the most effective at higher

temperatures were the metal-based catalysts – the Pt-alumina catalyst, the NREL 60

catalyst, and Vendor A's tar cracking catalyst. No catalyst was able to produce a tar

loading below 2.5 g/dscm at temperatures at or below 800°C. It is also apparent that a

major change in the rate of reaction occurs between 800°C and 900°C since the bed outlet

tar loading decreases for all the catalysts tested except the spray-dried $CaCO_3$, and, in

some cases, quite dramatically. This could be due to a change in the structure in the bond or a change in the bond state or energy of the tar molecules; however, further study is needed to prove this. Another possible explanation for the greater extent of cracking at 900°C may be fouling of the catalyst surface by coking at lower temperatures, but more study would be needed to prove this as well (Martin and Dunham, 2013). Figure 4-4 shows the equilibrium-based carbon deposition boundary for the fuel mixture fired in the gasifier. The gasfier was run at approximately a 0.45-0.55 equivalence ratio, which would border the carbon deposition boundary (Martin and Dunham, 2013).
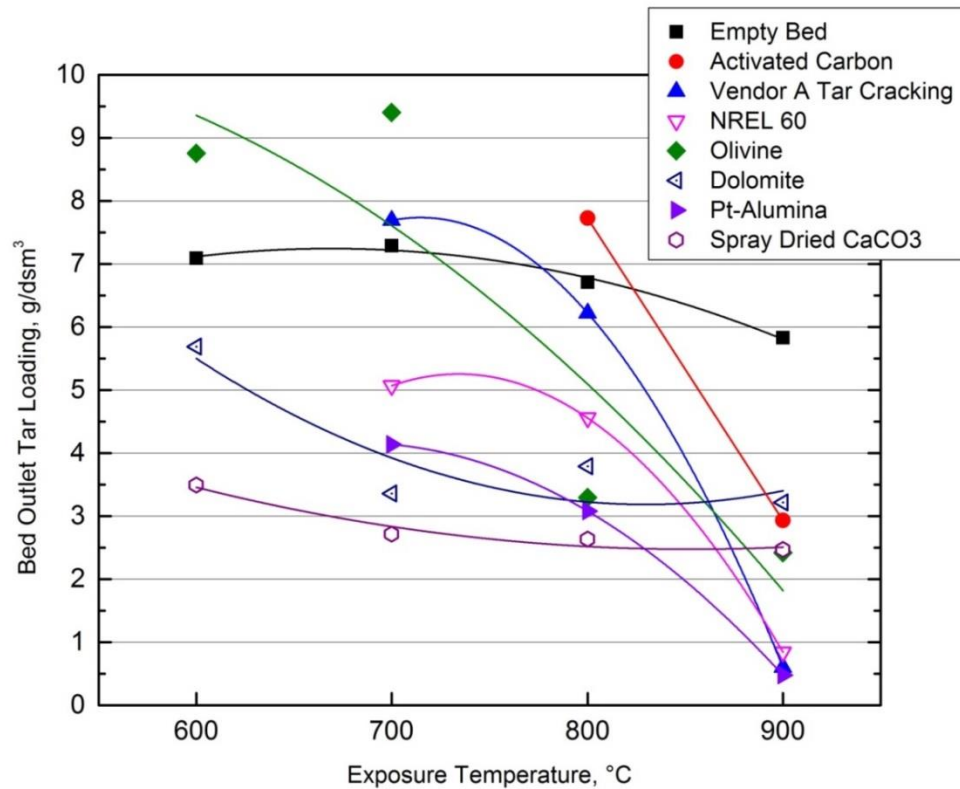
Figure 4-3. Temperature screening of various catalysts. Lines are included only to assist in seeing trends.
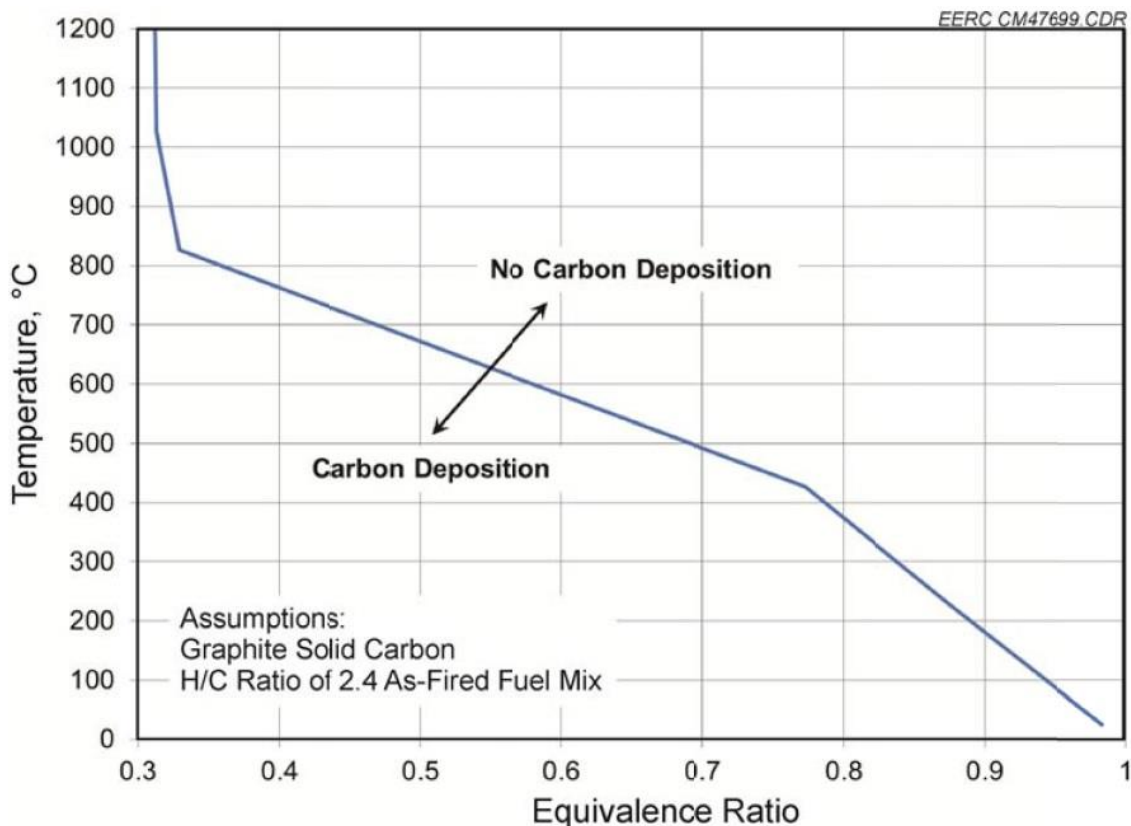
Figure 4-4. Equilibrium-based carbon deposition boundary (Martin and Dunham, 2013).

Because of the concern about coking at lower temperatures, the remainder of the work focused on cracking tars at 900°C. Figure 4-5 shows the bed outlet tar loadings for each of the catalysts at 900°C; Table 4-1 shows the number of replicates for each catalyst. Several catalysts were able to decrease the tar loading to less than 1 g/dscm (< 97% tar destruction), including the Pt-alumina, Vendor A's methane reforming, Vendor A's tar cracking, the NREL 2.5 mm spheres, Vendor B's tar cracking, Vendor C's tar cracking, and the NREL 60 catalyst. These catalysts were metal-based reforming and/or cracking catalysts intended for use in reducing conditions. The remaining catalysts were generally natural materials or metal-based catalysts intended for use under oxidizing conditions. Thermal cracking did account for 85% of tar destruction on average. The variability

observed may be attributed to the measurement method, as the sensitivity of the equipment used decreases with lower tar loading, and the gasifier operating conditions, which affect the inlet tar loading and possibly even the specific tar species. While the variability does not affect interpretation of performance of specific catalysts, it does lead to difficulty in selecting the best catalyst for tar cracking. Further experimentation, including a wider set of design parameters, would be necessary to select the optimal candidate. Another possibility is that there is no single "best" candidate but rather a series of equally effective catalysts, and the optimal catalyst may depend on the final application.
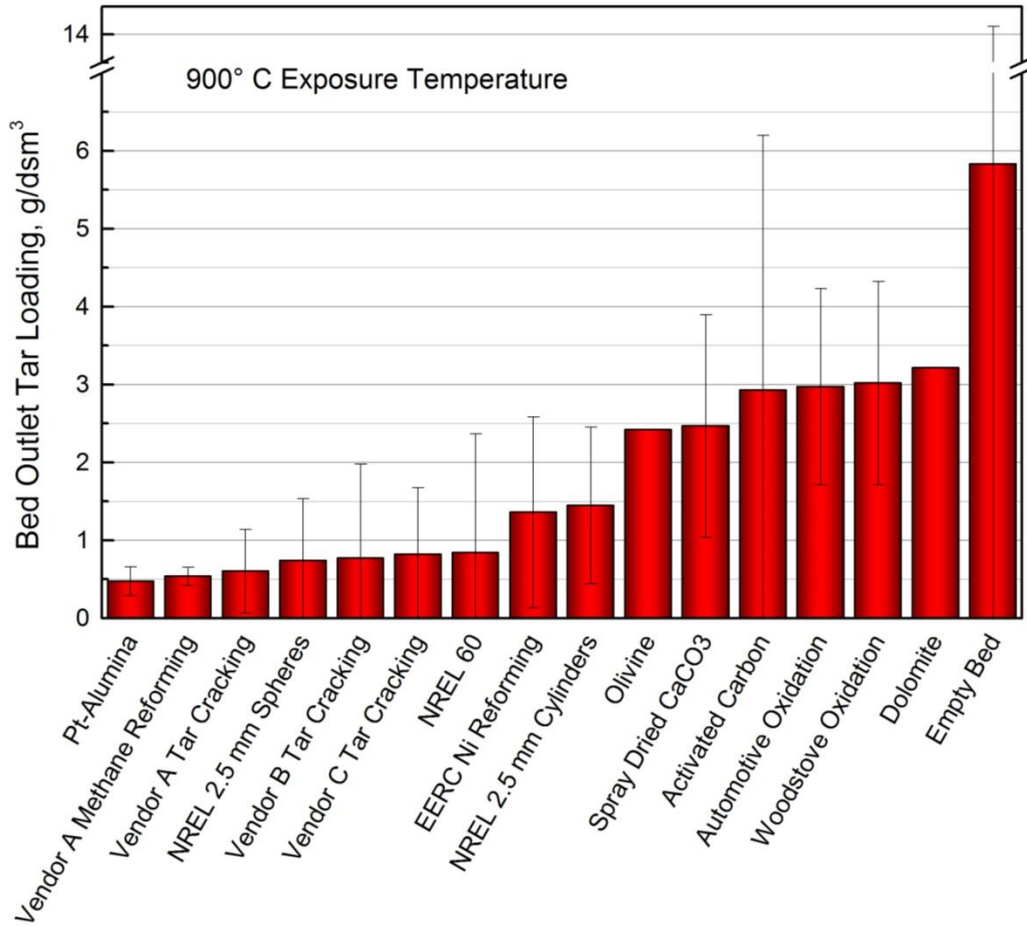
Figure 4-5. Bed outlet tar loading for various catalysts at 900°C. Error bars represent ± 1 standard deviation.

Table 4-1. Number of replicates for each catalyst at 900°C.

Catalyst	Number of Replicates
Pt-Alumina	3
Vendor A Methane Reforming	2
Vendor A Tar Cracking	3
NREL 2.5 mm Spheres	4
Vendor B Tar Cracking	8
Vendor C Tar Cracking	7
NREL 60	11
EERC Ni Reforming	2
NREL 2.5 mm Cylinders	9
Olivine	1
Spray Dried CaCO3	2
Activated Carbon	3
Automotive Oxidation	2

Table 4-1, cont.

Catalyst	Number of Replicates
Woodstove Oxidation	2
Plum Run dolomite	1
Empty Bed	23

Metal-based catalysts, on average, reduce tar loadings to 25-50% those of mineral catalysts. However, mineral catalysts still show significant tar reductions and warrant further studies, especially in light of their lower costs. Therefore, a selection of mineral catalysts were studied in a bench-scale reactor using naphthalene as a model tar compound, as it is the most difficult compound to crack according to literature.

4.2 Bench-Scale Tar Cracking Reactor
4.2.1 Catalyst Characterizations

Table 4-2 shows the average particle sizes and bulk densities for the tested catalysts. The catalysts varied widely in particle size, and this could have affected their performances in tar cracking as more surface area would be exposed for a smaller particle size. Surface areas were estimated assuming that the catalyst particles were perfect spheres randomly packed (64% packing efficiency).

Table 4-2. Catalyst average particle sizes, bulk densities, and surface areas.

Catalyst	Average Particle Size (μm)	Bulk Density (g/mL)	Estimated Surface Area (mm^2/mL)
Nahcolite	180	0.59	21,000
NREL Ni-based Catalyst	250	1.41	15,000
Olivine	2100	2.03	1800
Plum Run Dolomite	1000	1.41	3800
Powder Dolomite	90	0.59	42,000
Trona	70	0.98	53,000

4.2.2 Reacted Tar Characterizations and Conversions

As described in the experimental section, naphthalene vapors were passed over the catalyst and collected in an impinger cooled with liquid nitrogen. Acetone was used

to recover the naphthalene and its cracked products form these experiments. These results were used to determine the conversion of naphthalene to intermediate compounds (i.e., the effectiveness of each catalyst and temperature combination in cracking tars).

Table 4-3 shows the naphthalene conversions observed for each catalyst. Naphthalene conversion was calculated as $\frac{naphthalene_{fed} - naphthalene_{collected}}{naphthalene_{fed}} x100\%$. At the conclusion of each run, the impinger was weighed, deposits were dissolved in acetone, and the resulting solution was analyzed using GC-MS to determine how much of the collected product was unreacted naphthalene. The right-most column indicates the conversion of naphthalene accounting for the incomplete closure of the system. In baseline testing, approximately 91% of the naphthalene fed was recovered. It is assumed that, for the experimental tests, there is a similar loss of or unaccounting for material due to test procedures and equipment. The naphthalene may have condensed in the heated lines or been unaccounted for due to measurement error. The mass loss may be caused by an incomplete measuring of all the system components, as gas samples were not collected after the cryogenic impinger. Products which did not condense near -321°F, primarily H_2, CO, and hydrocarbons smaller than butane (C_4H_{10}), are likely to have escaped the system. In addition, in baseline runs, not all the naphthalene fed to the system was collected in the impinger. This is also assumed to be part of the uncollected mass.

Table 4-3. Bench-scale naphthalene conversion.

Carrier Gas	Catalyst	Temperature (°C)	% Conversion of Naphthalene	
			As-determined	Accounting for average mass loss
N_2	Empty bed	900	67	61
Syngas	Empty bed	750	57	52
Syngas	Empty bed	800	57	52
Syngas	Empty bed	850	61	56
Syngas	Empty bed	900	60	55
Syngas	No catalyst	750	39	35
Syngas	No catalyst	800	21	19
Syngas	No catalyst	850	83	76
Syngas	No catalyst	900	52	47
Syngas	Trona	750	27	25
Syngas	Trona	800	42	38
Syngas	Trona	850	*	*
Syngas	Trona	900	86	78
Syngas	Nahcolite	750	28	25
Syngas	Nahcolite	800	24	22
Syngas	Nahcolite	850	36	33
Syngas	Nahcolite	850	68	62
Syngas	Nahcolite	900	*	*
Syngas	Olivine	750	28	25
Syngas	Olivine	800	95	86
Syngas	Olivine	800	100	91
Syngas	Olivine	850	72	66
Syngas	Olivine	900	45	41
Syngas	Powder dolomite	750	42	38
Syngas	Powder dolomite	800	96	87
Syngas	Powder dolomite	850	100	91
Syngas	Powder dolomite	900	95	86
Syngas	Plum Run dolomite	750	**	**
Syngas	Plum Run dolomite	800	49	45
Syngas	Plum Run dolomite	850	66	60
Syngas	Plum Run dolomite	900	90	82

Table 4-3, cont.

Carrier Gas	Catalyst	Temperature (°C)	% Conversion of Naphthalene	
			As-determined	Accounting for average mass loss
Syngas	NREL Ni catalyst	750	66	60
Syngas	NREL Ni catalyst	800	79	72
Syngas	NREL Ni catalyst	850	100	91
Syngas	NREL Ni catalyst	900	100	91

* Measurements indicated a weight gain.
** Measurements indicated a weight loss in excess of the naphthalene fed.

The conversion of naphthalene to intermediate compounds in an empty bed, which would capture the effects of thermal cracking, was nearly steady at about 55% for all the temperatures tested. This does not match the results seen in the laboratory-scale gasifier and tar cracking system, in which significant increases in conversion were generally observed between 800°C and 900°C. However, naphthalene is a difficult compound to crack (secondary tar) as compared to the primary tars formed in updraft gasification; consequently, naphthalene requires higher temperatures for more complete thermal cracking. Figure 4-6 shows the GC-MS results for the empty bed runs with syngas as the carrier gas for the naphthalene. The chromatograms show similar compounds for all temperatures tested, demonstrating similar conversion of naphthalene to intermediate compounds, as the conversion data indicates.
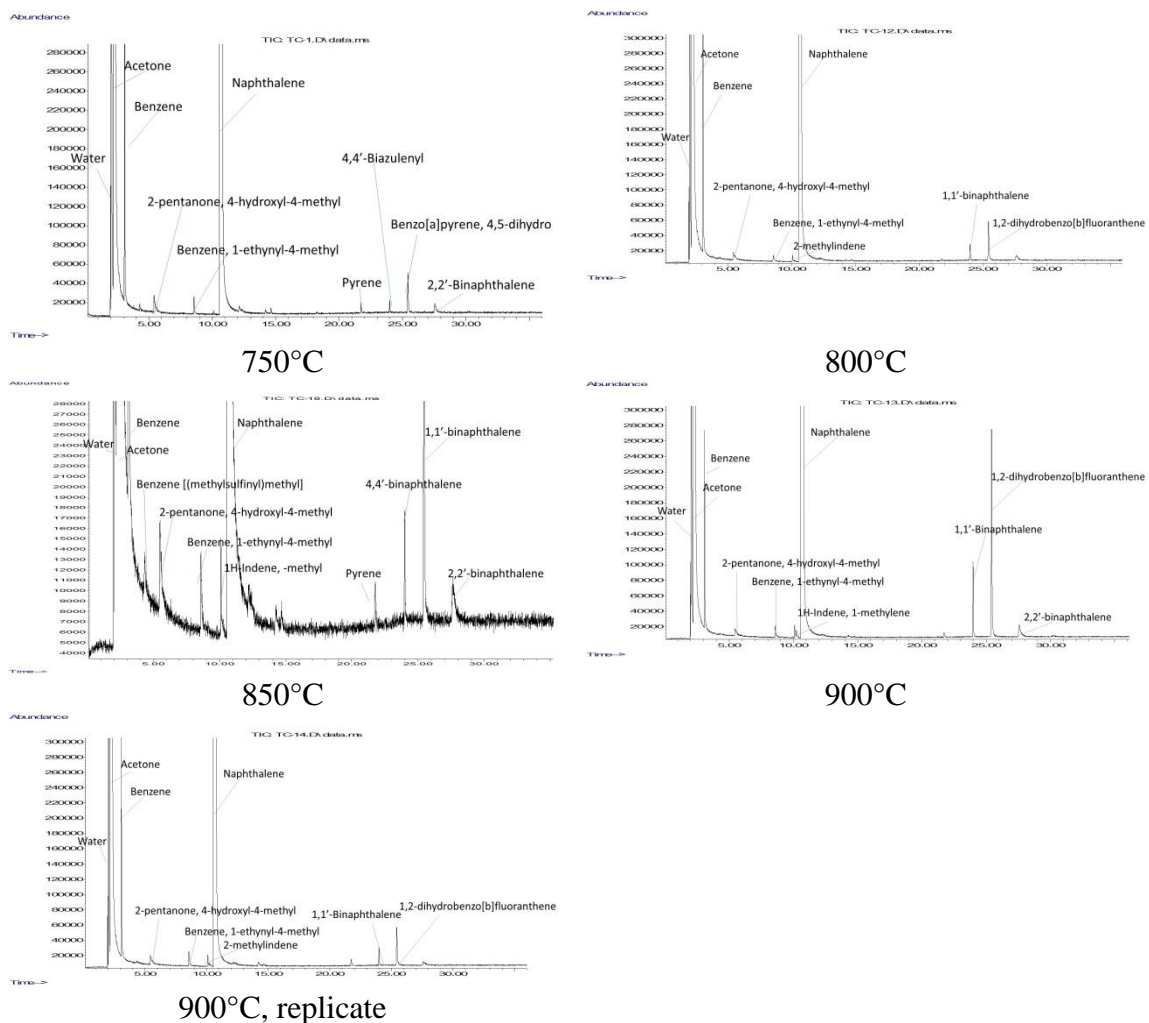
Figure 4-6. GC-MS results for empty bed runs using syngas blend.

The conversion of naphthalene to intermediate compounds in a bed without

catalytic material varied from 21% at 800°C to 83% at 850°C. The lower than 55%

conversions (empty bed average conversion) may indicate that the naphthalene or its

cracked intermediate products may have absorbed on the alumina pellets, quartz wool,

and/or mesh screen used in packing the bed. This could lead to the later observed runs in

which residual compounds would occasionally elute out of the system in runs after those

in which they were formed. Alternatively, the higher than 55% conversion may indicate

the bed materials themselves may have had some activity for conversion of naphthalene

to intermediate compounds. Figure 4-7 shows the GC-MS results for runs performed

using all the bed materials (quartz wool, alumina pellets, and mesh screens) without

catalyst. Significantly fewer compounds were detected using GC-MS for the no catalyst

runs than for the empty bed runs, lending more credence to the theory that the compounds

may have absorbed on the packing material.
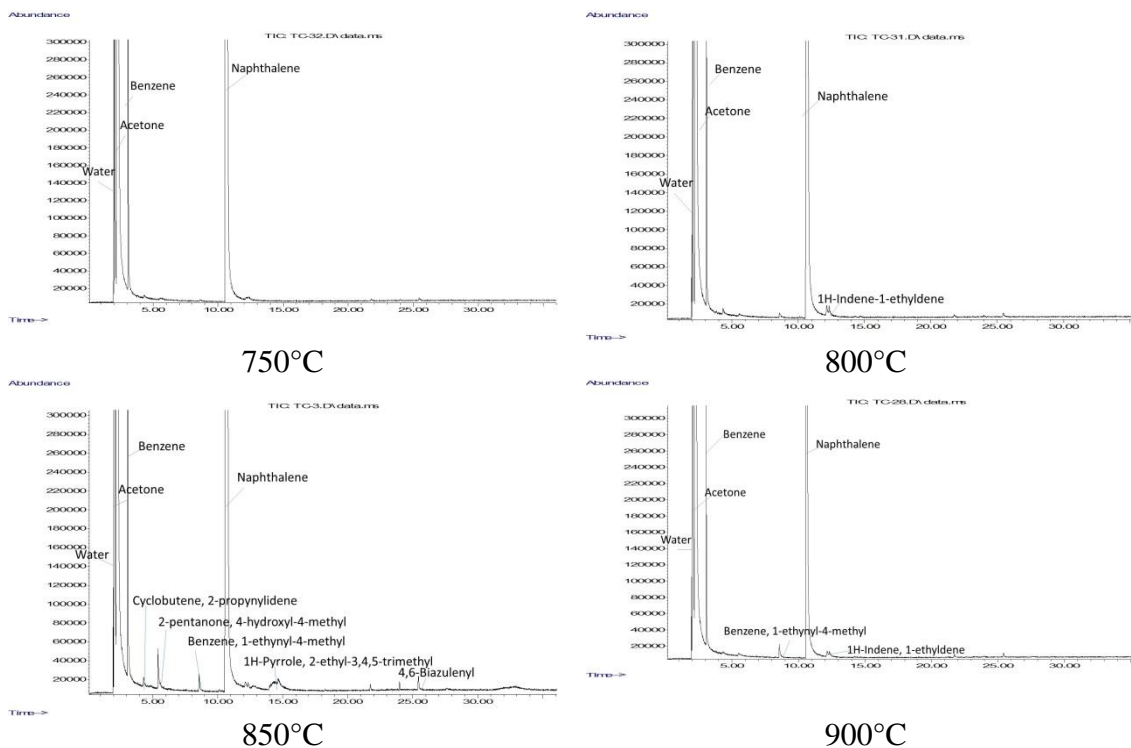
Figure 4-7. GC-MS results for no catalyst runs using syngas blend.

The conversion of naphthalene to intermediate compounds over a trona catalyst

varied from 27% at 750°C to 86% at 900°C. The conversion to intermediate compounds

rose as the temperature rose. The conversion at 750°C being lower than the conversion at

the same temperature with an empty bed or no catalytic material present indicates the

large error present (at least ±15% based on the mass balance closure). At 900°C, the trona

catalyst exhibited a higher conversion of naphthalene to intermediate products, indicating

its efficacy as a cracking catalyst over using no catalytic material at all. In addition, at 900°C, this was an effective catalyst by the parameters set forth in the hypothesis for this work. Figure 4-8 shows the GC-MS results for the trona runs with syngas as the carrier gas for the naphthalene. With increasing temperatures, a greater variety of intermediate compounds is detected, indicating increasing naphthalene conversion to these compounds.
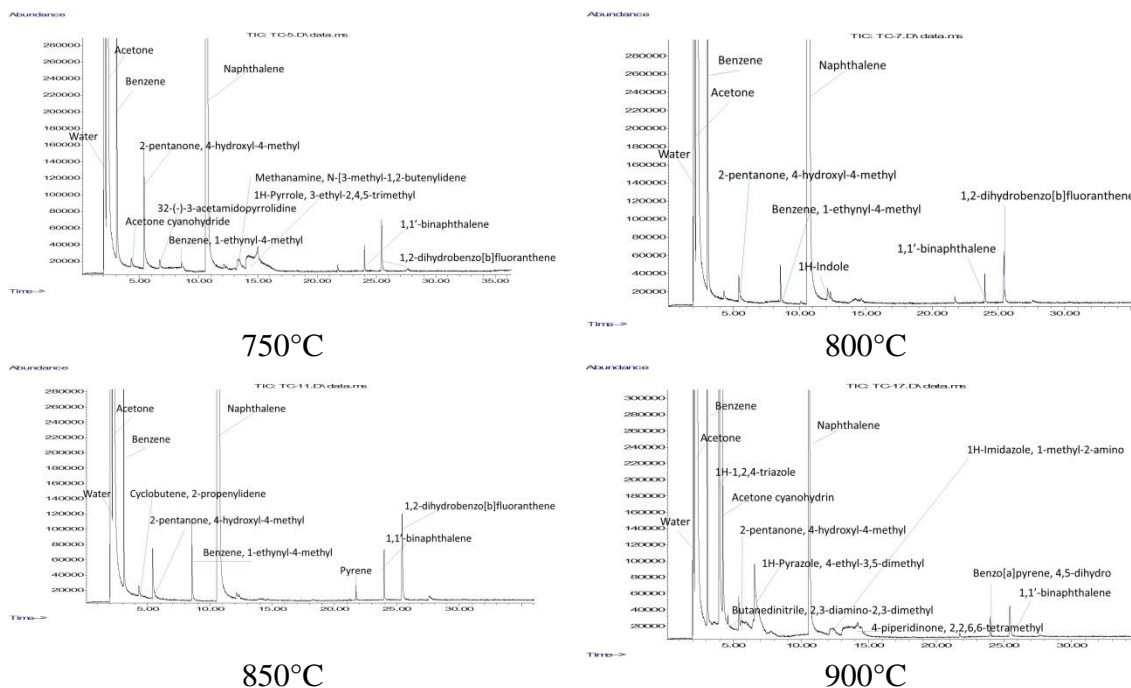
Figure 4-8. GC-MS results for trona runs using syngas blend.

The conversion of naphthalene to intermediate compounds over a nahcolite catalyst varied from 24% at 800°C to 68% at 900°C. The conversion to intermediate compounds rose as the temperature rose. The conversion at 750°C, 800°C, and 850°C being lower than the conversion at the same temperature with an empty bed or no catalytic material present indicates the large error present (at least ±15% based on the mass balance closure). In addition, at no point did the conversion rise to 75%,

66

demonstrating that nahcolite was not an effective catalyst for converting naphthalene to intermediate compounds as set forth in the hypothesis of this work. Figure 4-9 shows the GC-MS results for the nahcolite runs with syngas as the carrier gas for the naphthalene.
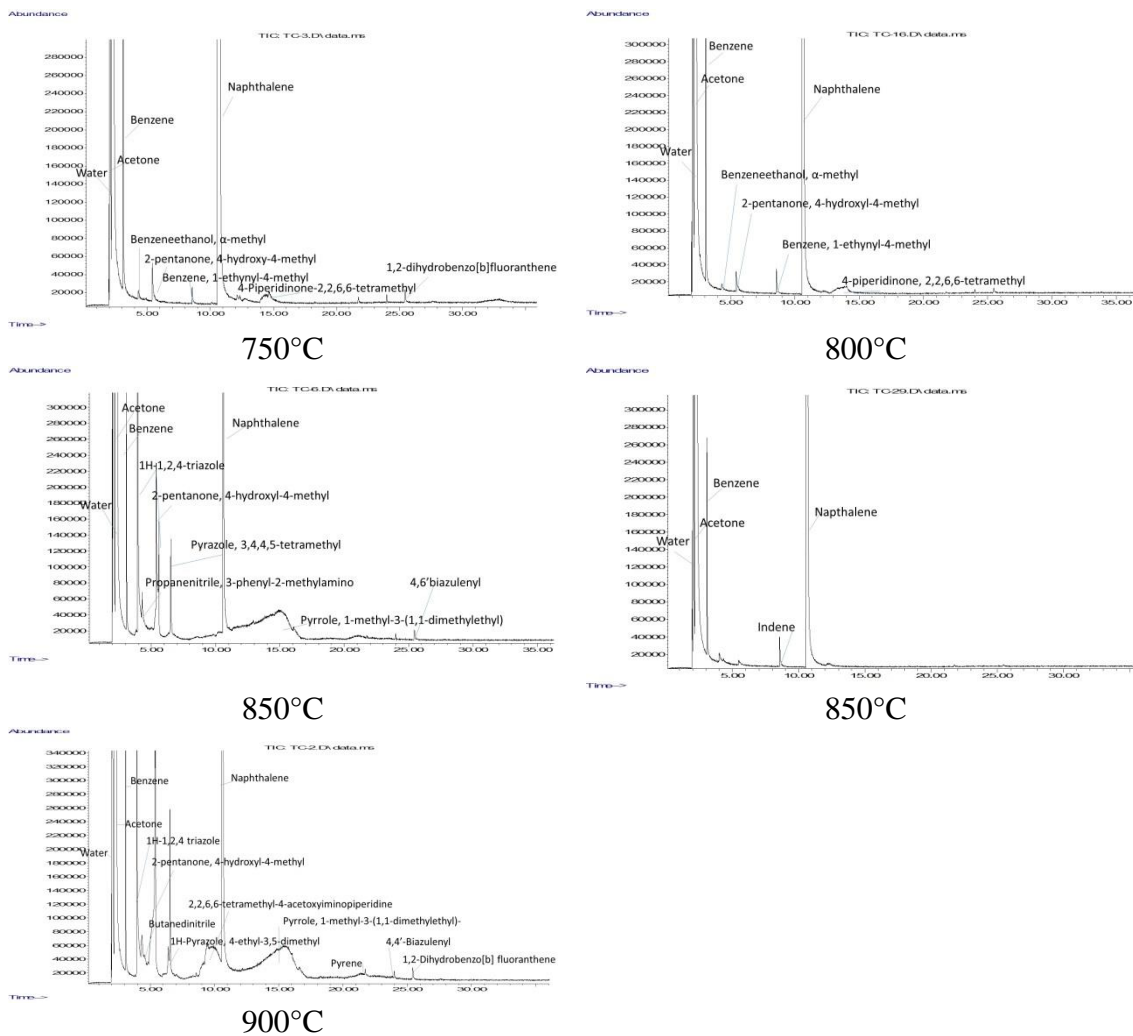
Figure 4-9. GC-MS results for nahcolite runs using syngas blend.

The conversion of naphthalene to intermediate compounds over olivine varied from 28% at 750°C to 100% at 850°C. This catalyst exhibited a much higher conversion of naphthalene to intermediate compounds at intermediate temperatures than expected. The conversion of naphthalene to intermediate compounds at 900°C is 45%, lower than

67

that observed for the runs in an empty bed or with no catalytic material present. It is possible that, above 850°C, the catalyst underwent a phase change or sintered, leading to the decrease in the availability of active sites and thus lower conversion levels (Bartholomew, 1996). Since the conversion of naphthalene to intermediate compounds was greater than 75%, olivine at 800°C and 850°C is an effective tar cracking catalyst at these conditions. In addition, olivine is a better catalyst than trona, as it requires a lower operating temperature to achieve superior conversion. Thus, a lower energy penalty would be incurred in heating the syngas to crack tars using olivine than using trona. Figure 4-10 shows the GC-MS results for the olivine runs with syngas as the carrier gas for the naphthalene.
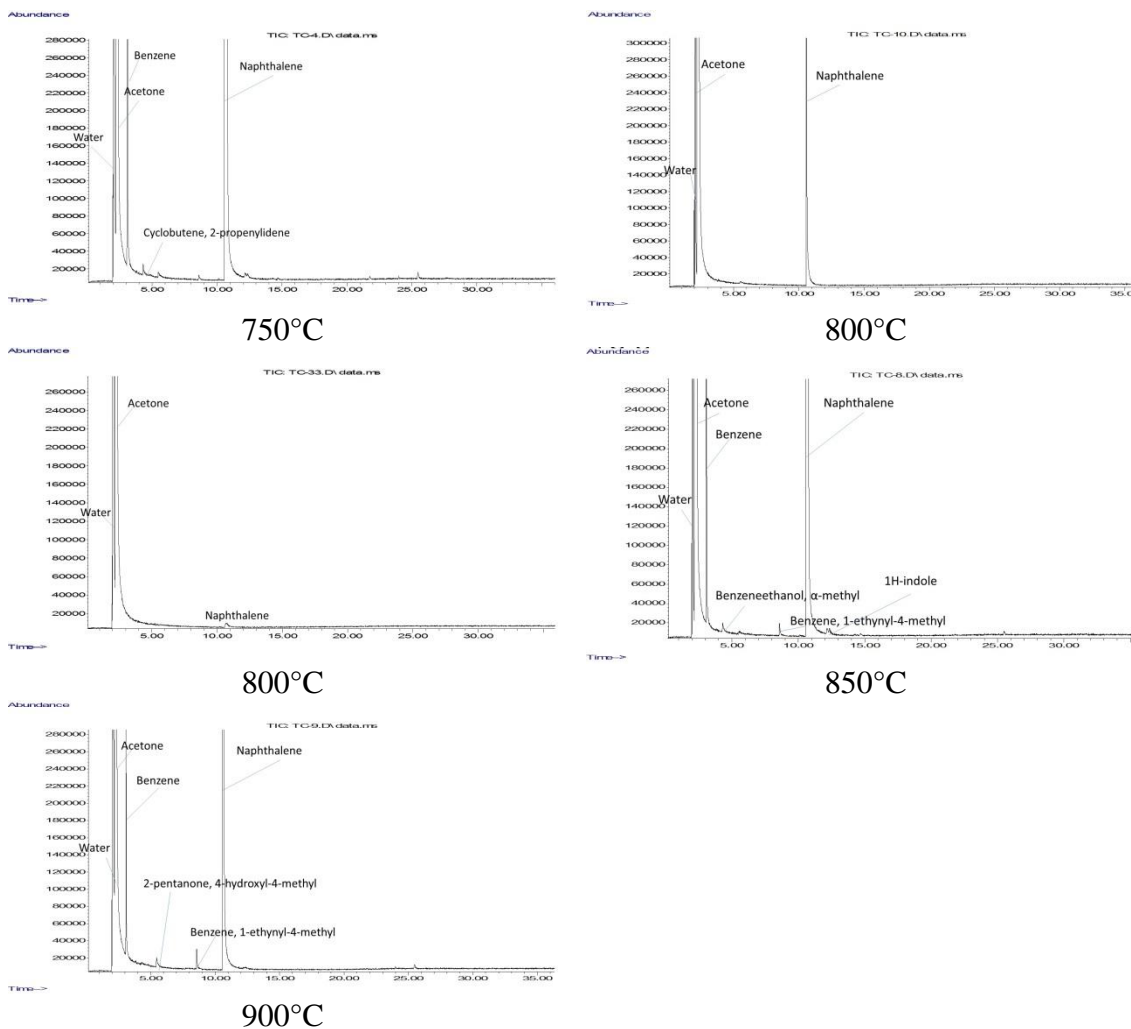
Figure 4-10. GC-MS results for olivine runs using syngas blend.

The conversion of naphthalene to intermediate compounds over powder dolomite varied from 42% at 750°C to 100% at 850°C. This catalyst exhibited a very high conversion of naphthalene to intermediate compounds at temperatures above 800°C; at no temperature above 800°C was the conversion of naphthalene to intermediate compounds less than 95%. Since the conversion of naphthalene to intermediate compounds was greater than 75%, powder dolomite at temperatures above 800°C is an effective tar cracking catalyst at the conditions studied. It is as effective as the olivine

studied and is a better catalyst than trona, as it requires a lower operating temperature to achieve superior conversion. Thus, a lower energy penalty would be incurred in heating the syngas to crack tars using powder dolomite than using trona. This may be due to the particle size of the powder dolomite, which was very fine and consequently would have a high surface area, leading to more active sites for catalytic activity. Figure 4-11 shows the GC-MS results for the powder dolomite runs with syngas as the carrier gas for the naphthalene.

750°C   800°C

850°C   900°C
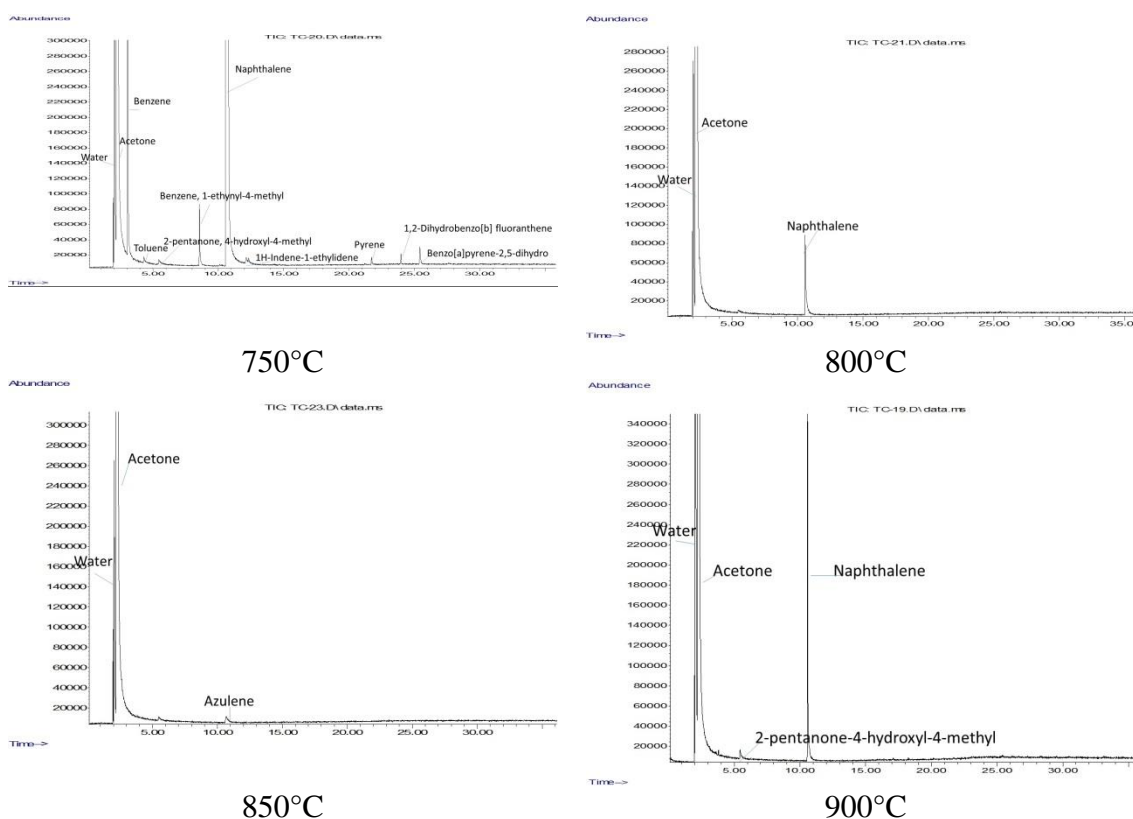
Figure 4-11. GC-MS results for powder dolomite runs using syngas blend.

The conversion of naphthalene to intermediate compounds over Plum Run dolomite varied from 49% at 800°C to 90% at 900°C. Since the conversion of naphthalene to intermediate compounds was greater than 75%, Plum Run dolomite at

900°C is an effective tar cracking catalyst at the conditions studied. It is as effective a catalyst as trona, but less energy efficient than olivine and powder dolomite, as it requires a higher temperature to convert naphthalene to intermediate compounds. Thus, a higher energy penalty would be incurred in heating the syngas to crack tars using Plum Run dolomite than olivine or trona. The difference in catalytic activity between the two dolomite samples studied may be partially attributed to their differences in particle size. Plum Run dolomite had an average particle size of approximately 0.8-1.0 mm, while the powder dolomite had an average particle size of approximately 90 μm. This significant difference in particle size could have led to the powder dolomite being a more effective catalyst as it would have a consequently larger surface area per gram and thus would have had more available active sites for naphthalene conversion to intermediate compounds. Another difference in catalytic activity between the two dolomite samples may be attributable to their differing compositions; the powder dolomite is at least 55% CaO, while the Plum Run dolomite is 66.6% CaO. Figure 4-12 shows the GC-MS results for the Plum Run dolomite runs with syngas as the carrier gas for the naphthalene.

750°C

800°C
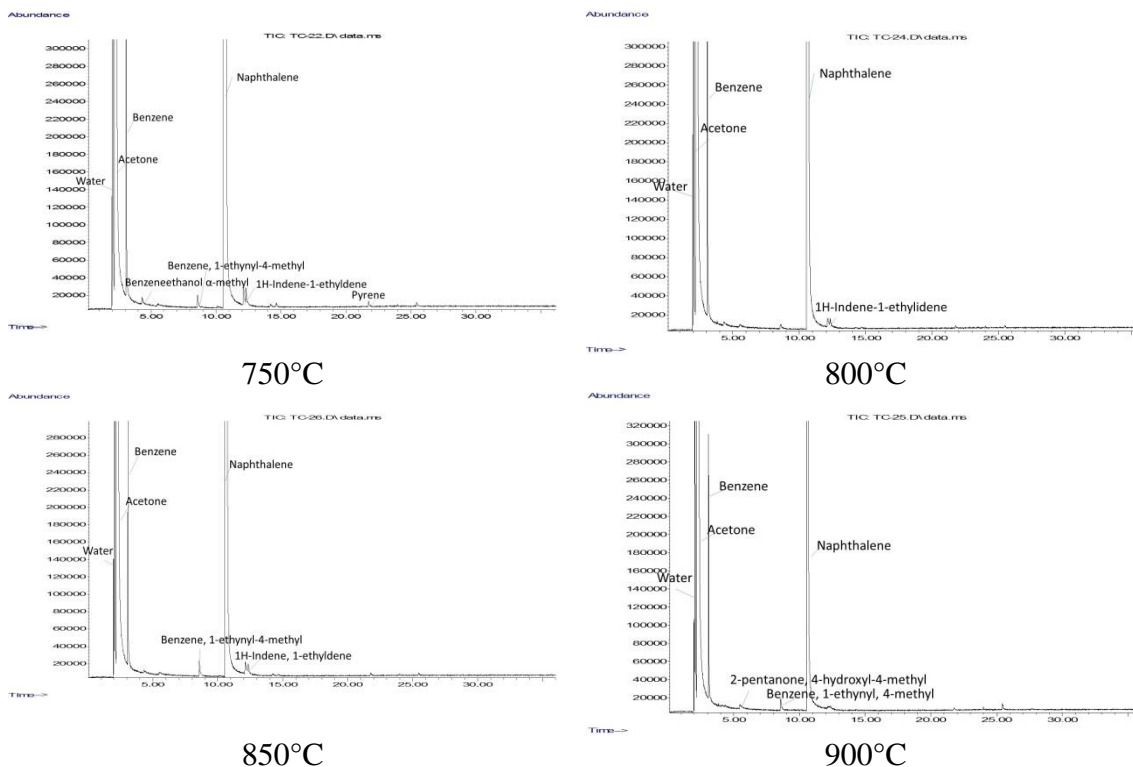
850°C

900°C

Figure 4-12. GC-MS results for Plum Run dolomite runs using syngas blend.

The conversion of naphthalene to intermediate compounds over the NREL Ni-based catalyst varied from 66% at 750°C to 100% at 850°C and 900°C. The Ni-based catalyst was very effective in cracking tars; this is expected, as transition metal-based catalysts have been shown to have very high conversion rates for tar cracking (Gerber, 2007; Xu *et al*., 2010; Anis and Zainal, 2011). Figure 4-13 shows the GC-MS results for runs performed using the NREL Ni-based catalyst.
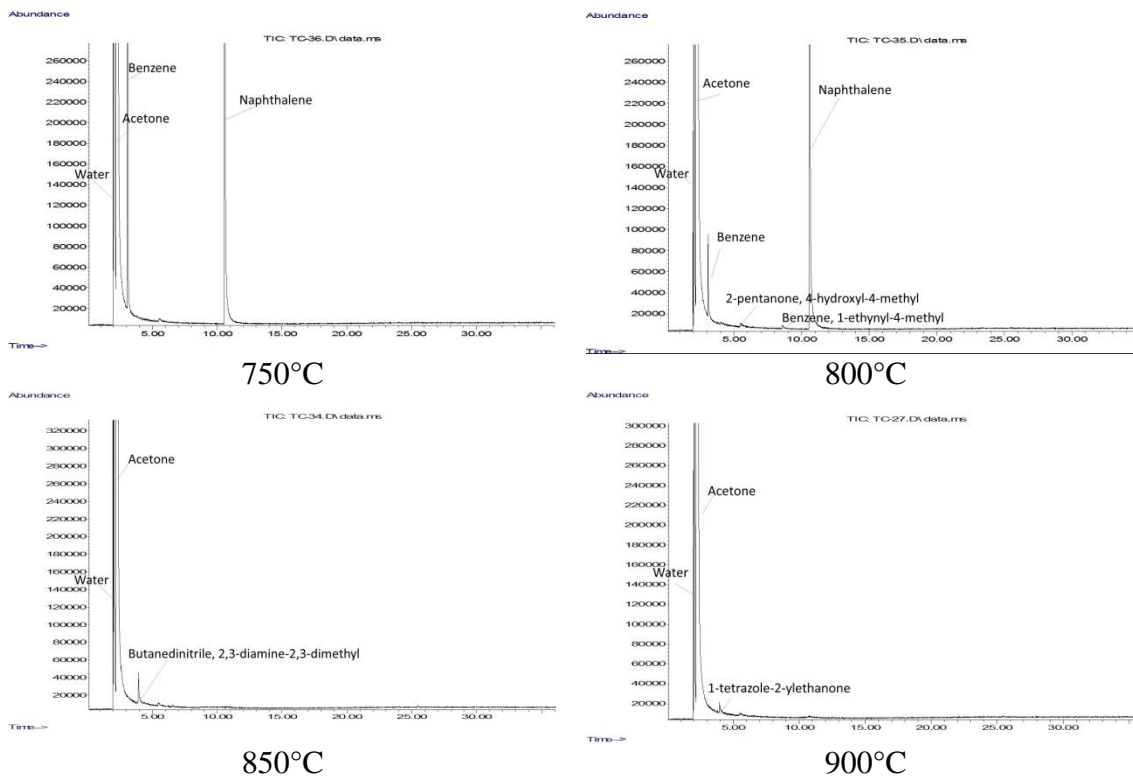
Figure 4-13. GC-MS results for NREL Ni-based catalyst runs using syngas blend.

Table 4-4 shows the composition of the collected tar samples as analyzed by gas chromatography-mass spectrometry (GC-MS).

Table 4-5 shows the tar compositions as collected by GC-MS, exclusive of the acetone. Since acetone was used to collect the naphthalene and other cracking products, the results should be considered in its absence.

Table 4-4. GC-MS composition analysis results.

Catalyst	Temperature (°C)	Carrier Gas	Acetone wt%	Naphthalene wt%	Water wt%	Benzene wt%	2-Pentanone wt%	Triazole wt%	Misc wt%
Empty bed	900	N_2	46.4	50.7	0.7	0	-	-	2.1
Empty bed	750	Syngas	43.7	55.1	0.7	0.4	-	-	0
Empty bed	800	Syngas	45.9	53.1	0.6	0.4	-	-	0.1
Empty bed	850	Syngas	48.5	50.4	0.6	0.5	-	-	0
Empty bed	900	Syngas	44.9	54.1	0.6	0.1	-	-	0.3
Empty bed	900	Syngas	45.3	53.7	0.6	0.2	-	-	0.1
Trona	750	Syngas	49.0	46.4	1.9	2.3	0.2	-	0.3
Trona	800	Syngas	43.1	54.5	1.5	0.8	-	-	0.1
Trona	850	Syngas	44.5	51.6	2.9	0.6	0.1	-	0.2
Trona	900	Syngas	80.3	11.9	1.2	0.6	-	4.6	1.3
Nahcolite	750	Syngas	42.8	54.5	1.5	1.2	0.1	-	0
Nahcolite	800	Syngas	61.5	35.7	2.4	0.4	-	-	0
Nahcolite	850	Syngas	83.8	9.9	2.4	0.4	-	1.2	2.4
Nahcolite	850	Syngas	67.06	30.9	1.8	0.2	-	-	0
Nahcolite	900	Syngas	68.1	24.3	2.0	0.4	-	1.7	3.5
Olivine	750	Syngas	44.6	52.1	1.6	1.7	-	-	0
Olivine	800	Syngas	97.5	1.7	0.8	0	-	-	0
Olivine	800	Syngas	96.94	0	3.01	0	-	-	0
Olivine	850	Syngas	51.8	47.0	0.6	0.7	-	-	0
Olivine	900	Syngas	72.2	23.4	4.0	0.4	-	-	0
Powder dolomite	750	Syngas	45.5	52.0	1.1	1.3	-	-	0.1
Powder dolomite	800	Syngas	99.21	0.2	0.6	0	-	-	0
Powder dolomite	850	Syngas	99.47	0	0.5	0	-	-	-0.01
Powder dolomite	900	Syngas	96.54	0.6	2.8	0	-	-	0

Table 4-4, cont.

Catalyst	Temperature (°C)	Carrier Gas	Acetone wt%	Naphthalene wt%	Water wt%	Benzene wt%	2-Pentanone wt%	Triazole wt%	Misc wt%
Plum Run dolomite	750	Syngas	41.96	56.7	0.6	0.8	-	-	0
Plum Run dolomite	800	Syngas	60.92	38.1	0.6	0.4	-	-	0
Plum Run dolomite	850	Syngas	58.79	40.5	0.5	0.2	-	-	0
Plum Run dolomite	900	Syngas	78.16	20.8	0.8	0.3	-	-	0
No catalyst	750	Syngas	58.64	39.9	0.9	0.6	-	-	0
No catalyst	800	Syngas	52.89	46.3	0.5	0.4	-	-	0
No catalyst	850	Syngas	57.92	40.8	0.5	0.8	-	-	0
No catalyst	900	Syngas	69.04	28.1	2.5	0.4	-	-	0
NREL Ni-based catalyst	750	Syngas	91.12	5.1	2.9	0.9	-	-	0
NREL Ni-based catalyst	800	Syngas	90.16	8.2	1.4	0.2	-	-	0
NREL Ni-based catalyst	850	Syngas	98.33	0	1.6	0	-	-	0.05
NREL Ni-based catalyst	900	Syngas	98.89	0	1.1	0	-	-	0

Table 4-5. GC-MS composition analysis results, normalized to acetone.

Catalyst	Temperature (°C)	Gas	Naphthalene wt%	Water wt%	Benzene wt%	2-Pentanone wt%	Triazole wt%	Misc wt%
Empty bed	900	N$_2$	98.5	1.5	0	0	0	4.1
Empty bed	750	Syngas	97.9	1.3	0.7	0	0	0
Empty bed	800	Syngas	98.2	1.1	0.7	0	0	0.1
Empty bed	850	Syngas	97.9	1.2	0.9	0	0	0
Empty bed	900	Syngas	98.7	1.1	0.3	0	0	0.5
Empty bed	900	Syngas	98.4	1.1	0.5	0	0	0.1
No catalyst	750	Syngas	96.4	2.2	1.5	0	0	0
No catalyst	800	Syngas	98.2	1.0	0.8	0	0	0
No catalyst	850	Syngas	97.0	1.1	1.9	0	0	0
No catalyst	900	Syngas	90.7	8.1	1.1	0	0	0
Trona	750	Syngas	91.5	3.7	4.5	0.3	0	0.6
Trona	800	Syngas	95.9	2.7	1.4	0	0	0.1
Trona	850	Syngas	93.4	5.3	1.1	0.2	0	0.4
Trona	900	Syngas	65.0	6.3	3.4	0	25.3	7.1
Nahcolite	750	Syngas	95.2	2.6	2.1	0.1	0	0
Nahcolite	800	Syngas	92.7	6.1	1.1	0	0	0
Nahcolite	850	Syngas	71.2	17.3	3.0	0	8.4	17.1
Nahcolite	850	Syngas	93.9	5.5	0.6	0	0	0
Nahcolite	900	Syngas	85.6	6.9	1.3	0	6.1	12.5
Olivine	750	Syngas	94.0	2.9	3.1	0	0	0
Olivine	800	Syngas	67.9	32.1	0	0	0	0
Olivine	800	Syngas	0	100	0	0	0	0
Olivine	850	Syngas	97.4	1.3	1.4	0	0	0
Olivine	900	Syngas	84.1	14.4	1.4	0	0	0

Table 4-5, cont.

Catalyst	Temperature (°C)	Gas	Naphthalene wt%	Water wt%	Benzene wt%	2-Pentanone wt%	Triazole wt%	Misc wt%
Powder dolomite	750	Syngas	95.6	2.1	2.3	0	0	0.1
Powder dolomite	800	Syngas	30.0	70.0	0	0	0	0
Powder dolomite	850	Syngas	0	100	0	0	0	-1.9
Powder dolomite	900	Syngas	18.4	81.6	0	0	0	0
Plum Run dolomite	750	Syngas	97.7	1.0	1.3	0	0	0
Plum Run dolomite	800	Syngas	97.6	1.4	1.0	0	0	0
Plum Run dolomite	850	Syngas	98.2	1.3	0.6	0	0	0
Plum Run dolomite	900	Syngas	95.1	3.5	1.4	0	0	0
NREL Ni-based catalyst	750	Syngas	57.9	32.5	9.6	0	0	0
NREL Ni-based catalyst	800	Syngas	83.5	14.5	1.9	0	0	0
NREL Ni-based catalyst	850	Syngas	0	100	0	0	0	3.1
NREL Ni-based catalyst	900	Syngas	0	100	0	0	0	0

Figure 4-14 shows structures of the detected intermediate compounds. The heteroatoms (here, any atom other than C or H) would have been donated by the inlet gas stream. O would have been donated by the CO when it decomposed, and N would have been donated by the N_2 when it decomposed. The source of the S is unclear; no inlet gas contained sulfur, and it is possible that this is a misidentification by the GC-MS. For highly effective catalysts and complete cracking, expected compounds would be H_2, CO_2, CO, and CH_4.

1,1'-binaphthalene   1,2-dihydrobenzo[b]fluoranthene   1H-1,2,4-triazole

1H-imidazole, 1-methyl-2-amino   1H-indene, 1-methylene   1H-indene, -methyl

1H-indene, 1-ethylidene   1H-indole   1H-pyrazole, 4-ethyl-3,5-dimethyl

1H-pyrrole, 2-ethyl-3,4,5-trimethyl   1H-pyrrole, 3-ethyl-2,4,5-trimethyl   1-tetrazole-2-yl-ethanone
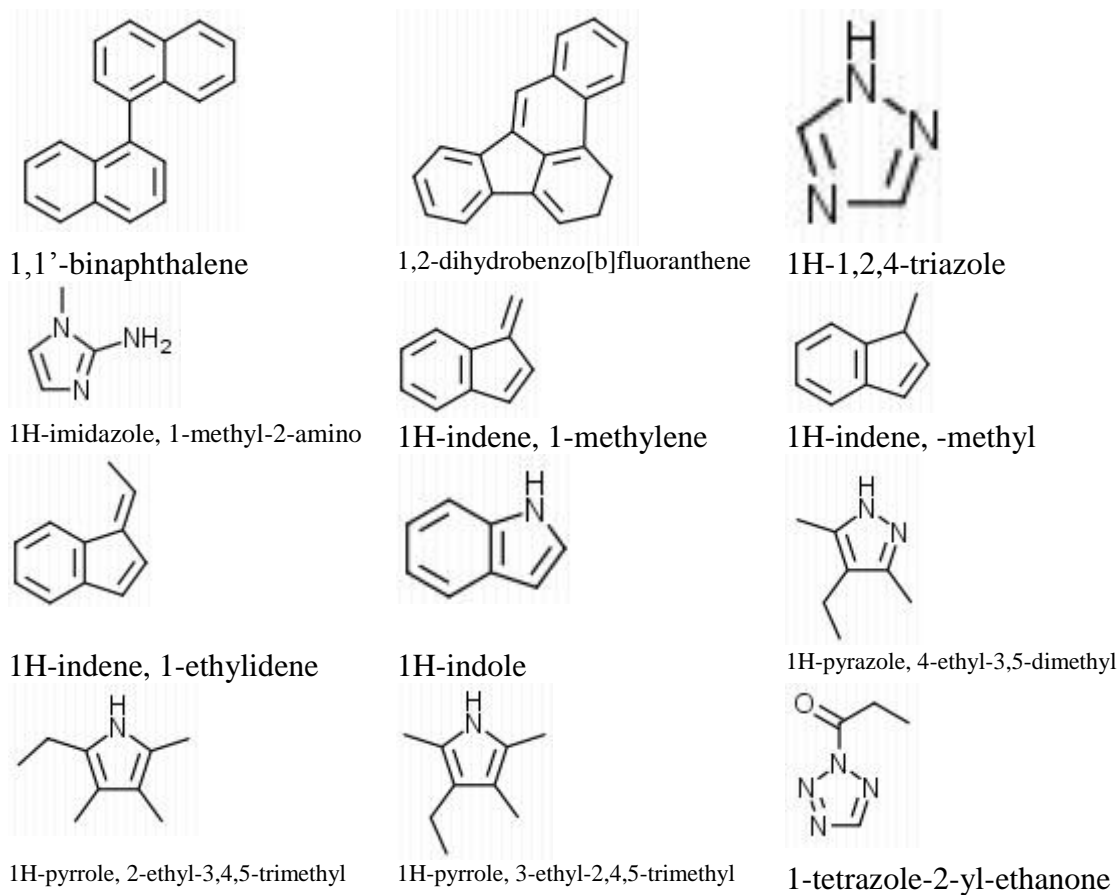
Figure 4-14. Structures of GC-MS detected compounds.

78
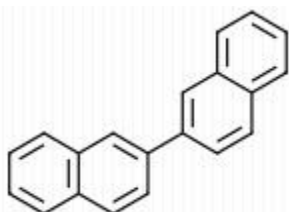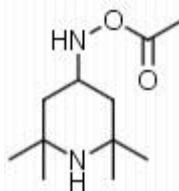
2,2'-binaphthalene

2,2,6,6-tetramethyl-4-acetoxyminopiperidine
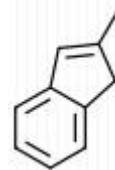
2-methylindene
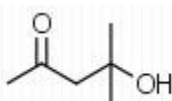
2-pentanone, 4-hydroxyl-4-methyl
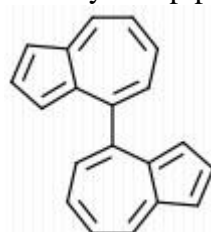
4,4'-biazulenyl
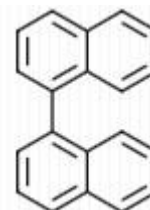
4,4'-binaphthalene
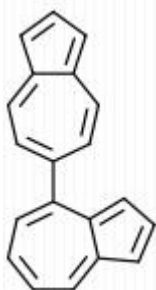
4,6'-biazulenyl
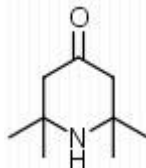
4-piperidinone, 2,2,6,6-tetramethyl

Acetone cyanohydride
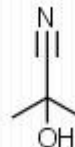
Acetone cyanohydrin

Acetone
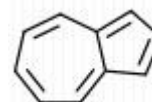
Azulene
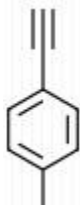
Benzene, 1-ethynyl-4-methyl
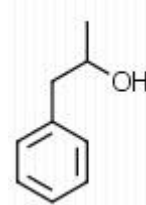
Benzeneethanol, α-methyl

Benzene

Figure 4-14, cont.
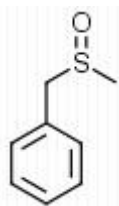
Benzene[(methylsulfinyl)methyl]
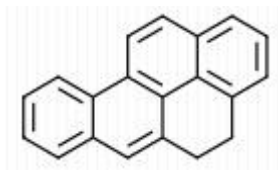
Benzo[a]pyrene, 4,5-dihydro
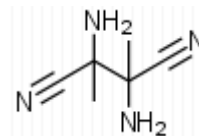
Butanedinitrile, 2,3-diamine-2,3-dimethyl
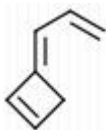
Cyclobutene, 2-propenylidene
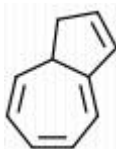
Indene
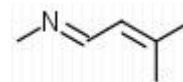
Methanamine, n-[3-methyl-1,2-butenylidene]
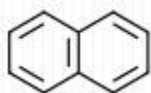
Naphthalene
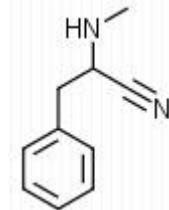
Propanenitrile, 3-phenyl-2-methylamino
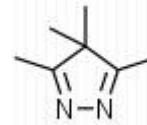
Pyrazole, 3,4,4,5-tetramethyl

Pyrene
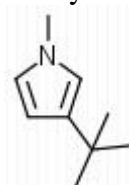
Pyrrole, 1-methyl-3-(1,1-dimethylethyl)
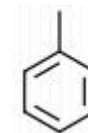
Toluene
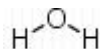
Water

Figure 4-14, cont.

Figure 4-15 shows the naphthalene conversion versus temperature for the bench-scale system. The highest overall conversions were observed above 800°C for the powder dolomite, NREL Ni-based catalyst, olivine, and Plum Run dolomite.
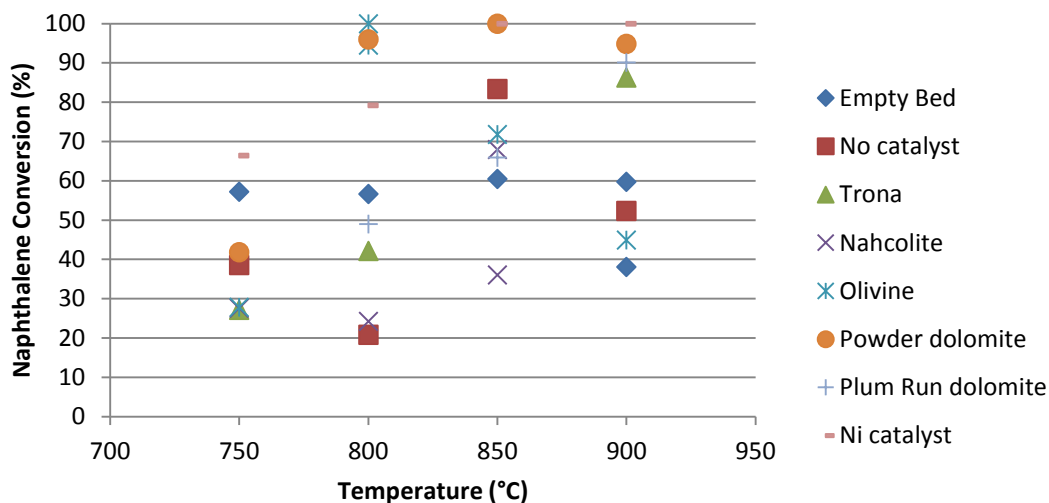
Figure 4-15. Naphthalene conversion versus temperature. Plotted without following runs: trona at 850°C, nahcolite at 900°C, Plum Run dolomite at 750°C.

Figure 4-16 show the naphthalene conversion versus the run order. This graph indicates that variance is due to the effect of temperature and not an artifact of the run order. For example, the run order for the powder dolomite catalyst was as follows: 1) 900°C, 2) 800°C, 3) 750°C, and 4) 850°C. If run order were a factor in the observed conversions, one would expect the conversions to increase or decrease as a function of the run order. This has not occurred; therefore run order did not significantly contribute to the variance.
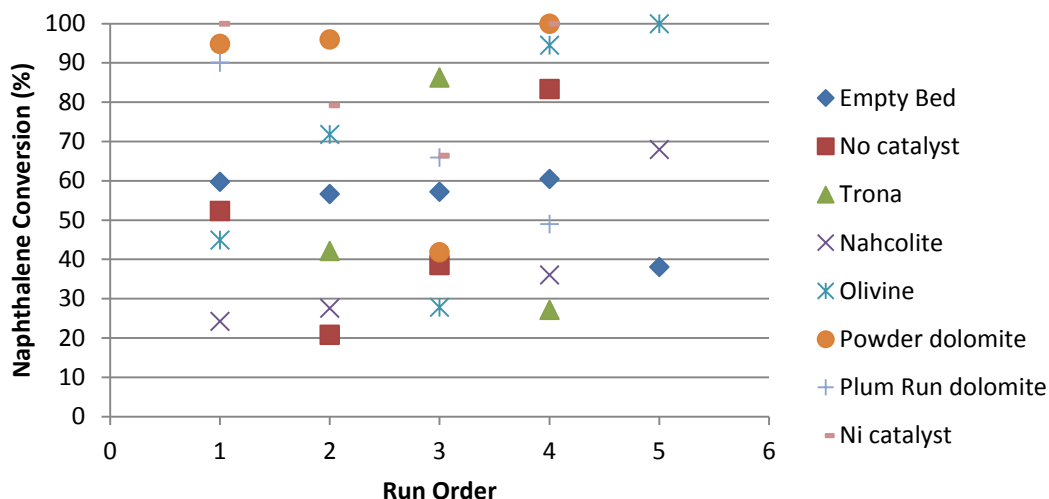
Figure 4-16. Naphthalene conversion versus run order. Plotted without following runs: trona at 850°C, nahcolite at 900°C, Plum Run dolomite at 750°C.

There are several suspect data points. First, the conversion of naphthalene over a trona catalyst at 850°C is reported as -49.5%. This is impossible and probably indicates residuals from a previous test in the system being released at a later point such that more naphthalene was collected than was fed. The second run in the empty bed at 900°C, which was the last test performed before the 850°C trona test, therefore, may have had less naphthalene reported than it should and thus an artificially higher conversion. The same issue is apparent for the conversion of naphthalene over a nahcolite catalyst at 900°C. These results indicate that the previous test may have had less naphthalene and condensable cracking products collected than there should have been; in the case of the nahcolite run, this would have been the run with nahcolite catalyst at 750°C. In addition, the conversion of naphthalene over a Plum Run dolomite catalyst at 750°C is reported as 240.1%. This is impossible and probably indicates a measurement error with the balance

used, as the mass of the collection pieces after the run was less than the mass of the same pieces before the run.

In addition, the mass balance closure was not complete. The mass balance closure results using liquid nitrogen indicated that the closure was 93±15%. Table 4-6 shows the range of conversions for the runs accounting for this incomplete mass balance closure. The greatest discrepancies are observed for runs with low conversion rates as opposed to runs with higher conversion rates.

Table 4-6. Conversion ranges, accounting for incomplete mass balance closure. Tabulated without following runs: trona at 850°C, nahcolite at 900°C, Plum Run dolomite at 750°C.

Catalyst	Carrier Gas	Temperature (°C)	% Conversion		
			As-measured	Low	High
Empty bed	N_2	900	67.0	62.0	71.9
Empty bed	Syngas	750	57.3	50.8	63.7
Empty bed	Syngas	800	56.7	50.2	63.2
Empty bed	Syngas	850	60.5	54.6	66.4
Empty bed	Syngas	900	59.8	53.7	65.8
Empty bed	Syngas	900	38.0	28.8	47.3
No catalyst	Syngas	750	38.6	29.4	47.8
No catalyst	Syngas	800	20.8	9.0	32.7
No catalyst	Syngas	850	83.4	80.9	85.9
No catalyst	Syngas	900	52.3	45.2	59.5
Trona	Syngas	750	27.2	16.3	38.1
Trona	Syngas	800	42.2	33.5	50.8
Trona	Syngas	900	86.3	84.3	88.4
Nahcolite	Syngas	750	27.6	16.7	38.5
Nahcolite	Syngas	800	24.3	12.9	35.6
Nahcolite	Syngas	850	36.1	26.5	45.6
Nahcolite	Syngas	850	68.0	63.2	72.8
Olivine	Syngas	750	27.8	17.0	38.6
Olivine	Syngas	800	94.5	93.7	95.4
Olivine	Syngas	800	100	100	100
Olivine	Syngas	850	71.8	67.6	76.1
Olivine	Syngas	900	44.9	36.6	53.2
Powder dolomite	Syngas	750	41.8	33.1	50.5
Powder dolomite	Syngas	800	95.9	95.3	96.6
Powder dolomite	Syngas	850	100	100	100
Powder dolomite	Syngas	900	94.9	94.1	95.6

Table 4-6, cont.

Catalyst	Carrier Gas	Temperature (°C)	% Conversion		
			As-measured	Low	High
Plum Run dolomite	Syngas	800	49.0	41.4	56.7
Plum Run dolomite	Syngas	850	65.9	60.8	71.0
Plum Run dolomite	Syngas	900	90.1	88.6	91.6
Ni catalyst	Syngas	750	66.4	61.4	71.5
Ni catalyst	Syngas	800	79.2	76.0	82.3
Ni catalyst	Syngas	850	100	100	100
Ni catalyst	Syngas	900	100	100	100

Table 4-7 shows the results of loss-on-ignition (LOI) testing for the spent catalyst and bed materials, and Figure 4-17 shows the recovered catalyst and bed materials post-experimental runs. The LOI tests were conducted at 750°C under air and were run in triplicate, and the average is reported. The dark material in the photographs is most likely carbon deposited by coking. In the case of the olivine catalyst, some of the carbon may have been used in the formation of iron carbide. After it was calcined, the olivine catalyst was a bright orange-red, similar to rust, which was expected as calcination drove off CO_2 and H_2O, leaving magnesium and iron oxides. In the presence of CO, the iron oxides may have been converted to iron carbides (Eliason, 1997). This is substantiated by the LOI for the olivine catalyst and bed materials, which was approximately half of that observed for most of the other catalysts. It is unclear why the LOI of the powder dolomite was so low, although this sample did qualitatively appear to have fewer carbon deposits than the others.

Table 4-7. Loss-on-ignition test results.

Spent Catalyst	% LOI	% Carbon Fed in Coking Deposits
Bed Material (no catalyst)	17 ± 4	2.5
Trona	19 ± 1	4.8
Plum Run Dolomite	18 ± 1	5.1
Powder Dolomite	8 ± 1	1.3
Nahcolite	18 ± 3	5.2
Olivine	9 ± 1	3.3

(a)   (b)

Figure 4-17. Recovered catalyst and bed materials. (a) – trona, (b) – nahcolite.
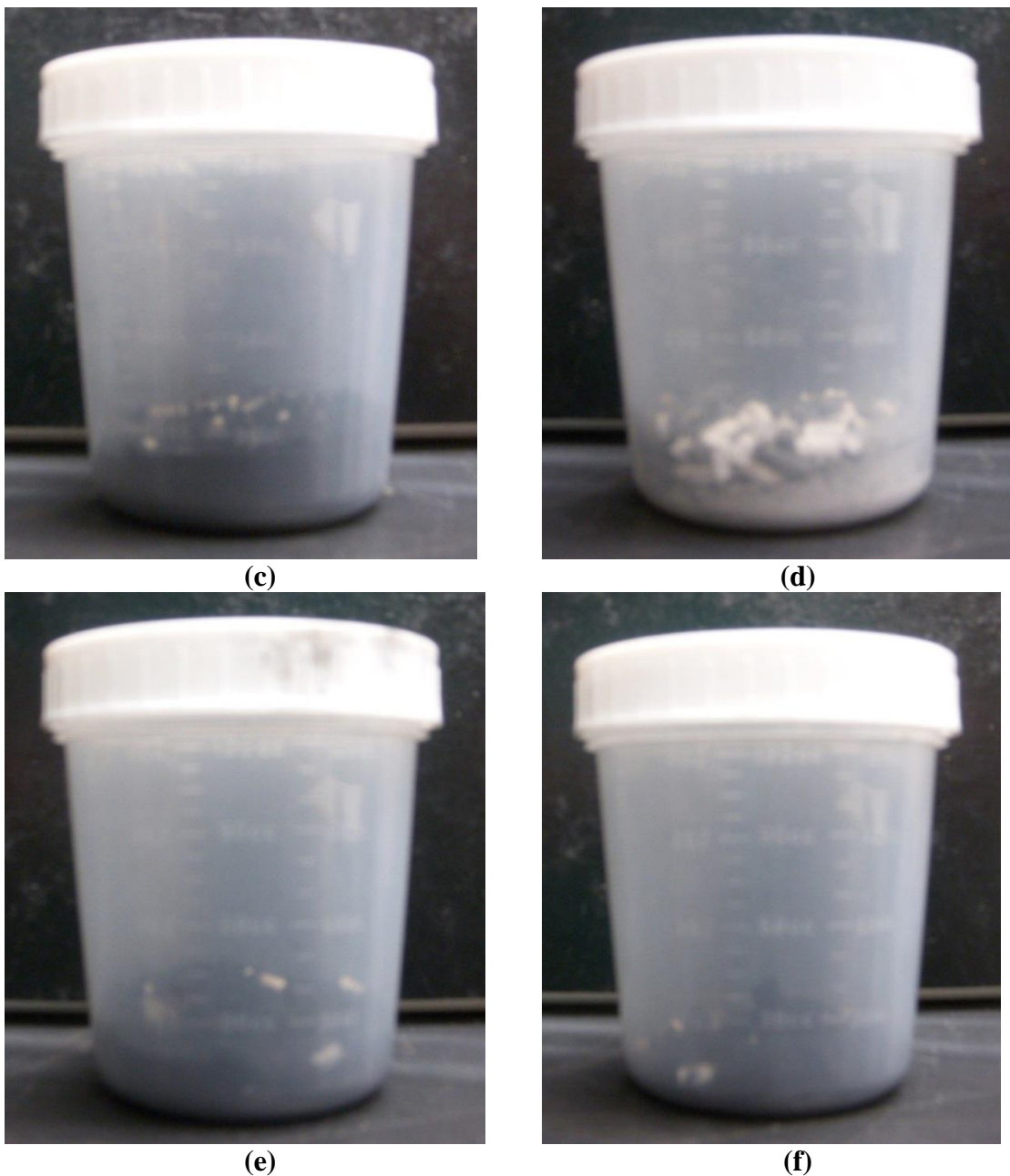
Figure 4-17, cont. (c) – olivine, (d) – powder dolomite, (e) – Plum Run dolomite, (f) – catalyst-free bed material.

4.3 Summary
4.3.1 Laboratory-Scale Updraft Gasifier and Tar Cracking System

It is clear that there is a transition in catalyst cracking performance between

800°C and 900°C. The optimal temperature for catalytic cracking is at least 800°C, as

coking is too prevalent at lower temperatures. Thermal cracking performance substantially increases between 800°C and 900°C as well.

Thermal cracking accounted for ~85% of the observed tar destruction, and depending on the application, thermal cracking may be sufficient. This would impose a balance between the energy penalty of heating the syngas from the gasifier to the degree required to crack the tars formed in gasification and the cost of operating a catalyst bed to incur a lesser energy penalty.

The data suggest that guard catalysts are of little value at 900°C because the tar is thermally destroyed. However, mineral-based guard catalysts may still be of use to protect more expensive transition metal-based catalysts against poisoning and coking.

The primarily transition metal-based reforming and cracking catalysts were the most promising, showing outlet tar loadings two to three times lower than the mineral catalysts, especially at 900°C. This is in agreement with the reviewed literature.

4.3.2 Bench-Scale Tar Cracking Reactor

The powder dolomite was the most effective catalyst for converting naphthalene to intermediate compounds, exhibiting conversions in excess of 95% at temperatures above 800°C. The NREL Ni-based catalyst and olivine were highly effective as well; the Ni-based catalyst exhibited conversions in excess of 79% at temperatures above 800°C, and the olivine exhibited conversions of 100% at 800°C and 72% at 850°C. The trona and Plum Run dolomite were effective catalysts at 900°C; the trona exhibited a conversion of 86%, and the Plum Run dolomite exhibited a conversion of 90%. Nahcolite was not an effective naphthalene-converting catalyst.

GC-MS data could not be used to determine which mineral-based catalyst was most effective based on the abundance of intermediate compounds formed in the conversion of naphthalene, as generally only small amounts of these compounds were present in comparison with the large amount of acetone present in the sample. That is, the method used is only semi-quantitative at the low values of the other compounds imposed by the use of the acetone solvent.

Generally higher temperatures led to greater conversion. This is as expected since thermal cracking effects would be more evident at higher temperatures. The exception to this rule was olivine: temperatures above 800°C led to a decrease in cracking activity. This may be due to a phase change within the mineral structure of the catalyst or sintering of the catalyst particles.

CHAPTER V
LITERATURE REVIEW – BIOFUELS

5.1 Bio-oil and Biodiesel Sources

Although there are many other sources of bio-oils and biofuels, this literature review is focused only on those used for the testing performed here. These oils were chosen because of their relative abundance and, consequently, availability.

Jatropha oil is derived from the *Jatropha* genus of flowering plants. Most of the species of this plant are native to the Americas. The main oil-bearing plant as identified by Goldman Sachs is *Jatropha curcas*, which is native to the North and Central American tropics. The seeds average 34.4% oil, which can be refined into biodiesel (Achten *et al*., 2008). The remaining cake may also be burned for further energy production (Jongschaap *et al*., 2009). The plant is simple to cultivate and grows in nearly every soil, although yields may be somewhat lower in poor and stony soils (von Reppert-Bismarck, 2011). Jatropha plants live for more than 40 years and produce seeds after 9-12 months, though maximum yield is not obtained until after the first 2-3 years. While seed yields vary widely, an average yield is around 1500 to 2000 kg / hectare, which equates to 540 to 640 liters of oil / hectare (Dar, 2007). However, the *Jatropha* genus of plants has not been domesticated. Furthermore, the *Jatropha curcas* plant requires a substantial amount of water to grow, potentially upwards of five times that of sugar cane and corn (McKenna, 2009). Currently, jatropha plants are mainly used for soap production, traditional medicine (the seeds act as a purgative), and live fence (Asselbergs *et al*., 2006).

Palm oil is derived from the fruit of the oil palm trees, especially the African oil palm *Elaeis guineensis*. Indonesia produces the most palm oil in the world at 20.9 million tonnes (2009), while Malaysia produces 18.79 million tonnes (2012) (Scientific American, 2012; USDA, 2012). Other producers of palm oil include Nigeria, Thailand, Colombia, and smaller producers in Africa (Ayodele, 2010). In 2012-2013, total world production of palm oil was 58.1 million metric tonnes (Index Mundi, 2013). Its principle use is as a cooking ingredient, especially in the tropical belt of Africa, southeast Asia, and Brazil. It has also been used in soap products (e.g., Unilever and Palmolive), in processed foods as a cheap substitute for butter, and in the production of biodiesel (although this does ignite a food vs. fuel debate) (Fedepalma, accessed 2013).

Animal and plant products can generally be recycled into biocrude fuel and refined into biodiesel. Several companies, including Griffin Industries and Darling International, recycle animal fats collected during animal rendering, used cooking oil, and other plant oils into renewable diesel. Some of the fats used in this process include inedible tallow, technical lard, choice white grease, poultry fat, yellow grease, flotation fat, prepared foods waste fats, soybean oil, corn oil, palm stearin, palm fatty acid distillate, tall oil, camelina oil, jatropha oil, and algal oil (Griffin Industries, 2010). As an example, the Diamond Green Diesel facility located in Norco, LA, is able to take in approximately 11% of the animal fats and used cooking oil generated in the United States and output 137 million gallons of renewable diesel annually (Zerman, 2013). Another plant processing these streams in the United States is the Dynamic Fuels plant in Geismar, LA. This plant is able to output 75 million gallons of renewable diesel per year (Dynamic Fuels LLC, accessed 2013).

5.2 Quick Assessment Tools for Biofuels
5.2.1 Critical Fuel Properties Impacting Performance In Power Production

The fuel properties which most greatly impact power production performance are viscosity, volatility, surface tension, corrosion, oxidative stability, acid number, water absorption, and deposit formation.

Higher viscosity in pure vegetable oils, waste oils, and greases can prevent adequate atomization of the fuel. This results in poorer mixing with combustion air and incomplete combustion in engines and turbines. Thus, this can lead to poor cold start performance, nozzle clogging, and lubricating oil contamination. Viscosity can be improved (lowered) by heating the fuel prior to injection, by diluting with lower viscosity fuels (e.g., petroleum diesel, alcohols, or fatty acid methyl esters [FAME]), emulsifying the oils, or converting the oils to FAME (Rehman *et al*., 2011). In one study, heating waste fryer oil to 135°C resulted in a reduction of its viscosity to be similar to that of diesel fuel at 30°C (Pugazhvadivu and Jeyachandran, 2005).

The viscosity of triglycerides is nearly ten times greater than that of their corresponding methyl esters, as indicated in Table 5-1. Due to the strong correlation between viscosity and the fraction of unreacted triglycerides in biodiesel, viscosity is a useful parameter to indirectly assess FAME purity (Knothe, 2001).

Table 5-1. Comparison of properties of vegetable oils and esters with diesel fuel (after Ramadhas *et al*., 2004).

Fuel Type	Calorific Value (kJ/kg)	Density (kg/m^3)	Viscosity (27°C, mm^2/s)	Cetane number
Diesel fuel	43,350	815	4.3	47.0
Sunflower oil	39,525	918	58.5	37.1
Sunflower methyl ester	40,579	878	10.3	45.5
Cottonseed oil	39,648	912	50.1	48.1
Cottonseed methyl ester	40,580	874	11.1	45.5
Soybean oil	39,623	914	65.4	38.0
Soybean methyl ester	39,760	872	11.1	37.0
Corn oil	37,825	915	46.3	37.6
Opium poppy oil	38,920	921	56.1	-
Rapeseed oil	37,620	914	39.2	37.6

Relatively low volatility makes vaporization of vegetable oils, waste oils, and greases difficult. Incomplete vaporization can lead to thermal cracking of the oils, resulting in excessive smoke emissions and carbon deposits in the combustion chamber (Rehman *et al*., 2011).

Higher surface tension can reduce spray atomization, increase droplet size, and impact other properties of spray atomization (Boucher *et al*., 2000; Graboski and McCormick, 1998). Limited data exists on the surface tension of neat biodiesel and blends. A typical value for No. 2 diesel is 22.5 dyne/cm at 100°C. Reported surface tension of biodiesel ranges from 34.9 dyne/cm at 60°C for neat soy methyl ester and 25.4 dyne/cm at 100°C for rapeseed oil methyl ester (Stotler and Human, 1995; Reece and Peterson, 1993).

The presence of free fatty acids (FFA) can lead to corrosion of metallic components in storage and transportation equipment. Copper is especially susceptible to

this attack; therefore, copper- and brass-containing components should ideally be replaced with steel. Additionally, grey cast iron has showed slight corrosion in the presence of FFA and should be avoided for these fuel mixtures (Geller *et al.*, 2007).

Oxidative stability is a measure of biodiesel fuel oxidation after exposure to air at elevated temperatures. It is determined through measurement of the induction period (IP) by CEN method EN14112; this is known as the Rancimat method. Increased oxidation of FAME can lead to the formation of peroxides, which may attach to elastomers or polymerize into insoluble high-molecular weight compounds that can clog fuel lines or filters or lead to incomplete combustion and associated engine deposits (Dunn, 2002). Some other tests, including kinematic viscosity, acid number, and iodine value, have been used as indicators of oxidation, but are generally not accurate (Moser, 2011).

The acid number is typically determined using Karl Fischer titration in accordance with ASTM D664. In renewable oil fuels, this is largely a measurement of the amount of FFA present in the fuel. Fuels with elevated acid numbers can cause corrosion in storage and feed systems. The specification for biodiesel calls for a maximum of 0.5 mg KOH / g fuel; however, fats and oils can posses acid numbers up to 10 mg KOH / g fuel (Espadafor *et al.*, 2009).

ASTM D975 indicates that up to 500 ppm water is acceptable in diesel fuel. No. 2 diesel fuel is typically 60 ppm water at 25°C, which is nearly equivalent to the water solubility in diesel at this temperature. The water solubility in 100% soy-based biodiesel is 1500 ppm; the water solubility in 20% biodiesel is around 40 ppm, which is statistically similar to 60 ppm with current measurement techniques. Blending saturated methyl ester with No. 2 diesel can lead to water separation. If enough water separates, a

water layer may form and provide a site for microbial growth and subsequent fuel degradation (Graboski and McCormick, 1998).

The formation of deposits in combustion engines is frequently attributed, therefore, to the high viscosity and low volatility of vegetable oil fuels. Heating the oil can significantly lower fuel viscosity and reduce deposit formation. However, the mechanisms that lead to deposit formation are not fully understood. Deposits are often attributed to the presence of triglycerides. For examples, in esterified oil fuels, the reduced amount of triglycerides correlates with lower levels of deposit formation. In some studies, diesel blends with less than 30% vegetable oil showed a performance similar to that of neat diesel (Sidibé *et al*., 2010).

5.2.2 Screening Methods for Fuel Quality Assessment

It is evident that it is important to analyze a fuel for, at a minimum, the aforementioned properties. While many standards are available to assess fuel properties, it may be beneficial to have a "quick and dirty" field test which can efficiently and accurately assess fuel properties. Table 5-2 outlines screening methods that oil-fired power plants could use to assess fuel quality.

Table 5-2. Summary of Screening Methods for Fuel Quality Assessment.

Property	Standard Method	Quick Method Available	Feasibility of Quick Method
Pour Point	ASTM D97 or D5949	Phase Technology – 70XI Cloud Analyzer (D5949)	Feasible for refined, particulate-free fuels. Not feasible for unrefined fuels due to presence of solids as this is an optical method.

Table 5-2, cont.

Property	Standard Method	Quick Method Available	Feasibility of Quick Method
Total Acid Number	ASTM D664	pHlip – color indicating aciditiy	Feasible for refined fuels. Unfeasible for unrefined fuels due to presence of solids and/or intense oil color.
		i-SPEC Q-100 ECON TAN Test, DIGI Field Kit, FG-K1-008-KW (0-3 TAN)	Feasible Feasible
		FFA/TAN Test, DIGI Biodiesel Test Kit FG-K16897-KW (Acid content / 0-6 TAN)	Feasible for refined fuels. Unfeasible for unrefined fuels due to presence of solids and/or intense oil color.
Moisture and impurities	ASTM D2709 (centrifuge)	Hot pan, > 500 ppm Sandy Brae, > 50 ppm – pressure calibrated to H_2O	Feasible Feasible
		Kittiwake Test Kit, DIGI Water in Oil Cell 0.02-1%, 200-10,000 ppm, 0-10%, 0-20%	Feasible
Heating value (HHV)	ASTM D240	None available	N/A
FFA	Per PORAM	None available	N/A
Iodine Value	AOCS Cd 1c-85	None available	N/A
Viscosity	ASTM D7042	DIGI Viscotube, DIGI Clean Oil Kit FG-K14971-KW (20-600 cSt @ 40°C)	Feasible
Flash Point	ASTM D93	None available	N/A
Sulfur	ASTM D1552, D2622, or D4294	None available	N/A
Nitrogen	ASTM D4629 or D5762	None available	N/A
Vanadium	ASTM D5863	None available	N/A

Table 5-2, cont.

Property	Standard Method	Quick Method Available	Feasibility of Quick Method
API gravity	ASTM D4052	None available	N/A
Density	ISO 3675 or 12185	Density Hydrometer, DIGI Biodiesel Test Kit FG-K16897-KW (850-950 kg/m^3)	Feasible for refined fuels. Unfeasible for unrefined fuels due to potentially intense oil color.
Cetane	FIA test	None available	N/A
CCAI	FIA test	None available	N/A
Total Sediment extant	ISO 10307-1	None available	N/A
Water, before engine	ISO 3733 (distillation)	None available	N/A
Micro carbon residue	ISO 10370	None available	N/A
Ash	ISO 6245 or LP 1001	None available	N/A
Phosphorus	ISO 10478 extended	None available	N/A
Aluminum	ISO 10478	None available	N/A
Calcium + Magnesium content	ISO 10478 extended	None available	N/A
Iron	ISO 10478 extended	None available	N/A
Silicon, organic	No method specified	None available	N/A
Silicon, inorganic	ISO 10478	None available	N/A
Alkali (sodium + potassium)	ISO 10478 extended	None available	N/A
Cloud Point	ISO 3015 or ASTM D5949	Phase Technology PSA-70Xi analyzer	Feasible for refined, particulate-free fuels. Not feasible for unrefined fuels due to presence of solids as this is an optical method.
Cold-Filter Plugging	IP 309	None available	N/A
Copper Strip Corrosion	ASTM D130	None available	N/A
Steel Corrosion	LP 2902	None available	N/A
Strong Acid Number	ASTM D664	None available	N/A
Synthetic Polymers	LP 2401 extended or LP 3402	None available	N/A
Ester content	EN 14103	None available	N/A

Table 5-2, cont.

Property	Standard Method	Quick Method Available	Feasibility of Quick Method
Linolenic acid content	EN 14103	None available	N/A
Total Glycerin	ASTM D6584	pHlip (qualitative – visible as interface)	Feasible for refined fuels. Unfeasible for unrefined fuels, especially particulate-rich or strongly colored fuels, as this is an optical method.
		Wilks IR Infraspec (<0.24% w/w)	Feasible
		i-SPEC Q-100, handheld analyzer for B-100	Feasible
Methanol	EN 14110	i-SPEC Q-100, handheld analyzer for B-100	Feasible
Carbon residue	ASTM D4530	None available	N/A
Oxidative stability	CEN method EN 14112 Rancimat	Metrohm USA, Inc. (Riverview, FL, USA) model 893 Rancimat instrument	Feasible
		AOCS CD 12-b-92 oil stability index, ISO 6886 Accelerated oxidation test Rancimat 892	Feasible
Water	ASTM D1744 – Karl Fischer titration	Mettler DL 18 titrator	Feasible
Total Base Number		Kittiwake DIGI Water in Oil/TBN cell (0-80 TBN)	Feasible
Insolubles		ECON Insolubles Test DIGI Basic Kit, FG-K1-003-KW (qualitative)	Feasible

pHlip is a quick field test available through CytoCulture International capable of measuring biodiesel acidity. The instrument can also indicate the presence of catalysts and measure soaps, monoglycerides, diglycerides, and triglycerides.

Wilks InfraSpec is a small infrared (IR) instrument designed for oils with total glycerin measurements below 0.24% w/w. The analysis time required is less than one minute. In addition, it can measure the presence of vegetable oil in methyl ester. The InfraSpec is available commercially as the InfraSpec VFA-IR Spectrometer manufactured by Wilks Enterprises, Inc.

The i-SPEC Q-100 is a handheld analyzer which uses impedance spectroscopy. It measures the blend percent, total glycerin, methanol, and acid number in B-100 samples.

The Mettler DL18 titrator uses the Hydranal Composite 5 reagent, which contains iodine, SO_2, and amine/methyl glycol to perform Karl Fischer titration for water determination. It meets the specifications set out in ASTM D1744.

Alkali metal content can be determined by using the Perkin-Elmer 100B Atomic Absorption Spectrometer, which uses nitric acid and hydrochloric acid digestion followed by spectrometry.

A quick test for water in oil involves placing drops of oil in a heated pan. "Popping" sounds are indicative of water in the oil; this method is accurate to 500 ppm (0.05% w/w).

Another test for water can be performed using the Sandy Brae Water Test Kit. This test involves reacting calcium hydride with water in an oil sample to produce H_2 gas. Since the reaction takes place in a closed container, the pressure of the container can be

calibrated to the amount of water in the sample. This method is accurate to a low level of 50 ppm.

A quick test for viscosity involves dipping a piece of cardboard in the oil and removing it, then observing the flow of oil off the cardboard. Smooth runny flow indicates good flow properties, while clumps indicate high viscosity at ambient temperature.

An optical cloud point analyzer can provide quick cold flow data provided the sample is clear and/or transparent.

Biodiesel test kits are available from Fleet Biodiesel, Inc., for B5/B20 and B100. The test kit allows for testing for water content, visual clarity, acid number, yeast/mold/anaerobic bacteria, and glycerin for ranges from 0.05% to 0.5%.

A relatively simple test to indicate the presence of triglycerides in biodiesel is the Warnquist 3/27 test. The test is carried out by mixing 27 mL of room temperature methanol with 3 mL of water-free biodiesel. Shake this mixture and let it settle. If oily material settles out in 30 minutes, the fuel contains more than trace amounts of triglycerides (and associated di- and monoglycerides).

Finally, another company that provides oil testing solutions is Kittiwake.

5.3 Key Temperature Parameters for Fuels

Table 5-3 shows melting points, boiling points, flash points, and autoignition temperatures for biodiesels, low-sulfur fuel oils, jatropha oil, palm oils, pyrolysis oils, and yellow greases. These data were acquired by examining a number of material safety data sheets (MSDS) and researcher-reported results (last row for each fuel in Table 5-3) (Tesoro, accessed 2012; National Biodiesel Board, accessed 2012; BioFlex Fuels,

accessed 2012; ConocoPhillips, accessed 2012; Biodiesel Industries, accessed 2012;

Cargill, accessed 2012; Bi, 2010; Goodrum, 2002; Ramadhas *et al*., 2005; Dooley *et al*.,

2008; Flint Hills Resources, accessed 2012; Philips Petroleum Company, accessed 2012;

Sprague, accessed 2012; Hess Corporation, accessed 2012; National Institute for

Occupational Safety and Health, 2014; Diligent Tanzania Ltd., accessed 2012; Olasheu *et*

al., 2015; Dubey *et al*., 2011; Sciencelab.com, Inc., accessed 2012; Natural Sourcing,

accessed 2012; Just a soap, accessed 2012; The Soap Kitchen, accessed 2012; Acme

Hardesty Oleochemicals, accessed 2012; Nassu and Gonçalves, 1999; Kiram, 2010;

CAMEO Chemicals, 1999; Cirad, 2006; ChevronPhillips, 2011; ChevronPhillips, 2011;

Unipetrol, 2010; Ensyn Technologies Inc., 2007; Olefins Panel of the American

Chemistry Council, 2005; Zhang *et al*., 2007; Wonkhorsub and Chindaprasert, 2013;

European Chemicals Agency, 2013; Griffin Industries, 2007; Backyard Biodiesel, LLC,

2011; Illinois Sustainable Technology Center – Waste Management and Research Center,

2006; Zhang *et al*., 2003; Liu and Kim, 1999).

Table 5-3. Summary of Temperature-Related Parameters for Various Fuels.

Fuel	Melting Point (°F)	Boiling Point (°F)	Flash Point (°F)	Autoignition Temperature (°F)
Biodiesel	n/a	298	100	351
	n/a	> 392	n/a	n/a
	n/a	300-691	126-140	611
	n/a	300-691	126-180	611
	n/a	> 399	n/a	n/a
	<< 8.6	> 392	266	n/a
	32-35.6	644-707	130	944-1088
Low-sulfur fuel oil	-20.2	325-700	n/a	n/a
	n/a	320-700	> 126	n/a
	n/a	340-675	n/a	n/a
	n/a	340-700	n/a	n/a
	-22 – -0.4	540-640	125.6	489-545

Table 5-3, cont.

Fuel	Melting Point (°F)	Boiling Point (°F)	Flash Point (°F)	Autoignition Temperature (°F)
Jatropha oil	n/a	n/a	464	n/a
	39-41	426	235	n/a
Palm oil	95	n/a	n/a	n/a
	97-100	n/a	n/a	n/a
	95-104	n/a	n/a	n/a
	77+	> 212	n/a	n/a
	108-140	568-689	> 212	> 482
	106	471	280	373
Pyrolysis oil	n/a	> 212	104-230?	932
	45	338	140-200	644
	n/a	336-1074	219	658
	59	392-572	> 214	> 842
	n/a	n/a	144-210	n/a
	2 – 77	212 – 482-536	154 – 212	851
Yellow grease	86	n/a – decomposes	399	n/a
	86	n/a – decomposes	399	n/a
	86	516	302	689 – 702

5.4 Fuel Corrosivity

Corrosion is a problem with biofuels as they generally have greater acid content, absorb more water, and have higher oxidative characteristics than petroleum-based fuels (Burton, 2008; Jayed *et al*., 2009). Generally corrosion is caused by a number of factors, including "free water, free FAME, corrosive acids (formic & acetic), free methanol, NaOH or KOH particles in fuel, high viscosity at low temperatures, iodine value, [and] total acid number" (Jayed *et al*., 2009). The corrosion behavior of Indian seed oil-derived biodiesels on engine parts was studied, and it was determined that *Salvadora oleoides*-derived biodiesels showed marked corrosion, while oils derived from *Jatropha curcas*, *Pongamia glabra*, and *Madhuca indica* showed little or no corrosion of the engine parts (Kaul *et al*., 2007). It was demonstrated that copper and/or brass components were most

susceptible to corrosion by poultry fat and diesel fuel mixtures and should generally be avoided; in addition, grey cast iron showed slight corrosion and should perhaps be avoided as well (Geller *et al*., 2007). Furthermore, it has been shown that anaerobic metabolism of biodiesel can lead to its degradation and subsequently increase corrosive activity (Aktas *et al*., 2010).

However, it has been demonstrated that even increasing the amount of incompletely converted soybean oil may not have a significant effect on its copper strip corrosion (Fernando *et al*., 2007). Other researchers have studied the effects of soybean- and sunflower-derived biodiesels on carbon steel and found that, while there was a low level of surface etching, the weight loss was minimal. HDPE polymers, however, underwent a weight gain in the order of 10^{-4} g due to absorption (Maru *et al*., 2009).

Additives may be used to reduce corrosion. It was demonstrated that use of an anticorrosion additive with a palm oil diesel not only reducee corrosion but also increasee brake power, reduced exhaust emissions, decreased wear metal, and decreased total base number (Kalam and Masjuki, 2002). Other researchers showed that *tert*-butylamine was a more effective corrosion inhibitor than ethylenediamine and *n*-butylamine for attack by palm-based biodiesel (Fazal *et al*., 2011).

5.5 Summary

Little to no information was available in the literature on the miscibility of crude bio-based oils with petroleum-based oils. It was decided to study the miscibility of blends of lo-pour fuel oil, hi-pour fuel oil, ultra-low sulfur diesel, crude jatropha oil, crude palm oil, biocrude derived from animal renderings, and biodiesel (refined biocrude) in order to determine if there were any adverse effects that arose from their blends. It was decided to

study these blends at 75°F (ambient temperature), 170°F (temperature in oil storage tanks), and 220°F (temperature to which oils are heated just before combustion) to determine any differences in the behavior of the oil blends at different temperatures. Adverse effects could include events such as excess settling of waxes, smoking, or semi-polymerization of the oils.

It was decided to study the pour point, flash point, and wax appearance temperature of select pure oils and oil blends to attempt to determine whether any synergistic properties might exist for these blends or whether a simple correlation could be used to predict, for example, what the wax appearance temperature for an oil blend would be given the wax appearance temperatures of its constituent pure oils.

While some information on corrosion is available in the literature, the potential corrosive activity of crude palm oil, biocrude derived from animal renderings, and biodiesel refined from the same does not seem to have been studied. It was decided to expose metal samples representative of those that might be encountered in a typical oil-fired power plant to these oils as well as crude jatropha oil, ultra-low sulfur diesel, lo-pour fuel oil, and hi-pour fuel oil in order to study any adverse effects these oils might have.

CHAPTER VI
EXPERIMENTAL METHODS – BIOFUELS

6.1   Fuels Tested

Seven different oils were sourced for testing. These oils, along with their original

sources, are listed in Table 6-1. The qualitative difference between hi-pour fuel oil and

lo-pour fuel oil is the viscosity: hi-pour fuel oil, which has a (reasonably) high reported

pour point of about 55°F, has the approximate viscosity of lard, while lo-pour fuel oil,

which has a reported pour point of about 30°F, has the approximate viscosity of slightly

cooled corn oil.

Table 6-1. Fuel oils tested.

Oil	Source
Hi-Pour Fuel Oil	Petrospect
Lo-Pour Fuel Oil	Petrospect
Crude Jatropha Oil	Original Source Unknown
Biocrude derived from animal renderings	REG Newton
Biodiesel (refined biocrude)	REG Newton
Crude Palm Oil	Sime Darby Biodiesel
Ultra-Low Sulfur Diesel	Purchased at Valley Dairy gas station in Grand Forks, ND – original source unknown

6.2   Miscibility Testing

Oils were mixed in ½ cup portions for a total of approximately 1 cup of blended

oils per sample. This mixing occurred at three distinct temperatures: 75°F (ambient

temperature for subtropical/tropical power stations), 170°F (storage temperature in the

tanks in the tank farm), and 220°F (temperature to which the oils are heated before

feeding to the burner.

For testing at 75°F, oils were combined in a beaker and (if necessarily) slightly heated to 75°F. The oils were then blended by stirring at the highest achievable RPM on the heating/stir plate (i.e., before the magnetic stir bar went out of balance) for five minutes; most oils were stirred at about 1200 RPM for five minutes.

For testing at 170°F, oils were combined in a beaker and heated to 170°F. The oils were then blended by stirring at the highest achievable RPM on the heating/stir plate, which was typically about 1200 RPM, for five minutes.

For testing at 220°F, oils were combined in a beaker and heated to 220°F. The oils were then blended by stirring at the highest achievable RPM on the heating/stir plate, which was typically about 1200 RPM, for five minutes.

After the oils were blended, they were photographed and visually examined for effective miscibility. The blended oils were then allowed to sit at the testing temperature (i.e., 75°F, 170°F, or 220°F) on a hot plate for a further 25 minutes without stirring, at which point they were examined again for separation of entrained solids or overall separation of oils. Again, the blends were photographed at the end of the 25 minutes. The oils were then placed in an oven maintained at the desired testing temperature and allowed to sit for an extended period of time (2 days – ~1.5 years, depending on the sample) in order to examine for further separation.

The samples heated to 170°F and 220°F were cooled to 75°F in order to test for any difficulties with the blends in the scenario that heating would be lost within the plant. The samples were allowed to sit for an extended period of time at the cooler temperature to examine for any separation of entrained solids, formation of sludge, or overall separation of oils. The samples were photographed again at the end of this period.

6.3   Characterization of Individual Fuels and Fuel Blends

In general, liquid fuels (petroleum-based) are analyzed for the following properties: composition and heating value by means of proximate and ultimate analysis, specific gravity, viscosity, flash point, and pour point. Each individual fuel in testing was analyzed for composition and heating value using proximate/ultimate analysis; this analysis was not performed on each blend of fuels, as these properties would be additive.

However, flash point, cloud point, and pour point may not be additive properties. Tests were consequently conducted to determine the flash point, pour point, and cloud point for select pure fuels and fuel blends. Viscosity testing was not conducted because of equipment limitations.

Flash point was determined using an Elcometer 6910/3 Setaflash Series 3 ActiveCool flash point tester. This is in accordance with ASTM D93.

Pour point was determined using a Multipoint Phase Technology 70X Series analyzer. This instrument operates in accordance with ASTM D97.

Cloud point was determined using a proprietary method developed in-house to find the wax appearance temperature. This method provides a conservative estimate of the wax point, as most wax points are determined by filter plugging. The cloud point determined by this method provided the first potential problem temperature.

6.4   Corrosion Testing

The main alloys in use at most power stations are 304 stainless steel, 316 stainless steel, brass/bronze, mild steel, aluminum, and Monel. In addition, 410 stainless steel is a common alloy in wetted parts in fuel pumps. It was determined that aluminum and Monel did not need to be analyzed for susceptibility to corrosion for two reasons: 1.) these

106

metals are usually not present in large amounts at power stations and 2.) these metals are not typically susceptible to corrosion because of passivating behavior. Therefore, five metals were selected for corrosion testing: 304 stainless steel, 316 stainless steel, brass, mild steel, and 410 stainless steel.

Samples of each metal were cut into 1" wide pieces (typically also 1" tall). These samples were then prepared by sanding all surfaces with 120 grit sandpaper. This was done in order to remove enough material to get below any variations in the metal surface, and remove any oil, grease, or other contaminants. Each metal type was polished with its own piece of sandpaper in order to avoid cross-contamination of metals, which could have led to erroneous results through galvanic corrosion effects.

All of the seven oils were used in the corrosion testing. The metal samples were each immersed in excess oil in 4oz jars, allowed to sit on the bottom of the jar, and placed in an oven at 175°F.

The metal samples were weighed, measured using a caliper, and photographed prior to corrosion testing and each time they were removed from the oven. The samples were removed from the oven and examined every two weeks for mass loss and change in appearance. Excess oils were removed by running the samples under water while scrubbing them with a rubber stopper.

CHAPTER VII
RESULTS AND DISCUSSION – BIOFUELS

7.1   Miscibility Test Results
7.1.1   Oils Blended at 75°F

This blending temperature represents a worst-case scenario for many tropical and subtropical plants, as this temperature should never be experienced unless the heating and stirring on the storage tanks fails for an extended period of time.

Blends are considered to be failures if the qualitative viscosity was too high, i.e., if the blend failed to flow, or if a significant amount of solids settled out of solution. For this chapter, "solids" is defined as waxes, which essentially are longer-chain fuel molecules which are too heavy to remain suspended in solution. The main cause of the failure at this temperature was solids settling, which could be problematic in the event of a prolonged heating and stirring failure in the storage tank and/or any heat-traced line. In addition, it was found that blends of crude palm oil with both hi-pour and lo-pour fuel oil were resistant to mechanical mixing. These blends could be manually stirred, and this may be a limitation of the magnetic stir plate used. The main problem with palm oil is its semi-solid characteristics at relatively low temperatures, in addition to its high concentration of solids.

Table 7-1 shows the elapsed time between initial blending and final photos of each oil blend. This indicates how long a blend was held at 75°F, which can affect factors such as particulate settling.

Table 7-1. Elapsed time between blending and final photos, 75°F.

Oil Blend	Elapsed Time (days)
Hi-Pour – Palm	8
Hi-Pour – Jatropha	556
Hi-Pour – Biocrude	8
Hi-Pour – Biodiesel	9
Hi-Pour – Ultra-low Sulfur Diesel	9
Lo-Pour – Palm	492
Lo-Pour – Jatropha	492
Lo-Pour – Biocrude	374
Lo-Pour – Biodiesel	492
Lo-Pour – Ultra-low Sulfur Diesel	374
Palm – Jatropha	567
Palm – Biocrude	560
Palm – Biodiesel	560
Palm – Ultra-low Sulfur Diesel	370
Jatropha – Biocrude	560
Jatropha – Biodiesel	560
Jatropha – Ultra-low Sulfur Diesel	373
Biocrude – Ultra-low Sulfur Diesel	373
Biodiesel – Ultra-low Sulfur Diesel	371

Figure 7-1 shows photos of a blend of hi-pour fuel oil and crude palm oil. This blend resisted stirring on the magnetic stir plate, but was able to be stirred by hand for the required five minutes. At ambient temperatures, this blend would be a poor fuel; however, it most likely would be pourable. The tops of the beakers in these photos indicate that the crude palm oil (yellow areas) did not fully blend with the hi-pour fuel oil.

(a)   **(b)**   **(c)**

Figure 7-1. Hi-pour fuel oil – crude palm oil blend, mixed and held at 75°F. (a) immediately after five minutes of stirring, (b) 25 minutes after stirring, (c) eight days after stirring.

Figure 7-2 shows photos of a blend of hi-pour fuel oil and crude jatropha oil. This blend could be easily mixed and was completely miscible; in fact, addition of the jatropha oil lowered the viscosity of the blend as compared to the hi-pour fuel oil. At ambient temperatures, this would be a good fuel. The qualitative viscosity of the blend did not change during storage. This indicates no formation of sludge or gels that would be evidence of chemical change, implying that this blend had an acceptable shelf life.

(a)   (b)   (c)

Figure 7-2. Hi-pour fuel oil – crude jatropha oil blend, mixed and held at 75°F. (a) immediately after five minutes of stirring, (b) 25 minutes after stirring, (c) 556 days after stirring.

Figure 7-3 shows photos of a blend of hi-pour fuel oil and biocrude derived from animal renderings. While initially this blend was resistant to stirring on the magnetic stir plate, a little manual stirring was sufficient to get it moving. This is most likely due to the high wax content of both the hi-pour fuel oil and biocrude derived from animal renderings. This combined wax content would make this a poor fuel blend at ambient temperatures.

| **(a)** | **(b)** | **(c)** |

Figure 7-3. Hi-pour fuel oil – biocrude blend, mixed and held at 75°F. (a) immediately after five minutes of stirring, (b) 25 minutes after stirring, (c) eight days after stirring.

Figure 7-4 shows photos of a blend of hi-pour fuel oil and biodiesel (refined biocrude). This blend was easily mixed and was completely miscible; in fact, addition of the biodiesel lowered the viscosity of the blend as compared to the hi-pour fuel oil. At ambient temperatures, based on the viscosity and miscibility, this would be a good fuel blend.

| **(a)** | **(b)** | **(c)** |

Figure 7-4. Hi-pour fuel oil – biodiesel blend, mixed and held at 75°F. (a) immediately after five minutes of stirring, (b) 25 minutes after stirring, (c) nine days after stirring.

Figure 7-5 shows photos of a blend of hi-pour fuel oil and ultra-low sulfur diesel. This blend was easily mixed and completely miscible; again, the addition of the ultra-low sulfur diesel lowered the viscosity of the hi-pour fuel oil. Based on the miscibility and the viscosity, this would be a good fuel blend at ambient temperatures.

111

| (a) | (b) | (c) |

Figure 7-5. Hi-pour fuel oil – ultra-low sulfur diesel blend, mixed and held at 75°F. (a) immediately after five minutes of stirring, (b) 25 minutes after stirring, and (c) nine days after stirring.

Figure 7-6 shows photos of a blend of lo-pour fuel oil and crude palm oil after attempted blending. This mixture resisted blending, even manually, and had the approximate consistency of cottage cheese. However, during storage, the two oils did mix together. This may be caused by the high concentration of saturated fatty acids and monounsaturated oleic acid of palm oil, which may have increased its polarity above that of the lo-pour fuel oil. Regardless, because of the high viscosity and low initial miscibility, this would be a poor fuel blend at ambient temperatures.

| (a) | (b) |
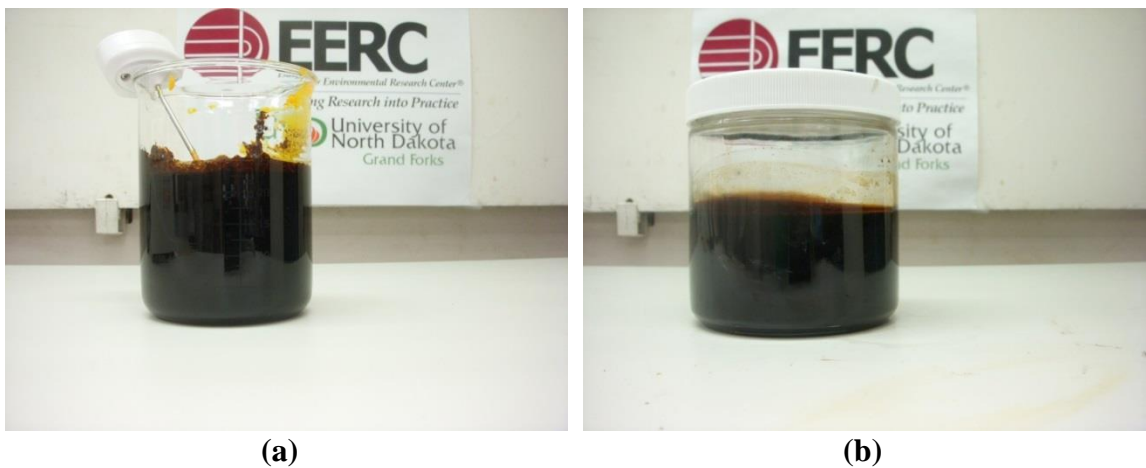
Figure 7-6. Lo-pour fuel oil – crude palm oil blend, mixed and held at 75°F. (a) immediately after attempted blending, (b) 492 days after attempted blending.

Figure 7-7 shows photos of a blend of lo-pour fuel oil and crude jatropha oil. This blend was easily mixed and completely miscible; in fact, the crude jatropha oil qualitatively improved the viscosity of the lo-pour fuel oil. At ambient temperatures, this would be a good fuel. The qualitative viscosity of the blend did not change during storage. This indicates no formation of sludge or gels that would be evidence of chemical change, implying that this blend had an acceptable shelf life.

(a)   (b)   (c)

Figure 7-7. Lo-pour fuel oil – crude jatropha oil blend, mixed and held at 75°F. (a) immediately after five minutes of stirring, (b) 25 minutes after stirring, (c) 492 days after stirring.

Figure 7-8 shows photos of a blend of lo-pour fuel oil and biocrude from animal renderings. This blend was initially resistant to mechanical stirring on the magnetic stir plate, though a little manual stirring was sufficient to overcome this. This is most likely due to the high wax content of both the hi-pour fuel oil and biocrude derived from animal renderings. This combined wax content, along with ambiguity about whether any waxes settled to the bottom of the jar in which it was stored due to the opacity of the hi-pour fuel oil, would make this a poor fuel blend at ambient temperatures.

113

(a)	**(b)**	**(c)**

Figure 7-8. Lo-pour fuel oil – biocrude blend, mixed and held at 75°F. (a) immediately after five minutes of stirring, (b) 25 minutes after stirring, (c) 374 days after stirring.

Figure 7-9 shows photos of a blend of lo-pour fuel oil and biodiesel (refined biocrude). This blend was easily mixed and completely miscible; in fact, the addition of the biodiesel lowered the viscosity of the blend as compared to the lo-pour fuel oil. At ambient temperatures, this would be a good fuel. The qualitative viscosity of the blend did not change during storage. This indicates no formation of sludge or gels that would be evidence of chemical change, implying that this blend had an acceptable shelf life.

(a)	**(b)**	**(c)**

Figure 7-9. Lo-pour fuel oil – biodiesel blend, mixed and held at 75°F. (a) immediately after five minutes of stirring, (b) 25 minutes after stirring, (c) 492 days after stirring.

Figure 7-10 shows photos of a blend of lo-pour fuel oil and ultra-low sulfur diesel. This blend was easily mixed and completely miscible; in fact, the addition of the ultra-low sulfur diesel lowered the viscosity of the blend as opposed to the lo-pour fuel oil. At ambient temperatures, this would be a good fuel. The qualitative viscosity of the

blend did not change during storage. This indicates no formation of sludge or gels that would be evidence of chemical change, implying that this blend had an acceptable life.

| (a) | (b) | (c) |

Figure 7-10. Lo-pour fuel oil – ultra-low sulfur diesel blend, mixed and held at 75°F. (a) immediately after five minutes of stirring, (b) 25 minutes after stirring, (c) 374 days after stirring.

Figure 7-11 shows photos of a blend of crude palm oil and crude jatropha oil. Immediately after stirring, the two oils appeared well-mixed; however, as soon as 25 minutes later, palm solids, which are primarily waxes, had already begun to settle out of solution. This indicates that, in the absence of constant stirring, a layer of solids could settle out in a storage tank. Over time, this layer of solids could plug the tank outlet, leading to additional maintenance costs. If the solids settled in a pipeline, they could plug the pipeline or lead to favorable environments for pitting or erosion corrosion. Thus, this blend is marginally acceptable because of the risk of waxes settling out of solution.

| (a) | (b) | (c) |

Figure 7-11. Crude palm oil – crude jatropha oil blend, mixed and held at 75°F. (a) immediately after five minutes of stirring, (b) 25 minutes after stirring, (c) 567 days after stirring.

Figure 7-12 shows photos of a blend of crude palm oil and biocrude from animal renderings. There is a high concentration of solids in this oil blend, making it fairly viscous. This is especially clear in Figure 7-12c, where a large amount of solids have settled to the bottom of the jar. In the absence of constant stirring, a layer of solids could settle out in a storage tank. Over time, this layer of solids could plug the tank outlet, leading to additional maintenance costs. If the solids settled in a pipeline, they could plug the pipeline or lead to favorable environments for pitting or erosion corrosion. Thus, this blend is marginally acceptable because of the risk of waxes settling out of solution.

| (a) | (b) | (c) |

Figure 7-12. Crude palm oil – biocrude blend, mixed and held at 75°F. (a) immediately after five minutes of stirring, (b) 25 minutes after stirring, (c) 560 days after stirring.

Figure 7-13 shows photos of a blend of crude palm oil and biodiesel (refined biocrude). In less than 25 minutes after stirring, a layer of palm solids settled to the

116

bottom of the beaker. In a fuel tank, this could lead to problems with solids settling out,

leading to long-term issues such as poor tank drainage and additional maintenance costs.

In the absence of constant stirring, a layer of solids could settle out in a storage tank.

Over time, this layer of solids could plug the tank outlet, leading to additional

maintenance costs. If the solids settled in a pipeline, they could plug the pipeline or lead

to favorable environments for pitting or erosion corrosion. Thus, this blend is marginally

acceptable because of the risk of waxes settling out of solution.

| (a) | (b) | (c) |

Figure 7-13. Crude palm oil – biodiesel blend, mixed and held at 75°F. (a) immediately after five minutes of stirring, (b) 25 minutes after stirring, (c) 560 days after stirring.

Figure 7-14 shows photos of a blend of crude palm oil and ultra-low sulfur diesel.

The whole blended fuel turned into a thick sludge. Upon initial addition of the diesel to

the palm oil, the mixture cooled by 6°F. Since this behavior was not observed with any

other oil blend, it was conjectured that some sort of endothermic reaction took place

between these oils.

Figure 7-14. Crude palm oil – ultra-low sulfur diesel blend, mixed and held at 75°F. (a) immediately after five minutes of stirring, (b) 25 minutes after stirring, (c) 370 days after stirring.

Figure 7-15 shows photos of a blend of crude jatropha oil and biocrude derived from animal renderings. Addition of jatropha oil to biocrude derived from animal renderings improved the viscosity as compared to the biocrude alone, but the high concentration of solids in biocrude could still potentially lead to processing problems, such as poor tank drainage, in an unheated and unstirred worst-case scenario. Thus, this blend is marginally acceptable because of the risk of solids settling and leading to pitting, erosion corrosion, and increased maintenance costs due to plugging.
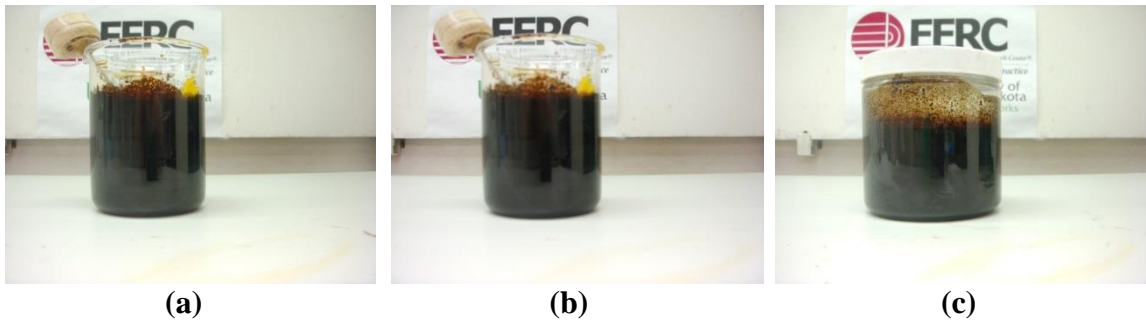

Figure 7-15. Crude jatropha oil – biocrude blend, mixed and held at 75°F. (a) immediately after five minutes of stirring, (b) 25 minutes after stirring, (c) 560 days after stirring.

Figure 7-16 shows photos of a bend of crude jatropha oil and biodiesel (refined biocrude). This blend could be easily mixed, had low viscosity, was completely miscible, and had no solids settling. Thus, this blend would be a good fuel at ambient temperatures.

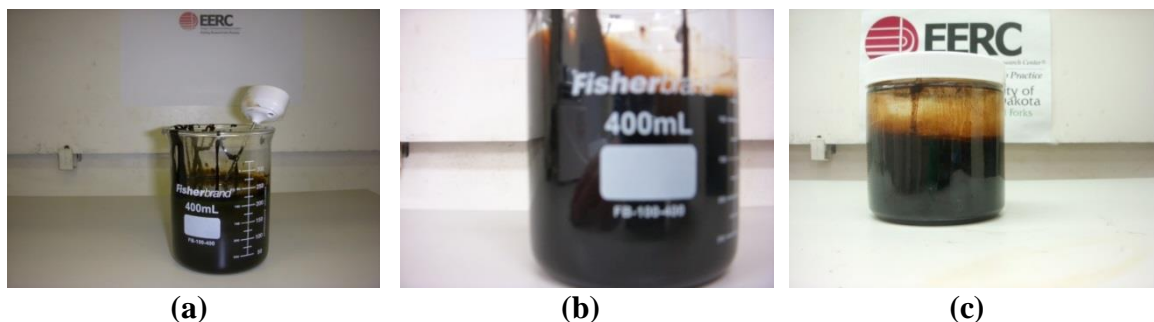|		
(a)	**(b)**	**(c)**

Figure 7-16. Crude jatropha oil – biodiesel blend, mixed and held at 75°F. (a) immediately after five minutes of stirring, (b) 25 minutes after stirring, (c) 560 days after stirring.

Figure 7-17 shows photos of a blend of crude jatropha oil and ultra-low sulfur diesel. This blend could be easily mixed, had low viscosity, was completely miscible, and had no solids settling. Thus, this blend would be a good fuel at ambient temperatures.

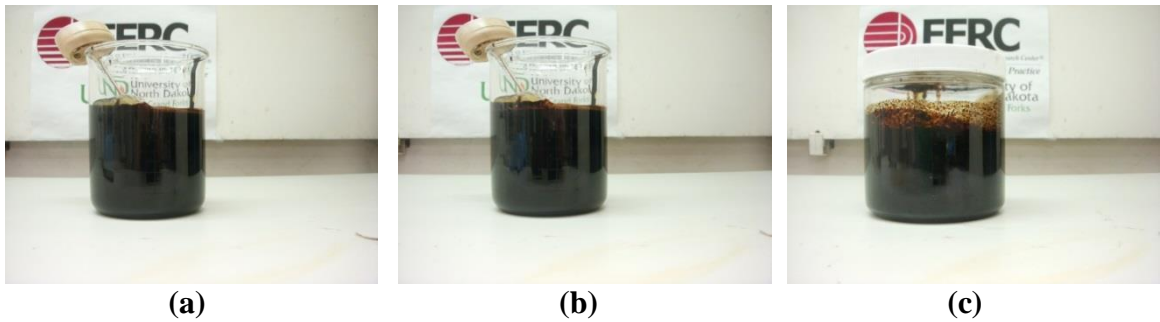|		
(a)	**(b)**	**(c)**

Figure 7-17. Crude jatropha oil – ultra-low sulfur diesel blend, mixed and held at 75°F. (a) immediately after five minutes of stirring, (b) 25 minutes after stirring, (c) 373 days after stirring.

Figure 7-18 shows photos of a blend of biocrude derived from animal renderings and ultra-low sulfur diesel. Within 25 minutes, a layer of biocrude-derived solids began settling out of solution. These solids could pose processing problems, such as poor tank

drainage, in an unheated worst-case scenario. Thus, this blend is marginally acceptable because of the risk of solids settling and leading to pitting, erosion corrosion, and increased maintenance costs due to plugging.

| (a) | (b) | (c) |

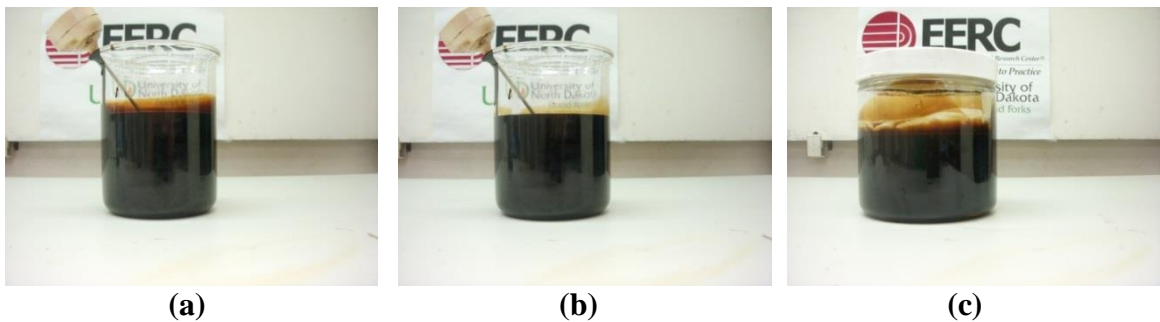**Figure 7-18.** Biocrude – ultra-low sulfur diesel blend, mixed and held at 75°F. (a) immediately after five minutes of stirring, (b) 25 minutes after stirring, (c) 373 days after stirring.

Figure 7-19 shows photos of a blend of biodiesel (refined biocrude) and ultra-low sulfur diesel. This blend could be easily mixed, had low viscosity, was completely miscible, and had no solids settling. Thus, this blend would be a good fuel at ambient temperatures.

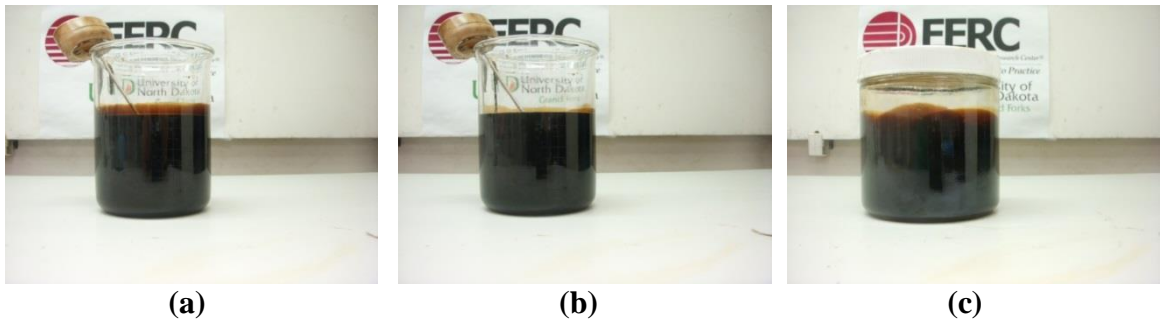| (a) | (b) | (c) |

Figure 7-19. Biodiesel – ultra-low sulfur diesel blend, mixed and held at 75°F. (a) immediately after five minutes of stirring, (b) 25 minutes after stirring, and (c) 371 days after stirring.

Based on the above results, Table 7-2 shows the miscibility of fuel blends at 75°F; duplicate blends are filled in with black boxes to alleviate confusion, and grey boxes

indicate pure oils. This is the acceptability at the worst-case scenario in which a storage

tank would lose heat for an extended period of time. The main cause of failure at this

temperature was entrained waxes that had a tendency to settle out of solution, as

discussed above for affected oil blends.

Table 7-2. Fuel blend acceptability at 75°F.

	Lo-Pour Fuel Oil	Hi-Pour Fuel Oil	Biocrude (animal)	Crude Jatropha Oil	Crude Palm Oil	Biodiesel (refined biocrude)	Ultra-low sulfur diesel
Lo-Pour Fuel Oil		Not Tested	Marginal	Yes	No	Yes	Yes
Hi-Pour Fuel Oil			Marginal	Yes	No	Yes	Yes
Biocrude (animal)				Marginal	No	Not Tested	Marginal
Crude Jatropha Oil					Marginal	Yes	Yes
Crude Palm Oil						Marginal	No
Biodiesel (refined biocrude)							Yes
Ultra-low sulfur diesel							

7.1.2 Oils Blended at 170°F

This blending temperature is approximately equal to the average temperature of oil

storage tanks in industry. Table 7-3 shows the elapsed time between initial blending and

final photos of each oil blend. This indicates how long a blend was held at 170°F.

Table 7-3. Elapsed time between blending and final photos, 170°F.

Oil Blend	Elapsed Time (days)
Hi-Pour – Palm	2
Hi-Pour – Jatropha	2
Hi-Pour – Biocrude	2
Hi-Pour – Biodiesel	2

Table 7-3, cont.

Oil Blend	Elapsed Time (days)
Hi-Pour – Ultra-low Sulfur Diesel	2
Lo-Pour – Palm	4
Lo-Pour – Jatropha	4
Lo-Pour – Biocrude	4
Lo-Pour – Biodiesel	5
Lo-Pour – Ultra-low Sulfur Diesel	5
Palm – Jatropha	5
Palm – Biocrude	5
Palm – Biodiesel	5
Palm – Ultra-low Sulfur Diesel	6
Jatropha – Biocrude	6
Jatropha – Biodiesel	6
Jatropha – Ultra-low Sulfur Diesel	6
Biocrude – Ultra-low Sulfur Diesel	6
Biodiesel – Ultra-low Sulfur Diesel	6

Figure 7-20 shows photos of a blend of hi-pour fuel oil and crude palm oil. This blend could be easily mixed, had low viscosity, and was completely miscible. Thus, this blend would be a good fuel at 170°F.
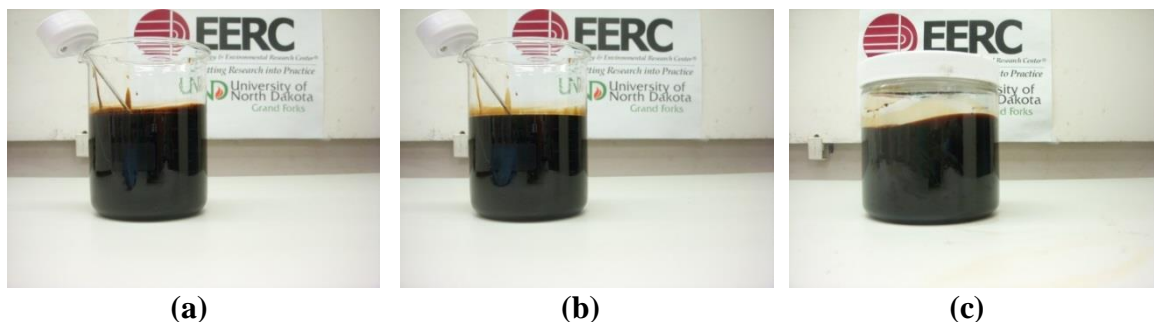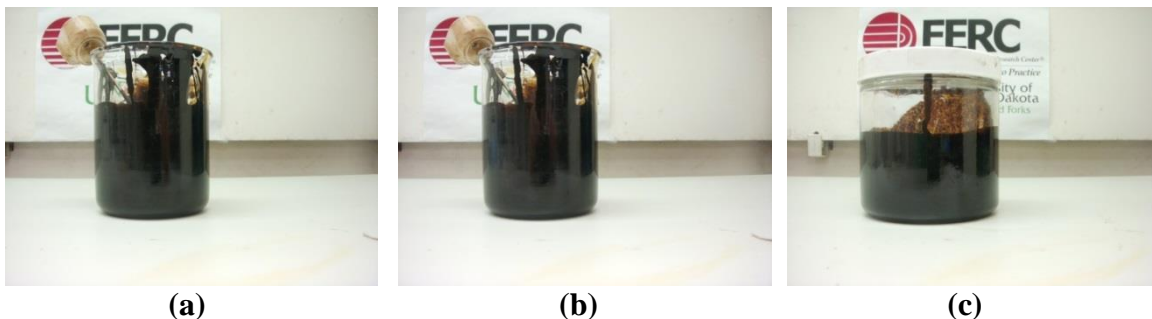

| (a) | (b) | (c) |

Figure 7-20. Hi-pour fuel oil – crude palm oil blend, mixed and held at 170°F. (a) immediately after five minutes of stirring, (b) 25 minutes after stirring, (c) two days after stirring.

Figure 7-21 shows photos of a blend of hi-pour fuel oil and crude jatropha oil. This blend could be easily mixed, had low viscosity, and was completely miscible. Thus, this blend would be a good fuel at 170°F.

| (a) | (b) | (c) |

Figure 7-21. Hi-pour fuel oil – crude jatropha oil blend, mixed and held at 170°F. (a) immediately after five minutes of stirring, (b) 25 minutes after stirring, (c) two days after stirring.

Figure 7-22 shows photos of a blend of hi-pour fuel oil and biocrude derived from animal renderings. This blend could be easily mixed, had low viscosity, and was completely miscible. Thus, this blend would be a good fuel at 170°F.
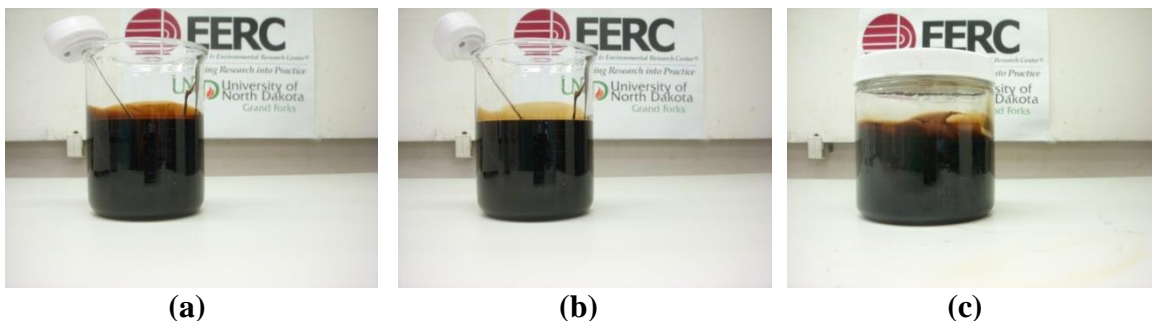

| (a) | (b) | (c) |

Figure 7-22. Hi-pour fuel oil – biocrude blend, mixed and held at 170°F. (a) immediately after five minutes of stirring, (b) 25 minutes after stirring, (c) two days after stirring.

Figure 7-23 shows photos of a blend of hi-pour fuel oil and biodiesel (refined biocrude). This blend could be easily mixed, had low viscosity, and was completely miscible. Thus, this blend would be a good fuel at 170°F.

123

| **(a)** | **(b)** | **(c)** |

Figure 7-23. Hi-pour fuel oil – biodiesel blend, mixed and held at 170°F. (a) immediately after five minutes of stirring, (b) 25 minutes after stirring, (c) two days after stirring.

Figure 7-24 shows photos of a blend of hi-pour fuel oil and ultra-low sulfur diesel. This blend could be easily mixed, had low viscosity, and was completely miscible. Thus, this blend would be a good fuel at 170°F.

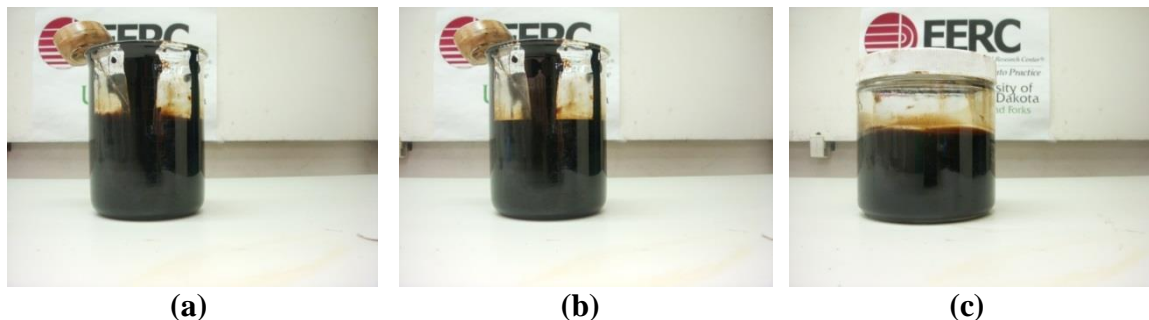| **(a)** | **(b)** | **(c)** |

Figure 7-24. Hi-pour fuel oil – ultra-low sulfur diesel blend, mixed and held at 170°F. (a) immediately after five minutes of stirring, (b) 25 minutes after stirring, (c) two days after stirring.

Figure 7-25 shows photos of a blend of lo-pour fuel oil and crude palm oil. This blend could be easily mixed, had low viscosity, and was completely miscible. Thus, this blend would be a good fuel at 170°F.

| (a) | (b) | (c) |

Figure 7-25. Lo-pour fuel oil – crude palm oil blend, mixed and held at 170°F. (a) immediately after five minutes of stirring, (b) 25 minutes after stirring, (c) four days after stirring.

Figure 7-26 shows photos of a blend of lo-pour fuel oil and crude jatropha oil. This blend could be easily mixed, had low viscosity, and was completely miscible. Thus, this blend would be a good fuel at 170°F.
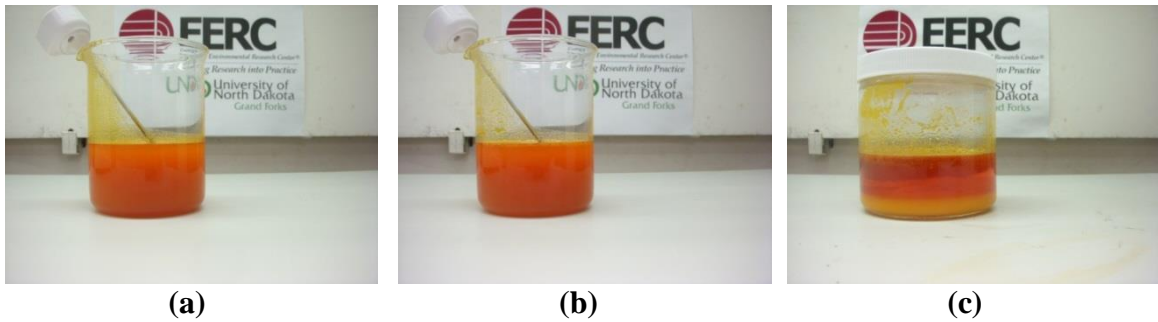

| (a) | (b) | (c) |

Figure 7-26. Lo-pour fuel oil – crude jatropha oil blend, mixed and held at 170°F. (a) immediately after five minutes of stirring, (b) 25 minutes after stirring, (c) four days after stirring.

Figure 7-27 shows photos of a blend of lo-pour fuel oil and biocrude derived from animal renderings. This blend could be easily mixed, had low viscosity, and was completely miscible. Thus, this blend would be a good fuel at 170°F.

(a)	**(b)**	**(c)**

Figure 7-27. Lo-pour fuel oil – biocrude blend, mixed and held at 170°F. (a) immediately after five minutes of stirring, (b) 25 minutes after stirring, (c) four days after stirring.

Figure 7-28 shows photos of a blend of lo-pour fuel oil and biodiesel (refined biocrude). This blend could be easily mixed, had low viscosity, and was completely miscible. Thus, this blend would be a good fuel at 170°F.

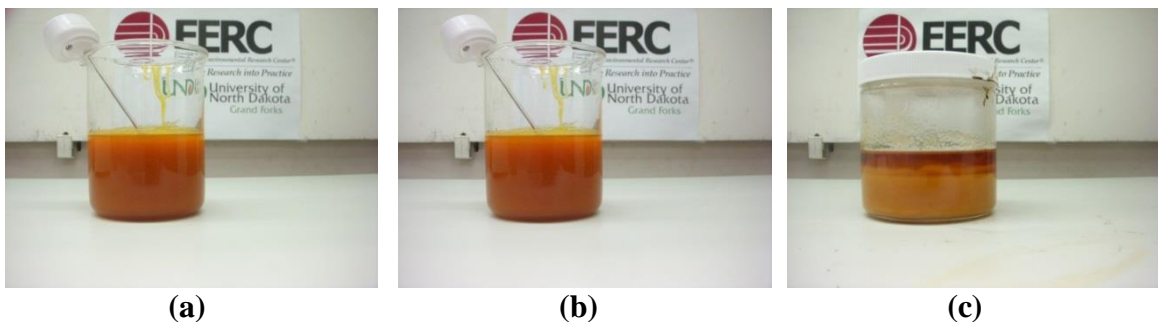|		
(a)	**(b)**	**(c)**

Figure 7-28. Lo-pour fuel oil – biodiesel blend, mixed and held at 170°F. (a) immediately after five minutes of stirring, (b) 25 minutes after stirring, (c) five days after stirring.

Figure 7-29 shows photos of a blend of lo-pour fuel oil and ultra-low sulfur diesel. This blend could be easily mixed, had low viscosity, and was completely miscible. Thus, this blend would be a good fuel at 170°F.

126

| (a) | (b) | (c) |

Figure 7-29. Lo-pour fuel oil – ultra-low sulfur diesel blend, mixed and held at 170°F. (a) immediately after five minutes of stirring, (b) 25 minutes after stirring, (c) five days after stirring.

Figure 7-30 shows photos of a blend of crude palm oil and crude jatropha oil. This blend could be easily mixed, had low viscosity, was completely miscible, and had zero solids settling. Thus, this blend would be a good fuel at 170°F.

| (a) | (b) | (c) |

Figure 7-30. Crude palm oil – crude jatropha oil blend, mixed and held at 170°F. (a) immediately after five minutes of stirring, (b) 25 minutes after stirring, (c) five days after stirring.

Figure 7-31 shows photos of a blend of crude palm oil and biocrude derived from animal renderings. This blend could be easily mixed, had low viscosity, was completely miscible, and had zero solids settling. Thus, this blend would be a good fuel at 170°F.

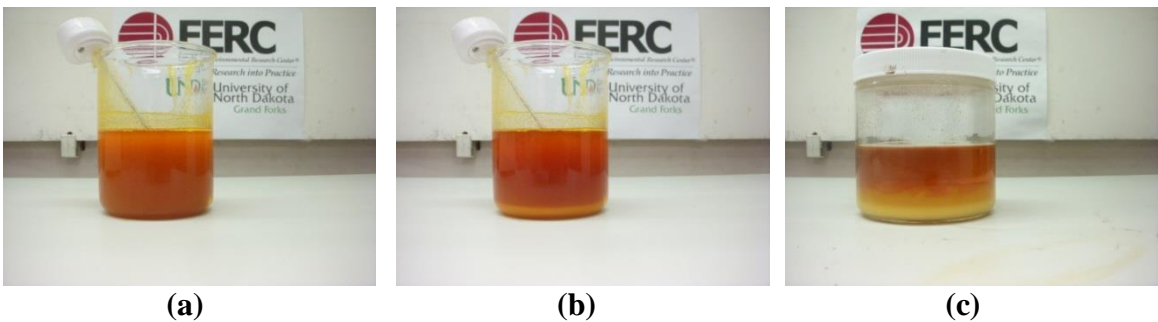**(a)**   **(b)**   **(c)**

Figure 7-31. Crude palm oil – biocrude blend, mixed and held at 170°F. (a) immediately after five minutes of stirring, (b) 25 minutes after stirring, (c) five days after stirring.

Figure 7-32 shows photos of a blend of crude palm oil and biodiesel (refined biocrude). This blend could be easily mixed, had low viscosity, was completely miscible, and had zero solids settling. Thus, this blend would be a good fuel at 170°F.

(a)   **(b)**   **(c)**

Figure 7-32. Crude palm oil – biodiesel blend, mixed and held at 170°F. (a) immediately after five minutes of stirring, (b) 25 minutes after stirring, (c) five days after stirring.

Figure 7-33 shows photos of a blend of crude palm oil and ultra-low sulfur diesel. This blend could be easily mixed, had low viscosity, was completely miscible, and had zero solids settling. Thus, this blend would be a good fuel at 170°F.

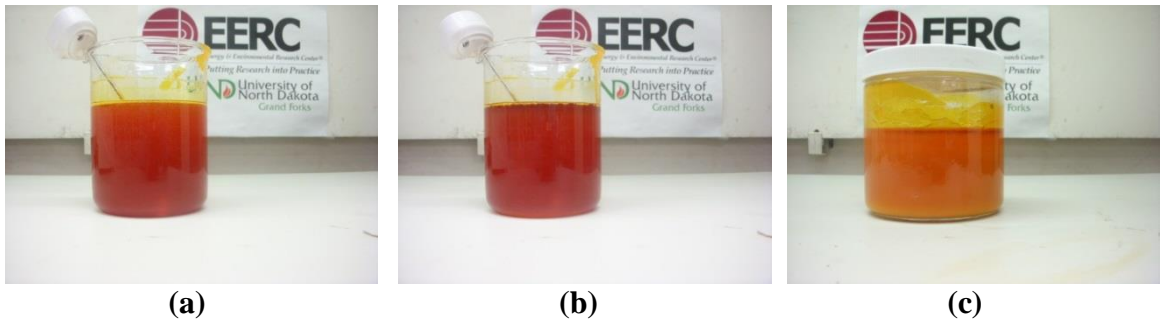| (a) | (b) | (c) |

Figure 7-33. Crude palm oil – ultra-low sulfur diesel blend, mixed and held at 170°F. (a) immediately after five minutes of stirring, (b) 25 minutes after stirring, (c) six days after stirring.

Figure 7-34 shows photos of a blend of crude jatropha oil and biocrude derived from animal renderings. This blend could be easily mixed, had low viscosity, was completely miscible, and had zero solids settling. Thus, this blend would be a good fuel at 170°F.
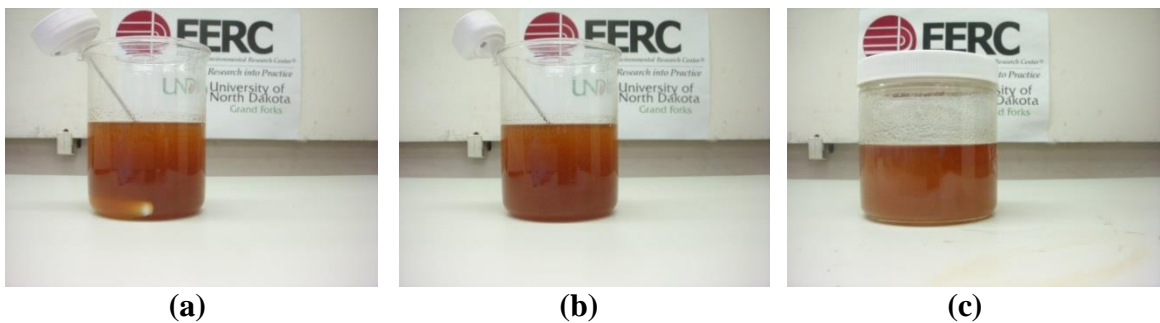

| (a) | (b) | (c) |

Figure 7-34. Crude jatropha oil – biocrude blend, mixed and held at 170°F. (a) immediately after five minutes of stirring, (b) 25 minutes after stirring, (c) six days after stirring.

Figure 7-35 shows photos of a blend of crude jatropha oil and biodiesel (refined biocrude). This blend could be easily mixed, had low viscosity, was completely miscible, and had zero solids settling. Thus, this blend would be a good fuel at 170°F.
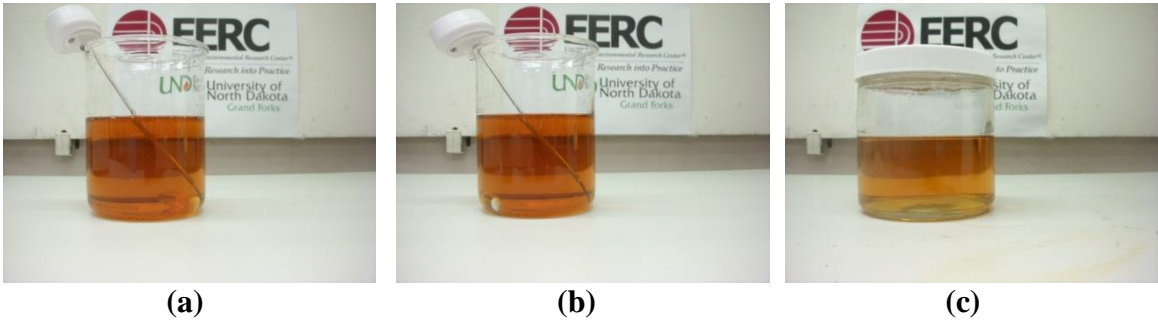
(a)   **(b)**   **(c)**

Figure 7-35. Crude jatropha oil – biodiesel blend, mixed and held at 170°F. (a) immediately after five minutes of stirring, (b) 25 minutes after stirring, (c) six days after stirring.

Figure 7-36 shows photos of a blend of crude jatropha oil and ultra-low sulfur diesel. This blend could be easily mixed, had low viscosity, was completely miscible, and had zero solids settling. Thus, this blend would be a good fuel at 170°F.

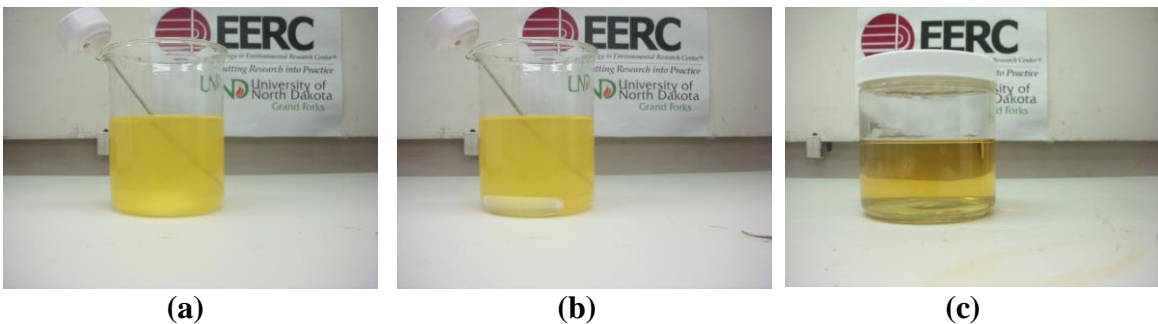**(a)**   **(b)**   **(c)**

Figure 7-36. Crude jatropha oil – ultra-low sulfur diesel blend, mixed and held at 170°F. (a) immediately after five minutes of stirring, (b) 25 minutes after stirring, (c) six days after stirring.

Figure 7-37 shows photos of a blend of biocrude derived from animal renderings and ultra-low sulfur diesel. This blend could be easily mixed, had low viscosity, was completely miscible, and had zero solids settling. Thus, this blend would be a good fuel at 170°F.

130

| (a) | (b) | (c) |

Figure 7-37. Biocrude – ultra-low sulfur diesel blend, mixed and held at 170°F. (a) immediately after five minutes of stirring, (b) 25 minutes after stirring, (c) six days after stirring.

Figure 7-38 shows photos of a blend of biodiesel (refined biocrude) and ultra-low sulfur diesel. This blend could be easily mixed, had low viscosity, was completely miscible, and had zero solids settling. Thus, this blend would be a good fuel at 170°F.
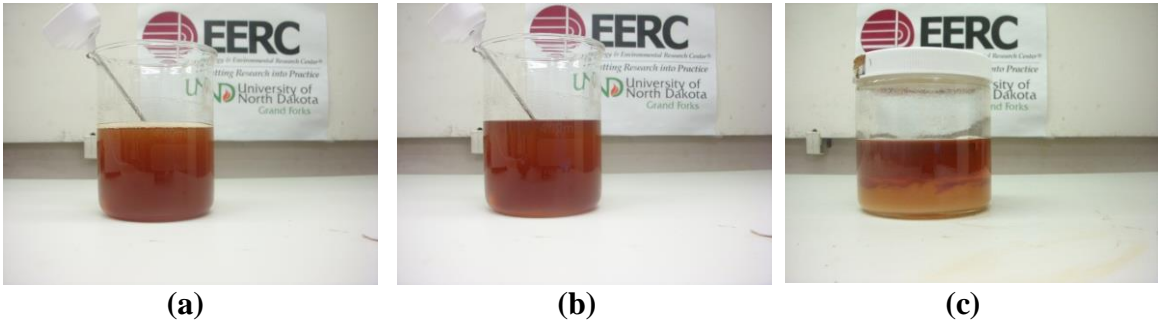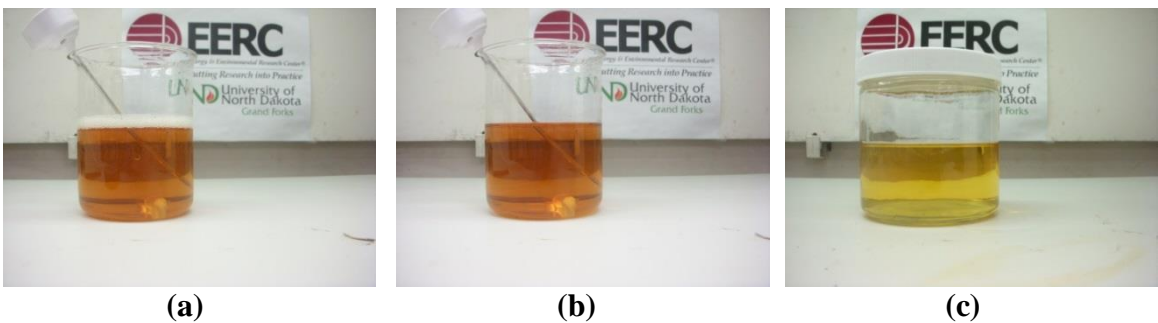

| (a) | (b) | (c) |

Figure 7-38. Biodiesel – ultra-low sulfur diesel blend, mixed and held at 170°F. (a) immediately after five minutes of stirring, (b) 25 minutes after stirring, (c) six days after stirring.

Based on the above results, Table 7-4 shows the miscibility of fuel blends at 170°F. This is approximately equal to the storage tank temperature. All blends were acceptable; entrained particles dissolved or melted into solution, and no blends smoked or formed semi-polymerized films on the testing beaker.

Table 7-4. Fuel blend acceptability at 170°F.

	Lo-Pour Fuel Oil	Hi-Pour Fuel Oil	Biocrude (animal)	Crude Jatropha Oil	Crude Palm Oil	Biodiesel (refined biocrude)	Ultra-low sulfur diesel
Lo-Pour Fuel Oil		Not Tested	Yes	Yes	Yes	Yes	Yes
Hi-Pour Fuel Oil			Yes	Yes	Yes	Yes	Yes
Biocrude (animal)				Yes	Yes	Not Tested	Yes
Crude Jatropha Oil					Yes	Yes	Yes
Crude Palm Oil						Yes	Yes
Biodiesel (refined biocrude)							Yes
Ultra-low sulfur diesel							

7.1.3 Oils Blended at 220°F

This blending temperature is approximately equal to the temperature to which industry heats the oils before firing them. It is also greater than the boiling point of water, so any water in the oils should be driven off.

Table 7-5 shows the elapsed time between initial blending and final photos of each oil blend. This indicates how long a blend was held at 220°F.

Table 7-5. Elapsed time between blending and final photos, 220°F.

Oil Blend	Elapsed Time (days)
Hi-Pour – Palm	3
Hi-Pour – Jatropha	3
Hi-Pour – Biocrude	3
Hi-Pour – Biodiesel	3
Hi-Pour – Ultra-low Sulfur Diesel	3
Lo-Pour – Palm	3
Lo-Pour – Jatropha	3
Lo-Pour – Biocrude	4

Table 7-5, cont.

Oil Blend	Elapsed Time (days)
Lo-Pour – Biodiesel	4
Lo-Pour – Ultra-low Sulfur Diesel	4
Palm – Jatropha	5
Palm – Biocrude	5
Palm – Biodiesel	5
Palm – Ultra-low Sulfur Diesel	5
Jatropha – Biocrude	6
Jatropha – Biodiesel	6
Jatropha – Ultra-low Sulfur Diesel	6
Biocrude – Ultra-low Sulfur Diesel	6
Biodiesel – Ultra-low Sulfur Diesel	6

Figure 7-39 shows photos of a blend of hi-pour fuel oil and crude palm oil. This blend could be easily mixed, had low viscosity, and was completely miscible. Thus, this blend would be a good fuel at 220°F.
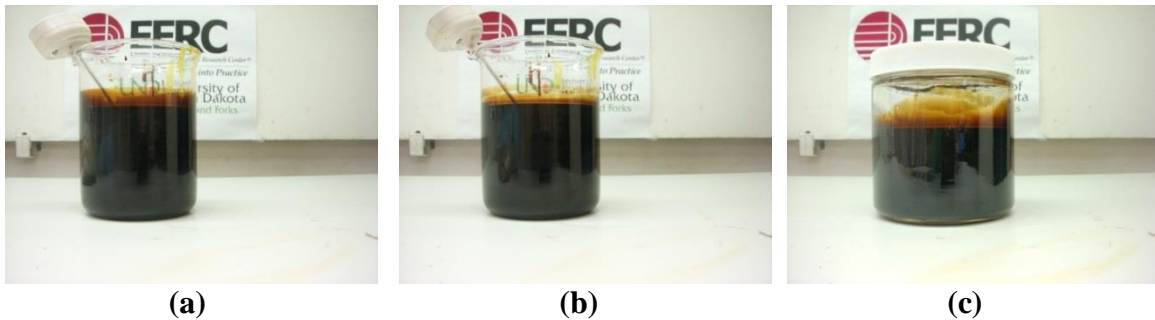

(a)	**(b)**	**(c)**
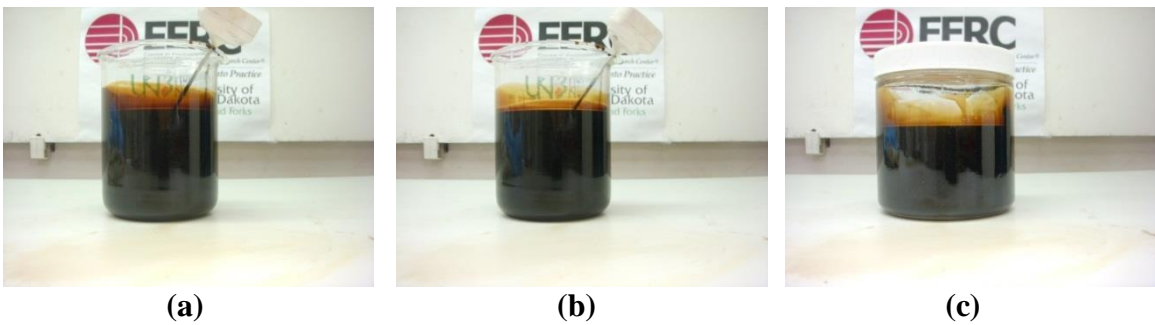
Figure 7-39. Hi-pour fuel oil – crude palm oil blend, mixed and held at 220°F. (a) immediately after five minutes of stirring, (b) 25 minutes after stirring, (c) three days after stirring.

Figure 7-40 shows photos of a blend of hi-pour fuel oil and crude jatropha oil. Figure 7-40a shows this blend immediately after stirring, Figure 7-40b shows this blend 25 minutes after stirring, and Figure 7-40c shows this blend three days after stirring. This blend could be easily mixed, had low viscosity, and was completely miscible. Thus, this blend would be a good fuel at 220°F.

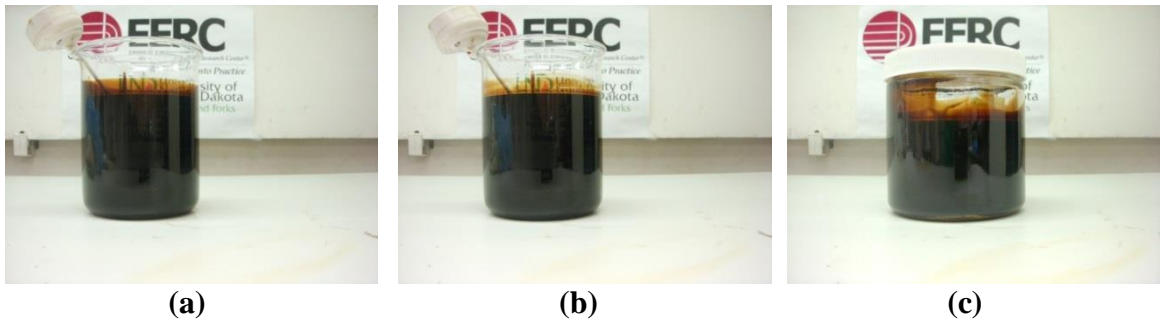|		
(a)	**(b)**	**(c)**
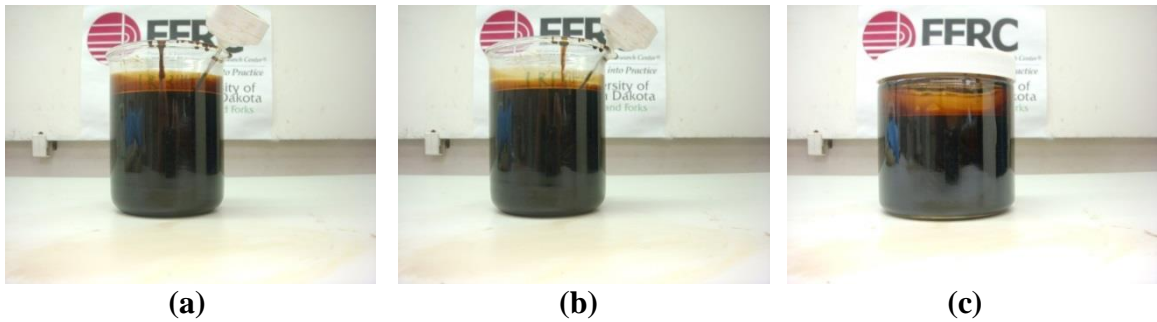
Figure 7-40. Hi-pour fuel oil – crude jatropha oil blend, mixed and held at 220°F. (a) immediately after five minutes of stirring, (b) 25 minutes after stirring, (c) three days after stirring.

Figure 7-41 shows photos of a blend of hi-pour fuel oil and biocrude derived from animal renderings. This blend could be easily mixed, had low viscosity, and was completely miscible. Thus, this blend would be a good fuel at 220°F.
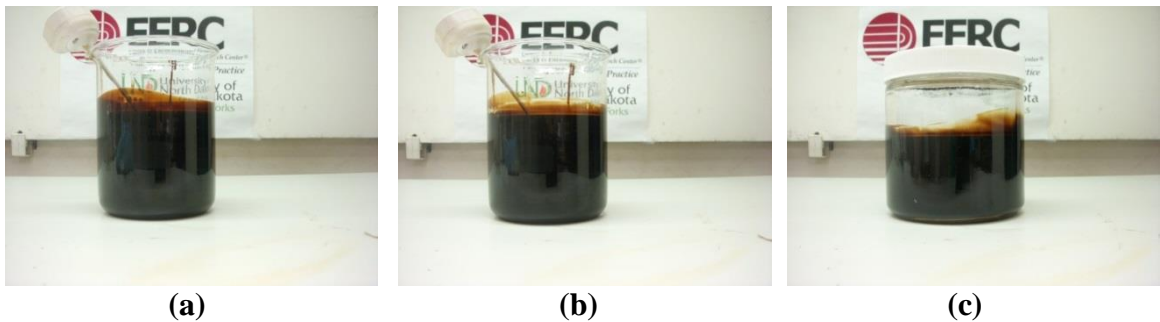

(a)	**(b)**	**(c)**

Figure 7-41. Hi-pour fuel oil – biocrude blend, mixed and held at 220°F. (a) immediately after five minutes of stirring, (b) 25 minutes after stirring, (c) three days after stirring.

Figure 7-42 shows photos of a blend of hi-pour fuel oil and biodiesel (refined biocrude). This blend could be easily mixed, had low viscosity, and was completely miscible. Thus, this blend would be a good fuel at 220°F.
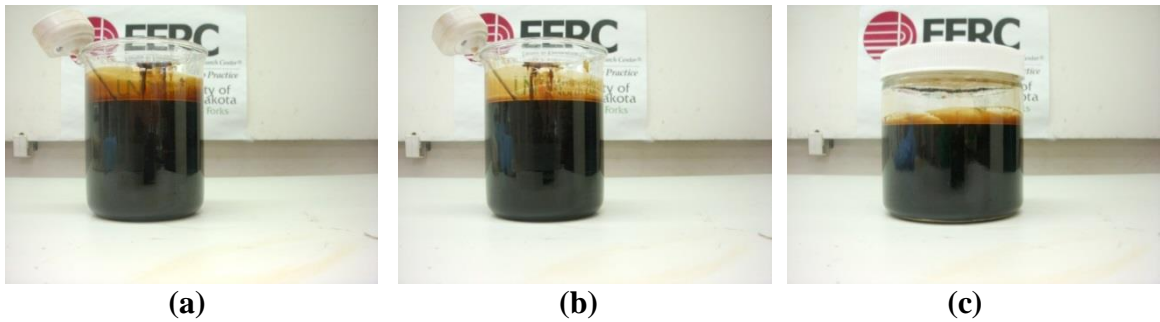
(a)   **(b)**   **(c)**

Figure 7-42. Hi-pour fuel oil – biodiesel blend, mixed and held at 220°F. (a) immediately after five minutes of stirring, (b) 25 minutes after stirring, (c) three days after stirring.

Figure 7-43 shows photos of a blend of hi-pour fuel oil and ultra-low sulfur diesel. This blend, and all blends containing ultra-low sulfur diesel, smoked slightly, both while being stirred and in the initial 25 minutes it was maintained at 220°F after stirring. Since this behavior was not observed with any other blends containing hi-pour fuel oil, the smoke was likely caused by the ultra-low sulfur diesel, which was blended without any additives to improve its performance. This behavior may be improved by the addition of a cetane number improver, which would reduce smoke (Bacha *et al*., 2007). Because of the smoke emitted by the blend, in the absence of a cetane number improver, this blend is marginally acceptable.
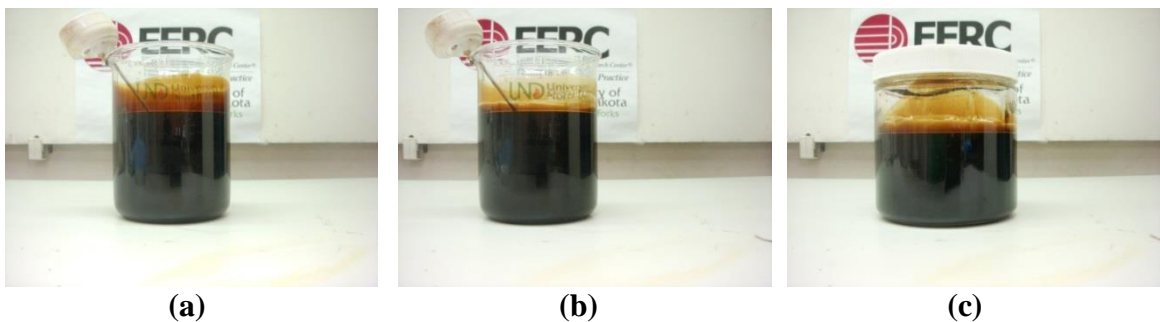

(a)   **(b)**   **(c)**
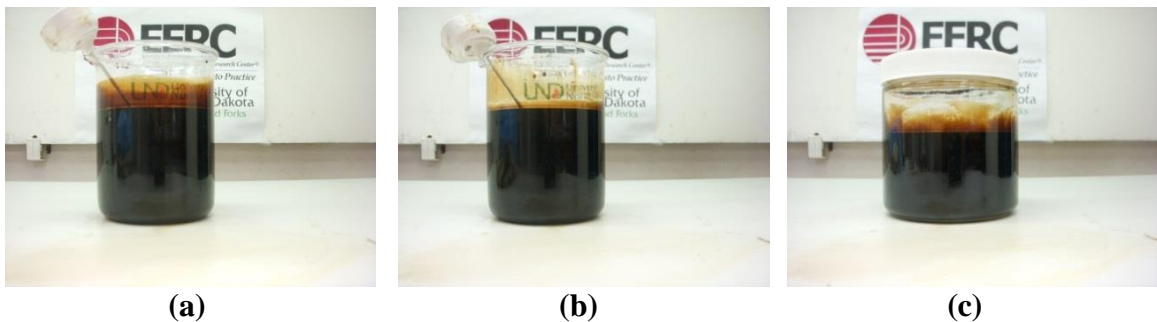
Figure 7-43. Hi-pour fuel oil – ultra-low sulfur diesel blend, mixed and held at 220°F. (a) immediately after five minutes of stirring, (b) 25 minutes after stirring, (c) three days after stirring.

Figure 7-44 shows photos of a blend of lo-pour fuel oil and crude palm oil. This blend could be easily mixed, had low viscosity, and was completely miscible. Thus, this blend would be a good fuel at 220°F.
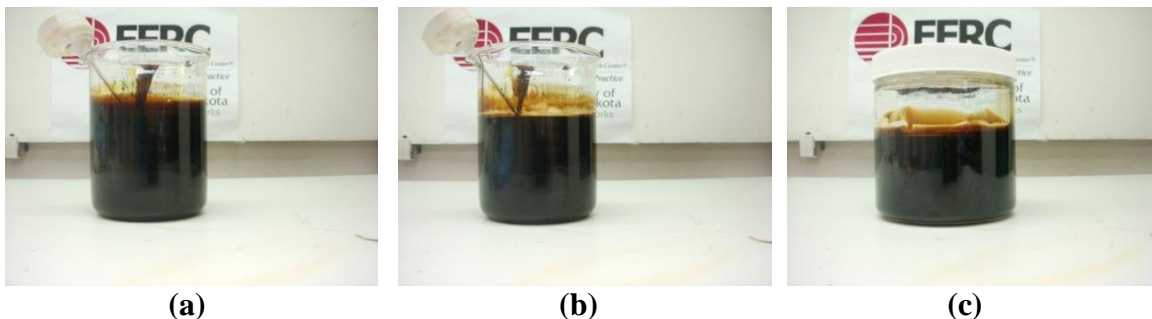

| (a) | (b) | (c) |
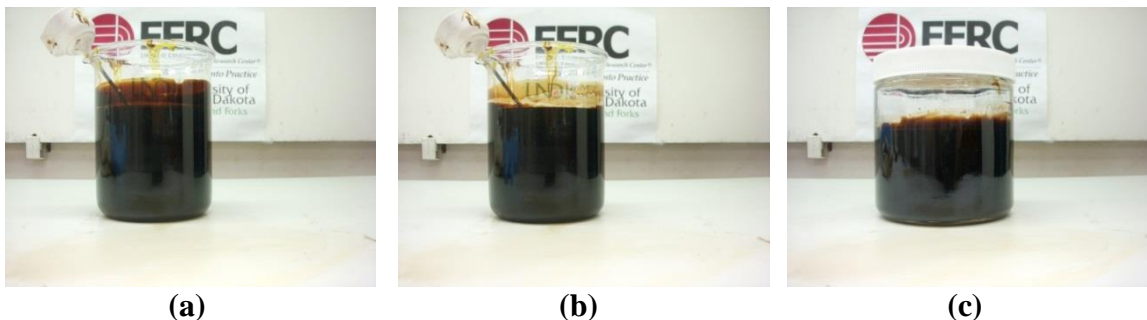
Figure 7-44. Lo-pour fuel oil – crude palm oil blend, mixed and held at 220°F. (a) immediately after five minutes of stirring, (b) 25 minutes after stirring, (c) three days after stirring.

Figure 7-45 shows photos of a blend of lo-pour fuel oil and crude jatropha oil. This blend could be easily mixed, had low viscosity, and was completely miscible. Thus, this blend would be a good fuel at 220°F.
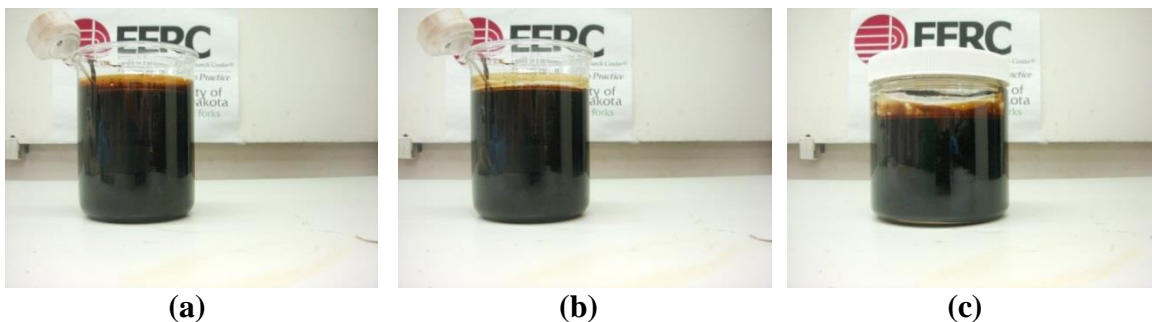

| (a) | (b) | (c) |
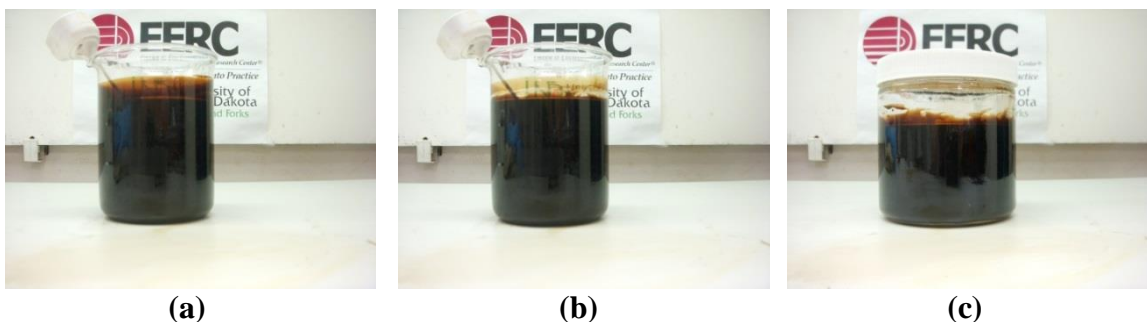
Figure 7-45. Lo-pour fuel oil – crude jatropha oil blend, mixed and held at 220°F. (a) immediately after five minutes of stirring, (b) 25 minutes after stirring, (c) three days after stirring.

Figure 7-46 shows photos of a blend of lo-pour fuel oil and biocrude derived from animal renderings. This blend could be easily mixed, had low viscosity, and was completely miscible. Thus, this blend would be a good fuel at 220°F.
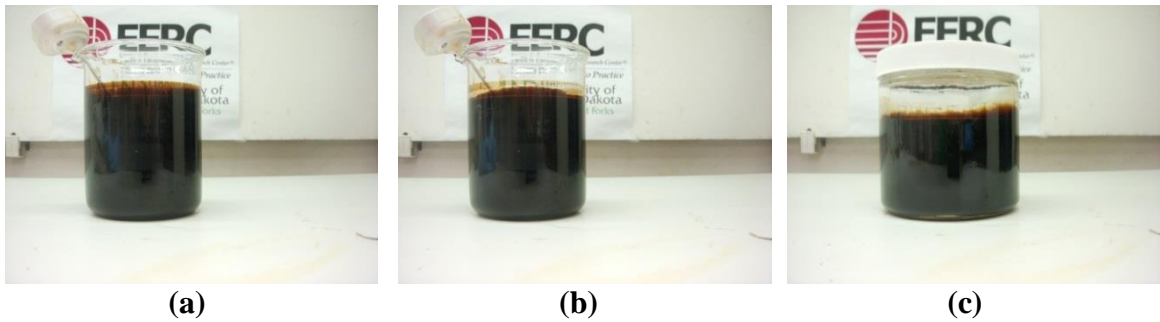
(a)   **(b)**   **(c)**
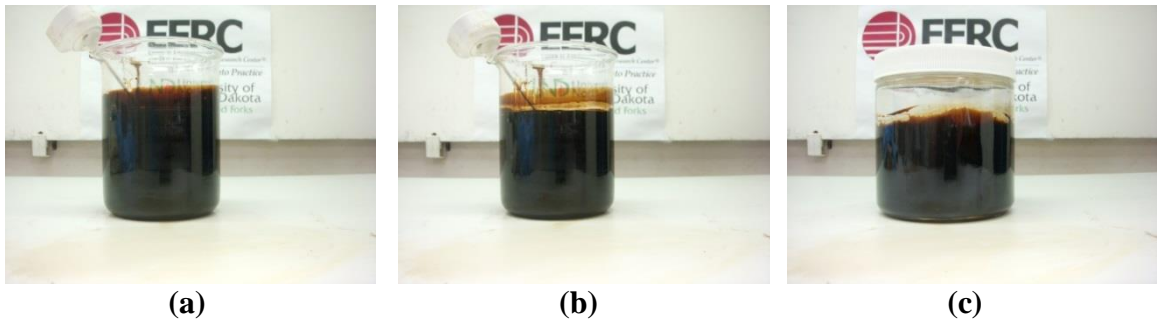
Figure 7-46. Lo-pour fuel oil – biocrude blend, mixed and held at 220°F. (a) immediately after five minutes of stirring, (b) 25 minutes after stirring, (c) four days after stirring.

Figure 7-47 shows photos of a blend of lo-pour fuel oil and biodiesel (refined biocrude). This blend could be easily mixed, had low viscosity, and was completely miscible. Thus, this blend would be a good fuel at 220°F.
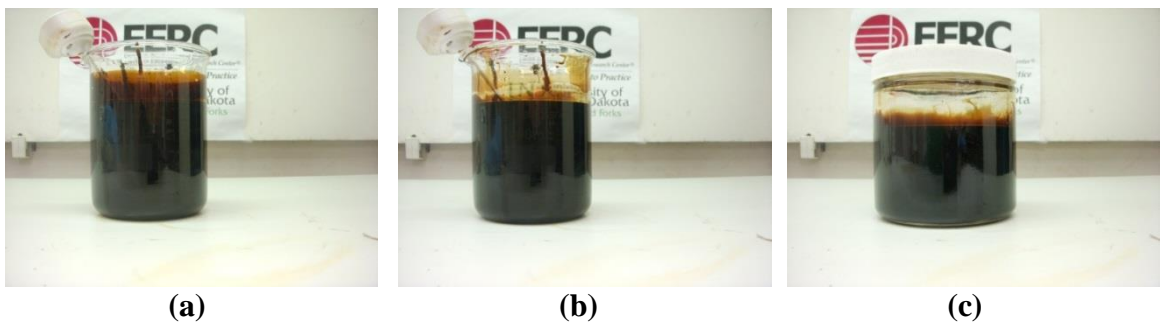

(a)   **(b)**   **(c)**
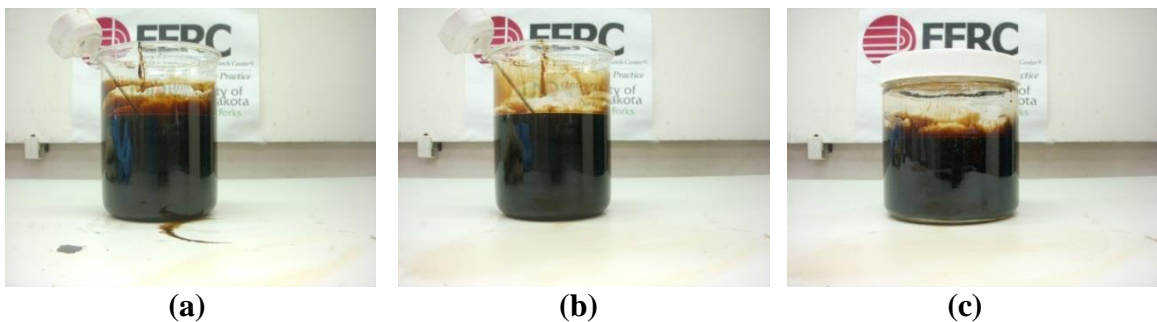
Figure 7-47. Lo-pour fuel oil – biodiesel blend, mixed and held at 220°F. (a) immediately after five minutes of stirring, (b) 25 minutes after stirring, (c) four days after stirring.

Figure 7-48 shows photos of a blend of lo-pour fuel oil and ultra-low sulfur diesel. This blend smoked heavily, both while being stirred and in the initial 25 minutes after stirring. Since this behavior was not observed with any other blends containing lo-pour fuel oil, the smoke was likely caused by the ultra-low sulfur diesel, which was blended without any additives to improve its performance. This behavior may be improved by the addition of a cetane number improver, which would reduce smoke

(Bacha *et al*., 2007). Because of the smoke emitted by the blend, in the absence of a

cetane number improver, this blend is marginally acceptable.

(a)   **(b)**   **(c)**
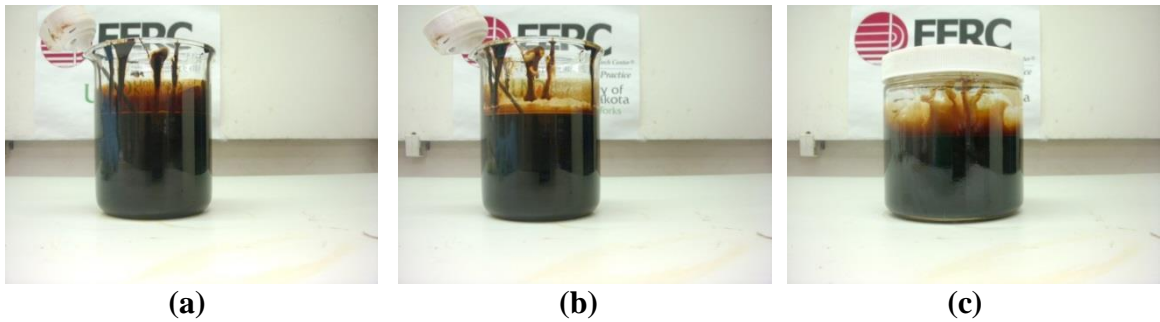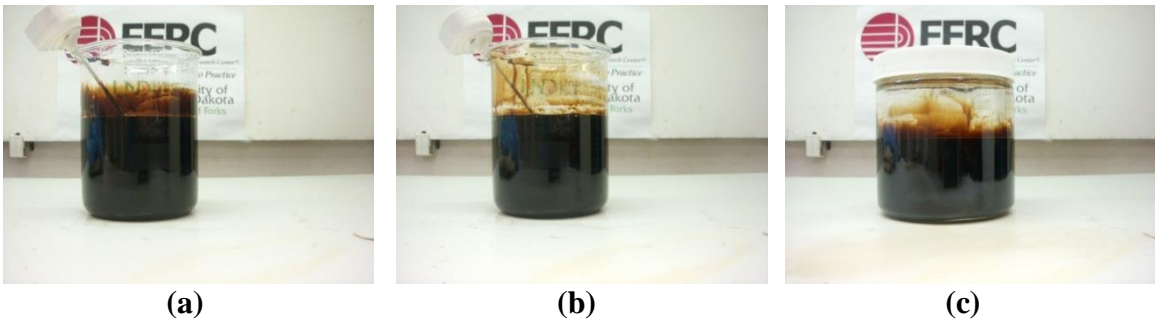
Figure 7-48. Lo-pour fuel oil – ultra-low sulfur diesel blend, mixed and held at 220°F. (a) immediately after five minutes of stirring, (b) 25 minutes after stirring, (c) four days after stirring.

Figure 7-49 shows photos of a blend of crude palm oil and crude jatropha oil. This

blend could be easily mixed, had low viscosity, was completely miscible, and had zero

solids settling out of solution. Thus, this blend would be a good fuel at 220°F.

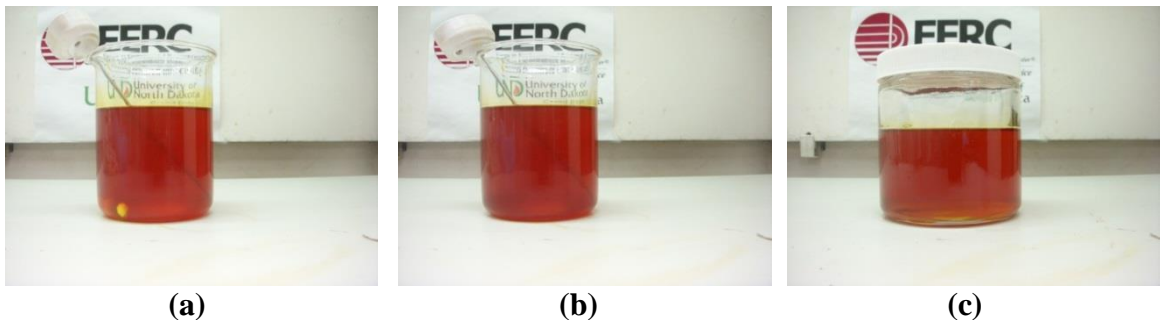**(a)**   **(b)**   **(c)**
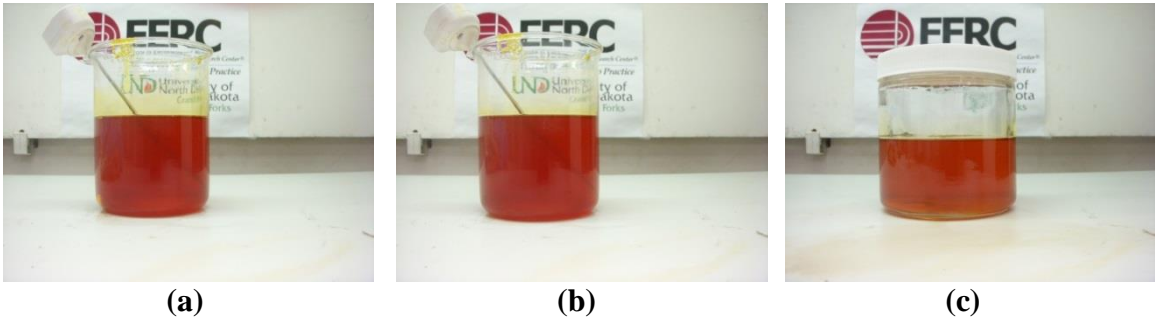
Figure 7-49. Crude palm oil – crude jatropha oil blend, mixed and held at 220°F. (a) immediately after five minutes of stirring, (b) 25 minutes after stirring, (c) five days after stirring.

Figure 7-50 shows photos of a blend of crude palm oil and biocrude derived from

animal renderings. A thin film appeared on the bottom of the beaker within 25 minutes

after it was stirred. Since this film was not observed with any other blends containing

crude palm oil, it was conjectured that this was caused by the biocrude derived from

animal renderings. It is conjectured that this film resulted from the semi-polymerization of the biocrude. This could lead to favorable environments for crevice corrosion or pitting. Because of the semi-polymerized oil, this blend is marginally acceptable.
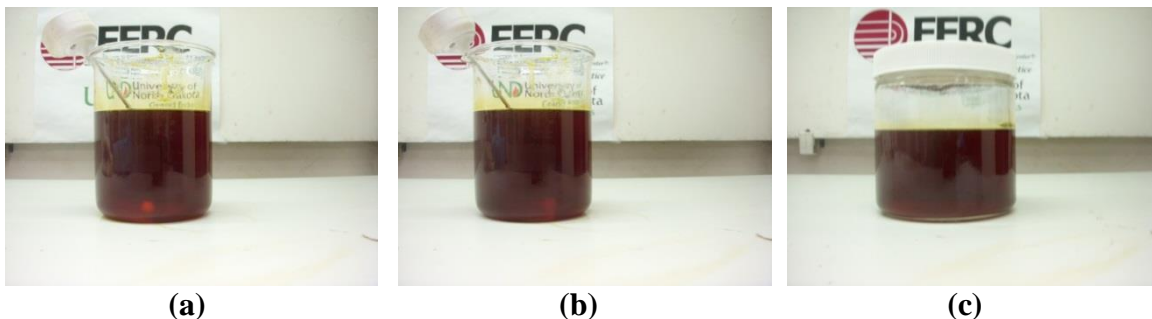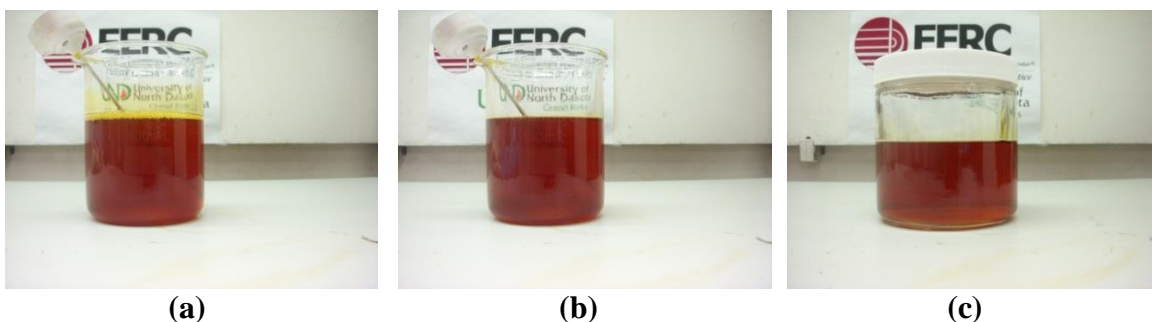

| (a) | (b) | (c) |
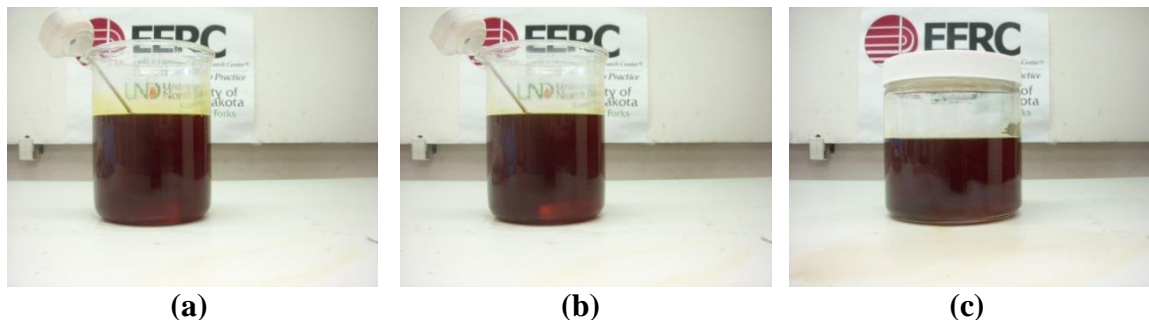
Figure 7-50. Crude palm oil – biocrude blend, mixed and held at 220°F. (a) immediately after five minutes of stirring, (b) 25 minutes after stirring, (c) five days after stirring.

Figure 7-51 shows photos of a blend of crude palm oil and biodiesel (refined biocrude). This blend could be easily mixed, had low viscosity, was completely miscible, and had zero solids settling out of solution. Thus, this blend would be a good fuel at 220°F.

| (a) | (b) | (c) |
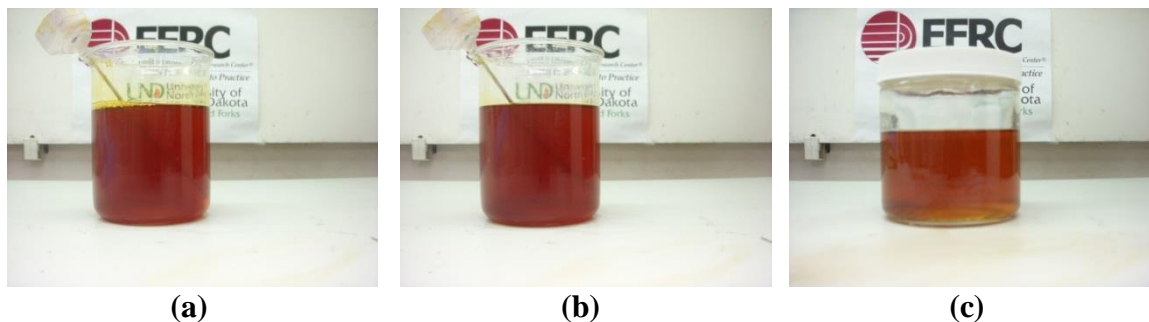
Figure 7-51. Crude palm oil – biodiesel blend, mixed and held at 220°F. (a) immediately after five minutes of stirring, (b) 25 minutes after stirring, (c) five days after stirring.

Figure 7-52 shows photos of a blend of crude palm oil and ultra-low sulfur diesel. This blend smoked slightly, both while being stirred and in the initial 25 minutes after stirring. Since this behavior was not observed with any other blends containing lo-pour

fuel oil, the smoke was likely caused by the ultra-low sulfur diesel, which was blended

without any additives to improve its performance. This behavior may be improved by the

addition of a cetane number improver, which would reduce smoke (Bacha *et al.*, 2007).

Because of the smoke emitted by the blend, in the absence of a cetane number improver,

this blend is marginally acceptable.

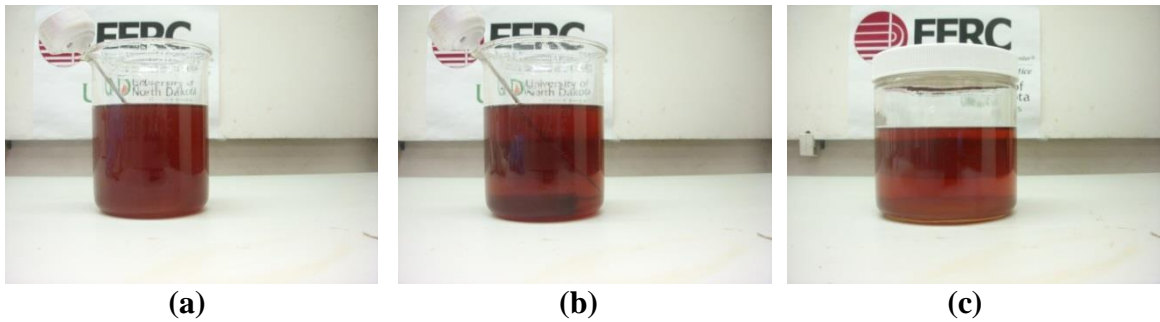| (a) | (b) | (c) |
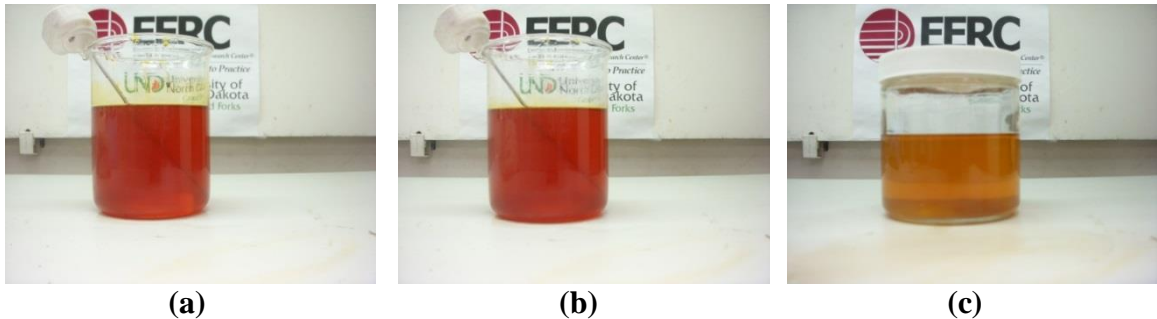
Figure 7-52. Crude palm oil – ultra-low sulfur diesel blend, mixed and held at 220°F. (a) immediately after five minutes of stirring, (b) 25 minutes after stirring, (c) five days after stirring.

Figure 7-53 shows photos of a blend of crude jatropha oil and biocrude derived

from animal renderings. A thin film appeared on the bottom of the beaker within 25

minutes after it was stirred. Since this film was not observed with any other blends

containing crude jatropha oil, it was conjectured that this was caused by the biocrude

derived from animal renderings. It is conjectured that this film resulted from the semi-

polymerization of the biocrude. This could lead to favorable environments for crevice

corrosion or pitting. Because of the semi-polymerized oil, this blend is marginally

acceptable.

(a)	**(b)**	**(c)**
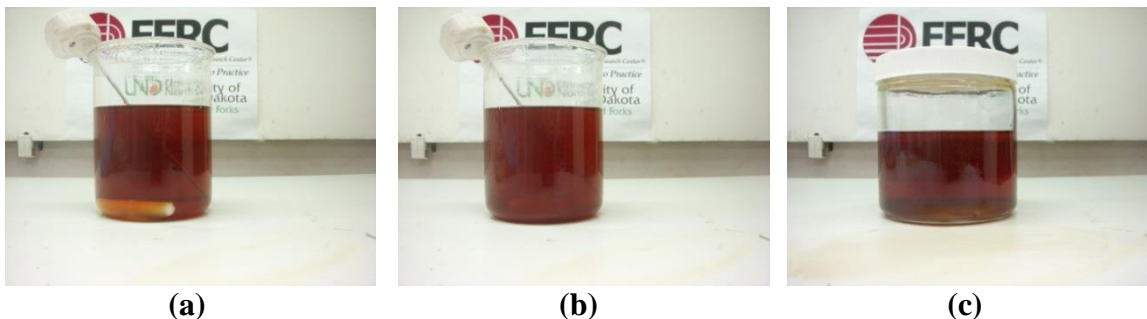
Figure 7-53. Crude jatropha oil – biocrude blend, mixed and held at 220°F. (a) immediately after five minutes of stirring, (b) 25 minutes after stirring, (c) six days after stirring.

Figure 7-54 shows photos of a blend of crude jatropha oil and biodiesel (refined biocrude). This blend could be easily mixed, had low viscosity, was completely miscible, and had zero solids settling out of solution. Thus, this blend would be a good fuel at 220°F.

(a)	**(b)**	**(c)**
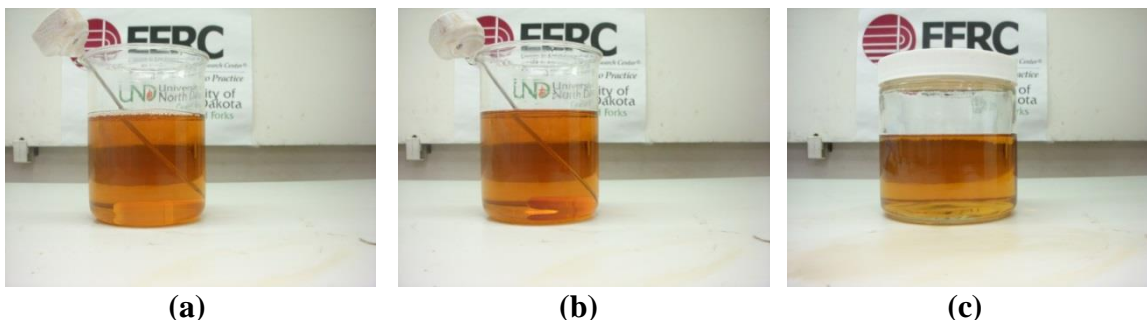
Figure 7-54. Crude jatropha oil – biodiesel blend, mixed and held at 220°F. (a) immediately after five minutes of stirring, (b) 25 minutes after stirring, (c) six days after stirring.

Figure 7-55 shows photos of a blend of crude jatropha oil and ultra-low sulfur diesel. This blend smoked slightly, both while being stirred and in the initial 25 minutes after stirring. Since this behavior was not observed with any other blends containing crude jatropha oil, the smoke was likely caused by the ultra-low sulfur diesel, which was blended without any additives to improve its performance. This behavior may be

improved by the addition of a cetane number improver, which would reduce smoke

(Bacha *et al*., 2007). Because of the smoke emitted by the blend, in the absence of a

cetane number improver, this blend is marginally acceptable.
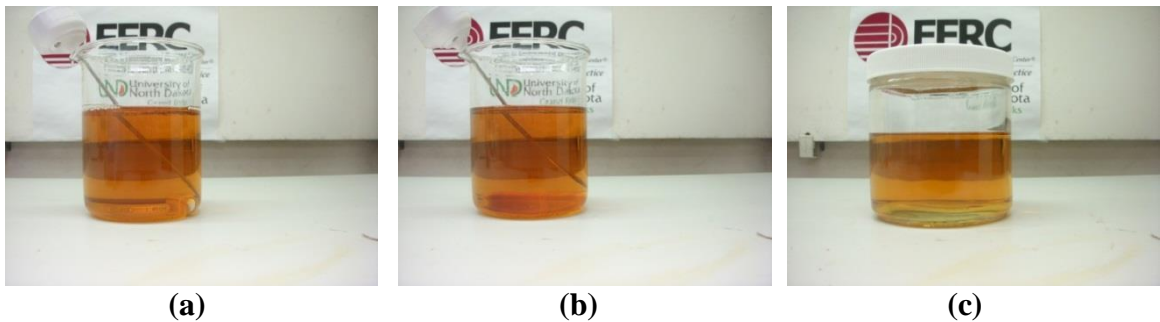

| (a) | (b) | (c) |
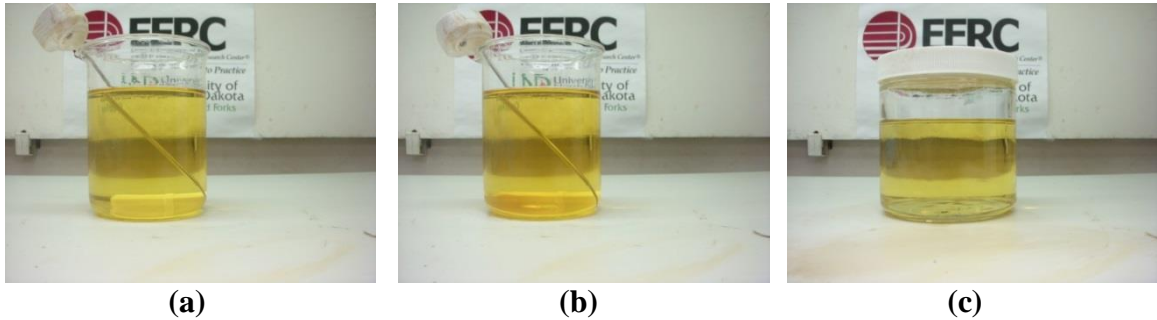
Figure 7-55. Crude jatropha oil – ultra-low sulfur diesel blend, mixed and held at 220°F. (a) immediately after five minutes of stirring, (b) 25 minutes after stirring, (c) six days after stirring.

Figure 7-56 shows photos of a blend of biocrude derived from animal renderings

and ultra-low sulfur diesel. A thin film appeared on the bottom of the beaker within 25

minutes after it was stirred. Since this film was not observed with any other blends

containing ultra-low sulfur diesel, it was conjectured that this was caused by the biocrude

derived from animal renderings. It is conjectured that this film resulted from the semi-

polymerization of the biocrude. This could lead to favorable environments for crevice

corrosion or pitting. Because of the semi-polymerized oil, this blend is marginally

acceptable.

(a)	**(b)**	**(c)**
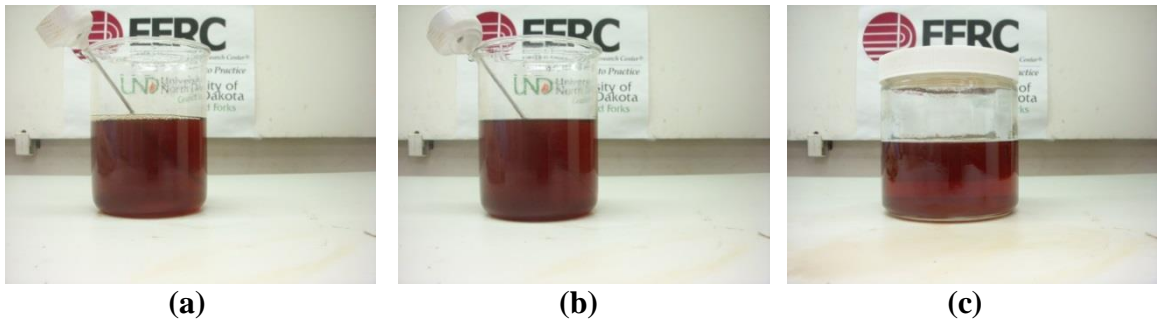
Figure 7-56. Biocrude – ultra-low sulfur diesel blend, mixed and held at 220°F. (a) immediately after five minutes of stirring, (b) 25 minutes after stirring, (c) six days after stirring.

Figure 7-57 shows photos of a blend of biodiesel (refined biocrude) and ultra-low sulfur diesel. This blend smoked slightly, both while being stirred and in the initial 25 minutes it was maintained at 220°F after stirring. Since this behavior was not observed with any other blends containing biodiesel, the smoke was likely caused by the ultra-low sulfur diesel, which was blended without any additives to improve its performance. This behavior may be improved by the addition of a cetane number improver, which would reduce smoke (Bacha *et al*., 2007). Because of the smoke emitted by the blend, in the absence of a cetane number improver, this blend is marginally acceptable.

(a)	**(b)**	**(c)**

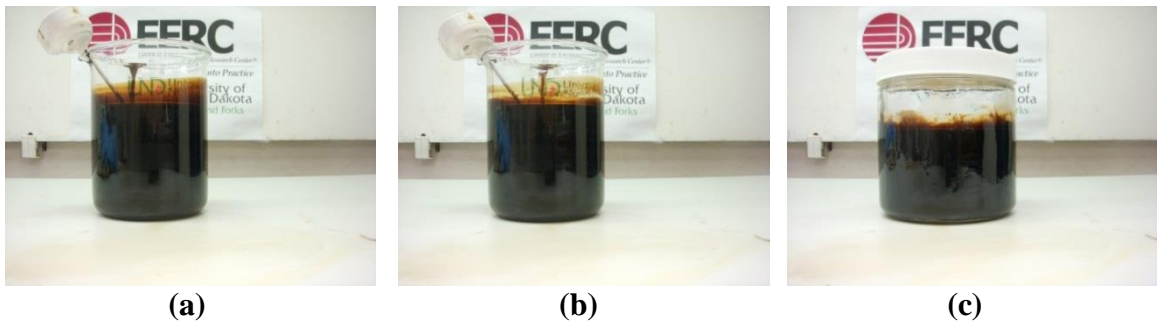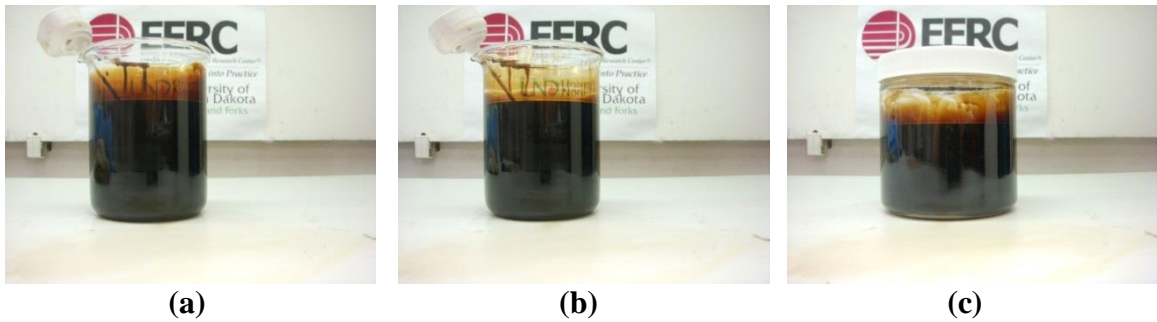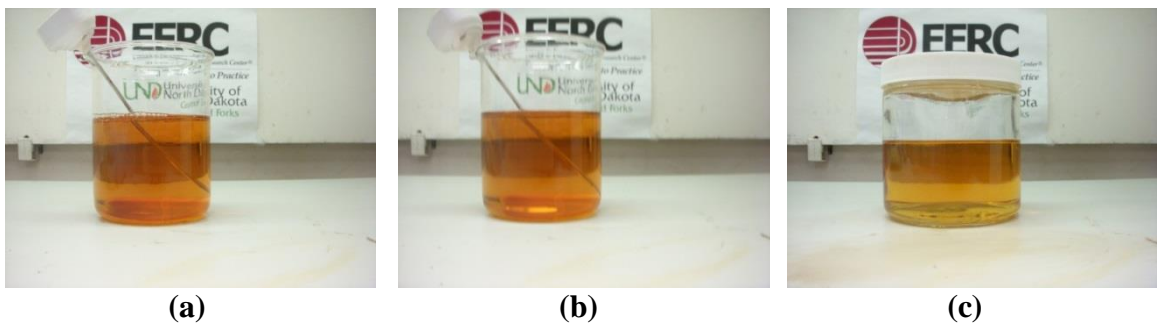**Figure 7-57.** Biodiesel – ultra-low sulfur diesel blend, mixed and held at 220°F. (a) immediately after five minutes of stirring, (b) 25 minutes after stirring, (c) six days after stirring.

Based on the above results, Table 7-6 shows the miscibility of fuel blends at 220°F. This is approximately the temperature to which oils are heated before firing. The main causes of marginal behavior were smoking and semi-polymerized films on the beaker.

Table 7-6. Fuel blend acceptability at 220°F.

	Lo-Pour Fuel Oil	Hi-Pour Fuel Oil	Biocrude (animal)	Crude Jatropha Oil	Crude Palm Oil	Biodiesel (refined biocrude)	Ultra-low sulfur diesel
Lo-Pour Fuel Oil		Not Tested	Yes	Yes	Yes	Yes	Yes
Hi-Pour Fuel Oil			Yes	Yes	Yes	Yes	Marginal
Biocrude (animal)				Marginal	Marginal	Not Tested	Marginal
Crude Jatropha Oil					Yes	Yes	Yes
Crude Palm Oil						Yes	Yes
Biodiesel (refined biocrude)							Yes
Ultra-low sulfur diesel							

7.1.4   Cooling Oil Blends from 170°F to 75°F

All the oils blended at 170°F were cooled overnight to 75°F and were allowed to settle for eight days. This represents a worst-case scenario for industry where the heating on the storage tanks would fail and oil blends would cool, potentially creating a situation where solids could settle or sludge-like compounds could form.

Figure 7-58 shows photos of a blend of hi-pour fuel oil and crude palm oil after it was cooled. This cooled blend was thicker than the heated fuel blend; qualitatively the

viscosity was similar to that of refrigerated vegetable oil. However, this viscosity was not

dissimilar to that of the same oils blended at 75°F, indicating that heating the oils did not

significantly change their overall properties. Nevertheless, the high opacity of the fuel oil

may have obscured any qualitatively-observable changes, such as solids settling out of

solution.

(a) **(b)**

Figure 7-58. Hi-pour fuel oil – crude palm oil blend, cooled from 170°F to 75°F. (a) shows the blend sitting flat, and (b) shows the blend tilted at an angle.

Figure 7-59 shows photos of a blend of hi-pour fuel oil and crude jatropha oil

after it was cooled. There was no difference between the viscosity of the cooled blend

and the viscosity of the same oils blended at 75°F, indicating that heating the oils did not

significantly change their properties. Thus, this cooled blend of oils is acceptable.

| (a) | (b) |

Figure 7-59. Hi-pour fuel oil – crude jatropha oil blend, cooled from 170°F to 75°F. (a) shows the blend sitting flat, and (b) shows the blend tilted at an angle.

Figure 7-60 shows photos of a blend of hi-pour fuel oil and biocrude derived from animal renderings after it was cooled. The qualitative viscosity of the cooled fuel blend was slightly lower than that of the same oils blended at 75°F. However, the high opacity of the fuel oil may be obscuring any qualitatively-observable changes, such as solids settling out of solution.

| (a) | (b) |

Figure 7-60. Hi-pour fuel oil – biocrude blend, cooled from 170°F to 75°F. (a) shows the blend sitting flat, and (b) shows the blend tilted at an angle.

Figure 7-61 shows photos of a blend of hi-pour fuel oil and biodiesel (refined biocrude) after it was cooled. There was no difference between the viscosity of the cooled blend and the viscosity of the same oils blended at 75°F, indicating that heating the oils did not significantly change their properties. Thus, this cooled blend of oils is acceptable.

(a)   (b)

Figure 7-61. Hi-pour fuel oil – biodiesel blend, cooled from 170°F to 75°F. (a) shows the blend sitting flat, and (b) shows the blend tilted at an angle.

Figure 7-62 shows photos of a blend of hi-pour fuel oil and ultra-low sulfur diesel after it was cooled. There was no difference between the viscosity of the cooled blend and the viscosity of the same oils blended at 75°F, indicating that heating the oils did not significantly change their properties. Thus, this cooled blend of oils is acceptable.

147

| (a) | (b) |

Figure 7-62. Hi-pour fuel oil – ultra-low sulfur diesel blend, cooled from 170°F to 75°F. (a) shows the blend sitting flat, and (b) shows the blend tilted at an angle.

Figure 7-63 shows photos of a blend of lo-pour fuel oil and crude palm oil after it was cooled. The qualitative viscosity of the cooled fuel blend was significantly lower than the initial viscosity of the same oils blended at 75°F. However, the high opacity of the fuel oil may be obscuring any qualitatively-observable changes, such as palm solids settling out of solution.

| (a) | (b) |

Figure 7-63. Lo-pour fuel oil – crude palm oil blend, cooled from 170°F to 75°F. (a) shows the blend sitting flat, and (b) shows the blend tilted at an angle.

Figure 7-64 shows photos of a blend of lo-pour fuel oil and crude jatropha oil after it was cooled. There was no difference between the viscosity of the cooled blend and the viscosity of the same oils blended at 75°F, indicating that heating the oils did not significantly change their properties. Thus, this cooled blend of oils is acceptable.

| (a) | (b) |

Figure 7-64. Lo-pour fuel oil – crude jatropha oil blend, cooled from 170°F to 75°F. (a) shows the blend sitting flat, and (b) shows the blend tilted at an angle.

Figure 7-65 shows photos of a blend of lo-pour fuel oil and biocrude derived from animal renderings after it was cooled. The qualitative viscosity of the cooled fuel blend was similar to that of the same oils blended at 75°F. However, the high opacity of the fuel oil may be obscuring any qualitatively-observable changes, such as solids settling out of solution.

(a)	**(b)**

Figure 7-65. Lo-pour fuel oil – biocrude blend, cooled from 170°F to 75°F. (a) shows the blend sitting flat, and (b) shows the blend tilted at an angle.

Figure 7-66 shows photos of a blend of lo-pour fuel oil and biodiesel (refined biocrude) after it was cooled. There was no difference between the viscosity of the cooled blend and the viscosity of the same oils blended at 75°F, indicating that heating the oils did not significantly change their properties. Thus, this cooled blend of oils is acceptable.

(a)	**(b)**

Figure 7-66. Lo-pour fuel oil – biodiesel blend, cooled from 170°F to 75°F. (a) shows the blend sitting flat, and (b) shows the blend tilted at an angle.

Figure 7-67 shows photos of a blend of lo-pour fuel oil and ultra-low sulfur diesel after it was cooled. There was no difference between the viscosity of the cooled blend

150

and the viscosity of the same oils blended at 75°F, indicating that heating the oils did not

significantly change their properties. Thus, this cooled blend of oils is acceptable.

<center>(a)   (b)</center>

Figure 7-67. Lo-pour fuel oil – ultra-low sulfur diesel blend, cooled from 170°F to 75°F.
(a) shows the blend sitting flat, and (b) shows the blend tilted at an angle.

Figure 7-68 shows photos of a blend of crude palm oil and crude jatropha oil after

it was cooled. A considerable amount of solids (most likely palm-based) settled out of

this blend. These solids could lead to favorable conditions for crevice corrosion or

erosion corrosion or could lead to plugging of tank outlets. Therefore, this blend is not

acceptable under these cooled conditions.

<center>(a)   (b)</center>

Figure 7-68. Crude palm oil – crude jatropha oil blend, cooled from 170°F to 75°F. (a)
shows the blend sitting flat, and (b) shows the blend tilted at an angle.

<center>151</center>

Figure 7-69 shows photos of a blend of crude palm oil and biocrude derived from animal renderings after it was cooled. This blend thickened quite a bit in cooling to the approximate consistency of honey. Overall, the viscosity of this cooled blend was higher than that of the same oils blended at 75°F, even though solids settled out of the latter blend as well. The thickened oil blend could lead to plugging of pipelines or tank outlets. Therefore, this blend is not acceptable under cooled conditions.

(a)   (b)

Figure 7-69. Crude palm oil – biocrude blend, cooled from 170°F to 75°F. (a) shows the blend sitting flat, and (b) shows the blend tilted at an angle.

Figure 7-70 shows photos of a blend of crude palm oil and biodiesel (refined biocrude) after it was cooled. A considerable amount of solids settled out; the solids at the bottom were more densely packed, while the solids nearer the top were less dense. These solids could lead to favorable conditions for crevice corrosion or erosion corrosion or could lead to plugging of tank outlets, especially as the solids became more densely packed from top to bottom through the blend, which may have been due to the actions of gravity. Therefore, this blend is not acceptable under these cooled conditions.

| (a) | (b) |

Figure 7-70. Crude palm oil – biodiesel blend, cooled from 170°F to 75°F. (a) shows the blend sitting flat, and (b) shows the blend tilted at an angle.

Figure 7-71 shows photos of a blend of crude palm oil and ultra-low sulfur diesel after it was cooled. A layer of moderately dense palm solids settled out. These solids could lead to favorable conditions for crevice corrosion or erosion corrosion or could lead to plugging of tank outlets, especially as the solids became more densely packed from top to bottom through the blend, which may have been due to the actions of gravity. Therefore, this blend is not acceptable under these cooled conditions.

| (a) | (b) |

Figure 7-71. Crude palm oil – ultra-low sulfur diesel blend, cooled from 170°F to 75°F. (a) shows the blend sitting flat, and (b) shows the blend tilted at an angle.

Figure 7-72 shows photos of a blend of crude jatropha oil and biocrude derived from animal renderings after it was cooled. A layer of moderately packed solids settled out, and more solids were visible throughout the solution. These solids could lead to favorable conditions for crevice corrosion or erosion corrosion or could lead to plugging of tank outlets, especially as the solids became more densely packed from top to bottom through the blend, which may have been due to the actions of gravity. Therefore, this blend is not acceptable under these cooled conditions.

| (a) | (b) |

Figure 7-72. Crude jatropha oil – biocrude blend, cooled from 170°F to 75°F. (a) shows the blend sitting flat, and (b) shows the blend tilted at an angle.

Figure 7-73 shows photos of a blend of crude jatropha oil and biodiesel (refined biocrude) after it was cooled. There was no difference between the viscosity of the cooled blend and the viscosity of the same oils blended at 75°F, indicating that heating the oils did not significantly change their properties. Thus, this cooled blend of oils is acceptable.

154

| (a) | (b) |

Figure 7-73. Crude jatropha oil – biodiesel blend, cooled from 170°F to 75°F. (a) shows the blend sitting flat, and (b) shows the blend tilted at an angle.

Figure 7-74 shows photos of a blend of crude jatropha oil and ultra-low sulfur diesel after it was cooled. There was no difference between the viscosity of the cooled blend and the viscosity of the same oils blended at 75°F, indicating that heating the oils did not significantly change their properties. Thus, this cooled blend of oils is acceptable.

| (a) | (b) |

Figure 7-74. Crude jatropha oil – ultra-low sulfur diesel blend, cooled from 170°F to 75°F. (a) shows the blend sitting flat, and (b) shows the blend tilted at an angle.

Figure 7-75 shows photos of a blend of biocrude derived from animal renderings and ultra-low sulfur diesel after it was cooled. A layer of crystalline solids settled out of

155

solution. These solids could lead to favorable conditions for crevice corrosion or erosion corrosion (particularly true for these crystalline solids) or could lead to plugging of tank outlets, especially as the solids became more densely packed from top to bottom through the blend, which may have been due to the actions of gravity. Therefore, this blend is not acceptable under these cooled conditions.

(a)   (b)

Figure 7-75. Biocrude – ultra-low sulfur diesel blend, cooled from 170°F to 75°F. (a) shows the blend sitting flat, and (b) shows the blend tilted at an angle.

Figure 7-76 shows photos of a blend of biodiesel (refined biocrude) and ultra-low sulfur diesel after it was cooled. There was no difference between the viscosity of the cooled blend and the viscosity of the same oils blended at 75°F, indicating that heating the oils did not significantly change their properties. Thus, this cooled blend of oils is acceptable.

156

| (a) | (b) |

Figure 7-76. Biodiesel – ultra-low sulfur diesel blend, cooled from 170°F to 75°F. (a) shows the blend sitting flat, and (b) shows the blend tilted at an angle.

Based on the above results, Table 7-7 shows the acceptability of the fuel blends after they were cooled from 170°F to 75°F. The main cause of failure was solids settling or the formation of sludge-like compounds. Generally, more solids were observed in blends containing crude palm oil which were cooled from 170°F to 75°F than were observed in blends containing this oil at 75°F. It is possible that the oil structure was changed by heating it. This may not have been entirely detrimental, though; the blend of lo-pour fuel oil with crude palm oil had a significantly lower viscosity after cooling than the initial blend of these same oils at 75°F. More solids were also observed in blends containing biocrude derived from animal renderings which were cooled from 170°F to 75°F than were observed in blends containing this oil at 75°F, though not enough is known about the fuel properties of the biocrude to make a determination as to why this would be the case.

Table 7-7. Acceptability of fuel blends after cooling from 170°F to 75°F.

	Lo-Pour Fuel Oil	Hi-Pour Fuel Oil	Biocrude (animal)	Crude Jatropha Oil	Crude Palm Oil	Biodiesel (refined biocrude)	Ultra-low sulfur diesel
Lo-Pour Fuel Oil		Not Tested	Yes	Yes	Marginal	Yes	Yes
Hi-Pour Fuel Oil			Yes	Yes	Marginal	Yes	Yes
Biocrude (animal)				No	No	Not Tested	No
Crude Jatropha Oil					No	Yes	Yes
Crude Palm Oil						No	No
Biodiesel (refined biocrude)							Yes
Ultra-low sulfur diesel							

7.1.5 Cooling Oil Blends from 220°F to 75°F

All the oils blended at 220°F were cooled overnight to 75°F and allowed to settle
for three days. This represents an unlikely scenario in industry where the heated lines to
the furnace would fail for some reason and the failure would go unnoticed for an
extended period of time. This would potentially create a situation where solids would
settle or sludge-like compounds would form.

Figure 7-77 shows photos of a blend of hi-pour fuel oil and crude palm oil after it
was cooled. This cooled blend was thicker than the heated fuel blend; the viscosity was
comparable to that of refrigerated vegetable oil, and the blend had the approximate
consistency of cottage cheese. The thickness of the blend could lead to plugging of

heated lines or tank outlets. Therefore, this blend is not acceptable under the cooled

conditions.

| (a) | (b) |
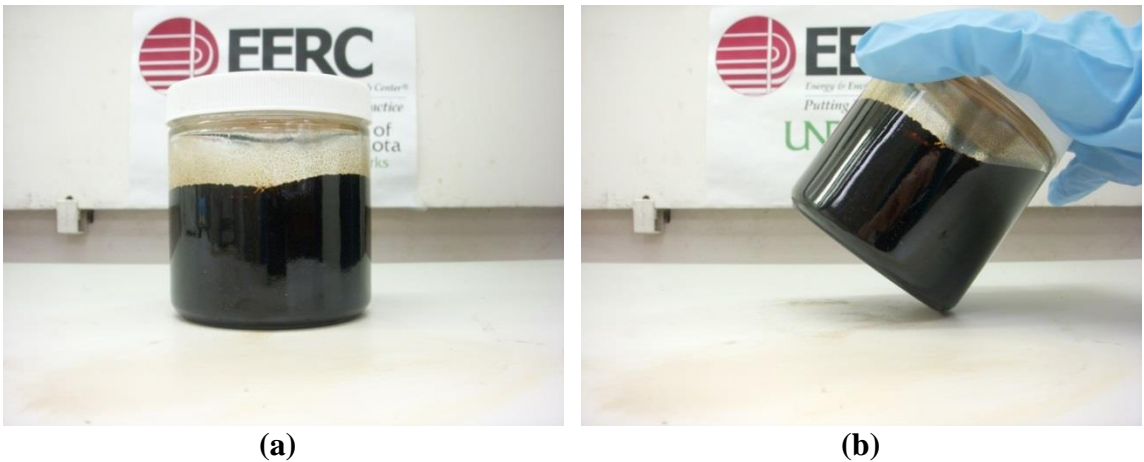
Figure 7-77. Hi-pour fuel oil – crude palm oil blend, cooled from 220°F to 75°F. (a) shows the blend sitting flat, and (b) shows the blend tilted at an angle.

Figure 7-78 shows photos of a blend of hi-pour fuel oil and crude jatropha oil

after it was cooled. There was no difference between the viscosity of the cooled blend

and the viscosity of the same oils blended at 75°F, indicating that heating the oils did not

significantly change their properties. However, the high opacity of the fuel oil may be

obscuring any qualitatively-observable changes, such as palm-based solids settling out of

solution.

| (a) | (b) |

Figure 7-78. Hi-pour fuel oil – crude jatropha oil blend, cooled from 220°F to 75°F. (a) shows the blend sitting flat, and (b) shows the blend tilted at an angle.

Figure 7-79 shows photos of a blend of hi-pour fuel oil and biocrude derived from animal renderings after it was cooled. The qualitative viscosity of the cooled fuel blend was slightly lower than that of the same oils blended at 75°F. However, the high opacity of the fuel oil may be obscuring any qualitatively-observable changes, such as biocrude-based solids settling out of solution.

| (a) | (b) |

Figure 7-79. Hi-pour fuel oil – biocrude blend, cooled from 220°F to 75°F. (a) shows the blend sitting flat, and (b) shows the blend tilted at an angle.

Figure 7-80 shows photos of a blend of hi-pour fuel oil and biodiesel (refined biocrude) after it was cooled. There was no difference between the viscosity of the cooled blend and the viscosity of the same oils blended at 75°F, indicating that heating the oils did not significantly change their properties. Thus, this blend of oils is acceptable.

(a)   (b)

Figure 7-80. Hi-pour fuel oil – biodiesel blend, cooled from 220°F to 75°F. (a) shows the blend sitting flat, and (b) shows the blend tilted at an angle.

Figure 7-81 shows photos of a blend of hi-pour fuel oil and ultra-low sulfur diesel after it was cooled. There was no difference between the viscosity of the cooled blend and the viscosity of the same oils blended at 75°F, indicating that heating the oils did not significantly change their properties. Thus, this cooled blend of oils is acceptable.

| (a) | (b) |

Figure 7-81. Hi-pour fuel oil – ultra-low sulfur diesel blend, cooled from 220°F to 75°F. (a) shows the blend sitting flat, and (b) shows the blend tilted at an angle.

Figure 7-82 shows photos of a blend of lo-pour fuel oil and crude palm oil after it was cooled. There was no difference between the viscosity of the cooled blend and the viscosity of the same oils blended at 75°F, indicating that heating the oils did not significantly change their properties. However, the high opacity of the fuel oil may be obscuring any qualitatively-observable changes, such as palm-based solids settling out of solution.

| (a) | (b) |

Figure 7-82. Lo-pour fuel oil – crude palm oil blend, cooled from 220°F to 75°F. (a) shows the blend sitting flat, and (b) shows the blend tilted at an angle.

Figure 7-83 shows photos of a blend of lo-pour fuel oil and crude jatropha oil after it was cooled. There was no difference between the viscosity of the cooled blend and the viscosity of the same oils blended at 75°F, indicating that heating the oils did not significantly change their properties. Thus, this cooled blend of oils is acceptable.

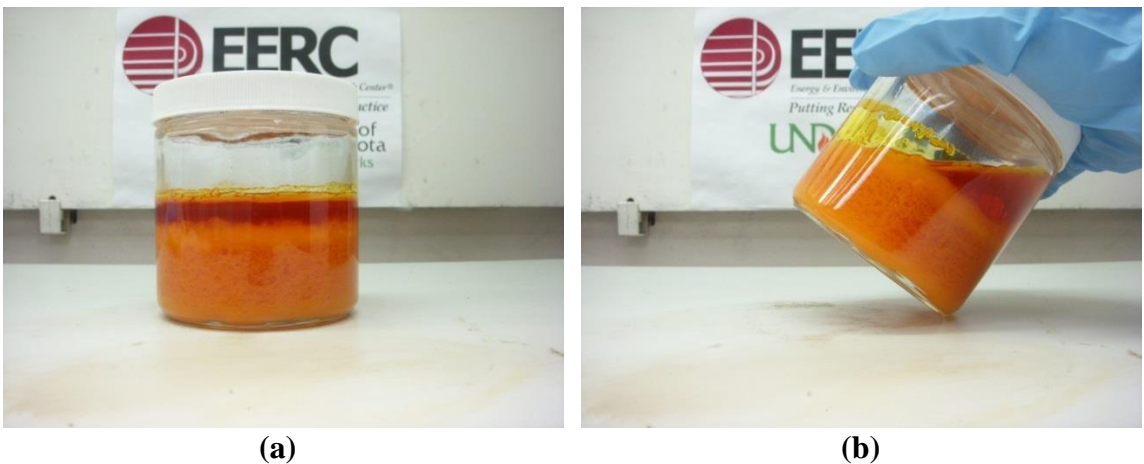
<table>
<tr><td>(a)</td><td>(b)</td></tr>
</table>

Figure 7-83. Lo-pour fuel oil – crude jatropha oil blend, cooled from 220°F to 75°F. (a) shows the blend sitting flat, and (b) shows the blend tilted at an angle.

Figure 7-84 shows photos of a blend of lo-pour fuel oil and biocrude derived from animal renderings after it was cooled. There was no difference between the viscosity of the cooled blend and the viscosity of the same oils blended at 75°F, indicating that heating the oils did not significantly change their properties. However, the high opacity of the fuel oil may be obscuring any qualitatively-observable changes, such as biocrude-based solids settling out of solution.

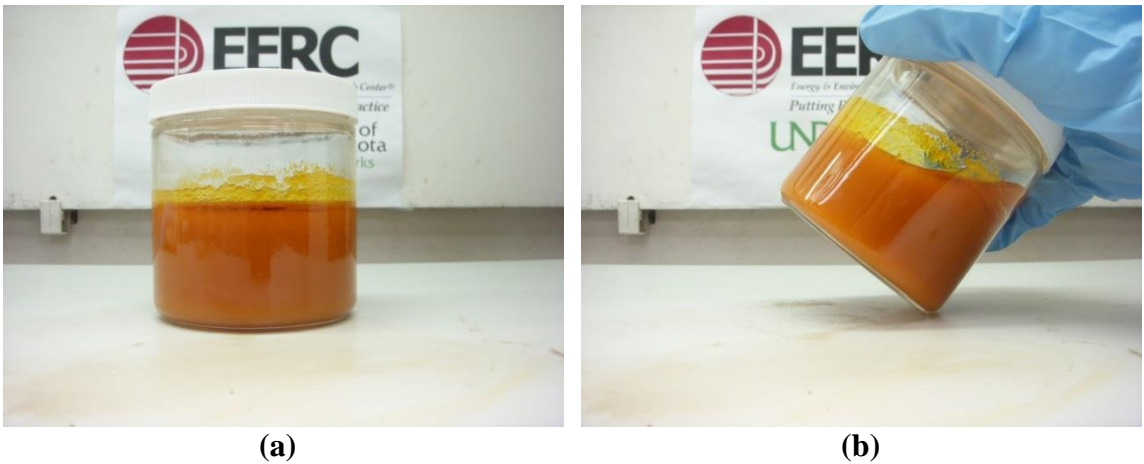|	
(a)	**(b)**
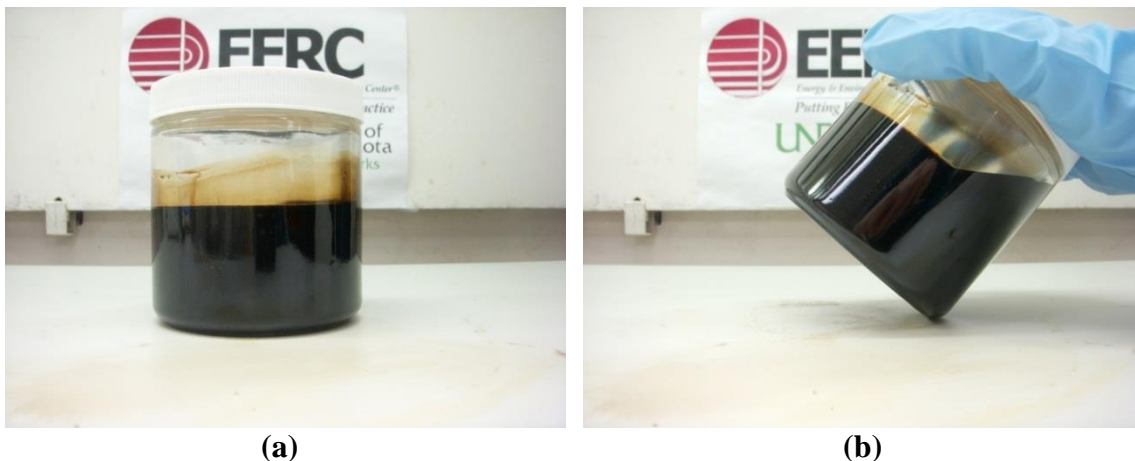
Figure 7-84. Lo-pour fuel oil – biocrude blend, cooled from 220°F to 75°F. (a) shows the blend sitting flat, and (b) shows the blend tilted at an angle.

Figure 7-85 shows photos of a blend of lo-pour fuel oil and biodiesel (refined biocrude) after it was cooled. There was no difference between the viscosity of the cooled blend and the viscosity of the same oils blended at 75°F, indicating that heating the oils did not significantly change their properties. Thus, this cooled blend of oils is acceptable.

(a)	**(b)**
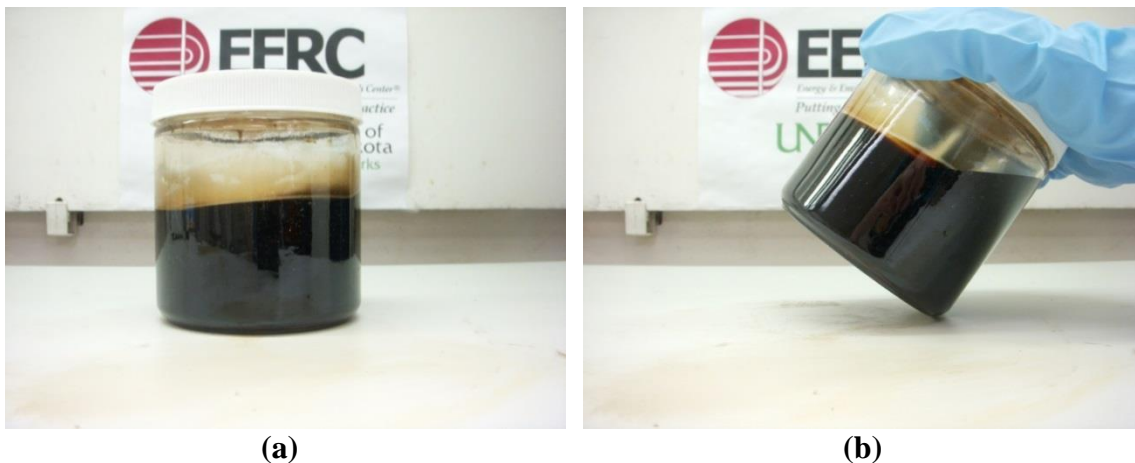
Figure 7-85. Lo-pour fuel oil – biodiesel blend, cooled from 220°F to 75°F. (a) shows the blend sitting flat, and (b) shows the blend tilted at an angle.

Figure 7-86 shows photos of a blend of lo-pour fuel oil and ultra-low sulfur diesel after it was cooled. There was no difference between the viscosity of the cooled blend

and the viscosity of the same oils blended at 75°F, indicating that heating the oils did not significantly change their properties. Thus, this cooled blend of oils is acceptable.

(a)   (b)

Figure 7-86. Lo-pour fuel oil – ultra-low sulfur diesel blend, cooled from 220°F to 75°F. (a) shows the blend sitting flat, and (b) shows the blend tilted at an angle.

Figure 7-87 shows photos of a blend of crude palm oil and crude jatropha oil after it was cooled. A large amount of solids settled out of this fuel blend, but they were not especially dense. However, under the right circumstances, they could still create environments suitable for erosion corrosion or perhaps crevice corrosion if they built up in a dead leg of piping. Therefore, this cooled blend is marginally acceptable.

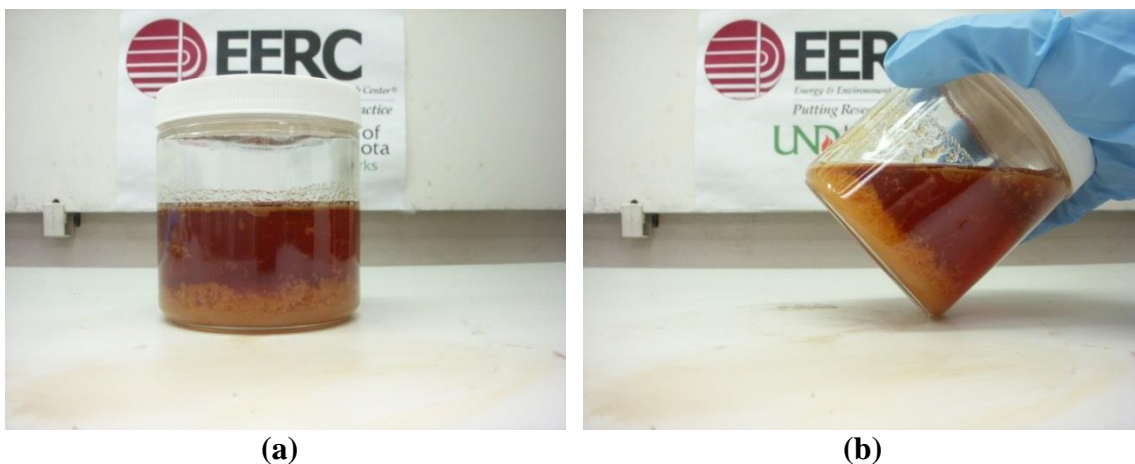(a)   (b)

Figure 7-87. Crude palm oil – crude jatropha oil blend, cooled from 220°F to 75°F. (a) shows the blend sitting flat, and (b) shows the blend tilted at an angle.

Figure 7-88 shows photos of a blend of crude palm oil and biocrude derived from animal renderings after it was cooled. The whole blend became a sludge comprised of congealed palm and biocrude solids. The thickness of the blend could lead to plugging of heated lines or tank outlets. Therefore, this blend is not acceptable under the cooled conditions.

| (a) | (b) |

Figure 7-88. Crude palm oil – biocrude blend, cooled from 220°F to 75°F. (a) shows the blend sitting flat, and (b) shows the blend tilted at an angle.

Figure 7-89 shows photos of a blend of crude palm oil and biodiesel (refined biocrude) after it was cooled. Some loosely packed solids settled out of this blend. Under the right circumstances, these solids could still create environments suitable for erosion corrosion or perhaps crevice corrosion if they built up in a dead leg of piping. The solids could also plug pipelines or, more likely, tank outlets, leading to additional maintenance costs. Therefore, this cooled blend is marginally acceptable.

| (a) | (b) |

Figure 7-89. Crude palm oil – biodiesel blend, cooled from 220°F to 75°F. (a) shows the blend sitting flat, and (b) shows the blend tilted at an angle.

Figure 7-90 shows photos of a blend of crude palm oil and ultra-low sulfur diesel after it was cooled. A layer of loosely packed solids settled out of the blend. Under the right circumstances, these solids could still create environments suitable for erosion corrosion or perhaps crevice corrosion if they built up in a dead leg of piping. The solids could also plug pipelines or, more likely, tank outlets, leading to additional maintenance costs. Therefore, this cooled blend is marginally acceptable.
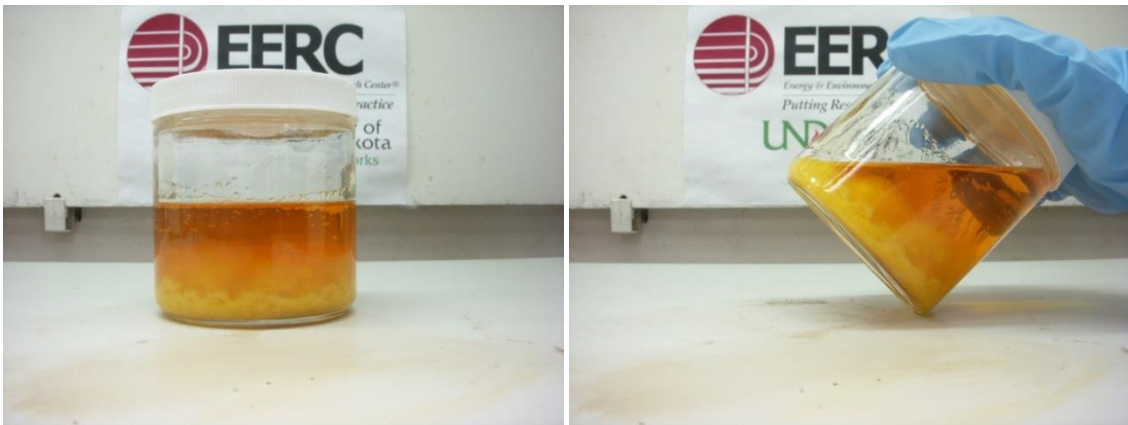
| (a) | (b) |

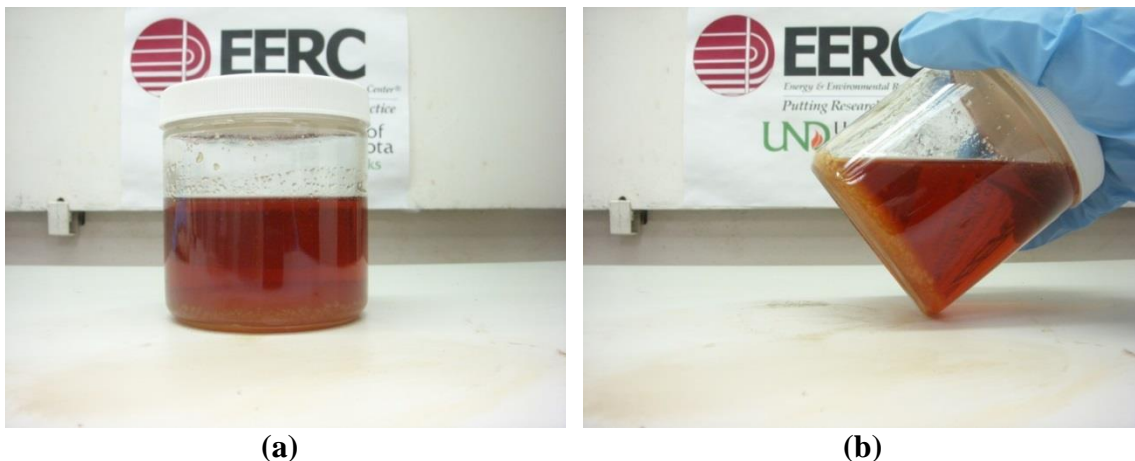**Figure 7-90.** Crude palm oil – ultra-low sulfur diesel blend, cooled from 220°F to 75°F. (a) shows the blend sitting flat, and (b) shows the blend tilted at an angle.

Figure 7-91 shows a blend of crude jatropha oil and biocrude derived from animal renderings after it was cooled. A large quantity of low-density solids settled out of the blend. Under the right circumstances, these solids could still create environments suitable for erosion corrosion or perhaps crevice corrosion if they built up in a dead leg of piping. Therefore, this cooled blend is marginally acceptable.

| (a) | (b) |

Figure 7-91. Crude jatropha oil – biocrude blend, cooled from 220°F to 75°F. (a) shows the blend sitting flat, and (b) shows the blend tilted at an angle.

Figure 7-92 shows a blend of crude jatropha oil and biodiesel (refined biocrude) after it was cooled. There was no difference between the viscosity of the cooled blend and the viscosity of the same oils blended at 75°F, indicating that heating the oils did not significantly change their properties. Thus, this cooled blend of oils is acceptable.

| **(a)** | **(b)** |

Figure 7-92. Crude jatropha oil – biodiesel blend, cooled from 220°F to 75°F. (a) shows the blend sitting flat, and (b) shows the blend tilted at an angle.

Figure 7-93 shows a blend of crude jatropha oil and ultra-low sulfur diesel after it was cooled. There was no difference between the viscosity of the cooled blend and the viscosity of the same oils blended at 75°F, indicating that heating the oils did not significantly change their properties. Thus, this cooled blend of oils is acceptable.

| **(a)** | **(b)** |

Figure 7-93. Crude jatropha oil – ultra-low sulfur diesel blend, cooled from 220°F to 75°F. (a) shows the blend sitting flat, and (b) shows the blend tilted at an angle.

Figure 7-94 shows a blend of biocrude derived from animal renderings and ultra-low sulfur diesel after it was cooled. There was no difference between the viscosity of the

169

cooled blend and the viscosity of the same oils blended at 75°F, indicating that heating

the oils did not significantly change their properties. Thus, this cooled blend of oils is

acceptable.

(a)   (b)
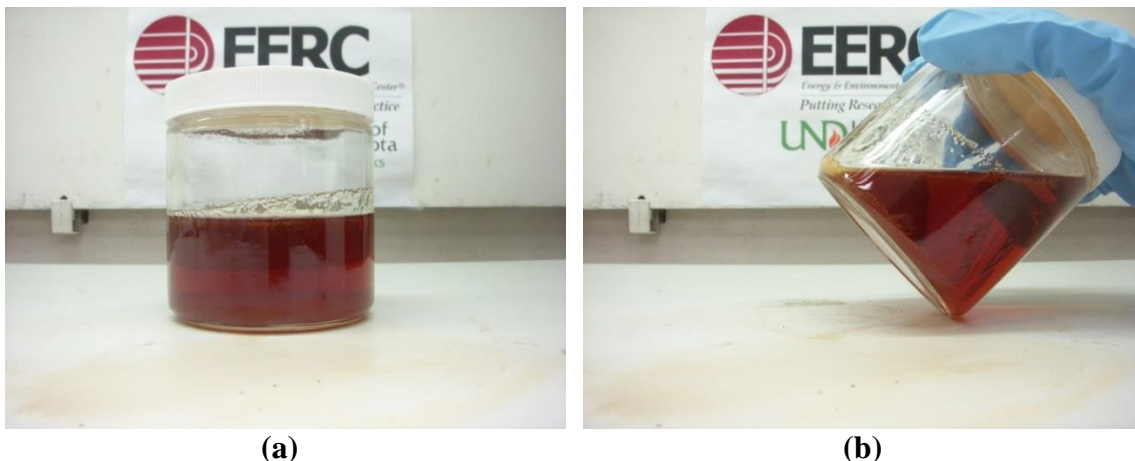
Figure 7-94. Biocrude – ultra-low sulfur diesel blend, cooled from 220°F to 75°F. (a) shows the blend sitting flat, and (b) shows the blend tilted at an angle.

Figure 7-95 shows a blend of biodiesel (refined biocrude) and ultra-low sulfur

diesel after it was cooled. There was no difference between the viscosity of the cooled

blend and the viscosity of the same oils blended at 75°F, indicating that heating the oils

did not significantly change their properties. Thus, this cooled blend of oils is acceptable.

(a)   (b)

Figure 7-95. Biodiesel – ultra-low sulfur diesel blend, cooled from 220°F to 75°F. (a) shows the blend sitting flat, and (b) shows the blend tilted at an angle.

Based on the above results, Table 7-8 shows the acceptability of the fuel blends after they were cooled from 220°F to 75°F. The main cause of failure was solids settling or the formation of sludge-like compounds. Fewer dense solids were observed in the crude jatropha oil – biocrude derived from animal renderings blend, the crude palm oil – biodiesel (refined biocrude) blend, and the crude palm oil – ultra-low sulfur diesel blend cooled from 220°F to 75°F than in the respective blends cooled from 170°F to 75°F. This may have been due to a change in structure for the blends containing crude palm oil; as outlined previously, the palm oil may have gone rancid from heating it rapidly, causing a change in the structure of the oil molecules. Not enough is known about the biocrude derived from animal renderings to determine why it would experience fewer solids settling out of solution under these conditions.

Table 7-8. Acceptability of fuel blends after cooling from 220°F to 75°F.

	Lo-Pour Fuel Oil	Hi-Pour Fuel Oil	Biocrude (animal)	Crude Jatropha Oil	Crude Palm Oil	Biodiesel (refined biocrude)	Ultra-low sulfur diesel
Lo-Pour Fuel Oil		Not Tested	Yes	Yes	Marginal	Yes	Yes
Hi-Pour Fuel Oil			Yes	Yes	Marginal	Yes	Yes
Biocrude (animal)				Marginal	No	Not Tested	No
Crude Jatropha Oil					No	Yes	Yes
Crude Palm Oil						Marginal	Marginal
Biodiesel (refined biocrude)							Yes
Ultra-low sulfur diesel							

7.1.6   Aggregate Photos of Oil Blends

Figure 7-96 shows a blend of hi-pour fuel oil and crude palm oil. These oils were resistant to blending at 75°F, but were fully miscible at 170°F and 220°F. In addition, these oil blends are highly opaque and darkly colored, contributing to difficulty in determining whether palm solids settled out of solution, especially in the blends which were cooled from 170°F and 220°F to 75°F. These oils are unlikely to store and pump well, especially if heating on the tanks or pipelines fails.

Figure 7-96. Hi-pour fuel oil – crude palm oil blend. In order from left to right, original blend temperatures were 75°F, 170°F, 220°F. All blends have been photographed at 75°F.

Figure 7-97 shows a blend of hi-pour fuel oil and crude jatropha oil. These oils were fully miscible at all three testing temperatures. However, these oil blends are highly

172

opaque and darkly colored, contributing to difficulty in determining whether any solids

settled out of solution, especially in the blends which were cooled from 170°F and 220°F

to 75°F. It is thought that this would be unlikely because of the low wax content of the

crude jatropha oil. Given these factors, this blend is likely to store and pump well.

Figure 7-97. Hi-pour fuel oil – crude jatropha oil blend. In order from left to right, original blend temperatures were 75°F, 170°F, 220°F. All blends have been photographed at 75°F.

Figure 7-98 shows a blend of hi-pour fuel oil and biocrude derived from animal

renderings. These oils were resistant to blending at 75°F, but were fully miscible at 170°F

and 220°F. In addition, these oil blends are highly opaque and darkly colored,

contributing to difficulty in determining whether biocrude-derived solids settled out of

solution, especially in the blends which were cooled from 170°F and 220°F to 75°F. These oils may store and pump well, but this is a little unclear because of the aforementioned difficulty in determining whether any solids settled out of the mixture.

Figure 7-98. Hi-pour fuel oil – biocrude blend. In order from left to right, original blend temperatures were 75°F, 170°F, 220°F. All blends have been photographed at 75°F.

Figure 7-99 shows a blend of hi-pour fuel oil and biodiesel (refined biocrude). These oils were fully miscible at all three testing temperatures. However, these oil blends are highly opaque and darkly colored, contributing to difficulty in determining whether any solids settled out of solution, especially in the blends which were cooled from 170°F and 220°F to 75°F. It is thought that this would be unlikely because of the low wax content of the biodiesel. Given these factors, this blend is likely to store and pump well.

Figure 7-99. Hi-pour fuel oil – biodiesel blend. In order from left to right, original blend temperatures were 75°F, 170°F, 220°F. All blends have been photographed at 75°F.

Figure 7-100 shows a blend of hi-pour fuel oil and ultra-low sulfur diesel. These oils were fully miscible at all three testing temperatures; however, this blend did smoke at 220°F. In addition, these oil blends are highly opaque and darkly colored, contributing to difficulty in determining whether any solids settled out of solution, especially in the blends which were cooled from 170°F and 220°F to 75°F. It is thought that this would be unlikely because of the low wax content of the ultra-low sulfur diesel. Given these factors, this blend is likely to store and pump well, especially with the addition of a cetane number improver. The improver would have the added effect of enhancing its combustion characteristics by raising the cetane number.

175

Figure 7-100. Hi-pour fuel oil – ultra-low sulfur diesel blend. In order from left to right, original blend temperatures were 75°F, 170°F, 220°F. All blends were photographed at 75°F.

Figure 7-101 shows a blend of lo-pour fuel oil and crude palm oil. These oils were resistant to blending at 75°F, but were fully miscible at 170°F and 220°F. In addition, these oil blends are highly opaque and darkly colored, contributing to difficulty in determining whether palm solids settled out of solution, especially in the blends which were cooled from 170°F and 220°F to 75°F. These oils are unlikely to store and pump well, especially if heating on the tanks or pipelines fails.
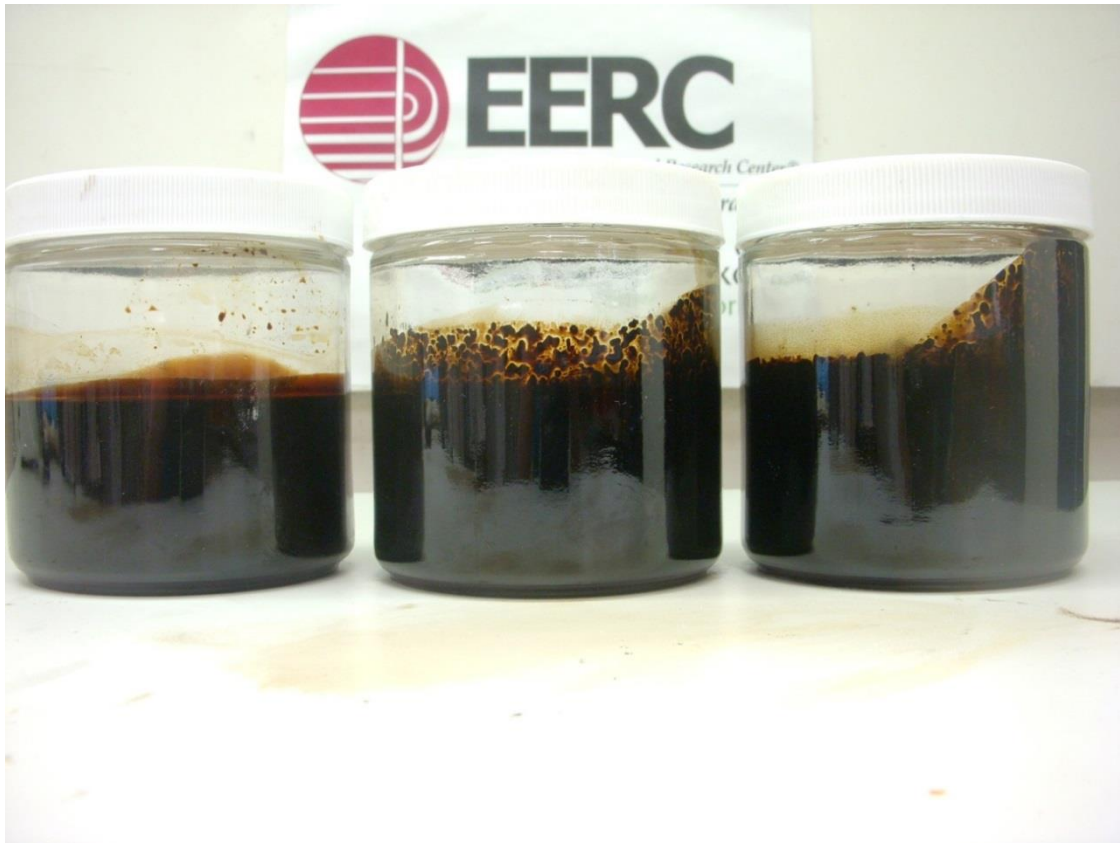
Figure 7-101. Lo-pour fuel oil – crude palm oil blend. In order from left to right, original blend temperatures were 75°F, 170°F, 220°F. All blends were photographed at 75°F.

Figure 7-102 shows a blend of lo-pour fuel oil and crude jatropha oil. These oils were fully miscible at all three testing temperatures. However, these oil blends are highly opaque and darkly colored, contributing to difficulty in determining whether any solids settled out of solution, especially in the blends which were cooled from 170°F and 220°F to 75°F. It is thought that this would be unlikely because of the low wax content of the crude jatropha oil. Given these factors, this blend is likely to store and pump well.
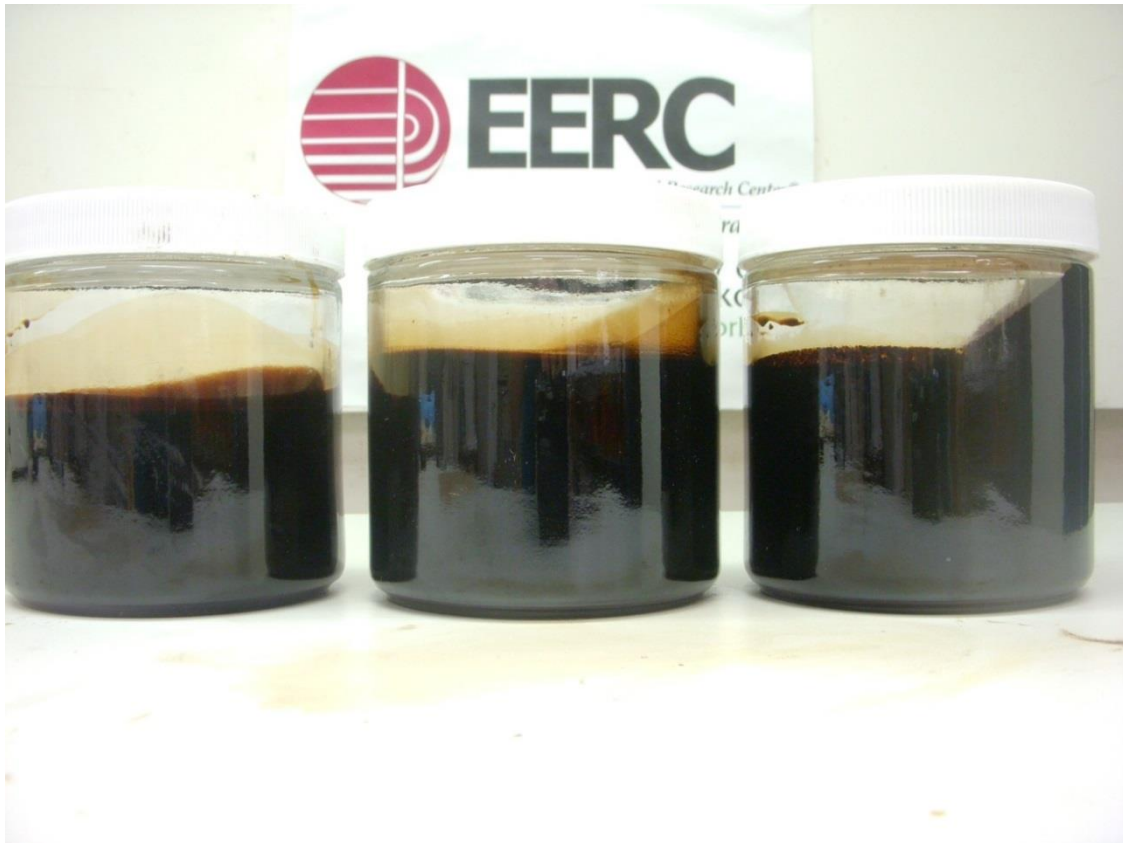
Figure 7-102. Lo-pour fuel oil – crude jatropha oil blend. In order from left to right, original blend temperatures were 75°F, 170°F, 220°F. All blends were photographed at 75°F.

Figure 7-103 shows a blend of lo-pour fuel oil and biocrude derived from animal renderings. These oils were resistant to blending at 75°F, but were fully miscible at 170°F and 220°F. In addition, these oil blends are highly opaque and darkly colored, contributing to difficulty in determining whether biocrude-derived solids settled out of solution, especially in the blends which were cooled from 170°F and 220°F to 75°F. These oils may store and pump well, but this is a little unclear because of the aforementioned difficulty in determining whether any solids settled out of the mixture.
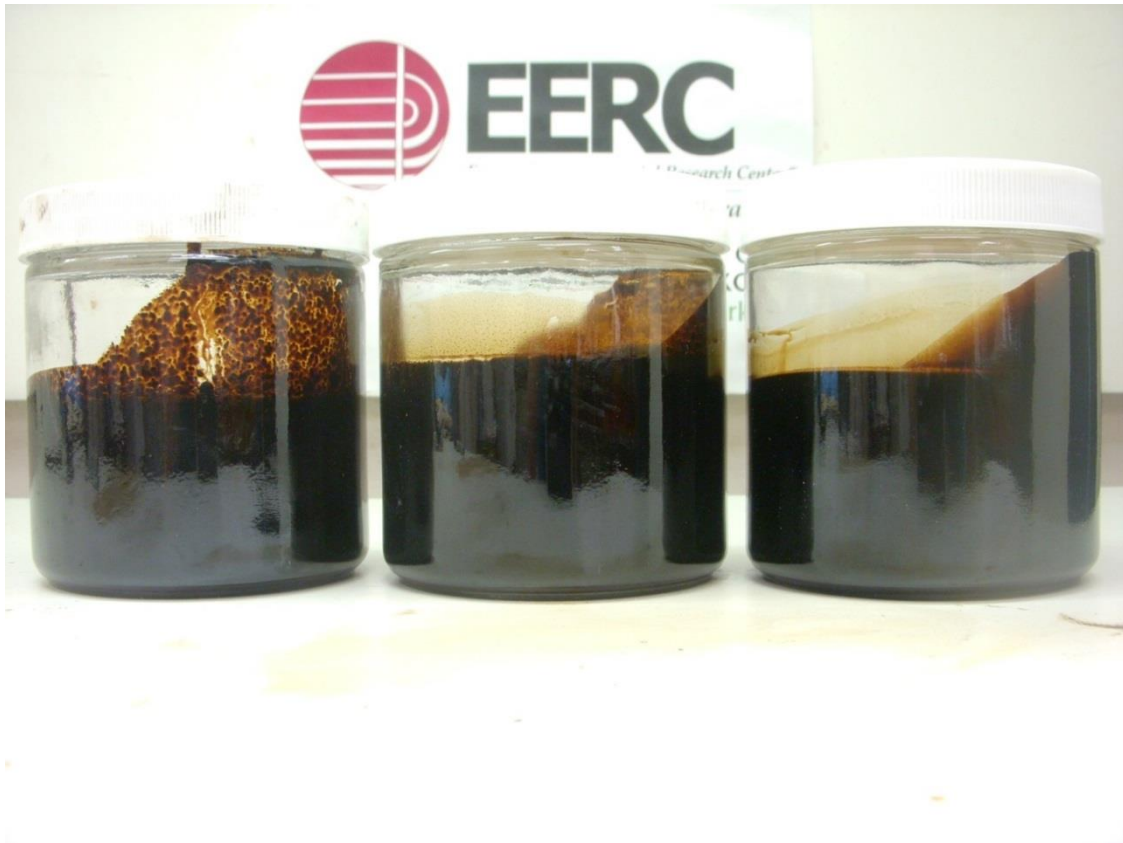
Figure 7-103. Lo-pour fuel oil – biocrude blend. In order from left to right, original blend temperatures were 75°F, 170°F, 220°F. All blends were photographed at 75°F.

Figure 7-104 shows a blend of lo-pour fuel oil and biodiesel. These oils were fully miscible at all three testing temperatures. However, these oil blends are highly opaque and darkly colored, contributing to difficulty in determining whether any solids settled out of solution, especially in the blends which were cooled from 170°F and 220°F to 75°F. It is thought that this would be unlikely because of the low wax content of the biodiesel. Given these factors, this blend is likely to store and pump well.
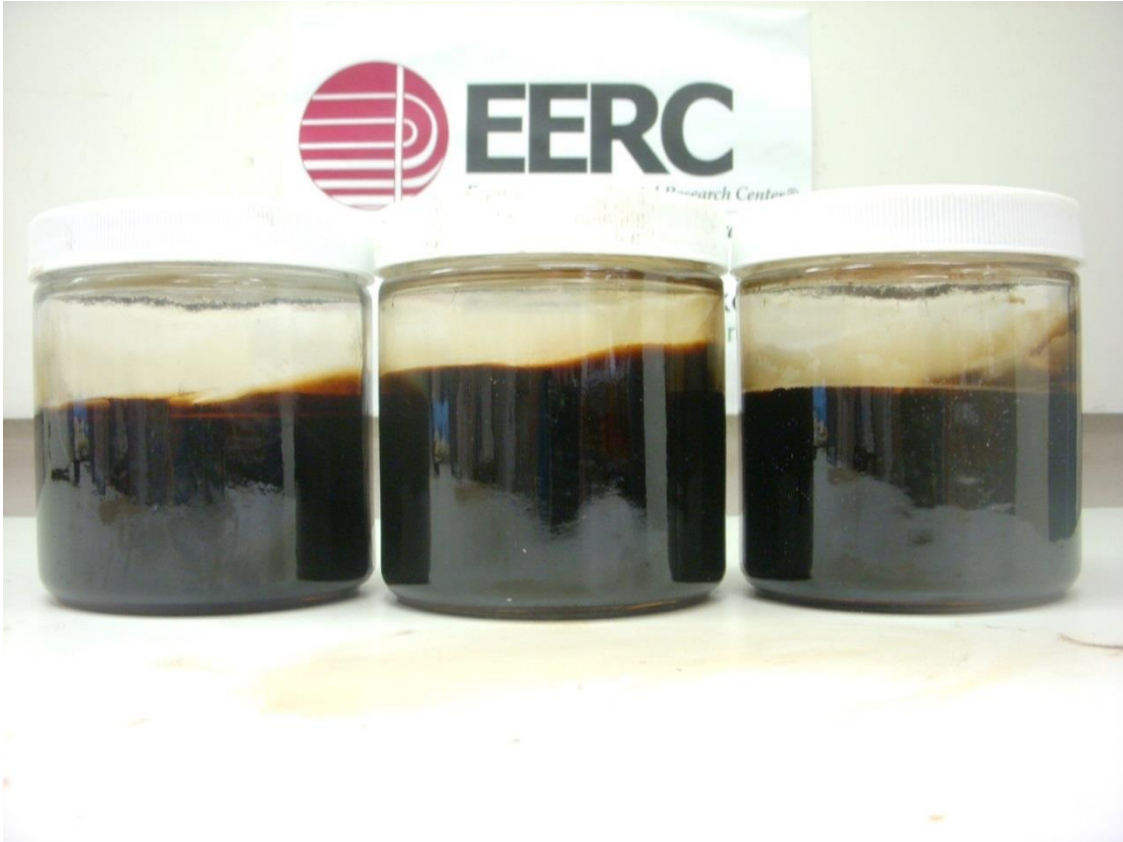
Figure 7-104. Lo-pour fuel oil – biodiesel blend. In order from left to right, original blend temperatures were 75°F, 170°F, 220°F. All blends were photographed at 75°F.

Figure 7-105 shows a blend of lo-pour fuel oil and ultra-low sulfur diesel. These oils were fully miscible at all three testing temperatures; however, this blend did smoke at 220°F. In addition, these oil blends are highly opaque and darkly colored, contributing to difficulty in determining whether any solids settled out of solution, especially in the blends which were cooled from 170°F and 220°F to 75°F. It is thought that this would be unlikely because of the low wax content of the ultra-low sulfur diesel. Given these factors, this blend is likely to store and pump well, especially with the addition of a cetane number improver. The improver would have the added effect of enhancing its combustion characteristics by raising the cetane number.

Figure 7-105. Lo-pour fuel oil – ultra-low sulfur diesel blend. In order from left to right, original blend temperatures were 75°F, 170°F, 220°F. All blends were photographed at 75°F.

Figure 7-106 shows a blend of crude palm oil and crude jatropha oil. Solids tended to settle out of this mixture at 75°F; however, this problem was not observed at 170°F and 220°F. When the mixtures blended at 170°F and 220°F were cooled to 75°F, solids settled out of the blends. If heat is not lost in the storage tanks and pipelines, this blend will pump and store well; however, if heat is lost, this blend may not pump or store well.

Figure 7-106. Crude palm oil – crude jatropha oil blend. In order from left to right, original blend temperatures were 75°F, 170°F, 220°F. All blends were photographed at 75°F.

Figure 7-107 shows a blend of crude palm oil and biocrude derived from animal renderings. A significant amount of solids settled out of this mixture at 75°F. At 220°F, a layer of semi-polymerized biocrude oil formed on the bottom of the beaker within 25 minutes of stirring at temperature. However, these problems were not observed at 170°F. When the blends at 170°F and 220°F were cooled to 75°F, solids settled out of the mixtures. Given these factors, this blend is unlikely to pump and store well.

Figure 7-107. Crude palm oil – biocrude blend. In order from left to right, original blend temperatures were 75°F, 170°F, 220°F. All blends were photographed at 75°F.

Figure 7-108 shows a blend of crude palm oil and biodiesel (refined biocrude). A significant amount of solids settled out of this mixture at 75°F. However, this problem was not observed at 170°F or 220°F. When the blends at 170°F and 220°F were cooled to 75°F, solids settled out of the mixtures. This blend may pump and store well if heating is not lost in the storage tanks or pipelines.

Figure 7-108. Crude palm oil – biodiesel blend. In order from left to right, original blend temperatures were 75°F, 170°F, 220°F. All blends were photographed at 75°F.

Figure 7-109 shows a blend of crude palm oil and ultra-low sulfur diesel. The blend at 75°F became a sludge; however, solids did not settle out of the blends at 170°F and 220°F. In addition, this blend smoked at 220°F. Solids settled out of the blends which were cooled from 170°F and 220°F to 75°F. Given these factors, this blend is unlikely to store and pump well.

Figure 7-109. Crude palm oil – ultra-low sulfur diesel blend. In order from left to right, original blend temperatures were 75°F, 170°F, 220°F. All blends were photographed at 75°F.

Figure 7-110 shows a blend of crude jatropha oil and biocrude derived from animal renderings. A significant amount of solids settled out of this mixture at 75°F. This problem was not observed at 170°F or 220°F; however, a film of semi-polymerized oil formed on the beaker at 220°F. When the blends at 170°F and 220°F were cooled to 75°F, solids settled out of the mixtures. Given these factors, this oil may not pump or store well.
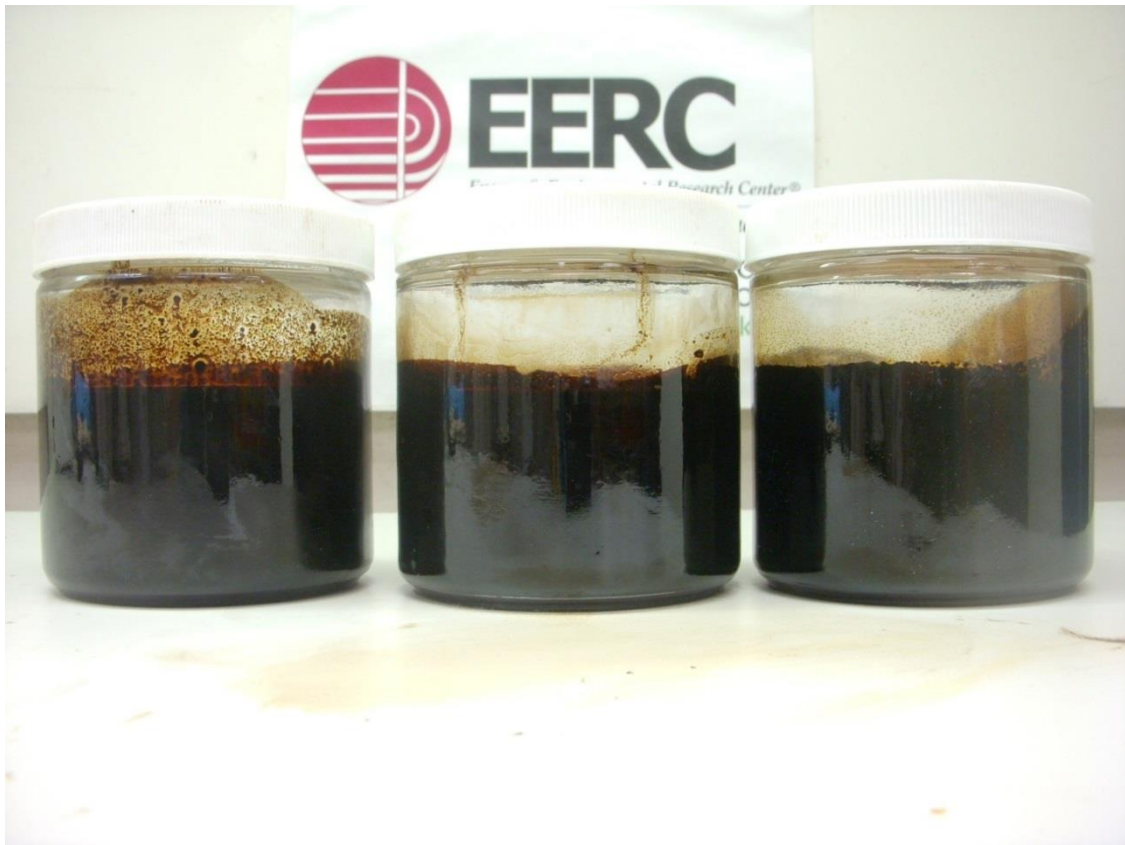
185

Figure 7-110. Crude jatropha oil – biocrude blend. In order from left to right, original blend temperatures were 75°F, 170°F, 220°F. All blends were photographed at 75°F.

Figure 7-111 shows a blend of crude jatropha oil and biodiesel (refined biocrude). These oils were fully miscible, completely mixed, and had zero solids settling at 75°F, 170°F, and 220°F. In addition, no solids settled out of the mixtures when the blends were cooled from 170°F and 220°F to 75°F. This blend would pump and store well.
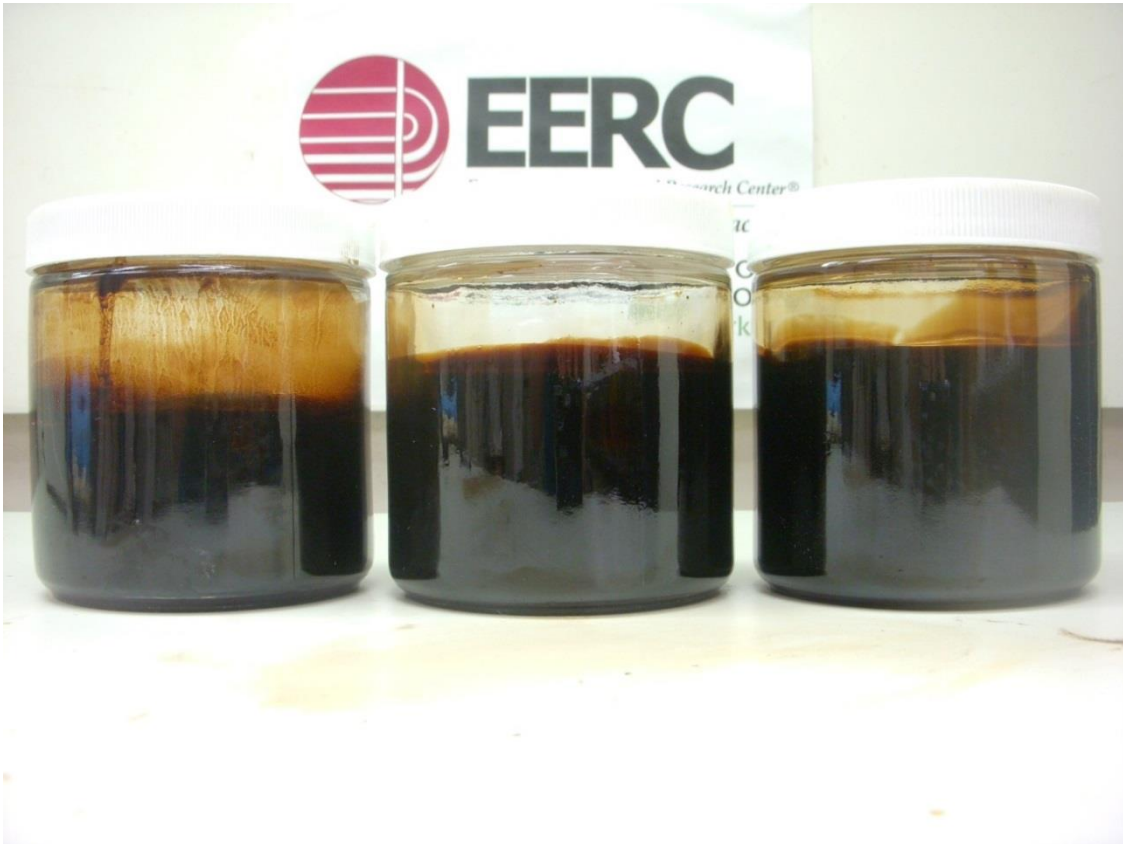
Figure 7-111. Crude jatropha oil – biodiesel blend. In order from left to right, original blend temperatures were 75°F, 170°F, 220°F. All blends were photographed at 75°F.

Figure 7-112 shows a blend of crude jatropha oil and ultra-low sulfur diesel. These oils were fully miscible, completely mixed, and had zero solids settling at 75°F, 170°F, and 220°F. However, this blend smoked at 220°F. Given these factors, this blend may store and pump well, especially with the addition of a cetane number improver.

Figure 7-112. Crude jatropha oil – ultra-low sulfur diesel blend. In order from left to right, original blend temperatures were 75°F, 170°F, 220°F. All blends were photographed at 75°F.

Figure 7-113 shows a blend of biocrude derived from animal renderings and ultra-low sulfur diesel. A significant amount of solids settled out of this mixture at 75°F. This problem was not observed at 170°F or 220°F; however, a film of semi-polymerized oil formed on the beaker at 220°F. When the blend at 170°F was cooled to 75°F, solids settled out of the mixture. This settling behavior was not observed in the blend cooled from 220°F to 75°F. Given these factors, this oil may pump and store well, especially if adequate heating in the storage tanks and pipelines is maintained.

Figure 7-113. Biocrude – ultra-low sulfur diesel blend. In order from left to right, original blend temperatures were 75°F, 170°F, 220°F. All blends were photographed at 75°F.

Figure 7-114 shows a blend of biodiesel (refined biocrude) and ultra-low sulfur diesel. These oils were fully miscible, completely mixed, and had zero solids settling at 75°F, 170°F, and 220°F. However, this blend smoked at 220°F. Given these factors, this blend may store and pump well, especially with the addition of a cetane number improver.
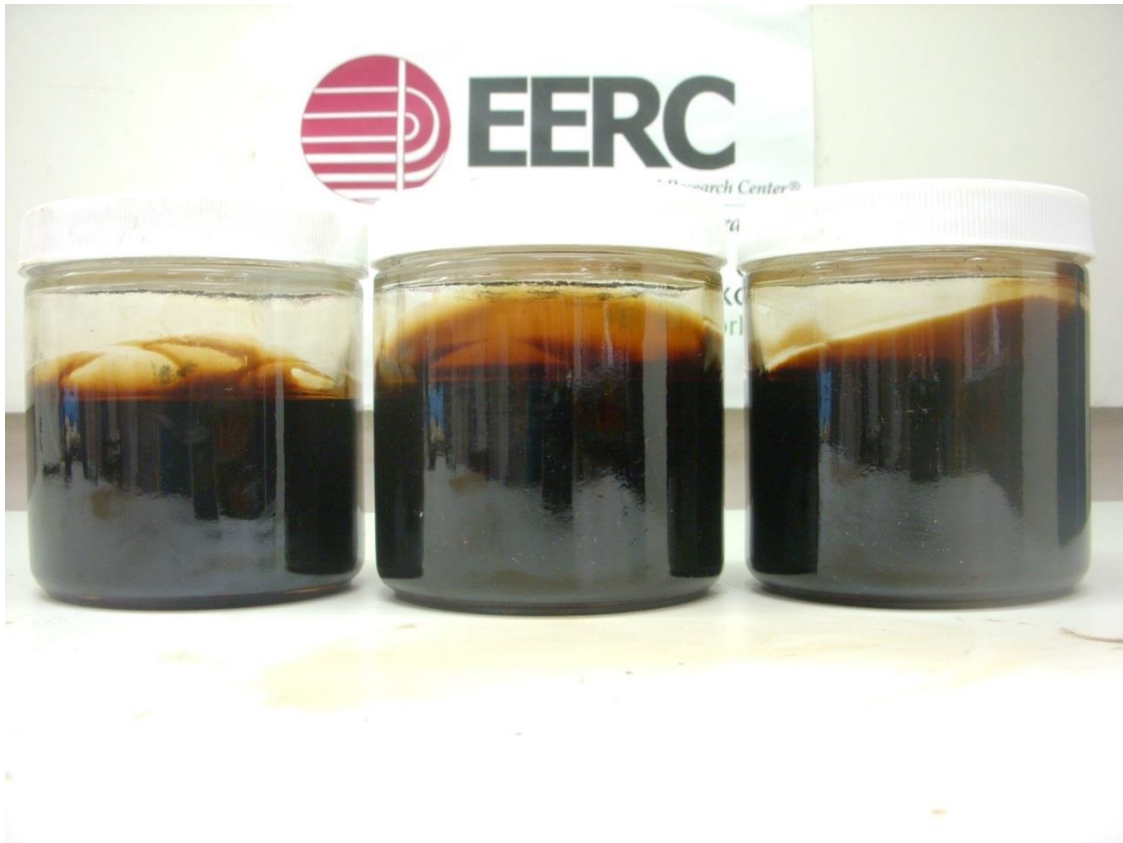
Figure 7-114. Biodiesel – ultra-low sulfur diesel blend. In order from left to right, original blend temperatures were 75°F, 170°F, 220°F. All blends were photographed at 75°F.

In summary, blends with high concentrations of waxes at ambient temperatures, such as those containing biocrude derived from animal renderings or crude palm oil, were more likely to be marginally acceptable or unacceptable as the waxes tended to settle out of solution at ambient temperature or when cooled to ambient temperature. Furthermore, blends containing biocrude derived from animal renderings were likely to form semi-polymerized oil layers at 220°F, making these blends more marginally acceptable. Blends containing ultra-low sulfur diesel tended to smoke at 220°F, making them marginally acceptable without the use of a cetane number improver. However, blends that contained

190

transparent bio-based oils, such as biodiesel or crude jatropha oil, were much more likely

to be acceptable because of their low solids content and low viscosity.

7.2   Characterization of Pure Fuels and Fuel Blends
7.2.1   Pour Points

Pour points were analyzed for six blends: crude jatropha oil – biodiesel (refined

biocrude), crude jatropha oil – biocrude derived from animal renderings, crude palm oil –

biocrude derived from animal renderings, crude jatropha oil – crude palm oil, crude palm

oil – biodiesel (refined biocrude), and hi-pour fuel oil – crude jatropha oil. The reported

pour points are listed in Table 7-9.

Table 7-9. Pour points of selected fuel blends.

Fuel Blend	Pour Point (±5°F)
Crude jatropha oil – biodiesel (refined biocrude)	45
Crude jatropha oil – biocrude derived from animal renderings	20
Biocrude derived from animal renderings – crude palm oil	40
Crude jatropha oil – crude palm oil	30
Crude palm oil – biodiesel (refined biocrude)	35
Hi-pour fuel oil – crude jatropha oil	40

These pour points indicate that all these blends would be pourable – and therefore

pumpable – at ambient temperatures, but would not pour or pump at colder temperatures

without heat-tracing on the pipelines. However, many of these blends have entrained

waxes, and these waxes can interfere with reported pour points on this apparatus,

especially if they settle to the bottom of the sample cup and the pour point of the liquid

above is measured. In addition, the optical nature of this measurement method adds to the

difficulty in determining pour points of darkly-colored blends, such as the hi-pour fuel oil

– crude jatropha oil blend.

7.2.2   Flash Points

Six fuel blends were tested for flash point: crude jatropha oil – biodiesel (refined biocrude), crude jatropha oil – biocrude derived from animal renderings, crude palm oil – biocrude derived from animal renderings, crude jatropha oil – crude palm oil, crude palm oil – biodiesel (refined biocrude), and hi-pour fuel oil – crude jatropha oil. While this analyzer is reported in the documentation to be able to determine flash points as high as 266°F, due to equipment failure, the analyzer did not heat above 155°F during testing. Therefore, since none of the blends flashed at 155°F or lower, it can be determined that all six of the blends had flash points in excess of 155°F, though how much in excess cannot be determined.

Table 7-10 shows the flash points of the pure oils studied in these blends as determined through literature review. Blends containing biodiesel and low-sulfur fuel oil may have had flash points higher than those of the pure oils.

Table 7-10. Flash points of pure oils.

Fuel Type	Flash Point (°F)
Biodiesel (refined biocrude)	100, 126-140, 266
Crude jatropha oil	464
Yellow grease	399
Crude palm oil	> 212
Low-sulfur fuel oil	> 126

7.2.3   Cloud Points

Cloud points were measured using a proprietary method. Table 7-11 shows the cloud points for selected pure oils and oil blends. Some oils and blends had a wax content too low to have a discernable cloud point using the aforementioned method. While this method, which more properly measures the wax appearance temperature, is conservative insofar as the exact temperatures where problems will be observed, a few trends do stand

out. At ambient temperatures, fuels and fuel blends with wax appearance temperatures ranging from approximately 70°F to 80°F will have little to no problems with filter clogging. However, fuels and fuel blends with higher wax appearance temperatures – i.e., those containing lo-pour fuel oil and hi-pour fuel oil – may experience issues with filters or orifices clogging or pipeline or heat exchanger fouling due to accumulation on cold surfaces. In addition, it was observed that the hi-pour fuel oil – crude jatropha oil blend had a higher wax appearance temperature than that of either the hi-pour fuel oil or the crude jatropha oil (for which a wax appearance temperature was not observed).

Table 7-11. Cloud points of selected oils and oil blends.

Oil/Oil Blend	Wax Appearance Temperature (°F)
Crude jatropha oil – biodiesel (refined biocrude)	Not observed
Biocrude derived from animal renderings – crude palm oil	81.1 ± 0.1
Crude jatropha oil – crude palm oil	73.2
Biocrude derived from animal renderings – crude jatropha oil	71.2 ± 1.8
Crude palm oil – biodiesel (refined biocrude)	80.1
Hi-pour fuel oil – crude jatropha oil	150.8 ± 4.6
Crude palm oil	73.4 ± 3.7
Biodiesel (refined biocrude)	Not observed
Biocrude derived from animal renderings	79.5 ± 2.0
Lo-pour fuel oil	144.3 ± 6.1
Hi-pour fuel oil	116.2 ± 7.0
Crude jatropha oil	Not observed

7.2.4   Proximate and Ultimate Analysis

Table 7-12 shows the ultimate analysis for the pure oils. As these properties are additive (Atkins and Jones, 2005), values for the blends may be calculated based upon the properties of the parent fuels. Thermogravimetric analysis (TGA) results indicated that there was more than 100% volatile matter for all of the oil samples; therefore, proximate

193

analysis could not be performed and moisture was determined by Karl Fisher titration. The moisture values indicate that, while many of the oils would present no problem for normal use, the biocrude derived from animal renderings and lo-pour fuel oil would need drying before use.

Table 7-12. Ultimate analysis of pure oils, as-determined basis.

	Biocrude	Biodiesel	Hi-Pour Fuel Oil	Crude Jatropha Oil	Lo-Pour Fuel Oil	Crude Palm Oil
Hydrogen	11.5%	12.3%	9.1%	11.7%	8.1%	11.6%
Carbon	75.7%	77.1%	87.0%	77.5%	84.3%	76.3%
Nitrogen	0.10%	0.01%	0.50%	0.01%	0.70%	0.20%
Sulfur	0.002%	0.01%	0.30%	0.01%	0.40%	0.01%
Oxygen (Ind)	12.7%	10.6%	3.1%	10.8%	6.6%	11.9%
Ash	0%	0%	0%	0%	0%	0%
Heating Value (Btu/lb)	16650	17068	18712	16922	18603	16942
Notes	Karl Fisher water = 1.21%	Karl Fisher water = 0.04%	Karl Fisher water = 0.10%	Karl Fisher water = 0.06%	Karl Fisher water = 1.15%	Karl Fisher water = 0.08%

7.3 Corrosion Test Results

Samples of 304 stainless steel, brass, 316 stainless steel, mild steel, and 410 stainless steel were exposed to pure samples of lo-pour fuel oil, hi-pour fuel oil, crude palm oil, crude jatropha oil, biocrude derived from animal renderings, biodiesel (refined biocrude), and ultra-low sulfur diesel at a temperature of 175°F. Samples were exposed for a total of 98 days, and were removed every 14 days for inspection.

The metal samples were photographed prior to exposure to the pure oils and each time they were removed from the oven. In addition, the masses of the metal samples were recorded each time they were removed from the oven.

Figure 7-115 shows the metal samples prior to exposure to the pure oils. Within each metal type, sample 1 was immersed in hi-pour fuel oil, sample 2 was immersed in lo-pour fuel oil, sample 3 was immersed in ultra-low sulfur diesel, sample 4 was immersed in crude palm oil, sample 5 was immersed in crude jatropha oil, sample 6 was immersed in biocrude derived from animal renderings, and sample 7 was immersed in biodiesel (refined biocrude). All corrosion products were removed to the extent possible to allow measurement of the weight loss.
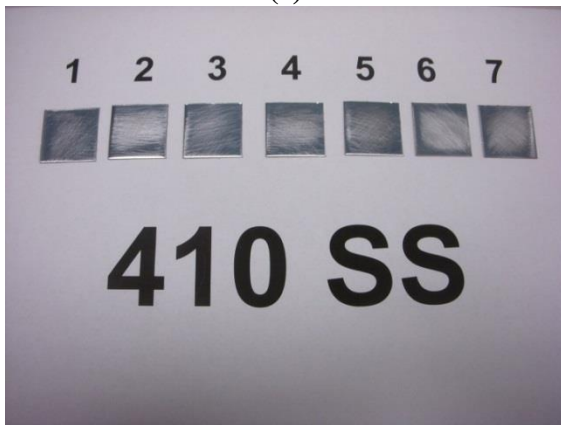
Figure 7-115. Metal samples, 0 hours of exposure to pure oils. (a) 304 stainless steel, (b) brass, (c) 316 stainless steel, (d) mild steel, and (e) 410 stainless steel.

Table 7-13 shows the masses of the metal samples in g throughout the testing period, and Table 7-14 shows the change in mass of the metal samples in mg throughout

the testing period. These changes in mass are calculated with respect to the masses of the samples before exposure to the pure fuels. Some samples, most noticeably the samples in ultra-low sulfur diesel, gained mass at several points in the testing due to deposits caused by fouling of the diesel, which had no thermal stabilizers added to it. These deposits were removed to the extent possible by scrubbing with a rubber stopper under running water and drying the samples before they were weighed.

Table 7-13. Masses in grams of corroded samples.

Sample ID	Metal Type	Oil Type	Mass 0 h	Mass 336 h	Mass 690 h	Mass 1020 h	Mass 1350 h	Mass 1680 h	Mass 2010 h	Mass 2340 h
1	304 SS	HPFO	31.523	31.527	31.528	31.528	31.527	31.527	31.528	31.527
2	304 SS	LPFO	31.205	31.211	31.21	31.212	31.209	31.21	31.211	31.21
3	304 SS	ULS Diesel	30.803	30.804	30.805	30.805	30.816	30.83	31.867	30.851
4	304 SS	Palm	31.736	31.741	31.74	31.74	31.738	31.739	31.74	31.739
5	304 SS	Jatropha	30.822	30.825	30.824	30.826	30.824	30.825	30.827	30.825
6	304 SS	Biocrude	31.656	31.663	31.66	31.661	31.66	31.66	31.664	31.661
7	304 SS	Biodiesel	31.075	31.077	31.078	31.077	31.077	31.078	31.078	31.078
8	Brass	HPFO	7.507	7.508	7.508	7.508	7.508	7.507	7.508	7.507
9	Brass	LPFO	7.261	7.259	7.257	7.256	7.254	7.253	7.253	7.253
10	Brass	ULS Diesel	7.362	7.363	7.363	7.364	7.363	7.363	7.371	7.382
11	Brass	Palm	7.503	7.502	7.499	7.498	7.496	7.496	7.496	7.495
12	Brass	Jatropha	7.402	7.402	7.401	7.4	7.401	7.4	7.401	7.4
13	Brass	Biocrude	7.247	7.241	7.237	7.238	7.237	7.236	7.236	7.238
14	Brass	Biodiesel	7.425	7.424	7.421	7.421	7.421	7.42	7.419	7.418
15	316 SS	HPFO	45.569	45.568	45.568	45.568	45.569	45.568	45.568	45.568
16	316 SS	LPFO	45.531	45.531	45.531	45.531	45.531	45.532	45.531	45.532
17	316 SS	ULS Diesel	49.234	49.235	49.241	49.235	49.238	49.242	49.248	49.249
18	316 SS	Palm	52.05	52.051	52.052	52.052	52.052	52.058	52.053	52.05
19	316 SS	Jatropha	49.735	49.734	49.735	49.734	49.735	49.736	49.736	49.734
20	316 SS	Biocrude	47.39	47.391	47.391	47.392	47.39	47.393	47.39	47.39
21	316 SS	Biodiesel	48.879	48.878	48.879	48.878	48.879	48.879	48.878	48.879

Table 7-13, cont.

Sample ID	Metal Type	Oil Type	Mass 0 h	Mass 336 h	Mass 690 h	Mass 1020 h	Mass 1350 h	Mass 1680 h	Mass 2010 h	Mass 2340 h
22	Mild steel	HPFO	12.235	12.236	12.234	12.234	12.234	12.235	12.233	12.235
23	Mild steel	LPFO	12.34	12.342	12.341	12.34	12.34	12.341	12.34	12.343
24	Mild steel	ULS Diesel	12.223	12.223	12.223	12.239	12.224	12.238	12.226	12.234
25	Mild steel	Palm	12.265	12.265	12.264	12.264	12.264	12.264	12.264	12.266
26	Mild steel	Jatropha	12.373	12.375	12.375	12.374	12.375	12.376	12.375	12.375
27	Mild steel	Biocrude	12.254	12.236	12.226	12.222	12.218	12.215	12.213	12.216
28	Mild steel	Biodiesel	12.269	12.269	12.268	12.268	12.268	12.268	12.267	12.271
29	410 SS	HPFO	2.48	2.481	2.481	2.481	2.482	2.48	2.48	2.479
30	410 SS	LPFO	2.487	2.488	2.488	2.487	2.487	2.487	2.486	2.486
31	410 SS	ULS Diesel	2.478	2.478	2.479	2.479	2.48	2.485	2.484	2.492
32	410 SS	Palm	2.477	2.478	2.477	2.477	2.477	2.478	2.477	2.477
33	410 SS	Jatropha	2.453	2.453	2.453	2.454	2.453	2.453	2.453	2.451
34	410 SS	Biocrude	2.486	2.487	2.487	2.487	2.486	2.487	2.487	2.486
35	410 SS	Biodiesel	2.478	2.477	2.478	2.478	2.477	2.477	2.478	2.477

Table 7-14. Change in mass of metal samples, mg.

Sample ID	Metal Type	Oil Type	ΔMass 336 h	ΔMass 690 h	ΔMass 1020 h	ΔMass 1350 h	ΔMass 1680 h	ΔMass 2010 h	ΔMass 2340 h
1	304 SS	HPFO	4	5	5	4	4	5	4
2	304 SS	LPFO	6	5	7	4	5	6	5
3	304 SS	ULS Diesel	1	2	2	13	27	1064	48
4	304 SS	Palm	5	4	4	2	1	4	3
5	304 SS	Jatropha	3	2	4	2	3	5	3
6	304 SS	Biocrude	7	4	5	4	4	8	5
7	304 SS	Biodiesel	2	3	2	2	3	3	3
8	Brass	HPFO	1	1	1	1	0	1	0
9	Brass	LPFO	-2	-4	-5	-7	-8	-8	-8
10	Brass	ULS Diesel	1	1	2	1	1	9	20
11	Brass	Palm	-1	-4	-5	-7	-7	-7	-8
12	Brass	Jatropha	0	-1	-2	-1	-2	-1	-2
13	Brass	Biocrude	-6	-10	-9	-10	-11	-11	-9
14	Brass	Biodiesel	-1	-4	-4	-4	-5	-6	-7
15	316 SS	HPFO	-1	-1	-1	0	-1	-1	-1
16	316 SS	LPFO	0	0	0	0	1	0	1
17	316 SS	ULS Diesel	1	7	1	4	8	14	15
18	316 SS	Palm	1	2	2	2	8	3	5
19	316 SS	Jatropha	-1	0	-1	0	2	2	-1
20	316 SS	Biocrude	1	1	2	0	3	0	0
21	316 SS	Biodiesel	-1	0	-1	0	0	-1	0

Table 7-14, cont.

Sample ID	Metal Type	Oil Type	ΔMass 336 h	ΔMass 690 h	ΔMass 1020 h	ΔMass 1350 h	ΔMass 1680 h	ΔMass 2010 h	ΔMass 2340 h
22	Mild steel	HPFO	1	-1	-1	-1	0	-2	0
23	Mild steel	LPFO	2	1	0	0	1	0	3
24	Mild steel	ULS Diesel	0	0	16	1	15	3	1
25	Mild steel	Palm	0	-1	-1	-1	-1	-1	1
26	Mild steel	Jatropha	2	2	1	2	3	2	2
27	Mild steel	Biocrude	-18	-28	-32	-36	-39	-41	-38
28	Mild steel	Biodiesel	0	-1	-1	-1	-1	-2	2
29	410 SS	HPFO	1	1	1	2	0	0	-1
30	410 SS	LPFO	1	1	0	0	0	-1	-1
31	410 SS	ULS Diesel	0	1	1	2	7	6	14
32	410 SS	Palm	1	0	0	0	1	0	0
33	410 SS	Jatropha	0	0	1	0	0	0	-2
34	410 SS	Biocrude	1	1	1	0	1	1	0
35	410 SS	Biodiesel	-1	0	0	-1	-1	0	-1

Each metal type will be discussed individually.

Figure 7-116 shows the changes in mass of the 304 stainless steel throughout the exposure process. With the exception of the sample immersed in ultra-low sulfur diesel, no 304 stainless steel sample underwent a change in mass greater than 8 mg. In addition, no sample experienced an overall loss in mass. This implies that no metal was lost from the samples due to corrosive processes.
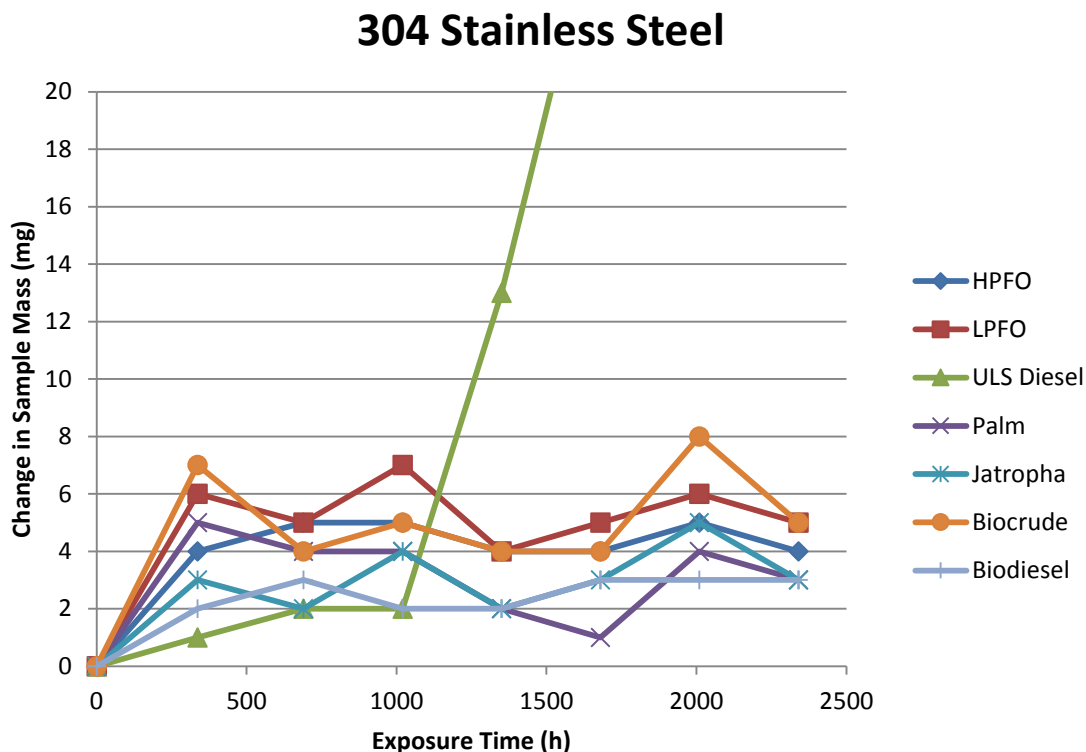
Figure 7-116. Changes in mass of 304 stainless steel samples during testing period. Change in mass of ultra-low sulfur diesel at 2010 hours and 2340 hours is an outlier and does not appear on the figure.

Figure 7-117 shows the rates of corrosion of the 304 stainless steel samples in mils per year (mpy). The corrosion rate was calculated by the formula:

$$mpy = \frac{534W}{DAT}$$

where W is the weight loss in mg, D is the density of the specimen in g/cm^3, A is the area

of the specimen in in.^{2}, T is the exposure time of the specimen in hours, and 534 is a

constant which allows for unit consistency throughout the equation (Fontana, 1986). As

expected for samples which saw very little mass change overall, no corrosion was

observed. The highest rate of gain of mass observed, with the exception of the ultra-low

sulfur diesel at 2010 hours, was for the biocrude sample at 336 hours and was 0.28 mpy.
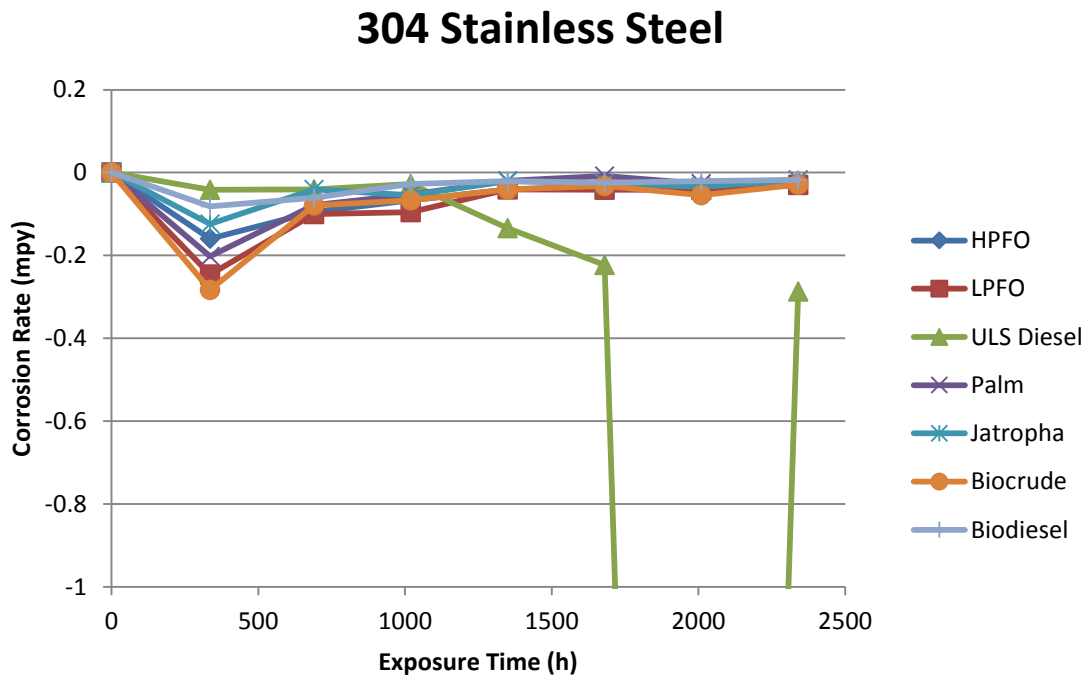
Figure 7-117. Rates of change of mass of 304 stainless steel samples during testing period. Rate of change of mass for ultra-low sulfur diesel at 2010 hours is an outlier and does not appear on the figure.

Figure 7-118 shows time lapse photos of the 304 stainless steel samples when

they were removed from the oven.

336 h (~2 weeks)

690 h (~4 weeks)

1020 h (~6 weeks)

1350 h (~8 weeks)

1680 h (~10 weeks)

2010 h (~12 weeks)

1 – exposed to hi-pour fuel oil
2 – exposed to lo-pour fuel oil
3 – exposed to ultra-low sulfur diesel
4 – exposed to crude palm oil
5 – exposed to crude jatropha oil
6 – exposed to biocrude derived from
    animal renderings
7 – exposed to biodiesel (refined biocrude)

2340 h (~14 weeks)
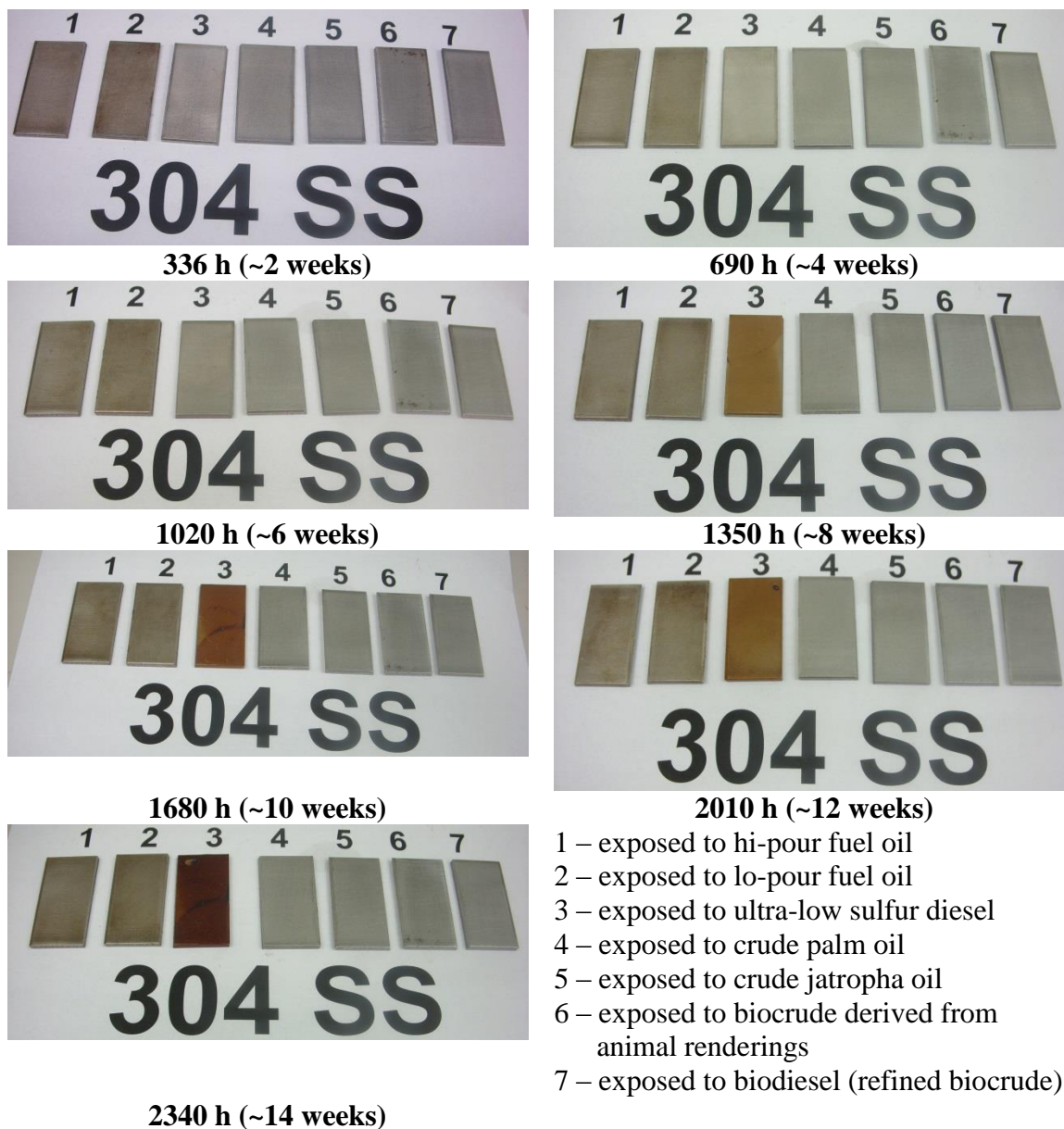
Figure 7-118. 304 stainless steel samples after exposure to pure oils.

The 304 stainless steel samples immersed in lo-pour fuel oil and biocrude derived

from animal renderings were selected for SEM analysis. Figure 7-119 shows the

backscatter images of the 304 stainless steel sample in lo-pour fuel oil, and Figure 7-120

shows the backscatter images of the 304 stainless steel sample in biocrude derived from

animal renderings. The rate of gain of mass for the sample in lo-pour fuel oil was 0.03 mpy at 2340 hours, and the rate of gain of mass for the sample in biocrude derived from animal renderings was 0.03 mpy at 2340 hours. Qualitative elemental analysis of the sample in biocrude indicates carbonaceous deposits on the sample in a line near the bottom of the coupon. This deposit appeared very early in testing and did not change in character throughout the exposure process. It is believed that this represents burned biocrude because of the high levels of carbon and oxygen rather than any corrosion-type deposits. Table 7-15 shows the elemental analysis of the spectrum points.
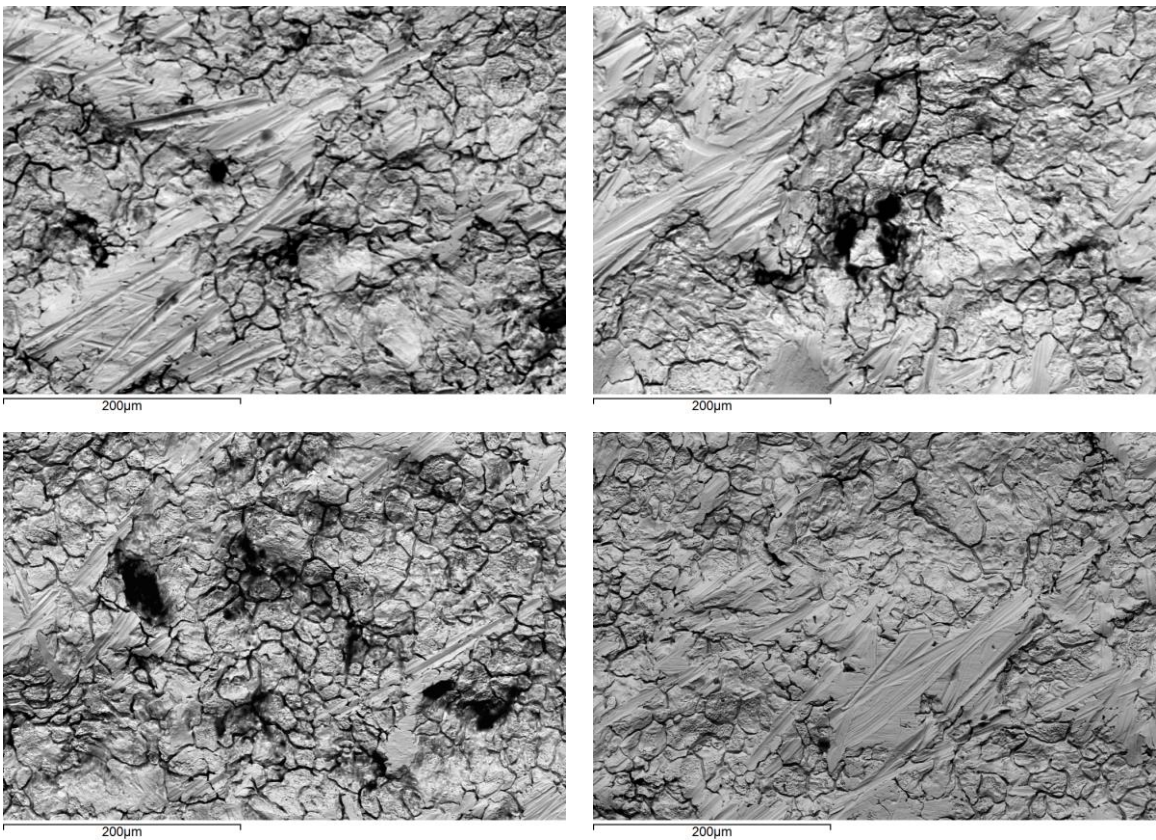
Figure 7-119. Backscatter electron images of 304 stainless steel after 2340 hours of exposure to lo-pour fuel oil.
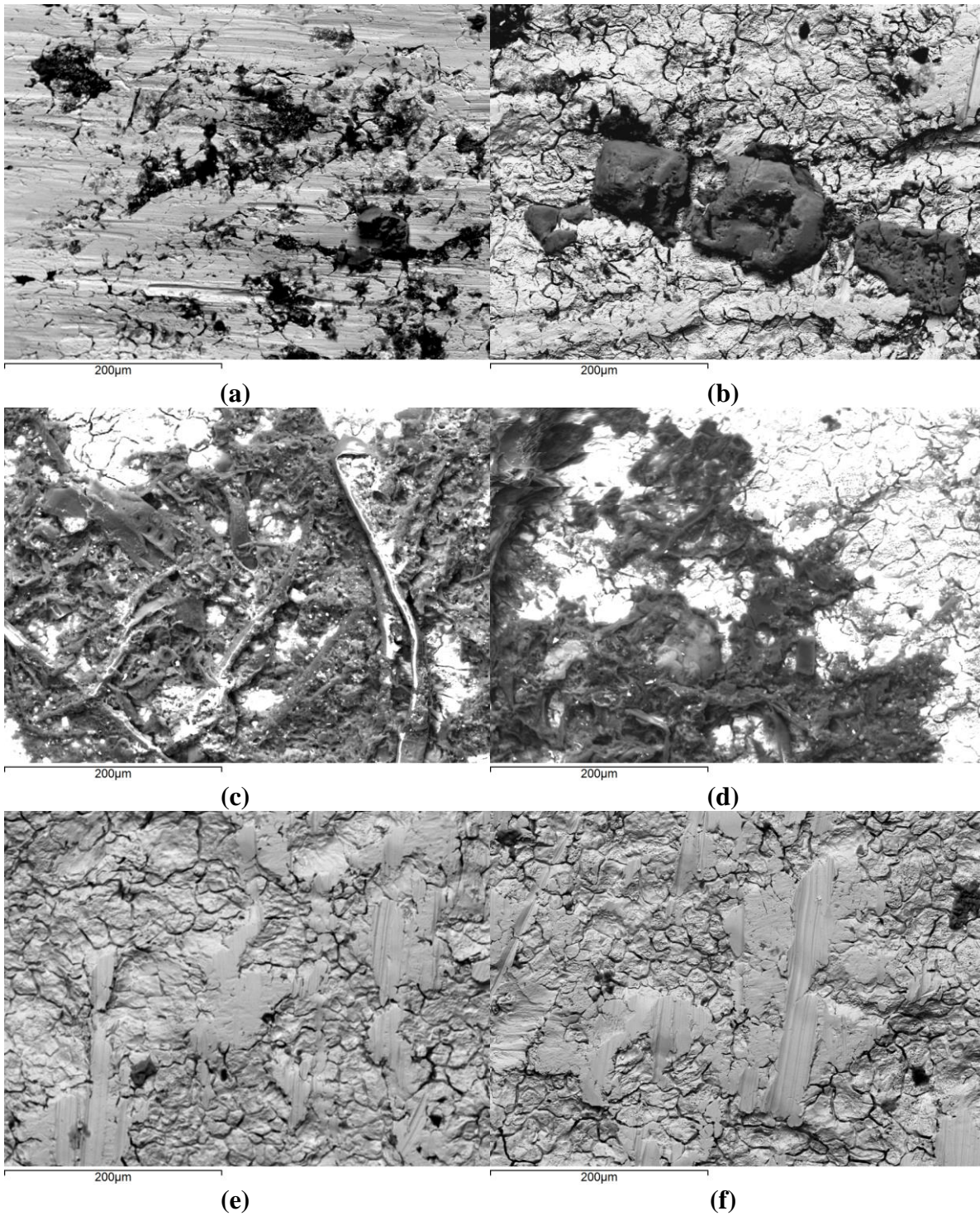
Figure 7-120. Backscatter electron images of 304 stainless steel after 2340 hours of exposure to biocrude derived from animal renderings. The dark areas in (c) and (d) are burned biocrude, not corrosion products.
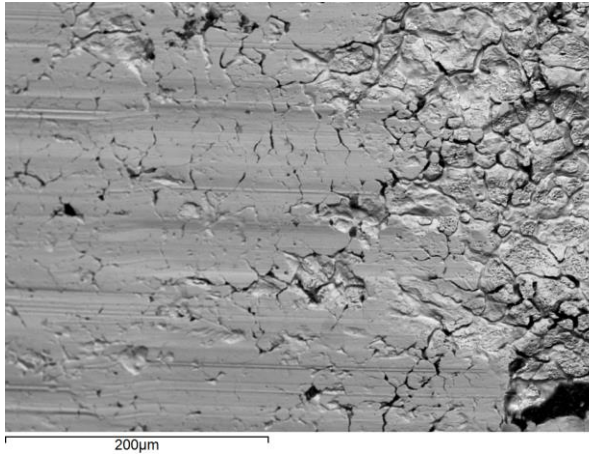
(g)
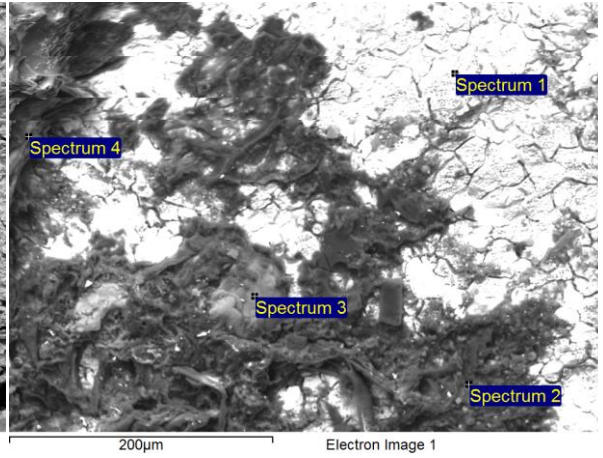
(h)

Figure 7-120, cont.

Table 7-15. Qualitiative elemental analysis of 304 stainless steel exposed to biocrude derived from animal renderings as indicated in Figure 7-120h.

Spectrum	C	O	Na	Mg	Al	Si	P	S	Cl	K	Ca	Mn	Fe	Sr	Total
1	23.81	10.34	1.32	0	0	1.97	0.53	0	0	0.29	0	2.86	58.89	0	100
2	51.96	15.5	1.43	1.04	0	0.24	2.79	0.28	0.32	1.42	0.13	1.12	23.45	0.33	100
3	12.07	45.38	6.99	1.86	0.48	0.11	5.48	9.56	0.23	16.94	0.16	0	0.47	0.39	100
4	53.97	22.86	0.57	0.17	0	0.33	0.62	0.19	17.29	0.74	0	0	3.25	0	100

Impacts of the lo-pour fuel oil on the 304 stainless steel were minimal. Some discoloration can be attributed to the fuel oil, but this is more likely a slight incorporation of the carbonaceous fuel in the surface matrix of the metal as opposed to a corrosive deposit. This may be substantiated by the utter lack of weight loss or gain in the samples after the small initial gain in mass. If corrosion was occurring on an ongoing basis, products would plate out onto the sample or flake away from the sample. Therefore, the lo-pour fuel oil did not corrode 304 stainless steel under these conditions.

Impacts of the hi-pour fuel oil on the 304 stainless steel were, again, minimal. Some discoloration can be attributed to the fuel oil, but again, this is more likely a slight incorporation of the carbonaceous fuel in the surface matrix of the metal as opposed to a corrosive deposit. This may be substantiated by the lack of weight loss or gain in the samples after the small initial gain in mass. If corrosion was occurring on an ongoing basis, products would plate out onto the sample or flake away from the sample. Therefore, the hi-pour fuel oil did not corrode 304 stainless steel under these conditions.

The ultra-low sulfur diesel had a significant impact on the 304 stainless steel sample. Starting at the 1020 hour mark, degraded diesel fuel was observed over the coupon. The deposits observed at 1350 hours, 1680 hours, 2010 hours, and 2340 hours could not be removed by the rubber stopper. The material was observed on the bottom of the coupon; the coupons were not suspended in the jars but were allowed to rest on the bottom, and it is possible that a thin layer of diesel fuel was trapped between the coupon and the bottom of the jar and was able to degrade and bond to the coupon there. The samples were flipped over after each weighing in which a deposit was observed to expose the face of the coupon with the deposit to the fuel and perhaps provide an opportunity for

it to diffuse away from the surface; this diffusion did not occur. In addition, this sample was ultrasonically cleaned in acetone prior to SEM analysis; the deposits were removed by the acetone, lending credence to the hypothesis that these were degraded diesel fuel as opposed to rust formed by corrosion. The diesel fuel probably decomposed because it was held at elevated temperatures without any additives to improve its thermal stability.

Impacts of the crude palm oil on the 304 stainless steel were minimal. The weight gains of the sample were minimal, and the weight was nearly constant throughout the entire process. Furthermore, no deposits were observed on the sample, and no material was removed from the sample. If corrosion was occurring on an ongoing basis, products would plate out onto the sample or flake away from the sample. Therefore, the crude palm oil did not corrode 304 stainless steel under these conditions.

Impacts of the crude jatropha oil on the 304 stainless steel were minimal. The weight gains of the sample were minimal, and the weight was nearly constant throughout the entire process. Furthermore, no deposits were observed on the sample, and no material was removed from the sample. If corrosion was occurring on an ongoing basis, products would plate out onto the sample or flake away from the sample. Therefore, the crude jatropha oil did not corrode 304 stainless steel under these conditions.

There were some slight impacts of the biocrude derived from animal renderings on the 304 stainless steel. At the 336 hour mark, a small amount of what was later determined to be burned biocrude was observed on the coupon. It is unclear why this adhered, and no further biocrude deposits were observed throughout the testing. Combining this with the minimal weight gain observed and the reasonably constant

210

weights leads to the conclusion that the biocrude derived from animal renderings did not significantly corrode 304 stainless steel under these conditions.

Impacts of the biodiesel (refined biocrude) on the 304 stainless steel were minimal. The weight gains of the sample were minimal, and the weight was nearly constant throughout the entire process. Furthermore, no deposits were observed on the sample, and no material was removed from the sample. If corrosion was occurring on an ongoing basis, products would plate out onto the sample or flake away from the sample. Therefore, the biodiesel did not corrode 304 stainless steel under these conditions.

Figure 7-121 shows the changes in mass of the brass samples during their exposure to pure oils. With the exception of the sample in hi-pour fuel oil, which experienced no change in mass, and the sample in ultra-low sulfur diesel, which gained mass, all the brass samples in oils lost mass over the testing period. This was especially noticeable for the sample in biocrude derived from animal renderings, although the mass did stabilize after the 690 hour mark. The sample in lo-pour fuel oil also lost mass until the 1680 hour mark, at which point the mass stabilized.
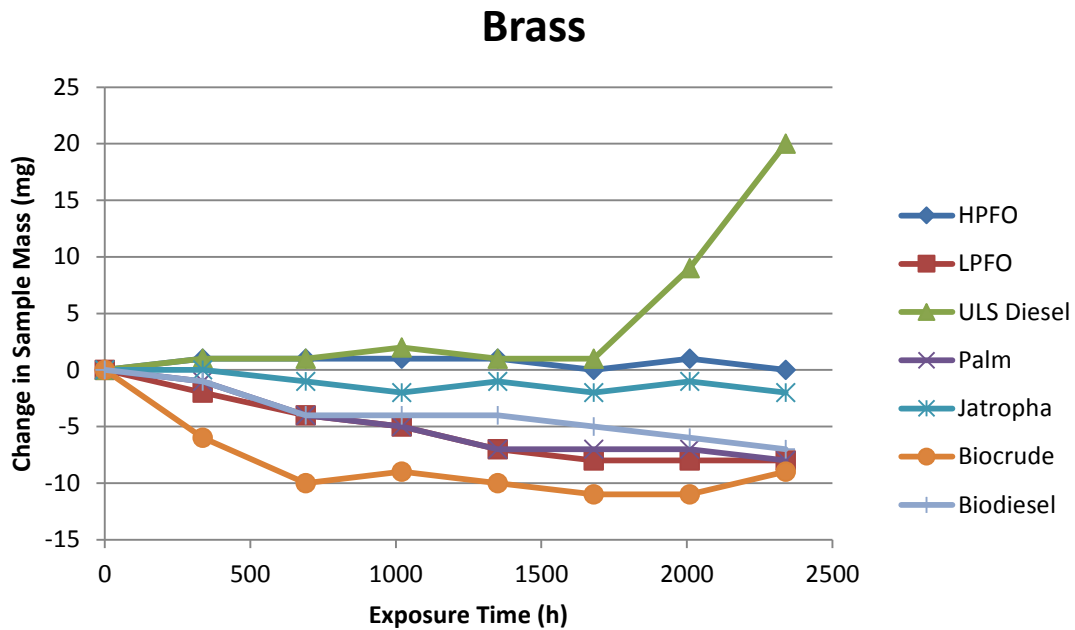
Brass

Figure 7-121. Changes in mass of brass samples during testing period.

Figure 7-122 shows the corrosion rates of the brass samples. These rates were calculated using the aforementioned equation as presented by Fontana (1986). Overall the corrosion rates were fairly low. A significant corrosion rate was observed at the 336 hour mark for the sample in biocrude derived from animal renderings (0.61 mpy) and at the 690 hour mark for the same sample (0.50 mpy), but this rate of corrosion slowed over time. The increase in the rate of corrosion for the brass sample in ultra-low sulfur diesel is due to the formation of bonded degraded fuel deposits by the same mechanisms observed for the 304 stainless steel samples.
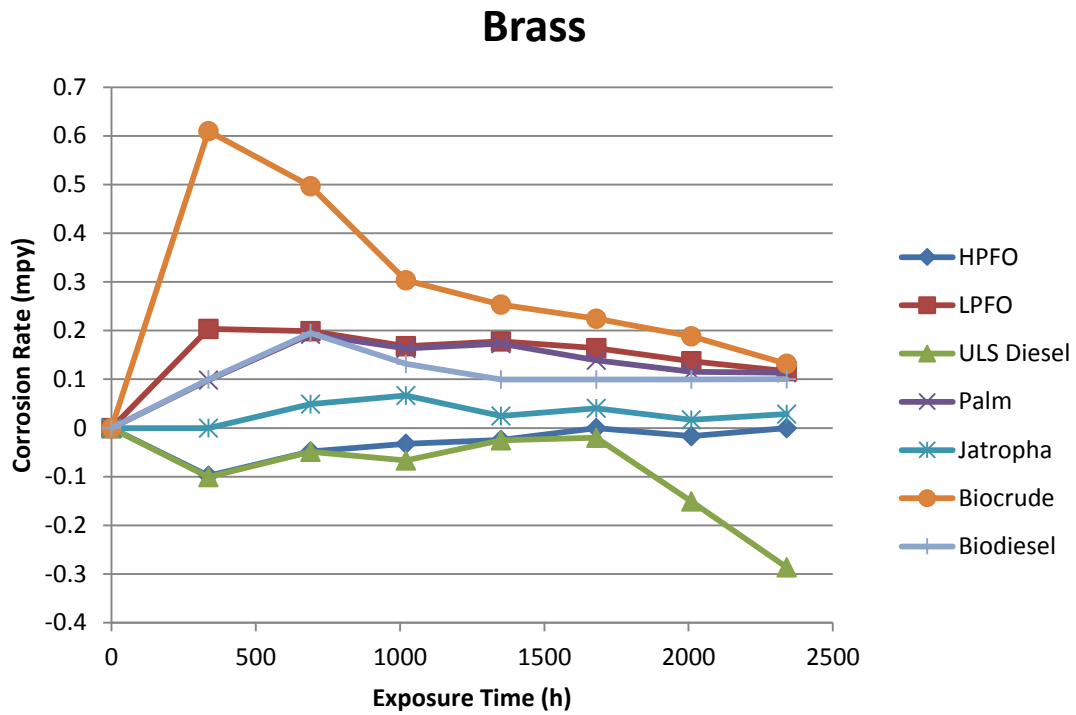
Figure 7-122. Corrosion rates of brass samples during testing period.

Figure 7-123 shows time lapse photos of the brass samples when they were removed from the oven.

336 h (~2 weeks)

690 h (~4 weeks)

1020 h (~6 weeks)

1350 h (~8 weeks)

1680 h (~10 weeks)

2010 h (~12 weeks)

1 – exposed to hi-pour fuel oil
2 – exposed to lo-pour fuel oil
3 – exposed to ultra-low sulfur diesel
4 – exposed to crude palm oil
5 – exposed to crude jatropha oil
6 – exposed to biocrude derived from
  animal renderings
7 – exposed to biodiesel (refined biocrude)

2340 h (~14 weeks)
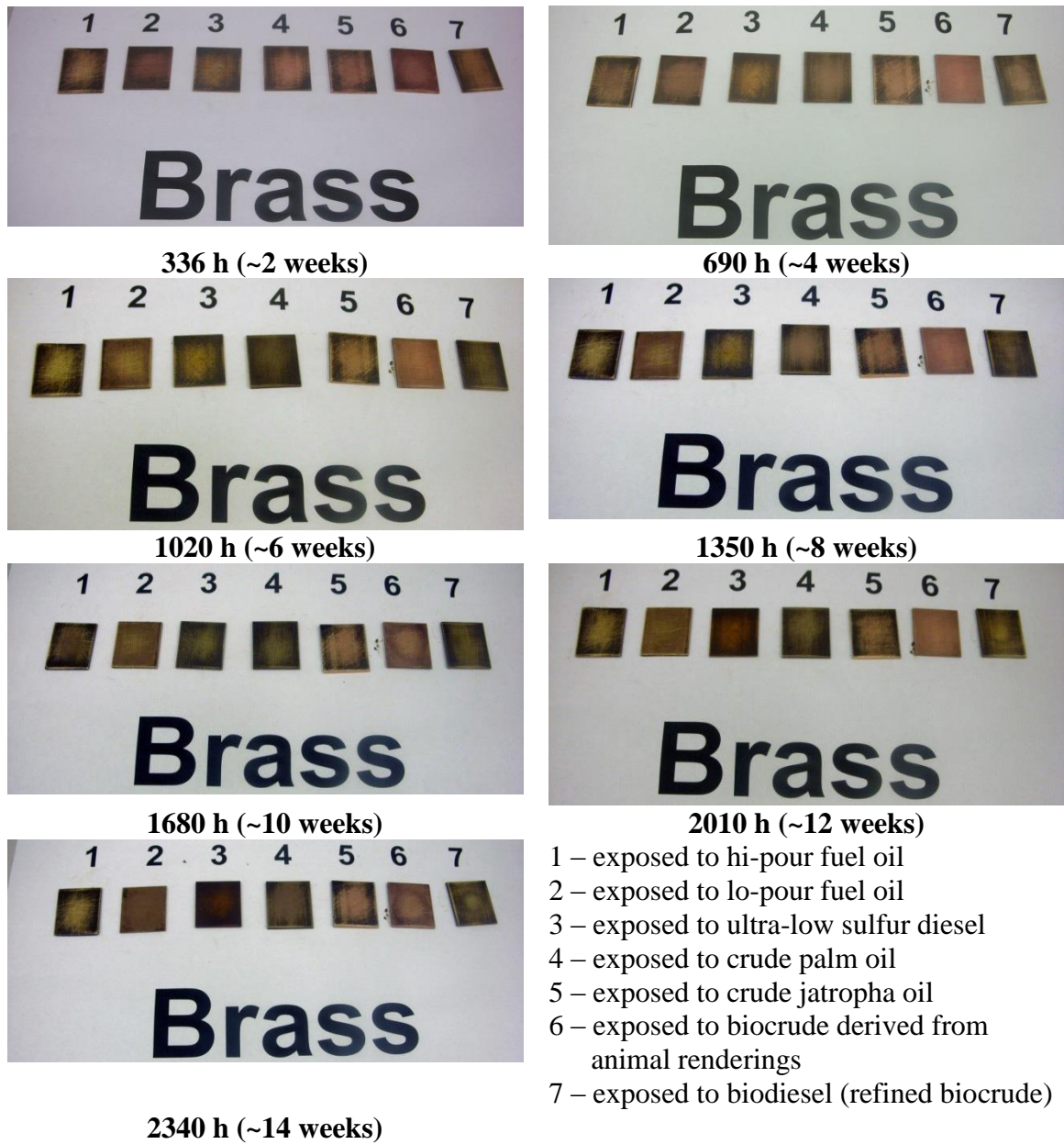
Figure 7-123. Brass samples after exposure to pure oils.

The brass samples immersed in biocrude derived from animal renderings and
biodiesel (refined biocrude) were selected for SEM analysis. Figure 7-124 shows the
backscatter images of the brass sample in biocrude derived from animal renderings, and
Figure 7-125 shows the backscatter images of the brass sample in biodiesel (refined

214

biocrude). The corrosion rate of the sample in biocrude derived from animal renderings was 0.13 mpy at 2340 hours, and the corrosion rate of the sample in biodiesel (refined biocrude) was 0.10 mpy at 2340 hours. Qualitative elemental analysis of the sample in biodiesel indicates carbonaceous deposits on the sample as well as the presence of iron. It is unknown why any iron would be present in this sample, and it is possible that this is a misreading for either copper or zinc, the two primary elements in brass alloys, neither of which were analyzed for. Table 7-16 shows the elemental analysis of the spectrum points.
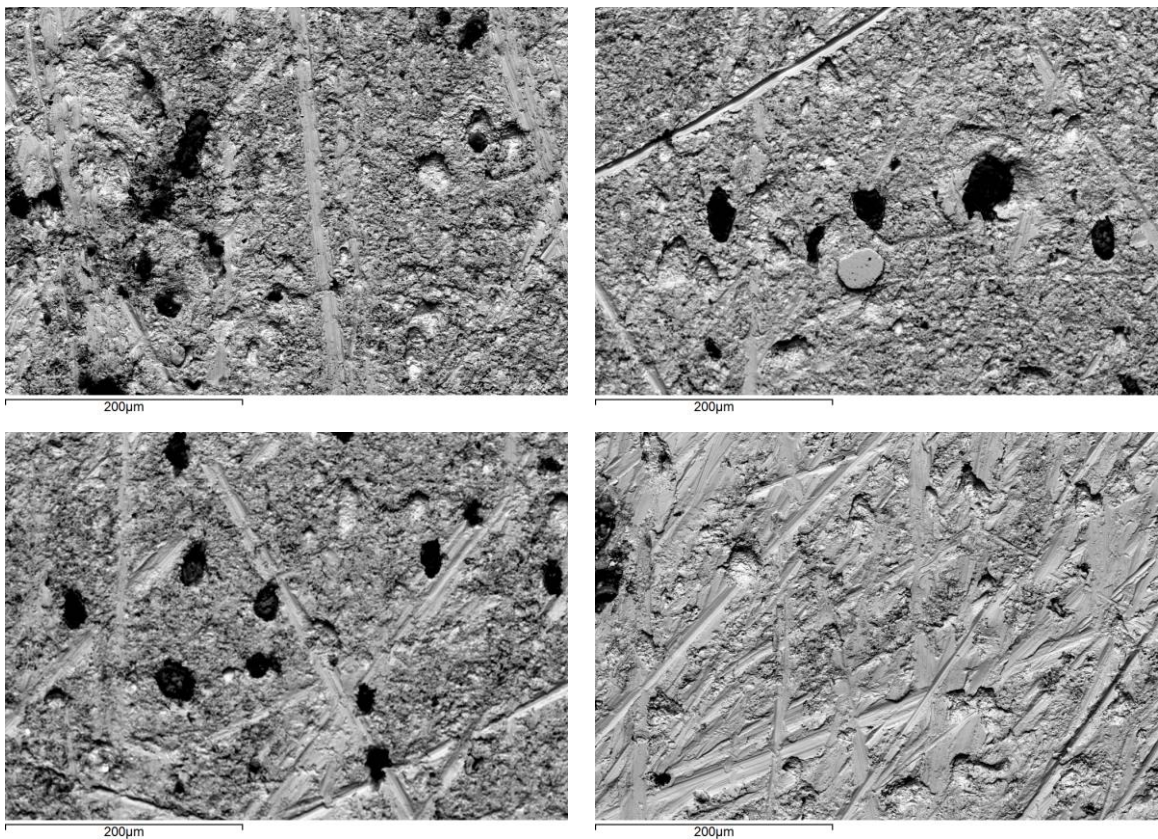
Figure 7-124. Backscatter electron images of brass after 2340 hours of exposure to biocrude derived from animal renderings.
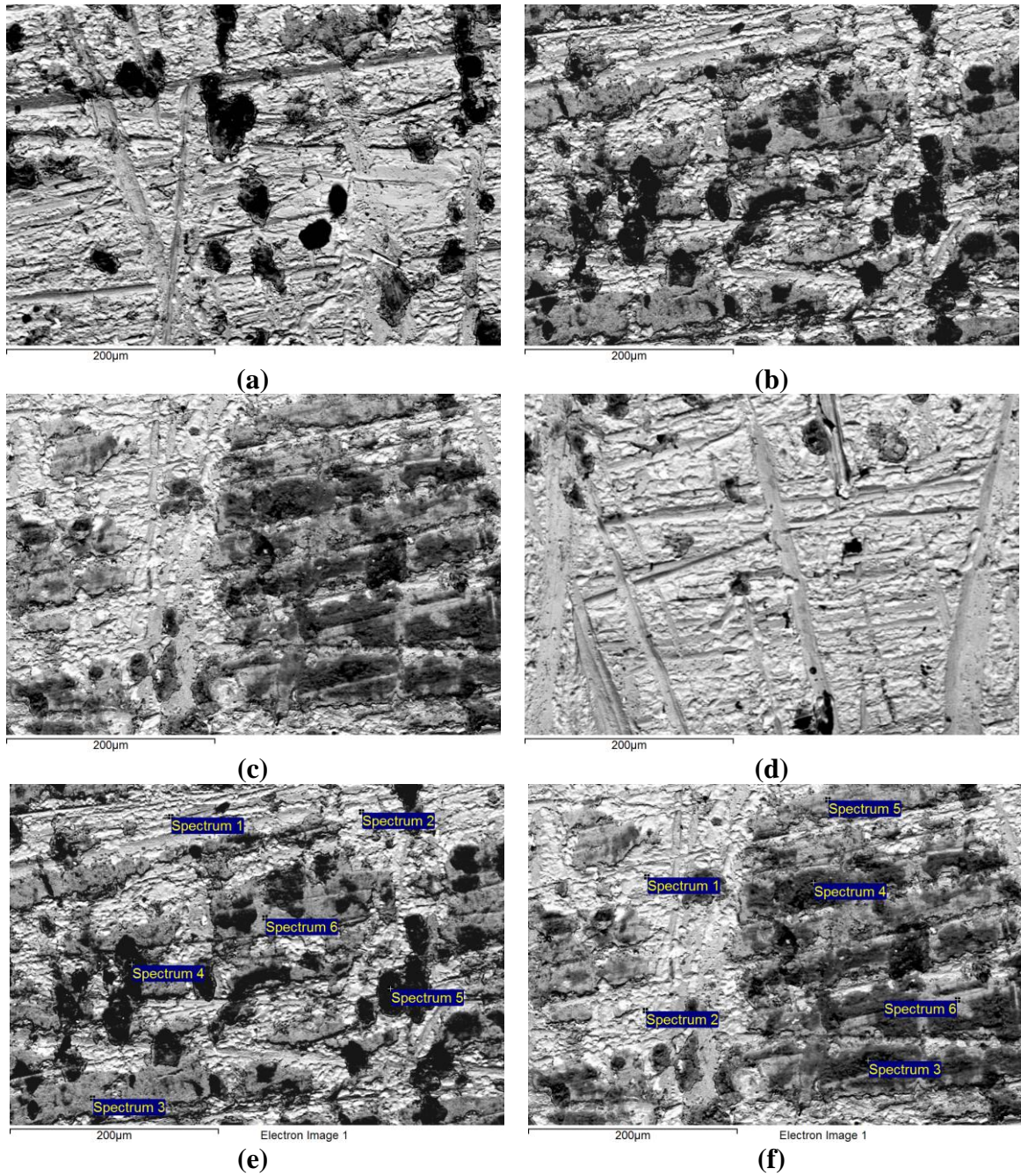
Figure 7-125. Backscatter electron images of brass after 2340 hours of exposure to biodiesel (refined biocrude).

Table 7-16. Qualitative elemental analysis of brass exposed to biocrude derived from animal renderings as indicated in Figure 7-125e and 7-125f.

7-125e

Spectrum	C	O	Mg	Al	Si	P	S	Cl	K	Ca	Ti	Fe	Total
1	0	70.77	29.23	0	0	0	0	0	0	0	0	7.46	100
2	62.02	29.87	6.59	0	1.51	0	0	0	0	0	0	0	100
3	0	82.29	5.5	2.67	1.44	0	2.42	4.06	0	0	0	1.62	100
4	0	65.74	9.36	2.71	9.63	1.5	0.71	0.79	0	0.19	0	9.37	100
5	0	56.28	0.83	1.52	5.39	4.25	0.95	0.45	0.36	0.37	7.81	21.8	100
6	25.25	49.56	1.21	0	2.23	2.45	1.52	1.5	0	0	0	16.28	100

7-125f

Spectrum	C	O	Na	Mg	Al	Si	P	S	Cl	Ca	Fe	Sr	Total
1	82.98	0	0	9.55	0	0	0	0	0	0	7.46	0	100
2	58.89	34.34	0	6.78	0	0	0	0	0	0	0	0	100
3	56.62	29.95	1.33	0	0.38	0.99	1.42	0.34	0.16	0.11	8.4	0.3	100
4	0	54.94	3.18	0.52	1.19	2.56	2.81	1.29	0.29	1.4	31.82	0	100
5	0	70.64	0	1.55	0	3.02	2.04	1.48	1.56	0	19.72	0	100
6	0	79.47	0	5.77	0	0.79	0	1.81	7.87	0	4.29	0	100

Effects of hi-pour fuel oil on brass were minimal. The weight gains of the sample were minimal, and the weight was nearly constant throughout the entire process. Furthermore, no deposits were observed on the sample, and no material was removed from the sample. If corrosion was occurring on an ongoing basis, products would plate out onto the sample or flake away from the sample. Therefore, the hi-pour fuel oil did not corrode brass under these conditions.

The brass sample in lo-pour fuel oil did lose about 8 mg of material over the testing period. The maximum corrosion rate of brass in lo-pour fuel oil was 0.20 mpy at the 336 hour mark; however, by the 2340 hour mark, the corrosion rate of brass in lo-pour fuel oil had dropped to 0.12 mpy, a 40% decrease. A small amount of matter was removed from the sample at each removal, as may be observed in the time-lapse pictures in Figure 7-123. Given the low rate of corrosion in mpy, however, it is difficult to call this "significant." However, brass wetted parts exposed to this lo-pour fuel oil should be monitored for evidence of corrosion.

The ultra-low sulfur diesel had several effects on the brass sample. At the 690 hour mark, the diesel had turned red and smelled strongly (probably decomposed), and the cap liner in the jar had disintegrated. The brass sample was reloaded into fresh ultra-low sulfur diesel. At the 2010 hour mark, bonded degraded diesel deposits were observed on the brass. These deposits could not be removed. The material was observed on the bottom of the coupon; the coupons were not suspended in the jars but were allowed to rest on the bottom, and it is possible that a thin layer of diesel fuel was trapped between the coupon and the bottom of the jar and was able to degrade and bond to the coupon there. The sample was flipped over after each weighing in which a deposit was observed

to expose the face of the coupon with the deposit to the fuel and perhaps provide an opportunity for it to diffuse away from the surface; this diffusion did not occur. In addition, this sample was ultrasonically cleaned in acetone after the 2340 hour mark; the deposits were removed by the acetone, lending credence to the hypothesis that these were degraded diesel fuel as opposed to corrosion products. The diesel fuel probably decomposed because it was held at elevated temperatures without any additives to improve its thermal stability.

The crude palm oil did affect the brass sample, though not immediately. The maximum corrosion rate was 0.17 mpy at the 1350 hour mark. Palm oils are very acidic (the oil is named for the palmitic acid which is a major component), and this acidity may, over time, have led to corrosion of the sample. Nevertheless, it is difficult to classify palm oil as being significantly corrosive, especially in light of the 0.11 mpy corrosion rate at the 2340 hour mark. Therefore, the crude palm oil had slight effects on the brass, and brass wetted components in the presence of palm oil should be monitored for corrosive activity.

Effects of crude jatropha oil on brass were minimal. The weight losses of the sample were minimal, and the weight was nearly constant throughout the entire process. Furthermore, no deposits were observed on the sample, and no material was removed from the sample. If corrosion was occurring on an ongoing basis, products would plate out onto the sample or flake away from the sample. Therefore, crude jatropha oil did not corrode brass under these conditions.

The effect of biocrude derived from animal renderings on brass was significant. The maximum corrosion rate was 0.61 mpy at the 336 hour mark. In addition, the brass

coupon took on an increasingly coppery appearance throughout the testing period. It is possible that zinc was selectively leached from the sample throughout the testing period, but additional testing would be required to prove this. At the 2340 hour mark, the corrosion rate was 0.13 mpy. Therefore, biocrude derived from animal renderings did corrode the brass sample, especially early in the process, and brass wetted parts exposed to biocrude derived from animal renderings should be monitored for corrosive activity.

The effect of biodiesel (refined biocrude) on brass was not insignificant. A total of 7 mg of mass was lost from the sample throughout the testing period. The highest rate of corrosion was 0.20 mpy at the 690 hour mark. The corrosion rate at the 336 hour mark and the corrosion rate at the 2340 hour mark was 0.10 mpy. While the corrosion rate of the brass sample in biodiesel was not high, it also was nonzero. By the hypothesis of this research, biodiesel did not have a significantly corrosive effect on brass; however, wetted brass parts exposed to biodiesel should be monitored for corrosive activity.

Figure 7-126 shows the changes in mass of the 316 stainless steel samples during their exposure to pure oils. The samples in hi-pour fuel oil, lo-pour fuel oil, crude jatropha oil, biocrude, and biodiesel all experienced minimal mass gains or losses throughout the testing period. The sample in ultra-low sulfur diesel experienced mass gains due to the formation of bonded degraded diesel fuel deposits. The sample in palm oil experienced a mass gain which peaked at 8 mg at the 1680 hour mark. It is clear from this chart that, overall, the fuels had very little effect on the 316 stainless steel samples.

316 Stainless Steel
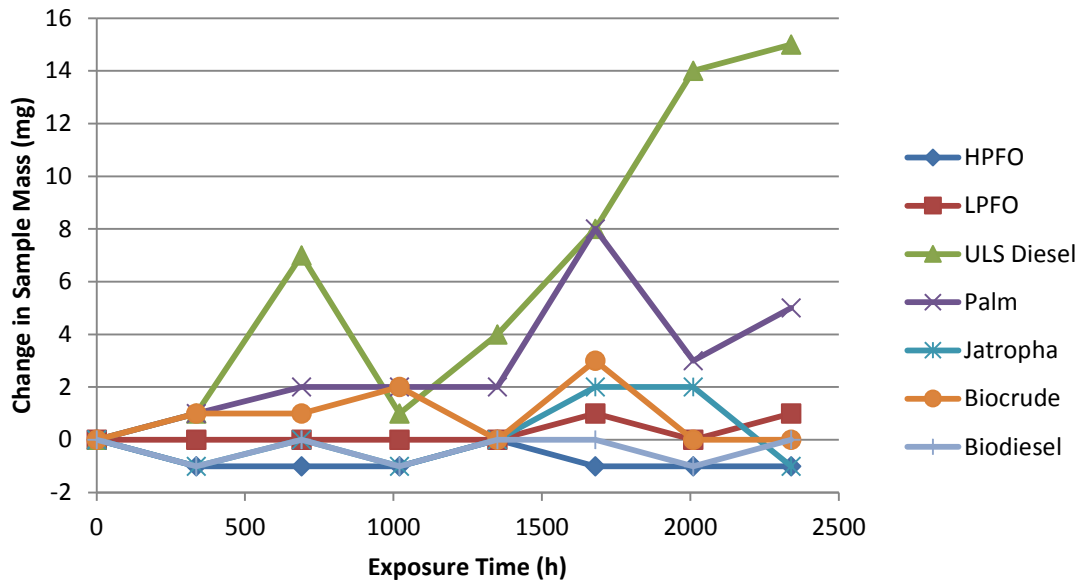
Figure 7-126. Changes in mass of 316 stainless steel samples during testing period.

Figure 7-127 shows the corrosion rates of the 316 stainless steel samples. These rates were calculated using the aforementioned equation as presented by Fontana (1986). Overall, the corrosion rates were very low. The highest corrosion rate was observed for the 316 stainless steel sample in ultra-low sulfur diesel and was 0.24 mpy at the 336 hour mark. The increase in the rate of corrosion for the 316 stainless steel sample in ultra-low sulfur diesel is due to the formation of bonded degraded fuel deposits by the same mechanisms observed for the 304 stainless steel and brass samples.

316 Stainless Steel
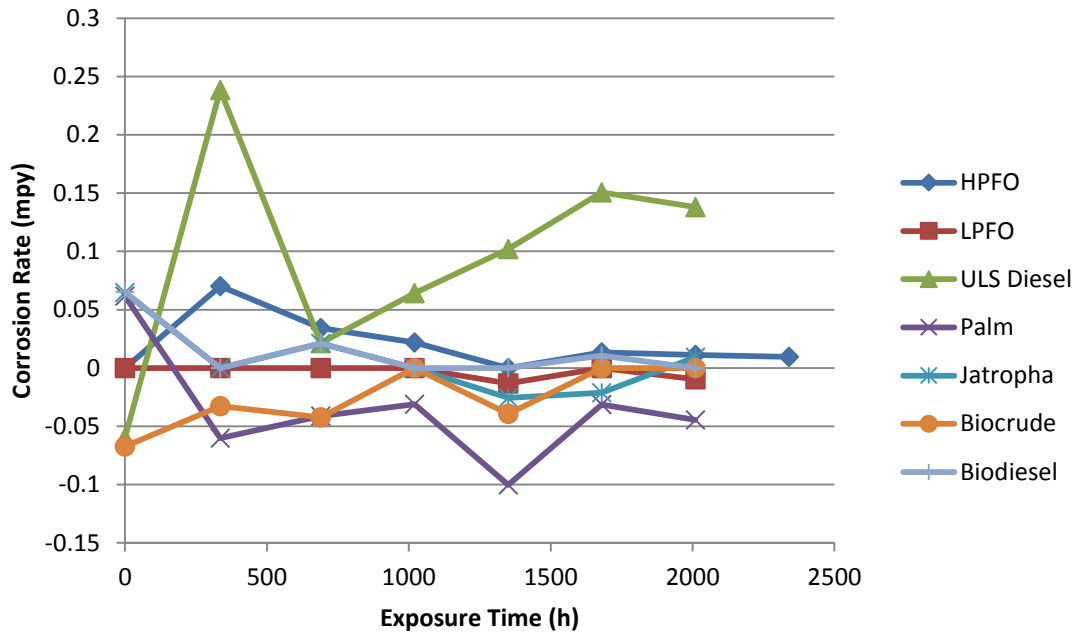
Figure 7-127. Corrosion rates of 316 stainless steel samples during testing period.

Figure 7-128 shows time lapse photos of the 316 stainless steel samples when they were removed from the oven.

336 h (~2 weeks)

690 h (~4 weeks)

1020 h (~6 weeks)

1350 h (~8 weeks)

1680 h (~10 weeks)

2010 h (~12 weeks)

1 – exposed to hi-pour fuel oil
2 – exposed to lo-pour fuel oil
3 – exposed to ultra-low sulfur diesel
4 – exposed to crude palm oil
5 – exposed to crude jatropha oil
6 – exposed to biocrude derived from
     animal renderings
7 – exposed to biodiesel (refined biocrude)

2340 h (~14 weeks)
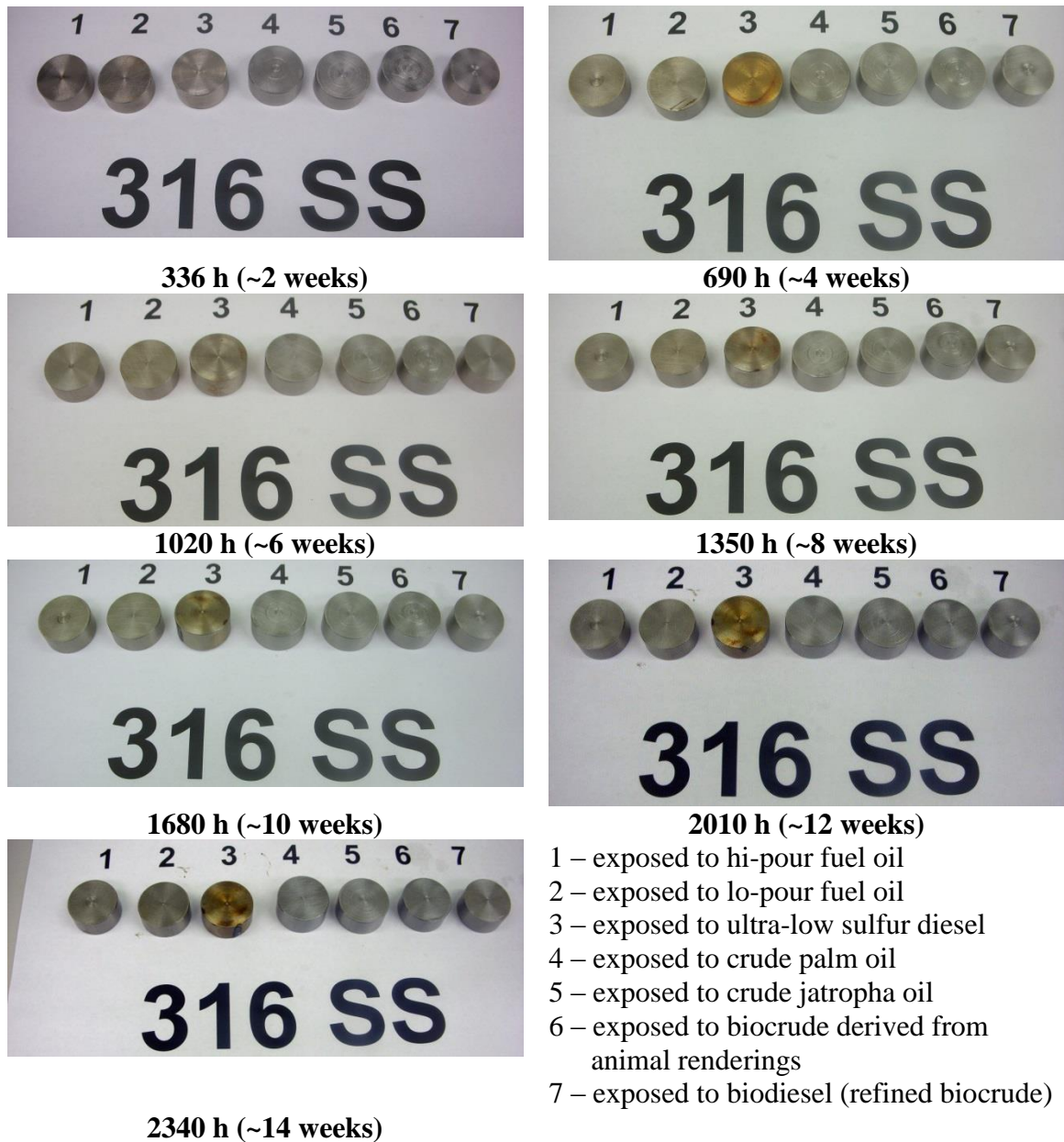
Figure 7-128. 316 stainless steel samples after exposure to pure oils.

The 316 stainless steel samples immersed in hi-pour fuel oil and ultra-low sulfur

diesel were selected for SEM analysis. Figure 7-129 shows the backscatter images of the

316 stainless steel sample in hi-pour fuel oil, and Figure 7-130 shows the backscatter

images of the 316 stainless steel sample in ultra-low sulfur diesel. The rate of change of

mass for the sample in hi-pour fuel oil was 0.01 mpy at 2340 hours, and the rate of

change of mass for the sample in ultra-low sulfur diesel was 0.14 mpy at 2340 hours.
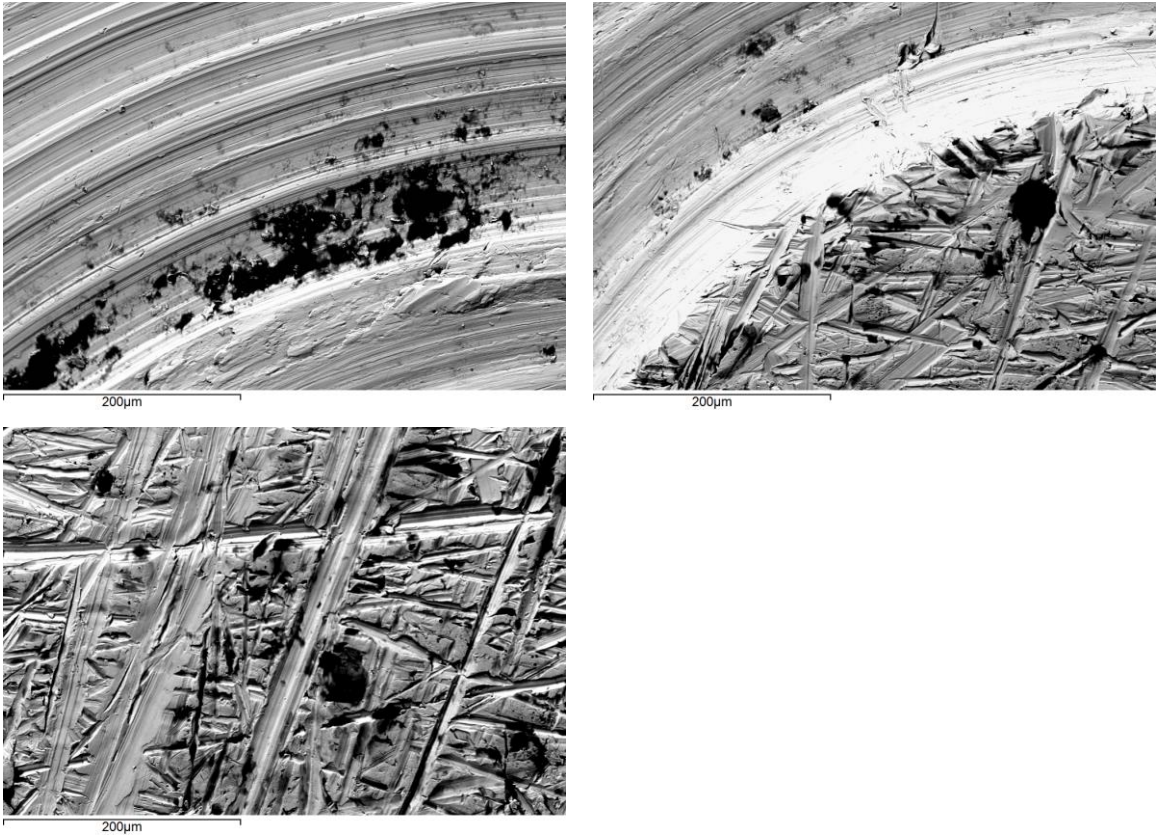
Figure 7-129. Backscatter electron images of 316 stainless steel after 2340 hours of exposure to hi-pour fuel oil.
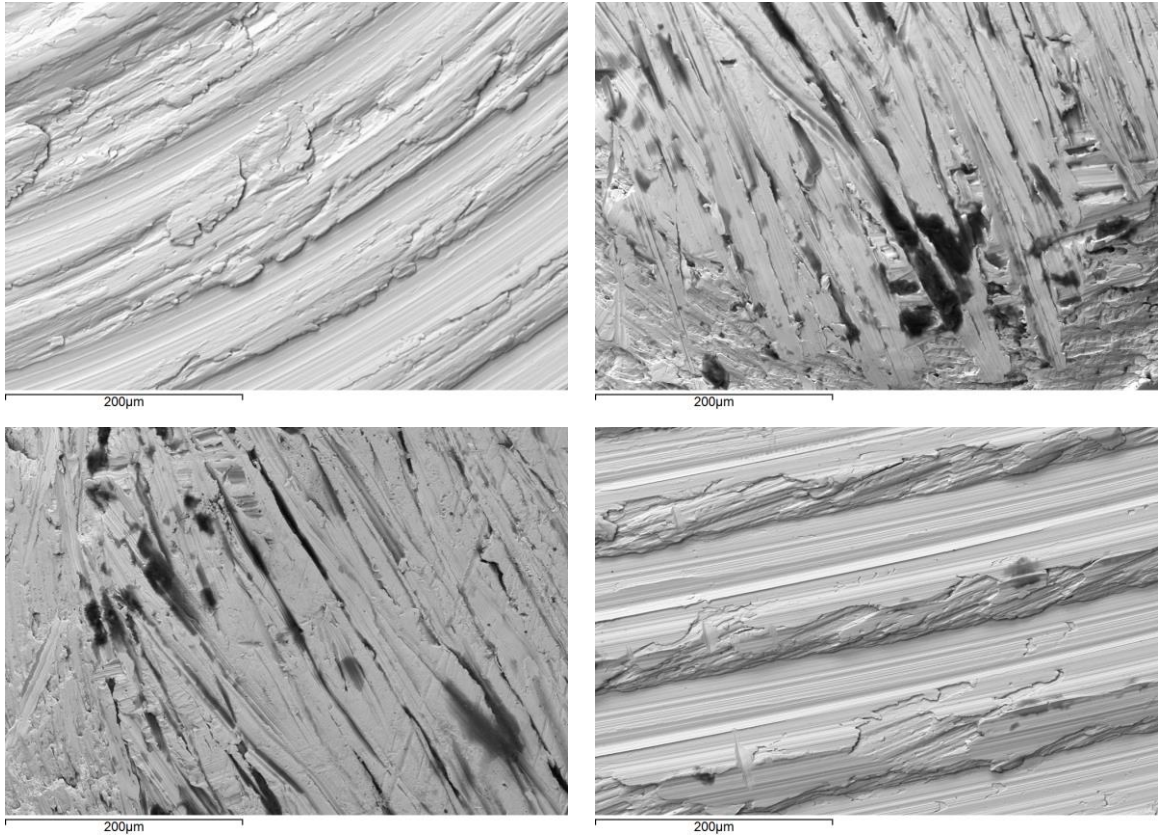
Figure 7-130. Backscatter electron images of 316 stainless steel after 2340 hours of exposure to ultra-low sulfur diesel.

Effects of hi-pour fuel oil on 316 stainless steel were minimal. The weight losses of the sample were minimal, and the weight of the sample was nearly constant throughout the entire process. Furthermore, no deposits were observed on the sample, and no material was removed from the sample. If corrosion was occurring on an ongoing basis, products would plate out onto the sample or flake away from the sample. Therefore, the hi-pour fuel oil did not corrode 316 stainless steel under these conditions.

Effects of lo-pour fuel oil on 316 stainless steel were minimal. The weight gains of the sample were minimal, and the weight of the sample was nearly constant throughout the entire process. Furthermore, no deposits were observed on the sample, and no material was removed from the sample. If corrosion was occurring on an ongoing basis,

products would plate out onto the sample or flake away from the sample. Therefore, the lo-pour fuel oil did not corrode 316 stainless steel under these conditions.

The ultra-low sulfur diesel affected the 316 stainless steel sample. At the 690 hour mark, significant quantities of decomposed diesel fuel which could not be removed were observed on the coupon. This deposit was only observed on the bottom face of the coupon; the coupons were not suspended in the jars but were allowed to rest on the bottom, and it is possible that a thin layer of diesel fuel was trapped between the coupon and the bottom of the jar and was able to degrade and bond to the coupon there. The sample was flipped over to expose the face of the coupon with the deposit to the fuel and perhaps provide an opportunity for it to diffuse away from the surface. At the 1020 mark, degraded diesel deposits were observed over the entire sample, though they were able to be removed with scrubbing by the rubber stopper. At the 1350 hour mark, bonded degraded diesel fuel was observed on the coupon; the coupon was reloaded with the bonded diesel fuel facing up. At the 1680 hour mark, more degraded diesel fuel was observed on the coupon. At the 2010 hour mark and the 2340 hour mark, additional bonded degraded diesel fuel deposits were observed on the coupon. This sample was ultrasonically cleaned in acetone after the 2340 hour mark; the deposits were removed by the acetone, lending credence to the hypothesis that these were degraded diesel fuel as opposed to rusts formed by corrosion. The diesel fuel probably decomposed because it was held at elevated temperatures without any additives to improve its thermal stability.

Effects of crude palm oil on 316 stainless steel were small. The weight gains of the sample were generally small, peaking at a weight gain of 8 mg at the 1680 hour mark. The maximum corrosion rate observed was 0.10 mpy at the 1680 hour mark. At the 2340

hour mark, the corrosion rate was 0.05 mpy. Given this small weight gain and low corrosion rate, the crude palm oil did not corrode 316 stainless steel under these conditions.

Effects of crude jatropha oil on 316 stainless steel were minimal. The weight gains and losses of the sample were minimal, and the weight of the sample was nearly constant throughout the entire process. Furthermore, no deposits were observed on the sample, and no material was removed from the sample. If corrosion was occurring on an ongoing basis, products would plate out onto the sample or flake away from the sample. Therefore, the crude jatropha oil did not corrode 316 stainless steel under these conditions.

Effects of biocrude derived from animal renderings on 316 stainless steel were minimal. The weight gains of the samples were minimal, and the weight of the sample was nearly constant throughout the entire process. Furthermore, no deposits were observed on the sample, and no material was removed from the sample. If corrosion was occurring on an ongoing basis, products would plate out onto the sample or flake away from the sample. Therefore, the biocrude derived from animal renderings did not corrode 316 stainless steel under these conditions.

Effects of biodiesel (refined biocrude) on 316 stainless steel were minimal. The weight losses of the sample were minimal, and the weight of the sample was nearly constant throughout the entire process. Furthermore, no deposits were observed on the sample, and no material was removed from the sample. If corrosion was occurring on an ongoing basis, products would plate out onto the sample or flake away from the sample.

227

Therefore, the biodiesel (refined biocrude) did not corrode 316 stainless steel under these conditions.

Figure 7-131 shows the changes in mass of the mild steel samples during their exposure to pure oils. The samples in hi-pour fuel oil, lo-pour fuel oil, crude palm oil, crude jatropha oil, and biodiesel (refined biocrude) all experienced minimal gains or losses throughout the testing period. The sample in ultra-low sulfur diesel experienced mass gains due to the formation of bonded degraded diesel fuel deposits. Most significantly, the sample in biocrude derived from animal renderings experienced a mass loss of about 40 mg throughout the testing period. It is clear from this chart that, with the exception of the biocrude derived from animal renderings, the fuels had very little effect on the mild steel samples.
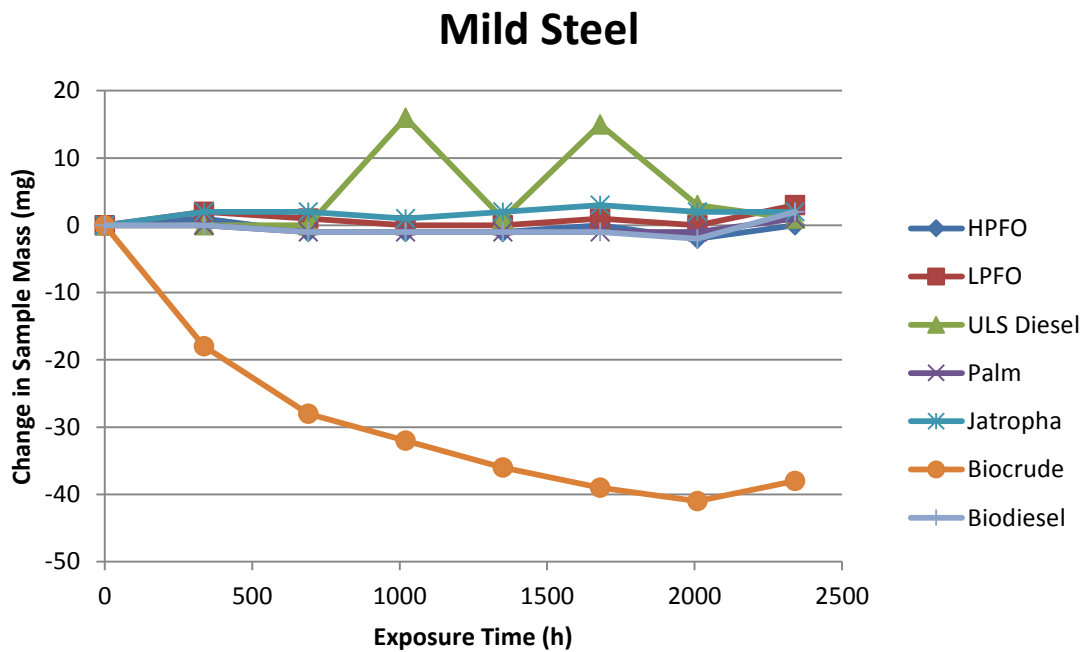
Figure 7-131. Changes in mass of mild steel samples during testing period.

Figure 7-132 shows the corrosion rates of the mild steel samples. These rates were calculated using the aforementioned equation as presented by Fontana (1986). Overall, the corrosion rates were low. The obvious exception is the corrosion rate of the mild steel sample in biocrude; the highest corrosion rate was observed for this sample at the 336 hour mark and was 1.50 mpy, and by the 2340 hour mark, the corrosion rate was still 0.45 mpy. The increase in the rate of corrosion for the mild steel sample in ultra-low sulfur diesel is due to the formation of bonded degraded fuel deposits by the same mechanisms observed for the 304 stainless steel, brass, and 316 stainless steel samples.
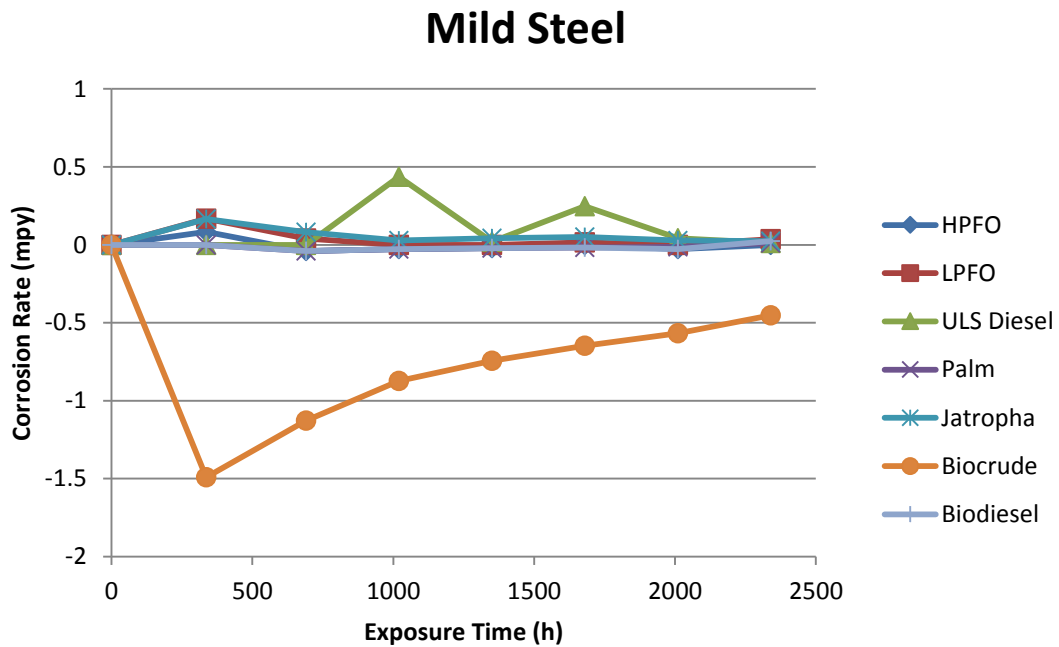
Mild Steel

Figure 7-132. Corrosion rates of mild steel samples during testing period.

Figure 7-133 shows time lapse photos of the mild steel samples when they were removed from the oven.

336 h (~2 weeks)

690 h (~4 weeks)

1020 h (~6 weeks)

1350 h (~8 weeks)

1680 h (~10 weeks)

2010 h (~12 weeks)

1 – exposed to hi-pour fuel oil
2 – exposed to lo-pour fuel oil
3 – exposed to ultra-low sulfur diesel
4 – exposed to crude palm oil
5 – exposed to crude jatropha oil
6 – exposed to biocrude derived from
     animal renderings
7 – exposed to biodiesel (refined biocrude)

2340 h (~14 weeks)
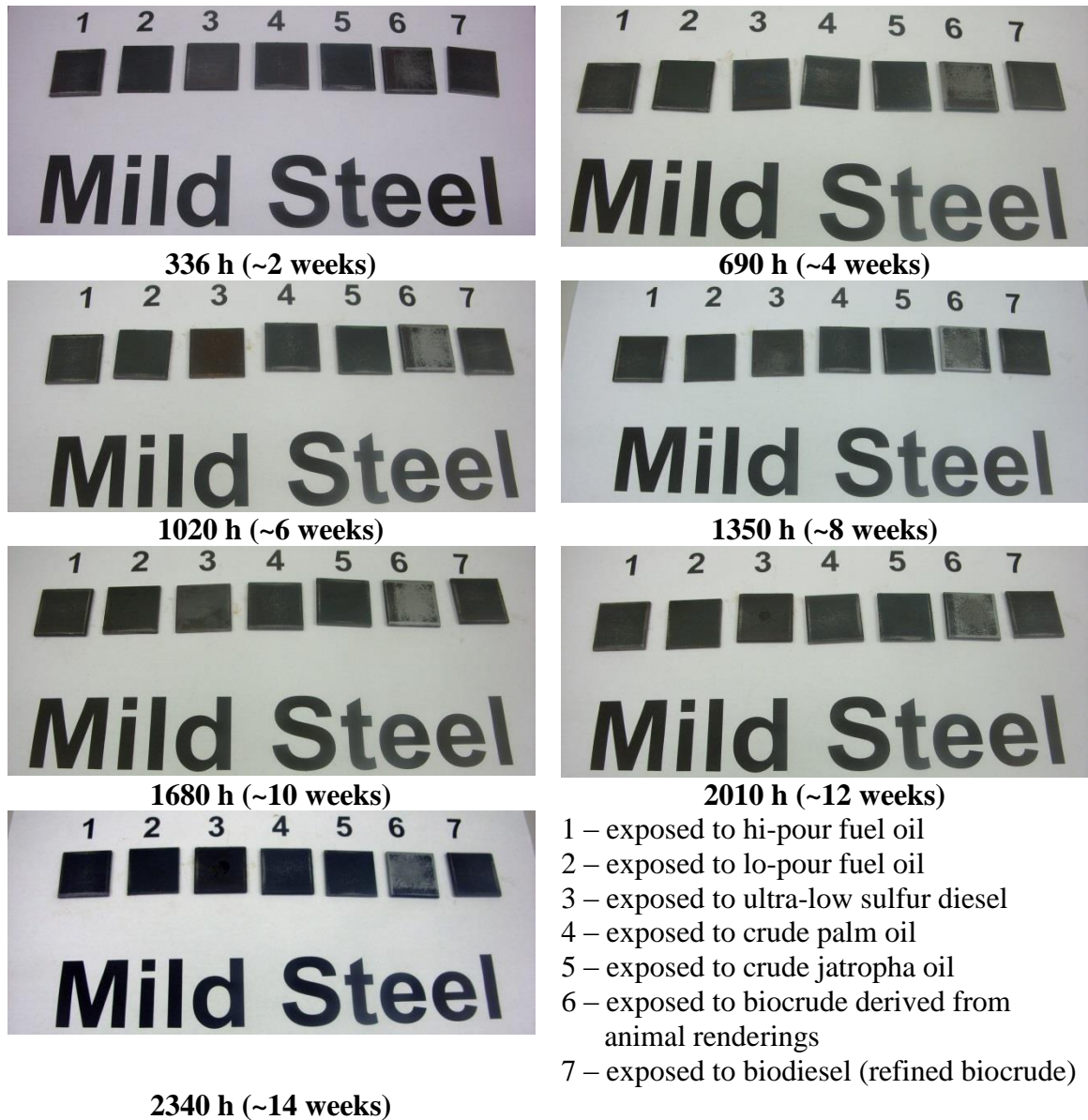
Figure 7-133. Mild steel samples after exposure to pure oils.

The mild steel samples immersed in crude palm oil and biocrude derived from animal renderings were selected for SEM analysis. Figure 7-134 shows the backscatter images of the mild steel sample in crude palm oil, and Figure 7-135 shows the backscatter images of the mild steel sample in biocrude derived from animal renderings. The corrosion rate of the sample in crude palm oil was 0.01 mpy at 2340 hours, and the

corrosion rate of the sample in biocrude derived from animal renderings was 0.45 mpy at

2340 hours. Qualitative elemental analysis indicated that the dark areas on both samples

were iron oxides, which were present on the sample before any exposure to the pure

fuels. Table 7-17 shows the elemental analysis of the spectrum points.

(a) **(b)** **(c)** **(d)** **(e)** **(f)**
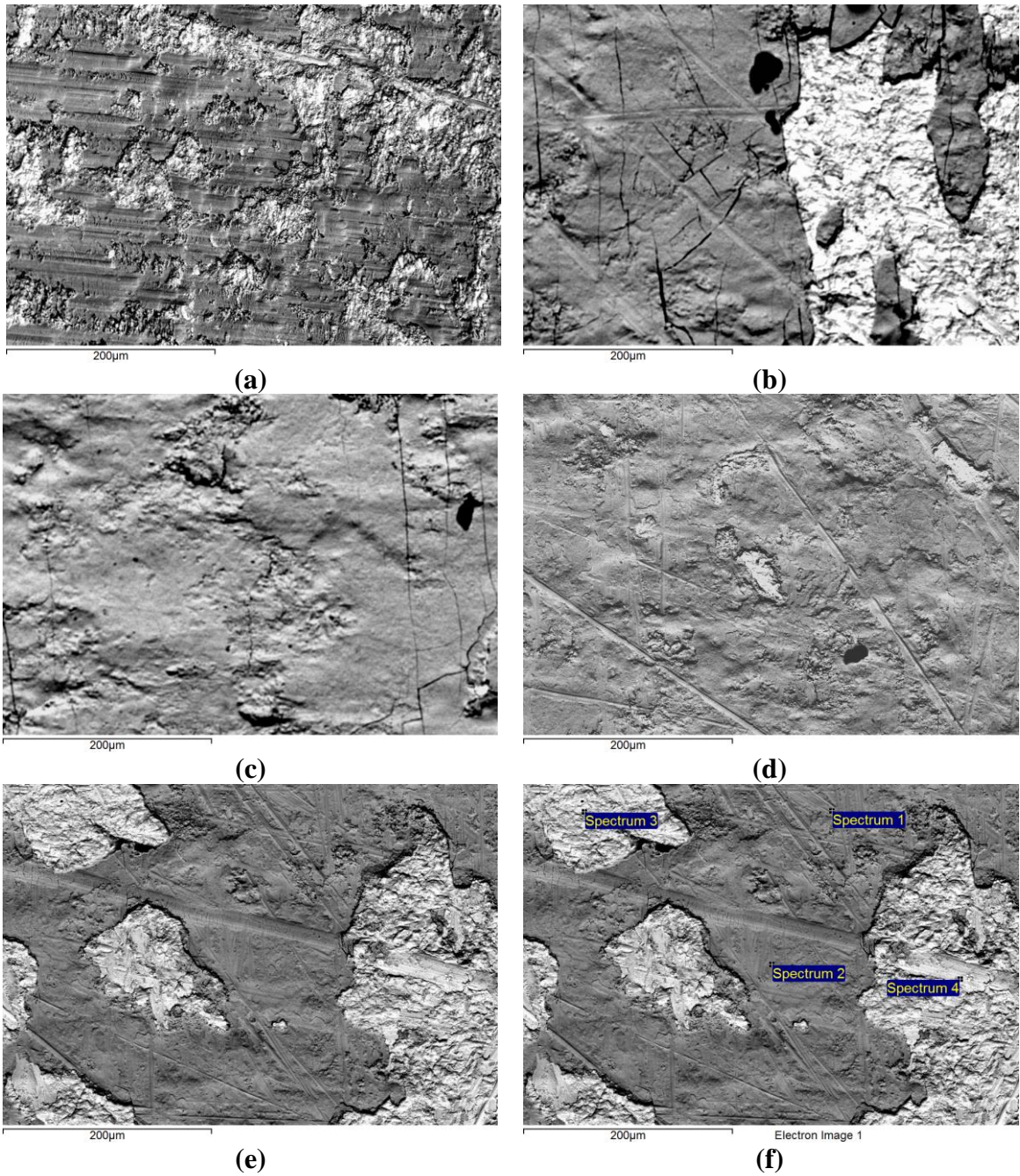
Figure 7-134. Backscatter electron images of mild steel after 2340 hours of exposure to crude palm oil.
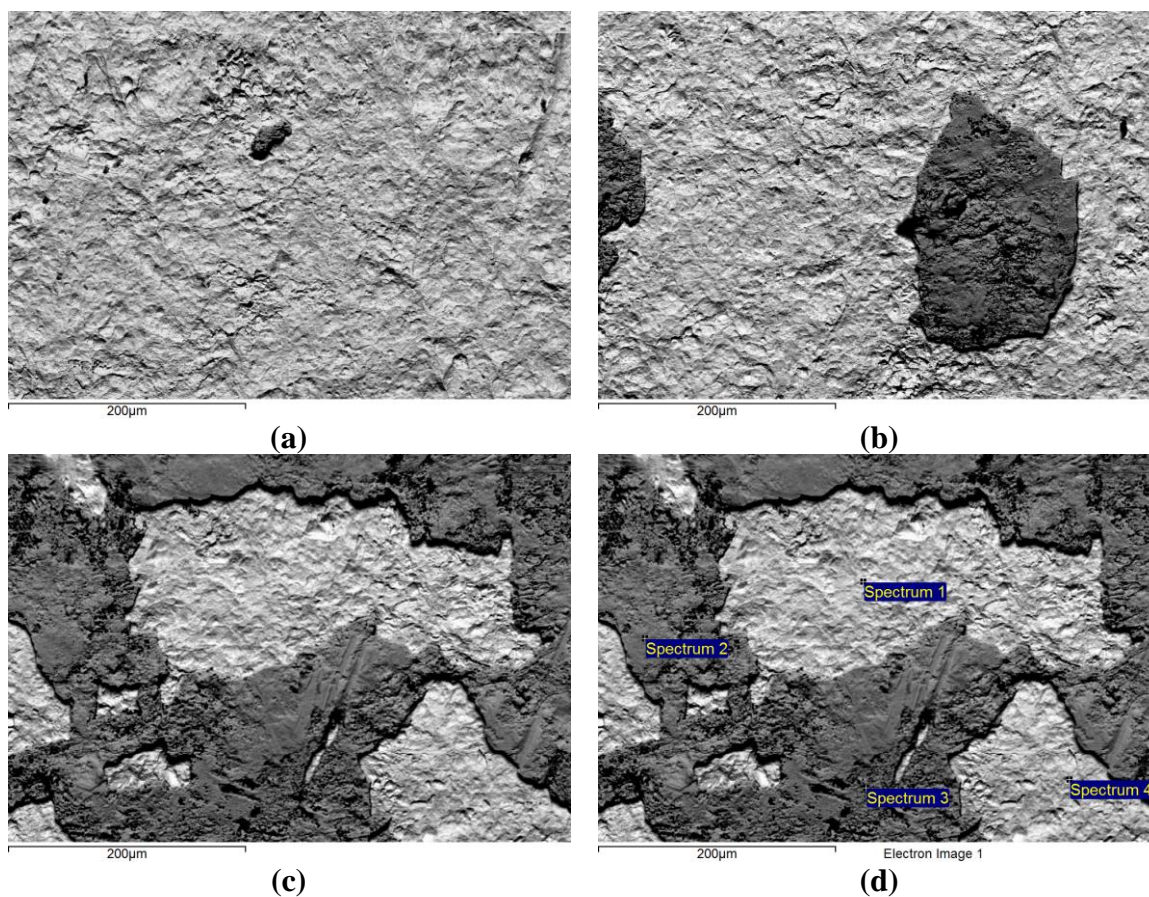
Figure 7-135. Backscatter electron images of mild steel after 2340 hours of exposure to biocrude derived from animal renderings. Dark areas are iron oxide.

Table 7-17. Qualitative elemental analysis of mild steel exposed to crude palm oil and exposed to biocrude derived from animal renderings as indicated in Figure 7-134f and 7-135d.

7-134f					
Spectrum	**C**	**O**	**Mn**	**Fe**	**Total**
1	0	35.38	0	64.62	100
2	0	37.95	0	62.05	100
3	21.73	4.91	0	73.36	100
4	15.95	7.38	0.49	76.18	100
7-135d					
Spectrum	**C**	**O**	**Mn**	**Fe**	**Total**
1	19.3	0	0.46	80.24	100
2	0	35.84	0.46	63.7	100
3	13.28	34.12	0	52.6	100
4	20.3	0	0.89	78.8	100

Effects of hi-pour fuel oil on the mild steel were minimal. The weight losses and gains of the sample were minimal, and the weight of the sample was nearly constant throughout the entire process. Furthermore, no deposits were observed on the sample, and no material was removed from the sample. If corrosion was occurring on an ongoing basis, products would plate out onto the sample or flake away from the sample. Therefore, the hi-pour fuel oil did not corrode mild steel under these conditions.

Effects of lo-pour fuel oil on the mild steel were also minimal. Again, the weight gains of the sample were minimal, and the weight of the sample was nearly constant throughout the entire process. Furthermore, no deposits were observed on the sample, and no material was removed from the sample. If corrosion was occurring on an ongoing basis, products would plate out onto the sample or flake away from the sample. Therefore, the lo-pour fuel oil did not corrode mild steel under these conditions.

The ultra-low sulfur diesel did affect the mild steel sample. At the 690 hour mark, some bluish discoloration was observed on the mild steel sample. It is unclear what caused this discoloration, as such changes would be more commonly observed in metals exposed to high-temperature (>900°F) applications (Fontana, 1986). At the 1350 hour mark, degraded diesel fuel deposits were observed on the sample, but they could be removed by scrubbing with the rubber stopper. At the 1680 hour mark, more degraded diesel fuel deposits were observed on the sample which could not be removed. These deposits could be removed at the 2010 hour mark, though. The diesel fuel probably decomposed because it was held at elevated temperatures without any additives to improve its thermal stability.

Effects of the crude palm oil on the mild steel were minimal. The weight losses and gains of the sample were minimal, and the weight of the sample was nearly constant throughout the entire process. Furthermore, no deposits were observed on the sample, and no material was removed from the sample. If corrosion was occurring on an ongoing basis, products would plate out onto the sample or flake away from the sample. Therefore, the crude palm oil did not corrode mild steel under these conditions.

Effects of the crude jatropha oil on the mild steel were minimal. The weight gains of the sample were minimal, and the weight of the sample was nearly constant throughout the entire process. Furthermore, no deposits were observed on the sample, and no material was removed from the sample. If corrosion was occurring on an ongoing basis, products would plate out onto the sample or flake away from the sample. Therefore, the crude jatropha oil did not corrode mild steel under these conditions.

Biocrude derived from animal renderings had a significant effect on the mild steel sample. At every removal from the oven, some material was removed from the sample; a total of about 40 mg of material, most likely iron oxides based on the SEM point elemental analysis, was lost throughout the process. This material was very loosely bonded and scrubbed away easily. The maximum corrosion rate observed was 1.49 mpy at the 336 hour mark, and the corrosion rate at the 2340 hour mark was 0.45 mpy. Since the material removed was iron oxides, it is uncertain what effect biocrude derived from animal renderings would have on unoxidized mild steel. Nevertheless, by the results of this study, biocrude derived from animal renderings had a significant corrosive effect on mild steel, and mild steel wetted parts should be avoided for service in the presence of biocrude derived from animal renderings.

Biodiesel (refined biocrude) did not have a significant effect on the mild steel sample. Some loosely bonded deposits were removed from the sample at the 690 hour, 1020 hour, and 2010 hour marks. However, the weight losses and gains of the sample were minimal, and the weight of the sample was nearly constant throughout the entire process. If significant corrosion was occurring on an ongoing basis, the mass of the sample would change significantly throughout the process, as observed for the mild steel sample in biocrude derived from animal renderings. While the nature of these deposits is not fully understood, the relative constancy of the mass of the coupon in biodiesel (refined biocrude) leads to the conclusion that biodiesel (refined biocrude) did not corrode the mild steel under these conditions.

Figure 7-136 shows the changes in mass of the 410 stainless steel samples during their exposure to pure oils. The samples in hi-pour fuel oil, lo-pour fuel oil, crude palm oil, crude jatropha oil, biocrude derived from animal renderings, and biodiesel (refined biocrude) all experienced minimal gains or losses during the testing period. The sample in ultra-low sulfur diesel experienced mass gains due the formation of bonded degraded diesel fuel deposits. It is clear from this chart that the fuels overall had very little effect on the 410 stainless steel samples.

410 Stainless Steel
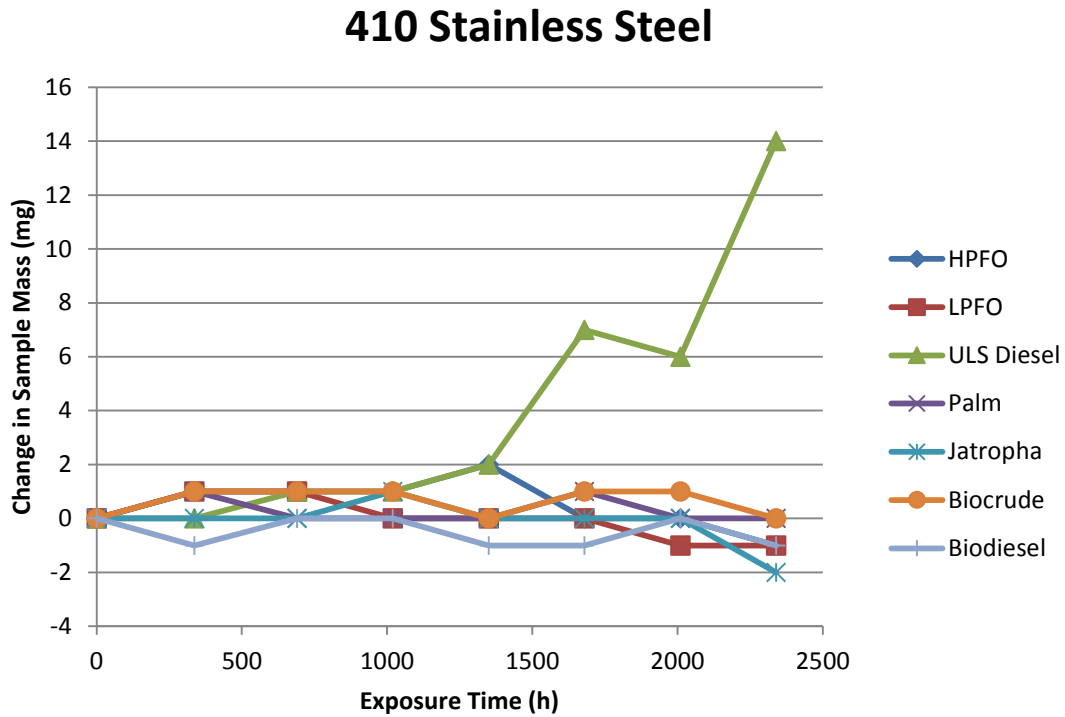
Figure 7-136. Changes in mass of 410 stainless steel samples during testing period.

Figure 7-137 shows the corrosion rates of the 410 stainless steel samples. These rates were calculated using the aforementioned equation as presented by Fontana (1986). Again, the overall corrosion rates were low. The exception is the corrosion rate of the 410 stainless steel sample in ultra-low sulfur diesel; this increase in the rate of corrosion is due to the formation of bonded degraded fuel deposits by the same mechanisms observed for the 304 stainless steel, brass, 316 stainless steel, and mild steel samples.

Figure 7-137. Corrosion rates of 410 stainless steel samples during testing period.

Figure 7-138 shows time lapse photos of the 410 stainless steel samples when they were removed from the oven.

336 h (~2 weeks)

690 h (~4 weeks)

1020 h (~6 weeks)

1350 h (~8 weeks)

1680 h (~10 weeks)

2010 h (~12 weeks)

1 – exposed to hi-pour fuel oil
2 – exposed to lo-pour fuel oil
3 – exposed to ultra-low sulfur diesel
4 – exposed to crude palm oil
5 – exposed to crude jatropha oil
6 – exposed to biocrude derived from
     animal renderings
7 – exposed to biodiesel (refined biocrude)

2340 h (~14 weeks)
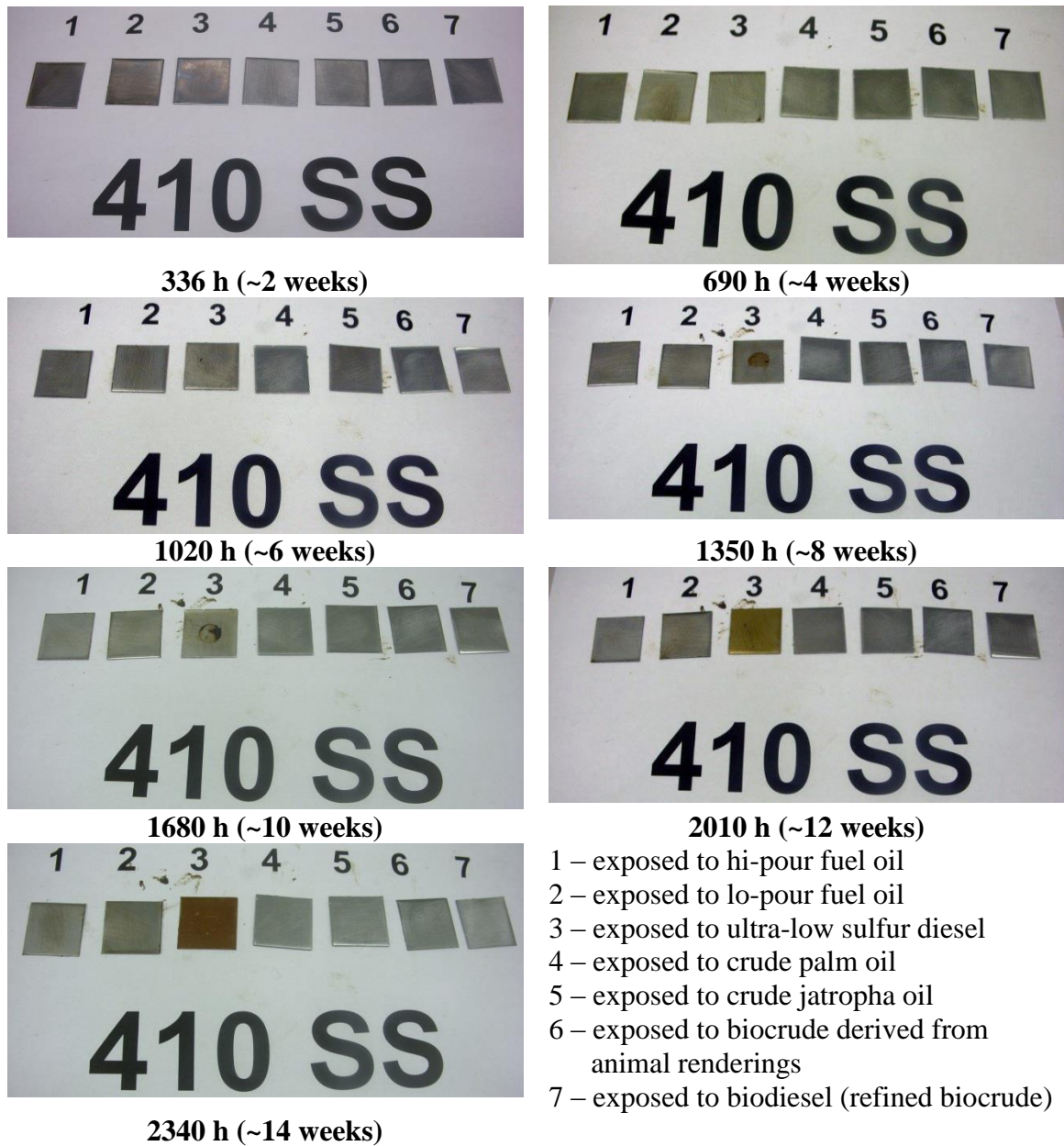
Figure 7-138. 410 stainless steel samples after exposure to pure oils.

The 410 stainless steel samples immersed in hi-pour fuel oil and crude jatropha

oil were selected for SEM analysis. Figure 7-139 shows the backscatter images of the 410

stainless steel sample in hi-pour fuel oil, and Figure 7-140 shows the backscatter images

of the 410 stainless steel sample in crude jatropha oil. The corrosion rate of the sample in

239

hi-pour fuel oil was 0.01 mpy at 2340 hours, and the corrosion rate of the sample in crude

jatropha oil was 0.03 mpy at 2340 hours.
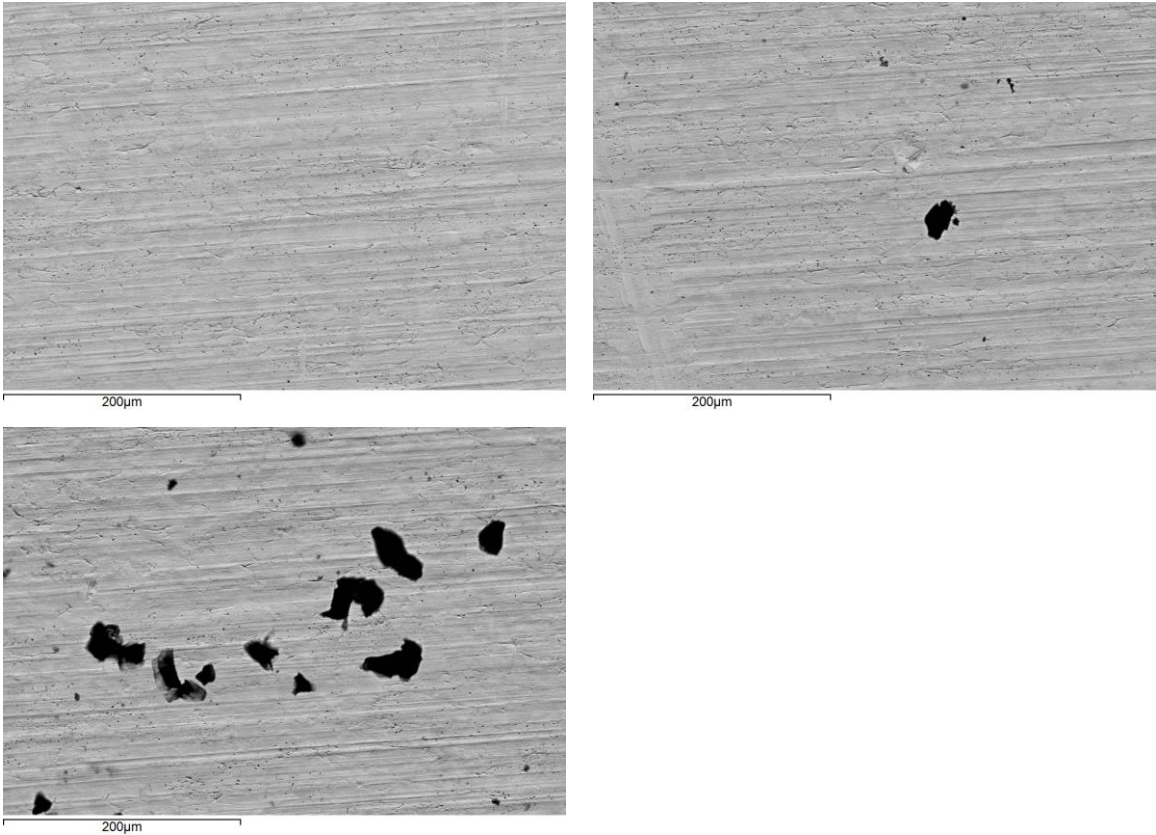
Figure 7-139. Backscatter electron images of 410 stainless steel after 2340 hours of exposure to hi-pour fuel oil.
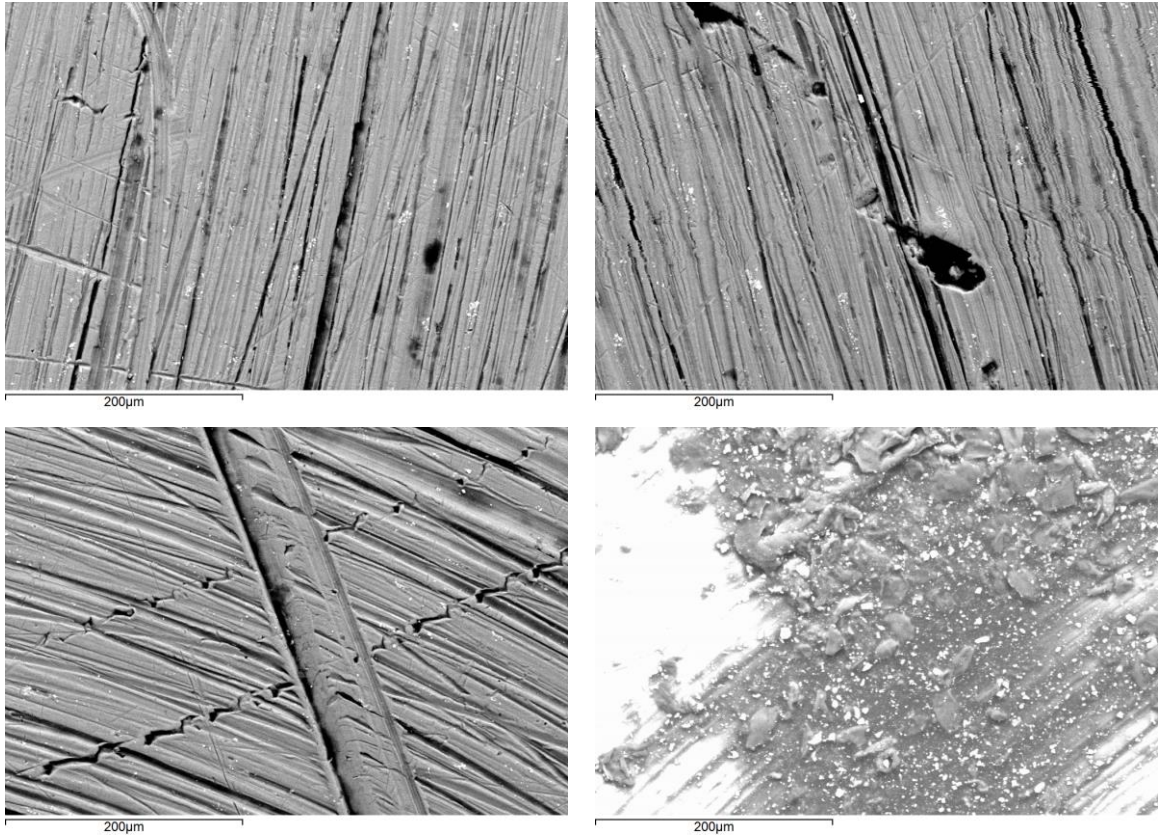
Figure 7-140. Backscatter electron images of 410 stainless steel after 2340 hours of exposure to crude jatropha oil.

Effects of the hi-pour fuel oil on the 410 stainless steel were minimal. The weight gains and losses of the sample were minimal, and the weight of the sample was nearly constant throughout the entire process. Furthermore, no deposits were observed on the sample, and no material was removed from the sample. If corrosion was occurring on an ongoing basis, products would plate out onto the sample or flake away from the sample. Therefore, the hi-pour fuel oil did not corrode 410 stainless steel under these conditions.

Effects of the lo-pour fuel oil on the 410 stainless steel were minimal. The weight gains and losses of the sample were minimal, and the weight of the sample was nearly constant throughout the entire process. Furthermore, no deposits were observed on the sample, and no material was removed from the sample. If corrosion was occurring on an

ongoing basis, products would plate out onto the sample or flake away from the sample. Therefore, the lo-pour fuel oil did not corrode 410 stainless steel under these conditions.

The ultra-low sulfur diesel did affect the 410 stainless steel sample. At the 690 hour mark, bonded degraded diesel fuel deposits were observed on the sample; while many of them could be removed, some were resistant to removal by scrubbing with the rubber stopper. At the 1020 hour mark, degraded diesel fuel deposits were again observed on the sample, though these could be removed by scrubbing with the rubber stopper. At the 1350 hour mark, degraded diesel fuel was again observed on the coupon; although most of it could be removed, some degraded fuel was resilient and remaining on the sample after cleaning. Similar resistant deposits were again observed at the 1680 hour and 2010 hour marks. These deposits were only observed on the bottom face of the coupon; the coupons were not suspended in the jars but were allowed to rest on the bottom, and it is possible that a thin layer of diesel fuel was trapped between the coupon and the bottom of the jar and was able to degrade and bond to the coupon there. The sample was flipped over when deposits were resistant to removal in order to expose the face of the coupon with the deposit to the fuel and perhaps provide an opportunity to for it to diffuse away from the surface. This sample was ultrasonically cleaned in acetone after the 2340 hour mark; the deposits were removed by the acetone, lending credence to the hypothesis that these were degraded diesel fuel as opposed to rusts formed by corrosion. The diesel fuel probably decomposed because it was held at elevated temperatures without any additives to improve its thermal stability.

Effects of the crude palm oil on the 410 stainless steel were minimal. The weight gains and losses of the sample were minimal, and the weight of the sample was nearly

constant throughout the entire process. Furthermore, no deposits were observed on the sample, and no material was removed from the sample. If corrosion was occurring on an ongoing basis, products would plate out onto the sample or flake away from the sample. Therefore, the crude palm oil did not corrode 410 stainless steel under these conditions.

Effects of the crude jatropha oil on the 410 stainless steel, again, were minimal. The weight gains and losses of the sample were minimal, and the weight of the sample was nearly constant throughout the entire process. Furthermore, no deposits were observed on the sample, and no material was removed from the sample. If corrosion was occurring on an ongoing basis, products would plate out onto the sample or flake away from the sample. Therefore, the crude jatropha oil did not corrode 410 stainless steel under these conditions.

Effects of the biocrude derived from animal renderings on the 410 stainless steel were minimal. The weight gains of the sample were minimal, and the weight of the sample was nearly constant throughout the entire process. Furthermore, no deposits were observed on the sample, and no material was removed from the sample. If corrosion was occurring on an ongoing basis, products would plate out onto the sample or flake away from the sample. Therefore, the biocrude derived from animal renderings did not corrode 410 stainless steel under these conditions.

Effects of the biodiesel (refined biocrude) on the 410 stainless steel, again, were minimal. The weight losses of the sample were minimal, and the weight of the sample was nearly constant throughout the entire process. Furthermore, no deposits were observed on the sample, and no material was removed from the sample. If corrosion was occurring on an ongoing basis, products would plate out onto the sample or flake away

from the sample. Therefore, the biodiesel (refined biocrude) did not corrode 410 stainless steel under these conditions.

Mars Fontana gives a correlation for minimum testing time as

$$\frac{2000}{mils\ per\ year} = hours(duration\ of\ test)\ \text{(Fontana, 1986).}$$

Table 7-18 shows the calculated minimum testing times for the samples using the corrosion rates observed at the 2340 hour mark to calculate the corrosion rate in mils per year as compared to the testing time used for the samples. The generally long calculated minimum testing times are expected with the low corrosion rates seen for many of the samples. The shorter minimum testing times observed for the brass samples are indicative of the corrosive action of many of the fuels on this alloy. The shorter testing times observed for the samples immersed in ultra-low sulfur diesel are due to the bonded degraded diesel fuel deposits rather than any corrosive activity.

Table 7-18. Comparison of calculated minimum testing times for samples to actual testing time.

Metal Type	Oil Type	Corrosion Rate at 2340 h (mpy)	Calculated Minimum Testing Time (h)	Actual Testing Time (h)
304 stainless steel	Hi-pour fuel oil	-0.02	23,000	2340
304 stainless steel	Lo-pour fuel oil	-0.03	18,000	2340
304 stainless steel	Ultra-low sulfur diesel	-0.29	1860	2340
304 stainless steel	Crude palm oil	-0.02	31,000	2340
304 stainless steel	Crude jatropha oil	-0.02	30,000	2340
304 stainless steel	Biocrude derived from animal renderings	-0.03	18,000	2340
304 stainless steel	Biodiesel (refined biocrude)	-0.02	30,000	2340
Brass	Hi-pour fuel oil	0.00	∞	2340
Brass	Lo-pour fuel oil	0.12	4560	2340
Brass	Ultra-low sulfur diesel	-0.29	1870	2340
Brass	Crude palm oil	0.11	4720	2340
Brass	Crude jatropha oil	0.03	18,000	2340
Brass	Biocrude derived from animal renderings	0.13	4040	2340
Brass	Biodiesel (refined biocrude)	0.10	5340	2340
316 stainless steel	Hi-pour fuel oil	0.01	53,000	2340
316 stainless steel	Lo-pour fuel oil	-0.01	53,000	2340
316 stainless steel	Ultra-low sulfur diesel	-0.14	3870	2340
316 stainless steel	Crude palm oil	-0.05	12,000	2340
316 stainless steel	Crude jatropha oil	0.01	59,000	2340
316 stainless steel	Biocrude derived from animal renderings	0.00	∞	2340
316 stainless steel	Biodiesel (refined biocrude)	0.00	∞	2340

Table 7-18, cont.

Metal Type	Oil Type	Corrosion Rate at 2340 h (mpy)	Calculated Minimum Testing Time (h)	Actual Testing Time (h)
Mild steel	Hi-pour fuel oil	0.00	∞	2340
Mild steel	Lo-pour fuel oil	-0.04	15,000	2340
Mild steel	Ultra-low sulfur diesel	-0.01	44,000	2340
Mild steel	Crude palm oil	-0.01	44,000	2340
Mild steel	Crude jatropha oil	-0.02	22,000	2340
Mild steel	Biocrude derived from animal renderings	0.45	1180	2340
Mild steel	Biodiesel (refined biocrude)	0.00	∞	2340
410 stainless steel	Hi-pour fuel oil	0.01	38,000	2340
410 stainless steel	Lo-pour fuel oil	0.01	38,000	2340
410 stainless steel	Ultra-low sulfur diesel	-0.20	2740	2340
410 stainless steel	Crude palm oil	0.00	∞	2340
410 stainless steel	Crude jatropha oil	0.03	19,000	2340
410 stainless steel	Biocrude derived from animal renderings	0.00	∞	2340
410 stainless steel	Biodiesel (refined biocrude)	0.01	38,000	2340

CHAPTER VIII
CONCLUSIONS AND FUTURE WORK

8.1   Conclusions
8.1.1   Tar Cracking
8.1.1.1 Laboratory-Scale Updraft Gasifier and Tar Cracking Reactor

Four main conclusions may be drawn from the lab-scale tar cracking tests: one

relating to testing temperature, one related to preconditioning (*i.e.*, the benefit of thermal

cracking and the benefit of guard catalysts), one related to the catalysts themselves, and

one related to the bed size.

Concerning testing temperature, it is clear that there is a transition in catalyst

cracking performance between 800°C and 900°C. The optimal temperature for catalytic

cracking is at least 800°C, as coking is too prevalent at lower temperatures. Figure 8-1

shows the equilibrium-based carbon deposition boundary for the fuel mixture fired in the

gasifier. The gasfier was run at approximately a 0.45-0.55 equivalence ratio, which would

border the carbon deposition boundary (Martin and Dunham, 2013). Thermal cracking

performance substantially increases between 800°C and 900°C as well.
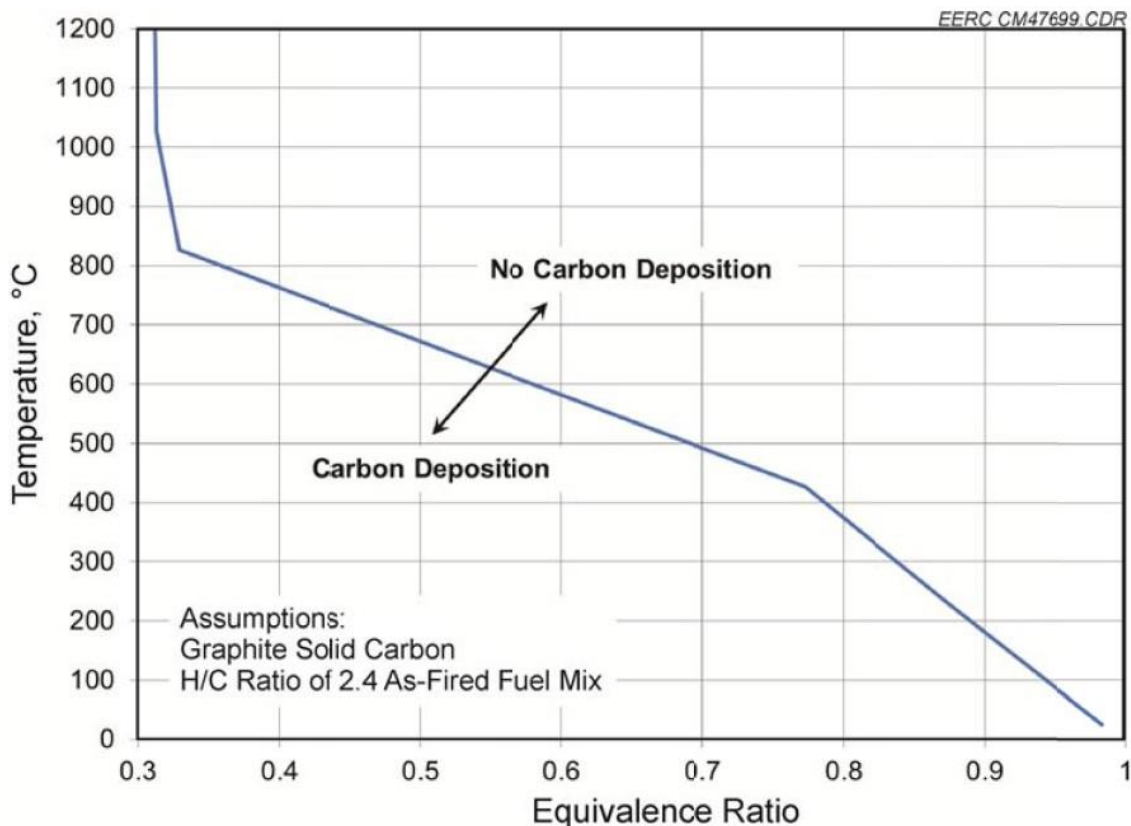
Figure 8-1. Equilibrium-based carbon deposition boundary (Martin and Dunham, 2013).

Concerning preconditioning, thermal cracking accounted for ~85% of the observed tar destruction, and depending on the application, thermal cracking may be sufficient. This would impose a balance between the energy penalty of heating the syngas from the gasifier to the degree required to crack the tars formed in gasification and the cost of operating a catalyst bed to incur a lesser energy penalty.

The data suggest that guard catalysts are of little use at 900°C because the tar is thermally destroyed. However, guard catalysts may still be of use to protect more expensive transition metal-based catalysts against poisoning and coking.

Concerning the catalysts themselves, the primarily transition metal-based reforming and cracking catalysts were the most promising, showing outlet tar loadings

248

two to three times lower than the mineral catalysts, especially at 900°C. This is in agreement with the reviewed literature.

Concerning the bed size, generous residence times were used to obtain the tar conversions reported (4000-5000 h^{-1}). The large bed (and consequent lower space velocity) was required to allow operation at a reasonable ΔP when higher flow rates were tested.

8.1.1.2 Bench-Scale Tar Cracking Reactor

The NREL Ni-based catalyst was the most effective overall; this is as expected since transition metal catalysts generally outperform basic mineral catalysts. Within the mineral catalysts, the powder dolomite was the most effective mineral catalyst. The trona catalyst, which had a similar particle size to the powder dolomite, did not perform as well as the powder dolomite but was an effective catalyst at 900°C. The Plum Run dolomite was also an effective catalyst at 900°C, and the nahcolite was not an effective mineral catalyst.

Concerning the testing temperature, generally higher temperatures led to greater conversion. This is as expected since thermal cracking effects would be more evident at higher temperatures. The exception to this rule was olivine: temperatures above 800°C led to a decrease in cracking activity. This may be due to phase change within the mineral structure of the catalyst or sintering of the catalyst particles.

Results observed on the bench-scale system overall were similar to those observed on the lab-scale system, which validates the results seen on both systems.

8.1.2   Biofuels
8.1.2.1 Overall Blend Acceptability

Table 8-1 shows an indication of the acceptability of the tested fuel blends. These were determined based on their miscibility at 75°F, 170°F, and 220°F as well as their behavior when cooled to 75°F from 170°F and 220°F. Blends containing biocrude and palm oil were marginal to unacceptable due to the large proportion of waxes at ambient temperatures. All other fuel blends were acceptable for use in industry.

Table 8-1. Overall fuel blend acceptability.

	Lo-Pour Fuel Oil	Hi-Pour Fuel Oil	Biocrude (animal)	Crude Jatropha Oil	Crude Palm Oil	Biodiesel (refined biocrude)	Ultra-low sulfur diesel
Lo-Pour Fuel Oil		Not Tested	Marginal	Yes	Marginal	Yes	Yes
Hi-Pour Fuel Oil			Marginal	Yes	Marginal	Yes	Yes
Biocrude (animal)				Marginal	No	Not Tested	Yes
Crude Jatropha Oil					No	Yes	Yes
Crude Palm Oil						Marginal	Marginal
Biodiesel (refined biocrude)							Yes
Ultra-low sulfur diesel							

8.1.2.2 Characterization of Oils and Oil Blends

The high wax content and/or opacity led to questionable pour point values in some tested blends. Of the tested blends, the crude jatropha oil – biodiesel (refined biocrude) blend would pour and therefore pump at ambient conditions, but may not at lower temperatures (< 45°F). Better pour point measurements could probably be obtained

by using the standard method in ASTM D92, but the high opacity of some of the oils and oil blends could make this difficult as well.

The method used to determine the wax appearance temperature was precise. However, it would not be simple to set up in the field, and it is impractical for widespread use.

Conventional ultimate analysis and Karl Fischer water titration was sufficient to characterize biofuels for composition, heating value, and water content.

8.1.2.3 Corrosion Testing

Significant corrosion was observed on the following samples: brass in biocrude derived from animal renderings, brass in crude jatropha oil, brass in biodiesel (refined biocrude), brass in crude palm oil, brass in lo-pour fuel oil, and mild steel in biocrude derived from animal renderings. The most significant corrosion was observed on the mild steel in biocrude derived from animal renderings; however, the majority of the metal loss occurred within the first 1020 hours, after which the mass of the sample began to stabilize. Table 8-2 shows the rates of corrosion at 2340 hours as compared to Fontana's standards for metal performance in corrosive environments. Fontana defines "outstanding" as <1 mpy, "excellent" as 1-5 mpy, "good" as 5-20 mpy, "fair" as 20-50 mpy, "poor" as 50-200 mpy, and "unacceptable" as >200 mpy (Fontana, 1986). In the case of mass gain, the absolute value of the gain was used to determine the classification. In spite of the varied effects of the oils on the metal samples, all samples had outstanding levels of performance in their respective oils.

Table 8-2. Performance of metals during exposure to pure oils.

Metal Type	Oil Type	Corrosion Rate at 2340 h (mpy)	Classification
304 stainless steel	Hi-pour fuel oil	-0.02	Outstanding
304 stainless steel	Lo-pour fuel oil	-0.03	Outstanding
304 stainless steel	Ultra-low sulfur diesel	-0.29	Outstanding
304 stainless steel	Crude palm oil	-0.02	Outstanding
304 stainless steel	Crude jatropha oil	-0.02	Outstanding
304 stainless steel	Biocrude derived from animal renderings	-0.03	Outstanding
304 stainless steel	Biodiesel (refined biocrude)	-0.03	Outstanding
Brass	Hi-pour fuel oil	0.00	Outstanding
Brass	Lo-pour fuel oil	0.12	Outstanding
Brass	Ultra-low sulfur diesel	-0.29	Outstanding
Brass	Crude palm oil	0.11	Outstanding
Brass	Crude jatropha oil	0.03	Outstanding
Brass	Biocrude derived from animal renderings	0.13	Outstanding
Brass	Biodiesel (refined biocrude)	0.10	Outstanding
316 stainless steel	Hi-pour fuel oil	0.01	Outstanding
316 stainless steel	Lo-pour fuel oil	-0.01	Outstanding
316 stainless steel	Ultra-low sulfur diesel	-0.14	Outstanding
316 stainless steel	Crude palm oil	-0.05	Outstanding
316 stainless steel	Crude jatropha oil	0.01	Outstanding
316 stainless steel	Biocrude derived from animal renderings	0.00	Outstanding
316 stainless steel	Biodiesel (refined biocrude	0.00	Outstanding
Mild steel	Hi-pour fuel oil	0.00	Outstanding
Mild steel	Lo-pour fuel oil	-0.04	Outstanding
Mild steel	Ultra-low sulfur diesel	-0.01	Outstanding
Mild steel	Crude palm oil	-0.01	Outstanding
Mild steel	Crude jatropha oil	-0.02	Outstanding
Mild steel	Biocrude derived from animal renderings	0.45	Outstanding

Table 8-2. Performance of metals during exposure to pure oils.

Metal Type	Oil Type	Corrosion Rate at 2340 h (mpy)	Classification
Mild steel	Biodiesel (refined biocrude)	0.00	Outstanding
410 stainless steel	Hi-pour fuel oil	0.01	Outstanding
410 stainless steel	Lo-pour fuel oil	0.01	Outstanding
410 stainless steel	Ultra-low sulfur diesel	-0.20	Outstanding
410 stainless steel	Crude palm oil	0.00	Outstanding
410 stainless steel	Crude jatropha oil	0.03	Outstanding
410 stainless steel	Biocrude derived from animal renderings	0.00	Outstanding
410 stainless steel	Biodiesel (refined biocrude)	0.01	Outstanding

Overall, the oils had the most effect on the brass samples. If possible, brass should be monitored when it is used in wetted parts in petroleum power plants intending to use biofuels.

8.2   Future Work
8.2.1   Tar Cracking
8.2.1.1 Laboratory-Scale Updraft Gasifier and Tar Cracking Reactor

The long-term effects of sulfur on the lab-synthesized catalysts manufactured by NREL and EERC need to be measured.

To avoid the pressure drop issues observed in testing, the most promising catalyst candidates should be synthesized in monolith form. This form would maximize mass transfer and lower the pressure drop. Thus, higher flow rates could be tested, and residence times would be decreased to more realistic levels. These tests could be used to verify the observed tar conversions.

8.2.1.2 Bench-Scale Tar Cracking Reactor

In order to ensure the validity of the conversions observed, replicates of every test run must be run. Ideally, these repeated tests would be performed on a system that has better mass balance closures than the one used for this testing. A consistent mass balance closure of 5-10% would be required to allow meaningful comparison of results.

A mechanistic study of the kinetics of nahcolite and trona should be performed, as the kinetics of these catalysts are not well understood.

To determine whether phase changes from crystalline to amorphous occurred in the olivine catalyst, x-ray powder diffraction (XRD) tests should be performed on olivine samples exposed to CO and heated to 750°C, 800°C, 850°C, and 900°C.

8.2.2   Biofuels

The fuel blends should be tested for miscibility and the occurrence of other undesired results at additional temperatures. Some temperatures that could be considered are 32°F, which is the freezing point of water; 50°F, which is near the pour point of several of the pure oils; and -10°F, which would simulate winter conditions in the northern United States. Other testing temperatures could be considered as well.

The cooled blends should be reheated to confirm that the blends are able to be reheated without additional negative effects occurring.

More blend ratios should be tested. All oils were blended at a 50:50 ratio. Using other ratios, such as a 20:80 ratio, may allow for the use of fuels which are problematic in higher proportions but are acceptable in lower proportions.

Viscosity testing should be performed on the pure oils and blends to determine whether the viscosity is additive or follows some other predictable relationship.

Further testing may be required to determine the exact effects of biocrude derived from animal renderings on mild steel.

REFERENCES

Z. Abu El-Rub, E.A. Bramer, and G. Brem. "Experimental comparison of biomass chars with other catalysts for tar reduction." Fuel 87 (2008) 2243-2252, doi: 10.1016/j.fuel.2008.01.004

W.M.J. Achten, L. Verchot, Y.J., Franken, E. Mathijs, V.P. Singh, R. Aerts, and B. Muys. "Jatropha bio-diesel production and use." Biomasss and Bioenergy 32.12 (2008): 1063-1084.

Acme Hardesty Oleochemicals. (Retrieved 29 May 2012). *Distilled Palm Oil Fatty Acid Blend B1650* [Material Safety Data Sheet].

S. Adusumilli. Desulfurization and tar removal from gasifier effluents using mixed rare earth oxides. Master's Thesis. Louisiana State University, 2009.

E. Afif, P. Azadi, and R. Farnood. "Catalytic hydrothermal gasification of activated sludge." Applied Catalysis B: Environmental 105 (2011) 136-143, doi: 10.1016/j.apcatb.2011.04.003

D.F. Aktas, J.S. Lee, B.J. Little, R.I. Ray, I.A. Davidova, C.N. Lyles, and J.M. Suflita. "Anaerobic Metabolism of Biodiesel and Its Impact on Metal Corrosion." *Energy & Fuels* 24(2010):2924-2928.

T. Ahmad, J. Nisar, I.A. Awan, and I. Ahmad. "Effect of Solid Additives on Pyrolysis Behaviour of Makerwal Coal." *Journal of the Chemical Society of Pakistan* 31(2009):11-15.

P. Ammendola, L. Lisi, B. Piriou, and G. Ruoppolo. "Rh-perovskite catalysts for
conversion of tar from biomass pyrolysis." <u>Chemical Engineering Journal</u> 154
(2009) 361-368, doi: 10.1016/j.cej.2009.04.010

P. Ammendola, B. Piriou, L. Lisi, G. Ruoppolo, R. Chirone, and G. Russo. "Dual bed
reactor for the study of catalytic biomass tars conversion." <u>Experimental Thermal
and Fluid Science</u> 34 (2010) 269-274, doi: 10.1016/j.expthermflusci.2009.10.019

S. Anis and Z. A. Zainal. "Tar reduction in biomass producer gas via mechanical,
catalytic and thermal methods: A review." <u>Renewable and Sustainable Energy
Reviews</u> 15 (2011) 2355-2377, doi: 10.1016/j.rser.2011.02.018

U. Arena, L. Zaccariello, and M.L. Mastellone. "Fluidized bed gasification of waste-
derived fuels." <u>Waste Management</u> (2010), doi: 10.1016/j.wasman.2010.01.038

U. Arena, F. Di Gregorio, C. Amorese, and M.L. Mastellone. "A techno-economic
comparison of fluidized bed gasification of two mixed plastic wastes." <u>Waste
Management</u> 31 (2011) 1494-1504, doi: 10.1016/j.wasman.2011.02.004

U. Arena, L. Zaccariello, and M.L. Mastellone. "Tar removal during the fluidized bed
gasification of plastic waste." <u>Waste Management</u> 29 (2009) 783-791, doi:
10.1016/j.wasman.2008.05.010

B. Asselbergs, J. Bokhorst, R. Harms, J. van Hemert, L. van der Noort, C. ten Velden, R.
Vervuurt, L. Wijnen, L. van Zon, and L. Woltjer. <u>Size does matter: The
possibilities for cultivating Jatropha curcas for biofuel production in Cambodia.</u>
University of Amsterdam: Expertise Centrum voor Duurzame Ontwikkeling
(ECDO), December 2006.

P. Atkins and L. Jones. *Chemical Principles: The Quest for Insight*. 3rd edition. W.H. Freeman and Company: New York, 2005.

T. Ayodele. "African Case Study: Palm Oil and Economic Development in Nigeria and Ghana; Recommendations for the World Bank's 2010 Palm Oil Strategy." Initiative For Public Policy Analysis. August 2010.

J. Bacha, J. Freel, A. Gibbs, L. Gibbs, G. Hemighaus, K. Hoekman, J. Horn, M. Ingham, L. Jossens, D. Kohler, D. Lesnini, J. McGeehan, M. Nikanjam, E. Olsen, R. Organ, B. Scott, M. Sztenderowicz, A. Teidemann, C. Walker, J. Lind, J. Jones, D. Scott, and J. Mills. "Diesel Fuels Technical Review." Chevron Products Company, San Ramon, CA: 2007.

Backyard Biodiesel, LLC. (1 July 2011). (Retrieved 24 May 2012). *Used Cooking Oil & Grease from Kitchens* [Material Safety Data Sheet].

C.H. Bartholomew and R.J. Farrauto. *Fundamentals of Industrial Catalytic Processes*. 2nd ed. Hoboken, N.J.: Wiley, 2006.

Y. Bi, D. Ding, and D. Wang. "Low-melting-point biodiesel derived from corn oil via urea complexation." Bioresource Technology 101.4 (2010): 1220-1226, doi: 10.1016/j.biortech.2009.09.036

Biodiesel Industries, Inc. (Retrieved 25 May 2012). *Biodiesel* [Material Safety Data Sheet].

BioFlex Fuels. (Retrieved 25 May 2012). *Biodiesel B5* [Material Safety Data Sheet].

"Bio G-3000 Premium Biodiesel Fuel: Renewable Fuels." Griffin Industries. www.griffinind.com. 2010.

M.E. Boucher, A. Chaala, and C. Roy. "Bio-oils obtained by vacuum pyrolysis of softwood bark as a liquid fuel for gas turbines. Part I: Properties of bio-oil and its blends with methanol and a pyrolytic aqueous phase." <u>Biomass and Bioenergy</u> 19.5 (2000): 337-350.

R. Burton. "An Overview of ASTM D6751: Biodiesel Standards and Testing Methods." Alternative Fuels Consortium, Central Carolina Community College and Piedmont Biofuels. 29 January 2008. Retrieved 2 October 2013 <http://www.collectivebiodiesel.org/presentations/2007presentations/pdf/rachelburton-BiodieselFuelQuality.pdf>.

CAMEO Chemicals. "Oils, Edible: Palm." National Oceanic and Atmospheric Administration, 1999.

Cargill. (Retrieved 25 May 2012). *Biodiesel* [Material Safety Data Sheet].

P. Chaiprasert and T. Vitidsant. "Promotion of Coconut Shell Gasification by Steam Reforming on Nickel-Dolomite." <u>American Journal of Applied Sciences</u> 6 (2009) 332-336.

W. Chaiwat, I. Hasegawa, and K. Mae. "Alternative Reforming Methods of Primary Tar Released from Gas Treatment of Biomass at Low Temperature for Development of Pyrolysis/Gasification Process." <u>Industrial and Engineering Chemistry Research</u> 49 (2010): 3577-3584, doi: 10.1021/ie901695r

ChevronPhillips. (5 December 2011). (Retrieved 25 May 2012). *Heavy Pyrolysis Oil* [Material Safety Data Sheet].

ChevronPhillips. (1 September 2011). (Retrieved 25 May 2012). *Light Pyrolysis Oil* [Material Safety Data Sheet].

Cirad. (31 May 2006). (Retrieved 25 May 2012). *Bio-oil* [Material Safety Data Sheet].

ConocoPhillips. (Retrieved 25 May 2012). *No. 2 Biodiesel Blend* [Material Safety Data Sheet].

D.A. Constantinou, J.L.G. Fierro, and A.M. Efstathiou. "A comparative study of the steam reforming of phenol towards H_2 production over natural calcite, dolomite and olivine materials." <u>Applied Catalysis B: Environmental</u> 95 (2010) 255-269, doi: 10.1016/j.apcatb.2010.01.003

J. Corella, J.M. Toledo, and G. Molina. "Performance of CaO and MgO for the hot gas clean up in gasification of a chlorine-containing (RDF) feedstock." <u>Bioresource Technology</u> 99 (2008) 7539-7544, doi: 10.1016/j.biortech.2008.02.018

J. Corella, J.M. Toledo, and G. Molina. "Steam Gasification of Coal at Low-Medium (600-800°C) Temperature with Simultaneous CO_2 Capture in a Bubbling Fluidized Bed at Atmospheric Pressure. 2. Results and Recommendations for Scaling Up." <u>Industrial and Engineering Chemistry Research</u> 47 (2008) 1798-1811, doi: 10.1021/ie0714192

W.D. Dar. "Research needed to cut risks to biofuel farmers." <u>Science and Development Network</u>, 12 June 2007.

L. Di Felice, C. Courson, N. Jand, K. Gallucci, P.U. Goscolo, and A. Kiennemann. "Catalytic biomass gasification: Simultaneous hydrocarbons steam reforming and CO_2 capture in a fluidised bed reactor." <u>Chemical Engineering Journal</u> 154 (2009) 375-383, doi: 10.1016/j.cej.2009.04.054.

Diligent Tanzania Ltd. (Retrieved 24 May 2012). *Diligent Jatropha Seed Oil* [Material Safety Data Sheet].

S. Dooley, H.J. Curran, and J.M. Simmie. "Autoignition measurements and a validated kinetic model for the biodiesel surrogate, methyl butanoate." <u>Combustion and Flame</u> 153.1-2 (2008) 2-32, doi: 10.1016/j.combustflame.2008.01.005

B. Dou, W. Pan, J. Ren, B. Chen, J. Hwang, and T.-U Yu. "Removal of tar component over cracking catalysts from high temperature fuel gas." <u>Energy Conversion and Management</u> 49 (2008) 2247-2253, doi: 10.1016/j.enconman.2008.01.027

A.K. Dubey, R.M. Sarviya, and A. Rehman. "Characterization of Processed Jatropha Oil for use as Engine Fuel." <u>Current World Environment</u> 6.1 (2011) 101-107

R.O. Dunn. "Effect of Oxidation Under Accelerated Conditions on Fuel Properties of Methyl Soyate (biodiesel)." <u>Journal of the American Oil Chemists' Society</u> 79.9 (2002): 915-920.

I. Elbaba, C. Wu, and P.T. Williams. "Hydrogen production from the pyrolysis – gasification of waste tyres with a nickel/cerium catalyst." <u>International Journal of Hydrogen Energy</u> 36 (2011) 6628-6637, doi: 10.1016/j.ijhydene.2011.02.135

"Electricity." <u>2010 International Energy Outlook</u>. U.S. Energy Information Administration. Accessed 29 August 2011 http://www.eia.gov/oiaf/ieo/electricity.html.

S.A. Eliason and C.H. Bartholomew. "Temperature-Programmed Reaction Study of Carbon Transformations on Iron Fischer-Tropsch Catalysts During Steady-State Synthesis." *Catalyst Deactivation*, C.H. Bartholomew and G.A. Fuentes, editors, 1997.

J.M. Encinar, J.F. González, G. Martínez, and J.M. González. "Two stages catalytic

    pyrolysis of olive oil waste." <u>Fuel Processing Technology</u> 89 (2008) 1448-1455,

    doi: 10.1016/j.fuproc.2008.07.005

Encyclopedaedia Britannica, "Coal utilization," retrieved February 10, 2009 (2009):

    http://www.brittanica.com/EBchecked/topic/1424725/coal-utilization

Energy and Environmental Research Center, "A Review of Large-Scale Commercial

    Gasification Technologies," PowerPoint (2007).

---, "The Effects of Fuel Impurities on Gasification and Gas Cleanup," PowerPoint

    (2007).

---, "Introduction to Gasification", PowerPoint (2007).

---, "Theory of Gasification," PowerPoint (2007).

Ensyn Technologies Inc. (26 November 2007). (Retrieved 25 May 2012). *Liquid MNRP*

    [Material Safety Data Sheet].

"EPA." *2013 Proposed Carbon Pollution Standard for New Power Plants*. 12 Jan. 2015.

    Web. 22 Apr. 2015. <http://www2.epa.gov/carbon-pollution-standards/2013-

    proposed-carbon-pollution-standard-new-power-plants>.

---. *FACT SHEET: Clean Power Plan*. 13 June 2014. Web. 22 Apr. 2015.

    <http://www2.epa.gov/carbon-pollution-standards/fact-sheet-clean-power-plan>.

---. *FACT SHEET: Clean Power Plan Flexibility*. 13 June 2014. Web. 22 Apr. 2015.

    <http://www2.epa.gov/carbon-pollution-standards/fact-sheet-clean-power-plan-

    flexibility>.

---. *FACT SHEET: Clean Power Plan Overview*. 13 June 2014. Web. 22 Apr. 2015.

    <http://www2.epa.gov/carbon-pollution-standards/fact-sheet-clean-power-plan-

    overview>.

---. *Proposed Carbon Pollution Standards for Modified and Reconstructed Power Plants*.

    12 Jan. 2015. Web. 19 Apr. 2015. <http://www2.epa.gov/carbon-pollution-

    standards/proposed-carbon-pollution-standards-modified-and-reconstructed-

    power>.

F.J. Espadafor, M.T. García, J.B. Villaneuva, and J.M. Gutiérrez. "The viability of pure

    vegetable oil as an alternative fuel for large ships." <u>Transportation Research Part

    D: Transport and Environment</u> 14.7 (2009): 461-469.

European Chemicals Agency. "Fast Pyrolysis Bio-oil: Auto flammability." Study report,

    2013.

M.A. Fazal, A.S.M.A. Haseeb, and H.H. Masjuki. "Effect of different corrosion

    inhibitors on the corrosion of cast iron in palm biodiesel." *Fuel Processing

    Technology* 92(2011):2154-2159.

S. Fernando, P. Karra, R. Hernandez, and S.K. Jha. "Effect of incompletely converted

    soybean oil on biodiesel quality." *Energy* 32(2007):844-851.

Flint Hills Resources. (Retrieved 24 May 2012). *Fuel Oil No. 2 (Low Sulfur)* [Material

    Safety Data Sheet].

B.C. Folkedahl, A.C. Snyder, J.R. Strege, and S.J. Bjorgaard. "Process Development and

    Demonstration of Coal and Biomass Indirect Liquefaction to Synthetic Iso-

    paraffinic Kerosene." *Fuel Processing Technology* 92.10 (2011): 1939-1945.

M.G. Fontana. *Corrosion Engineering*. 3rd ed. New York: McGraw-Hill, 1986.

"Frequently Ask Questions." <u>Dynamic Fuels LLC</u>. www.dynamicfuelsllc.com, accessed
10 May 2013.

P.K. Frolich and P.I. Wieszevich. "Cracking and Polymerization of Low Molecular
Weight Hydrocarbons." <u>Industrial and Engineering Chemistry</u> 27 (1935) 1055-
1062.

D.P. Geller, T.T. Adams, J.W. Goodrum, and J. Pendergrass. "Storage stability of poultry
fat and diesel fuel mixtures: specific gravity and viscosity." <u>Fuel</u> 87.1 (2007): 92-
102.

M. A. Gerber. "Review of Novel Catalysts for Biomass Tar Cracking and Methane
Reforming." Pacific Northwest National Laboratory. October 2007.

J.W. Goodrum. "Volatility and boiling points of biodiesel from vegetable oils and
tallow." <u>Biomass and Bioenergy</u> 22.3 (2002): 205-211, doi: 10.1016/S0961-
9534(01)00074-5

M.S. Graboski and R.L. McCormick. "Combustion of Fat and Vegetable Oil Derived
Fuels in Diesel Engines." <u>Progress in Energy and Combustion Science</u> 24.2
(1998): 125-164.

Griffin Industries. (19 March 2007). (Retrieved 24 May 2012). *Yellow Grease* [Material
Safety Data Sheet].

M. Guo, S. Weiping, and J. Buhain. "Bioenergy and Biofuels: History, Status, and
Perspective." <u>Renewable and Sustainable Energy Reviews</u> 42 (2014): 712-25, doi:
10.1016/j.rser.2014.10.013

E.S. Gusta. "Tar Elimination using Dolomites During the Gasification of Pine Sawdust."
Master's Thesis. University of Saskatchewan, August 2008.

J. Han and H. Kim. "The reduction and control technology of tar during biomass

gasification/pyrolysis: An overview." Renewable and Sustainable Energy

Reviews, 12 (2008) 397-416, doi: 10.1016/j.rser.2006.07.015

Q. Hao, C. Wang, D. Lu, Y. Wang, D. Li, and G. Li. "Production of hydrogen-rich gas

from plant biomass by catalytic pyrolysis at low temperature." International

Journal of Hydrogen Energy 35 (2010) 8884-8890, doi:

10.1016/j.ijhydene.2010.06.039

M. He, B. Xiao, Z. Hu, S. Liu, X. Guo, and S. Luo. "Syngas production from catalytic

gasification of waste polyethylene: Influence of temperature on gas yield and

composition." International Journal of Hydrogen Energy 34 (2009) 1342-1348,

doi: 10.1016/j.ijhydene.2008.12.023

M. He, B. Xiao, S. Liu, Z. Hu, X. Guo, S. Luo, and F. Yang. "Syngas production from

pyrolysis of municipal solid waste (MSW) with dolomite as downstream

catalysts." Journal of Analytical and Applied Pyrolysis 87 (2010) 181-187, doi:

10.1016/j.jaap.2009.11.005

Hess Corporation. (Retrieved 24 May 2012). *No. 2 Fuel Oil* [Material Safety Data Sheet].

Illinois Sustainable Technology Center – Waste Management and Research Center.

"Feasibility Report: Small Scale Biodiesel Production." Champaign, IL: 2006.

M.h. Jayed, H.h. Masjuki, R. Saidur, M.a. Kalam, and M.i. Jahirul. "Environmental

Aspects and Challenges of Oilseed Produced Biodiesel in Southeast Asia."

Renewable and Sustainable Energy Reviews 13 (2009): 2452-2462.

R.E.E. Jongschaap, R.A.R. Blesgraaf, T.A. Boogaard, E.N. Van Loo, and H.H.G. Savenije. "The water footprint of bioenergy from Jatropha curcas L." <u>Proceedings of the National Academy of Sciences of the United States of America</u> 106.42 (2009): E119.

Just a soap. (Retrieved 24 May 2012). *Palm Oil – Standard & Organic* [Material Safety Data Sheet].

M.A. Kalam and H.H. Masjuki. "Biodiesel from palmoil – an analysis of its properties and potential." <u>Biomass and Bioenergy</u> 23(2002) 471-479.

T. Kan, J. Xiong, X. Li, T. Ye, L. Yuan, Y. Torimoto, M. Yamamoto, and Q. Li. "High efficient production of hydrogen from crude bio-oil via an integrative process between gasification and current-enhanced catalytic steam reforming." <u>International Journal of Hydrogen Energy</u> 35 (2010) 518-532, doi: 10.1016/j.ijhydene.2009.11.010

S.K.B.A. Karim. <u>Production of Biodiesel from Crude Palm Oil (CPO) and Waste Cooking Oil (WCO) through Transesterification Method</u>. Thesis. MARA University of Technology, Shah Alam, Selangor, Malaysia: November 2010.

S. Kaul, R.C. Saxena, A. Kumar, M.S. Negi, A.K. Bhatnagar, H.B. Goyal, and A.K. Gupta. "Corrosion behavior of biodiesel from seed oils of Indian origin on diesel engine parts." <u>Fuel Processing Technology</u> 88 (2007) 303-307.

K. Kawamoto, W. Wu, and H. Kuramochi. "Development of Gasification and Reforming Technology using Catalyst at Lower Temperature for Effective Energy Recovery: Hydrogen Recovery Using Waste Wood." <u>Journal of Environment and Engineering</u> 4 (2009) 409-421, doi: 10.1299/jee.4.409.

A. Ketcong, T. Vitidsant, and K. Fujimoto. "The Development of Ni/Dolomite Catalyst in Simultaneous Biomass Gasification and Reforming in Fluidized Bed." American Journal of Environmental Sciences 5 (2009) 273-277.

J.-W. Kim, T.-Y. Mun, J.-O Kim, J.S.-Kim. "Air gasification of mixed plastic wastes using a two-stage gasifier for the production of producer gas with low tar and a high caloric value." Fuel (2011), doi: 10.1016/j.fuel.2011.02.021

J.B. Kitto. *Steam, Its Generation and Use*. 41st ed. Barberton, OH: Babcock & Wilcox, 2005.

H. Kitzler, C. Pfeifer, and H. Hofbauer. "Pressurized gasification of woody biomass – Variation of parameter." Fuel Processing Technology (2011), doi: 10.1016/j.fuproc.2010.12.009

G. Knothe. "Analytical Methods Used in the Production and Fuel Quality Assessment of Biodiesel." Transactions of the ASAE: 2001 American Society of Agricultural Engineers 44.2 (2001): 193-200.

S. Koppatz, T. Proll, C. Pfeifer, and H. Hofbauer. "Investigation of reforming activity and oxygen transfer of olivine in a dual circulating fluidized bed system with regard to biomass gasification." 2010 ECI Conference on the 13th International Conference on Fluidization – New Paradigm in Fluidization Engineering, 2011.

J.N. Kuhn, Z. Zhao, A. Senefeld-Naber, L.G. Felix, R.B. Slimane, C.W. Choi, and U.S. Ozkan. "Ni-olivine catalysts prepared by thermal impregnation: Structure, steam reforming activity, and stability." Applied Catalysis A: General 341 (2008) 43-49, doi: 10.1016/j.apcata.2007.12.037.

J.N. Kuhn, Z. Zhao, L.G. Felix, R.B. Slimane, C.W. Choi, and U.S. Ozkan. "Olivine
catalysts for methane- and tar-steam reforming." <u>Applied Catalysis B:
Environmental</u> 81 (2008) 14-26, doi: 10.1016/j.apcatb.2007.11.040

B.N. Kuzentsov. "Catalytic methods in coal processing to syn-gas, carboneous and liquid
fuels contributing to sustainable development." <u>International Journal of Hydrogen
Energy</u> 34 (2009) 7057-7063, doi: 10.1016/j.ijhydene.2008.10.049

A. Łamacz, A. Krztoń, and A. Musi. "Reforming of Model Gasification Tar
Compounds." <u>Catalysis Letters</u> 128 (2009) 40-48, doi: 10.1007/s10562-008-9712-
1

A. Łamacz, A. Krztoń, and G. Djéga-Mariadassou. "Steam reforming of model
gasification tars compounds on nickel based ceria-zirconia catalysts." <u>Catalysis
Today</u> (2010), doi: 10.1016/j.cattod.2010.11.067

C. Li, Y. Yamamoto, M. Suzuki, D. Hirabayashi, and K. Suzuki. "Study on the
combustion kinetic characteristics of biomass tar under catalysts." <u>Journal of
Thermal Analysis and Calorimetry</u> 95 (2009) 991-997.

C. Li and K. Suzuki. "Tar property, analysis, reforming mechanism and model for
biomass gasification – An overview." <u>Renewable and Sustainable Energy
Reviews</u> 13 (2009) 594-604, doi: 10.1016/j.rser.2008.01.009

J. Li, B. Xiao, R. Yan, and X. Xu. "Development of a supported tri-metallic catalyst and
evaluation of the catalytic activity in biomass steam gasification." <u>Bioresource
Technology</u> 100 (2009) 5295-5300, doi: 10.1016/j.bioretech.2009.05.030

L. Li, K. Morishita, and T. Takarada. "Light fuel gas production from nascent coal volatiles using a natural limonite ore." Fuel 86 (2007) 1570-1576, doi: 10.1016/j.fuel.2006.10.024

"Liquid Fuels." 2010 International Energy Outlook. U.S. Energy Information Administration. Accessed 29 August 2011 http://www.eia.gov/oiaf/ieo/liquid_fuels.html.

J. Liu, H. Hu, L. Jin, and P. Wang. "Effects of the Catalyst and Reaction Conditions on the Integrated Process of Coal Pyrolysis with CO_2 Reforming of Methane." Energy & Fuels 23 (2009) 4782-4786, doi: 10.1021/ef099272n

Z. Liu and A.K. Kim. "Fire Protection of a Restaurant Cooking Area with Water Mist Suppression Systems." Proceedings of the Third International Conference on Fire Research and Engineering. Chicago, IL, 4-8 October 1999.

P. Lv, Z. Yuan, C. Wu, L. Ma, Y. Chen, and N. Tsubaki. "Bio-syngas production from biomass catalytic gasification." Energy Conversion and Management 48 (2007) 1132-1139, doi: 10.1016/j.enconman.2006.10.014

L. Ma, H. Verelst, and G.V. Baron. "Integrated high temperature gas cleaning: Tar removal in biomass gasification with a catalytic filter." Catalysis Today 105 (2005) 729-734.

K. Magrini, M. Gerber, and R. Dagle. "Catalyst Fundamentals: Thermochemical Conversion Platform Review." 2011 DOE Biomass Program Review, February 17, 2011.

"MALAYSIA: Stagnating Palm Oil Yields Impede Growth." USDA Foreign Agricultural Service. usda.gov. 11 December 2012.

C. Martin. "Thermal Catalytic Syngas Cleanup for High-Efficiency Waste-to-Energy Converters." Proposal to SERDP, SERDP Number 12 WP03-015. March 9, 2011.

C. Martin. "Thermal Catalytic Syngas Cleanup for High-Efficiency Waste-to-Energy Converters." In-Progress Review Meeting presentation to SERDP, WP-2210. April 22, 2013.

C. Martin and D. Dunham. "Thermal Catalytic Syngas Cleanup for High Efficiency Waste-to-Energy Converters." Interim Report (Year 1). Prepared for: Robin Nissan, SERDP Project WP-2210. May 2013.

M.M. Maru, M.M. Lucchese, C. Legnani, W.G. Quirino, A. Balbo, I.B. Aranha, L.T. Costa, C. Vilani, L.Á. de Sena, J.C. Damasceno, T. dos Santos Cruz, L.R. Lidízo, R.F. e Silva, A. Jorio, and C.A. Achete. "Biodiesel compatibility with carbon steel and HDPE parts." *Fuel Processing Technology* 90(2009):1175-1182.

M.L. Mastellone and U. Arena. "Olivine as a Tar Removal Catalyst During Fluidized Bed Gasification of Plastic Waste." AIChE Journal 54 (2008) 1656-1667, doi: 10.1002/aic.11497

B.J. McCoy. "Continuous Kinetics of Cracking Reactions: Thermolysis and Pyrolysis." Chemical Engineering Science 51 (1996) 2903-2908

P. McKenna. "All Washed Up for Jatropha? The draught-resistant "dream" biofuel is also a water hog." MIT Technology Review 9 June 2009.

T. Mendiara, J.M. Johansen, R. Utrilla, A.D. Jensen, and P. Glarborg. "Evaluation of different oxygen carriers for biomass tar reforming (II): Carbon deposition in experiments with methane and other gases." Fuel 90 (2011) 1370-1382, doi: 10.1016/j.fuel.2010.12.034

270

Mg Engineering. Lurgi Oel Gas Chemie. (2002). *State Of The Art Gas Technologies* U. Koss.

F. Miccio, B. Piriou, G. Ruoppolo, and R. Chirone. "Biomass gasification in a catalytic fluidized reactor with beds of different materials." <u>Chemical Engineering Journal</u> 154 (2009) 369-374, doi: 10.1016/j.cej.2009.04.002

R. Michel, S. Rapagnà, M. Di Marcello, P. Burg, M. Matt, C. Courson, and R. Gruber. "Catalytic steam gasification of Miscanthus X giganteus in fluidised bed reactor on olivine based catalysts." <u>Fuel Processing Technology</u> (2010), doi: 10.1016/j.fuproc.2010.12.005

T.A. Milne, R.J. Evans, and N. Abatzoglou. "Biomass Gasifier 'Tars': Their Nature, Formation, and Conversion." National Renewable Energy Laboratory. November 1998.

Z. Min, M. Asadullah, P. Yimsiri, S. Zhang, H. Wu, and C.-Z. Li. "Catalytic reforming of tar during gasification. Part I. Steam reforming of biomass tar using ilmenite as a catalyst." <u>Fuel</u> (2011), doi: 10.1016/j.fuel.2010.12.039

B.R. Moser. "Influence of extended storage on fuel properties of methyl esters prepared from canola, palm, soybean and sunflower oils." <u>Renewable Energy</u> 36.4 (2011): 1221-1226.

L.K. Mudge, S.L. Weber, D.H. Mitchell, L.J. Sealock, Jr., and R.J. Robertus. "Investigations on Catalyzed Steam Gasification of Biomass." Prepared for the U.S. Department of Energy under Contract DE-AC06-76RLO1830. Pacific Northwest Laboratory. January 1981.

271

T.-Y. Mun, J.-O Kim, J.-W. Kim, and J.-S. Kim. "Influence of operation conditions and additives on the development of producer gas and tar reduction in air gasification of construction woody wastes using a two-stage gasifier." Bioresource Technology 102 (2011) 7196-7203, doi: 10.1016/j.biortech.2011.04.068

R.T. Nassu and L.A.G. Gonçalves. "Determination of melting point of vegetable oils and fats by differential scanning calorimetry (DSC) technique." Grasas y Aceites 50.1 (1999) 16-22

National Biodiesel Board. (Retrieved 25 May 2012). *Biodiesel* [Sample Material Safety Data Sheet].

National Institute for Occupational Safety and Health. "Diesel Fuel No. 2 [International Chemical Safety Cards (ICSC)]." Centers for Disease Control and Prevention, 1 July 2014.

Natural Sourcing. (Retrieved 24 May 2012). *Organic Palm Oil, RBD* [Material Safety Data Sheet].

V. Nemanova, T. Nordgreen, K. Engvall, and K. Sjöström. "Biomass gasification in an atmospheric fluidised bed: Tar reduction with experimental iron-based granules from Höganäs AB, Sweden." Catalysis Today (2010), doi: 10.1016/j.cattod.2010.12.019

H. Noichi, A. Uddin, and E. Sasoka. "Steam reforming of naphthalene as model biomass tar over iron-aluminum and iron-zirconium oxide catalyst catalysts." Fuel Processing Technology 91 (2010) 1609-1616, doi: 10.1016/j.fuproc.2010.06.009

T.R. Nunn, J.B. Howard, J.P. Longwell, and W.A. Peters. "Product Compositions and Kinetics in the Rapid Pyrolysis of Sweet Gum Hardwood." <u>Industrial Engineering Chemistry Process Design and Development</u> 24 (1985) 836-844

Y. Ohtsuka, N. Tsbouchi, T. Kikuchi, and H. Hashimoto. "Recent progress in Japan on hot gas cleanup of hydrogen chloride, hydrogen sulfide and ammonia in coal-derived fuel gas." <u>Powder Technology</u> 190 (2009) 340-347, doi: 10.1016/j.powtec.2008.08.012

"Oil Uses." Federación Nacional de Cultivatores de Palma de Aceite. portal.fedepalma.org/oil_uses.htm. Accessed 10 May 2013.

T.I. Olasheu, K.A. Adebiyi, M.O. Durowoju, and K.O. Odesanya. "Determination of Some Physical Properties of Jatropha (*Jatropha Curcas*) Oil." <u>International Journal of Engineering Research</u> 4.6 (2015) 331-338

Olefins Panel of the American Chemistry Council. "US High Production Volume Chemical Program: Category Summary for Fuel Oils Category." Prepared for the Environmental Protection Agency, March 28, 2005.

"Palm Oil Production by Country in 1000 MT." <u>Index Mundi</u>. www.indexmundi.com. 2013.

S.S. Pansare, J.G. Goodwin, Jr., and S. Gangwal. "Simultaneous Ammonia and Toluene Decomposition on Tungsten-Based Catalysts for Hot Gas Cleanup." <u>Industrial and Engineering Chemistry Research</u> 47 (2008) 8602-8611, doi: 10.1021/ie800525c

R.H. Perry, C.H. Chilton, and S.D. Kirkpatrick. *Perry's Chemical Engineers' Handbook*. 4th edition. McGraw Hill (1963), p. 9-6.

C. Pfeifer and H. Hofbauer. "Development of catalytic tar decomposition downstream

    from a dual fluidized bed biomass steam gasifier." <u>Powder Technology</u> 180

    (2008) 9-16, doi: 10.1016/j.powtec.2007.03.008.

Phillips Petroleum Company. (Retrieved 24 May 2012). *No. 2 Diesel Fuel* [Material

    Safety Data Sheet Summary Sheet].

T. Phuphuakrat, T. Namioka, and K. Yoshikawa. "Tar removal from biomass pyrolysis

    gas in two-step function of decomposition and adsorption." <u>Applied Energy</u> 87

    (2010) 2203-2211, doi: 10.1016/j.apenergy.2009.12.002

F. Pinto, R.N. André, C. Franco, H. Lopes, I. Gulyurtlu, and I. Cabrita. "Co-gasification

    of coal and wastes in a pilot-scale installation 1: Effect of catalysts in syngas

    treatment to achieve tar abatement." <u>Fuel</u> 88 (2009) 2392-2402, doi:

    10.1016/j.fuel.2008.12.012

M. Pugazhvadivu and K. Jeyachandran. "Investigations on the performance and exhaust

    emissions of a diesel engine using preheated waste frying oil as fuel." <u>Renewable</u>

    <u>Energy</u> 30.14 (2005) 2189-2202.

A.S. Ramadhas, S. Jayaraj, and C. Muraleedharan. "Biodiesel production from high FFA

    rubber seed oil." <u>Fuel</u> 84.4 (2005) 335-340, doi; 10.1016/j.fuel.2004.09.016

A.S. Ramadhas, S. Jayaraj, and C. Muraleedharan. "Use of vegetable oils as I.C. engine

    fuels – A review." <u>Renewable Energy</u> 29.5 (2004) 727-742.

S. Rapagnà, K. Gallucci, M. Di Marcello, M. Matt, and P.U. Foscolo. "Improvement of

    gas yield from biomass gasification by using Fe/olivine as gasifier bed inventory."

    <u>Chemical Engineering Transactions</u> 21 (2010) 415-420, doi:

    10.3303/CET102101770

D. Reece and C.L. Peterson. "Progress report Idaho on road test with vegetable oil as a diesel fuel." *Proceedings: First Biomass Conference of the Americas, National Renewable Laboratory, 30 August-2 September, 1993*. Pergamon/Elsevier Publishers: p. 891.

A. Rehman, D.R.Phalke, and R. Pandey. "Alternative fuel for gas turbine: Esterified jatropha oil-diesel blend." Renewable Energy 36.10 (2011): 2635-2640.

J. von Reppert-Bismarck. "Biofuel jatropha falls from wonder-crop pedestal." Reuters 21 Jan 2011.

G. Ruoppolo, F. Miccio, and R. Chirone. "Fluidized Bed Cogasification of Wood and Coal Adopting Primary Catalytic Method for Tar Abatement." Energy & Fuels 24 (2010) 2034-2041, doi: 10.1021/ef9012054

Sciencelab.com, Inc. (Retrieved 24 May 2012). *Palm oil* [Material Safety Data Sheet].

Scientific American Board of Editors. "The Other Oil Problem." Scientific American 307.6 (2012): 10.

S.S. Sidibé, J. Blin, G. Vaitilingom, and Y. Azoumah. "Use of crude filtered vegetable oil as a fuel in diesel engines state of the art: Literature review." Renewable and Sustainable Energy Reviews 14.9 (2010) 2748-2759.

M. Siedlecki, W. de Jong, and A.H.M. Verkooijen. "Fluidized Bed Gasification as a Mature And Reliable Technology for the Production of Bio-Syngas and Applied in the Production of Liquid Transportation Fuels – A Review."Energies 4 (2011) 389-434, doi: 10.3990/en4030389

E. Simeone, E. Holsken, M. Nacken, S. Heindreich, and W. De Jong. "Study of the
    Behaviour of a Catalytic Candle Filter in a Lab-Scale Unit at High
    Temperatures." <u>International Journal of Chemical Reactor Engineering</u> 8 (2010)
    1-16.

J.G. Singer. *Combustion, Fossil Power Systems: A Reference Book on Fuel Burning and
    Steam Generation*. 3rd ed. Windsor, CT (1000 Prospect Hill Rd., Windsor
    06095): Combustion Engineering, 1981.

The Soap Kitchen. (Retrieved 29 May 2012). *Palm oil Refined (Organic)* [Material
    Safety Data Sheet].

Sprague. (Retrieved 24 May 2012). *#2 Fuel Oil* [Material Safety Data Sheet].

R. Stotler and D. Human. "Transient emission evaluation of biodiesel fuel blend in a
    1987 Cummins L-10 and DDC 6V-92-TA." ETS Report No. ETS-95-128 to
    National Biodiesel Board, 30 November 1995.

Q. Sun, S. Yu, F. Wang, and J. Wang. "Decomposition and gasification of pyrolysis
    volatiles from pine wood through a bed of hot char." <u>Fuel</u> 90 (2011) 1041-1048,
    doi: 10.1016/j.fuel.2010.12.015

D. Świerczyński, C. Courson, L. Bedel, A. Kiennemann, and S. Vilminot. "Oxidation
    Reduction Behavior of Iron-Bearing Olivines $(Fe_XMg_{1-X})_2SiO_4$ Used as Catalysts
    for Biomass Gasification." <u>Chemistry of Materials</u> 18 (2006) 897-905, doi:
    10.1021/cm051433+

D. Świerczyński, S. Libs, C. Courson, and A. Kiennemann. "Steam reforming of tar from a biomass gasification process over Ni/olivine catalyst using toluene as a model compound." Applied Catalysis B: Environmental 74 (2007) 211-222, doi: 10.1016/j.apcatb.2007.01.017

D. Świerczynski, C. Courson, and A. Kiennemann. "Study of steam reforming of toluene used as model compound of tar produced by biomass gasification." Chemical Engineering and Processing 47 (2008) 508-513, doi: 10.1016/j.cep.2007.01.012.

G. Taralas, M.G. Kontominas, and X. Kakatsios. "Modeling the Thermal Destruction of Toluene (C7H8) as Tar-Related Species for Fuel Gas Cleanup." Energy & Fuels 17 (2003) 329-337, doi: 10.1021/ef0201533

Tesoro. (Retrieved 25 May 2012). *Biodiesel* [Material Safety Data Sheet].

M. Virginie, C. Courson, D. Niznansky, N. Chaoui, and A. Kiennemann. "Characterization and reactivity in toluene reforming of a Fe/olivine catalyst designed for gas cleanup in biomass gasification." Applied Catalysts B: Environmental 101 (2010) 90-100, doi: 10.1016/j.apcatb.2010.09.011

M. Virginie, C. Courson, and A. Kinnemann. "Toluene steam reforming as tar model molecule produced during biomass gasification with an iron/olivine catalyst." Compts Rendus Chimie 13 (2010) 1319-1325, doi: 10.1016/j.crci.2010.03.022

M.A. Uddin, H. Tsuda, S. Wu, and E. Sasaoka. "Catalytic decomposition of biomass tars with iron oxide catalysts." Fuel 87 (2008) 451-459, doi: 10.1016/j.fuel.2007.06.021

Unipetrol. (1 December 2010). (Retrieved 25 May 2012). *Pyrolysis Fuel Oil* [Material Safety Data Sheet].

The United States Department of Energy National Energy Technology Laboratory.

(2002). *The Cost of Mercury Removal in an IGCC Plant*. Reading, Pennsylvania:

Parsons Infrastructure and Technology Group, Inc.

UOP LLC. (2002). *Selexol Process* [PDF]. Des Plaines, IL.

D. Wang, W. Yuan, and W. Ji. "Char and char-supported nickel catalysts for secondary

syngas cleanup and conditioning." Applied Energy 88 (2011) 1656-1663, doi:

10.1016/j.apenergy.2010.11.041

Web. 22 April 2015. <http://www2.epa.gov/sites/production/files/2014-05/ghg-

chart.png>.

M. Widyawati, T.L. Church, N.H. Florin, and A.T. Harris. "Hydrogen synthesis from

biomass pyrolysis with in situ carbon dioxide capture using calcium oxide."

International Journal of Hydrogen Energy 36 (2011) 4800-4813, doi:

10.1016/j.ijhydene.2010.11.103

C. Wongkhorsub and N. Chindaprasert. "A Comparison of the Use of Pyrolysis Oils in

Diesel Engine." Energy and Power Engineering 5 (2013) 350-355, doi:

10.5236/epe.2013.54B068

 "World Energy Demand and Economic Outlook." 2010 International Energy Outlook.

U.S. Energy Information Administration. Accessed 29 August 2011

http://www.eia.gov/oiaf/ieo/world.html.

X. Xiao, X. Meng, D.D. Le, and T. Takarada. "Two-stage steam gasification of waste

biomass in fluidized bed at low temperature: Parametric investigations and

performance optimization." Bioresource Technology 102 (2011) 1975-1981, doi:

10.1016/j.biortech.2010.09.016

C. Xu, J. Donald, E. Byambajav, and Y. Ohtsuka. "Recent advances in catalyst for hot-gas removal of tar and NH_3 from biomass gasification." Fuel 89 (2010) 1784-1795, doi: 10.1016/j.fuel.2010.02.014

J. Yang, X. Wang, L. Li, K. Shen, X. Lu, and W. Ding. "Catalytic conversion of tar from hot coke oven gas using 1-methylnaphthalene as a tar model compound." Applied Catalysis B: Environmental 96 (2010) 232-237, doi: 10.1016/j.apcatb.2010.02.026

S.J. Yoon, Y.-C. Choi, and J.-G. Lee. "Hydrogen production from biomass tar by catalytic steam reforming." Energy Conversion and Management 51 (2010) 42-47, doi: 10.1016/j.econman.2009.08.017

B.C. Young and R.C. Timpe. "Task 3.9 – Catalytic Tar Cracking. Semi-Annual Report: January 1 – June 30, 1995." Work Performed Under Contract No.: DE-FC21-93MC30097. For U.S. Department of Energy, Office of Fossil Energy, by Energy and Environmental Research Center.

Q.-Z. Yu, C. Brage, T. Nordgreen, and K. Sjöström. "Effects of Chinese dolomites on tar cracking in gasification of birch." Fuel 88 (2009) 1922-1926, doi: 10.1016/j.fuel.2009.04.020

B. Yue, X. Wang, X. Ai, J. Yang, L. Li, X. Lu, and W. Ding. "Catalytic reforming of model tar compounds from hot coke oven gas with low steam/carbon ratio over Ni/MgO-Al_2O_3 catalysts." Fuel Processing Technology 91 (2010) 1098-1104, doi: 10.1016/j.fuproc.2010.03.020

N. Zerman. "Valeros Renewable Diesel Plant Nears Start-Up." ENR: Texas & Louisiana. 22 April 2013.

R. Zhang, Y. Wang, and R.C. Brown. "Steam reforming of tar compounds over Ni/olivine catalysts doped with CeO_2." Energy Conversion and Management 48 (2007) 68-77, doi: 10.1016/j.enconman.2006.05.001

Q. Zhang, J. Chang, T. Wang, and Y. Xu. "Review of biomass pyrolysis oil properties and upgrading research." Energy Conversion and Management 48.1 (2007) 87-92, doi: 10.1016/j.enconman.2006.05.010

S.-Y. Zhang, X.-J. Wang, J.-P. Cao, and T. Takarada. "Low temperature catalytic gasification of pig compost to produce H_2 rich gas." Bioresource Technology 102 (2011) 2033-2039, doi: 10.1016/j.biortech.2010.09.070

Y. Zhang, M.A. Dubé, D.D. McLean, and M. Kates. "Biodiesel production from waste cooking oil: 1. Process design and technological assessment." Bioresource Technology 89.1 (2003) 1-16, doi: 10.1016/S0960-8524(03)00040-3

C. Zhao, L. Lin, K. Pang, W. Xiang, and X. Chen. "Experimental study on catalytic steam gasification of natural coke in a fluidized bed." Fuel Processing Technology 91 (2010) 805-809, doi: 10.1016/j.fuproc.2009.08.010

H. Zhao, D.J. Darelants, and G.V. Baron. "Performance of a Nickel-Activated Candle Filter for Naphthalene Cracking in Synthetic Biomass Gasification Gas." Industrial and Engineering Chemistry Research 39 (2000) 3195-3201, doi:10.1021/ie000213x

H. Zhou, B. Jin, Z. Zhong, Y. Huang, R. Xiao, and Y. Zheng. "Catalytic coal partial gasification in an atmospheric fluidized bed." Korean Journal of Chemical Engineering 24 (2007) 489-494.